THERMAL IMPACT ON SOIL-STRUCTURE INTERACTION FOR INTEGRAL BRIDGES

EDET OKON EFRETUEI
(200359251)

Submitted in accordance with the requirements for the degree of
Doctor of Philosophy

University of Leeds
School of Civil Engineering

March
2013

The candidate confirms that the work submitted is his own and that appropriate credit has been given where reference has been made to the work of others.

ACKNOWLEDGEMENTS

I wish to express my sincere gratitude to my supervisor, Prof. B. G. Clarke for being extremely dedicated and providing hands-on guidance and support throughout this study. I appreciate Prof. Clarke for his insight and knowledgeable contributions strategically aimed at critically reviewing every approach and decision in this research. This contributed greatly to the success of this thesis. I am grateful.

I also wish to thank Dr. T. W. Cousens for his critical review of my 1st year transfer report and input towards improving the research. Thanks also to Dr. D. I. Stewart and Dr. Y. Sheng for their guidance within the first year of this study. These inputs helped define this research more appropriately. I would like to thank Mrs. Marcia Martell for her dependable administrative support. Many thanks to the staff of the School of Civil Engineering for the kind advice and able support I received through my studies. I am also thankful to my friends and colleagues in the Civil Engineering department for their support.

Finally, I would like to thank the management and staff of Frekan Consultants, Nigeria, for professional and financial support thus making this study possible. I am eternally grateful to my God and family members, my wife Ekaete Efretuei, my sons Joshua and Joseph Efretuei, my parents Engr. Okon Efretuei and Ms Arit Uyo, my parents in-law Prof. J. G. Ottong, and Dr. Mrs Eno Ottong, and my siblings.

Thank you all for your invaluable support.

ABSTRACT

Integral bridges are generally considered an attractive alternative to conventional bridges presenting the economic advantage of lower construction and maintenance costs. However, the concept of the integral bridge presents other challenges primarily arising from the monolithic connection that exists between the superstructure and the substructure. Thermal loading leads to daily cycles of expansion and contraction superimposed on seasonal cycles. This results in significantly higher soil-structure interaction activity that may lead to excessive earth pressures behind the abutment and potential failure of the soil and structure.

A parametric study was carried out to evaluate the impact of change in the backfill soil parameters and change in the season of construction on the earth pressures developed behind the abutment. The frequency of the daily and seasonal cycles of expansion and contraction is such that granular soils respond as fully drained materials. This is seldom the case for fine grained soils. Excess pore pressures are developed and some drainage may occur. However, data and resource limitations make it not feasible to accurately model this over the long term. Further the need to make assumptions about the temperature cycles and the permeability characteristics weakens the strength of the analysis. Therefore, an envelope of earth pressure generation was created in these parametric studies by modelling fine grained soils as fully drained and fully undrained. Plaxis 2D was used to model the bridge and surrounding soil.

In developing a realistic model of an integral bridge, the first stage was to simulate a constructed instrumented integral bridge which presented measured values of temperature, deformation and earth pressures in time. This allowed the model to be validated and the sensitivity of the analysis to the parameters assessed. A second simulation was undertaken to compare the output of an integral bridge analysis using Plaxis 2D finite element software with a published study output carried out using the finite difference method.

There were a number of challenges to overcome in modelling an integral bridge. These are described in some detail, highlighting the impact the assumptions made within this studies,

had upon the output. It was found that the backfill stiffness parameter was the dominant factor that controlled the magnitude of earth pressure. The parametric study revealed that the season of construction affected the earth pressures generated behind the abutment with autumn and summer construction often leading to cumulatively lower earth pressures than spring and winter respectively.

In integral bridge construction, it is common to use granular soils in backfill construction. However, the use of granular soils in foundation construction may not be sustainable as a result of material availability and construction cost. Fine grained soils are alternatively used where granular soils are not. It was found that modelling fine grained foundation soils as fully drained and fully undrained produced significant variations in the behaviour of the backfill soil and the resulting earth pressure pattern. It is therefore necessary to take into account the impact of thermal loading on the envelope of earth pressure to ensure that the capacity of the structure and soils are not exceeded or underutilised.

TABLE OF CONTENTS

LIST OF FIGURES

LIST OF TABLES

NOMENCLATURE

Symbols

α	Coefficient of thermal expansion
σ	Normal stress
$\boldsymbol{\sigma}'$	Effective normal stress
ΔL	Change in length
Δt	Change in temperature
Δp_f	Increment in pore pressure
$\delta\varepsilon_s$	Increment of shear strain
$\delta q'$	Increment of deviator stress
$\delta\varepsilon_v$	Increment of volumetric strain
$\delta p'$	Increment in mean stress
ε	Total strain
γ	Unit weight of soil
γ_w	Unit weight of water
$\gamma_{0.7}$	Threshold shear strain
κ	Cam clay swelling index
κ^*	Modified swelling index
λ	Cam clay compression index
λ^*	Modified compression index
ρ	Fluid density
ø	Friction angle
$\boldsymbol{\phi}_m$	Mobilized angle of shearing resistance
τ	Shear stress
μ	Viscosity
μ^*	Modified creep index
ν	Poisson's ratio
ψ	Dilatancy
[B]	Matrix with derivatives of shape functions
$\{\Delta d\}_n$	Nodal displacement for the finite element
$\{\Delta d\}_{nG}$	Vector containing the unknown nodal displacements

$\{\Delta d\}^T$	Displacement vector
$\{\Delta F\}^T$	Body force vector
$\{\Delta R_E\}$	Right hand side load vector
$\{\Delta R_G\}$	Global right hand side load vector
$\{\Delta T\}^T$	Surface traction vector
$[D]$	Constitutive matrix in a two dimensional plane strain analysis
$[K_E]$	Element stiffness matrix
$[K_G]$	Global stiffness matrix
$[N]$	Matrix of shape functions
A	Cross-sectional area of flow
c	Cohesion
$c_{increment}$	Cohesion increase with depth
c_k	Change in Permeability
C_c	Compression Index
C_s	Swelling Index
CL	Current length
Ct	Current temperature
$d\boldsymbol{\sigma}_a$	Axial stress
$d\boldsymbol{\sigma}_r$	Radial stress
$d\varepsilon_a$	Axial strain
$d\varepsilon_r$	Radial strain
e	Void ratio
e_{int}	Initial void ratio
E	Mean square error of the estimator
E_i	Initial stiffness
E	Total potential energy of a body
E	Young's modulus
E_{oed}	Oedometer modulus
E_{ur}	Unloading and reloading stiffness
E_{50}	Secant modulus at 50% of the material strength
g	Gravitational acceleration
G'	Shear modulus

G_0^{ref}	Reference shear modulus at very small strain
h	Depth of the water table
i	Hydraulic gradient
k	Intrinsic permeability
k_x	Horrizontal Permeability
k_y	Vertical Permeability
k_o^{nc}	Coefficient of earth pressure at rest
K	Coefficient of permeability or hydraulic conductivity
K	Coefficient of earth pressure
K_a	Coefficient of active earth pressure
K_p	Coefficient of passive earth pressure
K_e	Equivalent bulk modulus of pore fluid
K_o	Coefficient of earth pressure at rest
K'	Bulk modulus
L	Length
L	Applied loads
m	Power for stress-level dependency of stiffness
M	Tangent of critical state line
n	Number of variables
n	Number of nodes in the element
N	Number of elements
q	Discharge
q_a	Asymptotic value of the shear strength
t	Time
u	Pore water pressure
v	Discharge velocity
v_{ur}	Poisson's ratio for unloading
V	Soil volume
w	Strain energy or work done
y	Estimator
y_{ref}	Referenced depth
$\hat{y}$	Data

Y	Yield
z	Depth of the soil element

Abbreviations

DMRB	Design Manual for Roads and Bridges
EBT	Effective Bridge Temperature

Chapter 1 : INTRODUCTION

1.1. Background

Economic growth in the 20th century led to rapid infrastructure development. As a result, an increasing number of bridges are being constructed to cope with the rising road transportation demand. In the United Kingdom, the cost of construction and maintenance of this rising number of bridges has been significant and accounts for a substantial part of the annual expenditure of public funds.

Bridges may be constructed from several materials and may take one of several forms. This includes the Arch Bridge, Beam Bridge, Cable-Stayed Bridge, Cantilever Bridge, Suspension Bridge and Truss Bridge. However, the construction of these bridges may be classified under two main structural configurations – bridges constructed with joints or bridges constructed without joints. Bridges constructed with joints (see Figure 1.1) are identified as conventional bridges. The joints provided in conventional bridges accommodate displacements mainly arising from thermal expansion and contraction of the bridge deck. These joints are usually found in the abutment and piers, providing spaces between the abutments or piers, and the longitudinal beams or slabs. The joints, known as expansion joints are designed to contain damaging forces resulting from torsion, compression or tension in all directions (Johnson, 1994). Bridges constructed without joints are known as integral bridges. Figure 1.2 shows an integral bridge. Figure 1.3 shows the connection between the deck and abutment for (a) a conventional beam bridge and (b) an integral beam bridge, highlighting the difference between a jointed connection and an integral connection. Modern integral bridges are usually Beam Bridges.

Expansion joints are adversely affected by exposure to precipitation and harsh weather conditions. In the 1950's when de-icing salt was introduced to combat the effect of ice and snow, it was found to accelerate the deterioration of these joints. Expansion joints have also

been identified as a major cause of bridge deterioration resulting from leakages and corrosion (Johnson, 1994, Tilly, 1994).

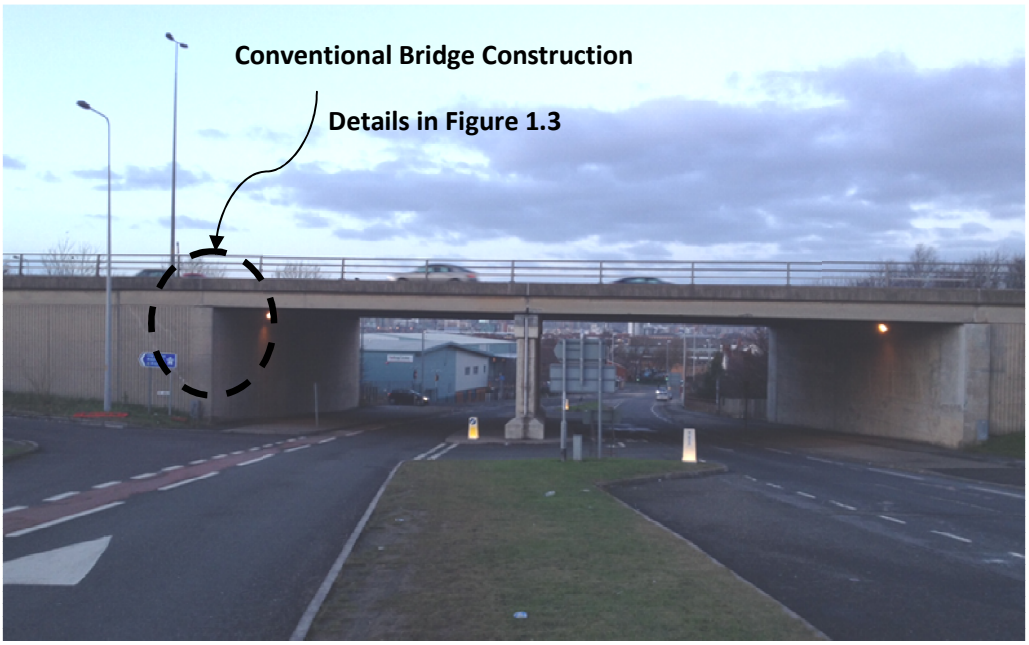

Figure 1.1: Double span conventional bridge in service located in Leeds (M621 Road Bridge over Belle Isle Road), United Kingdom.

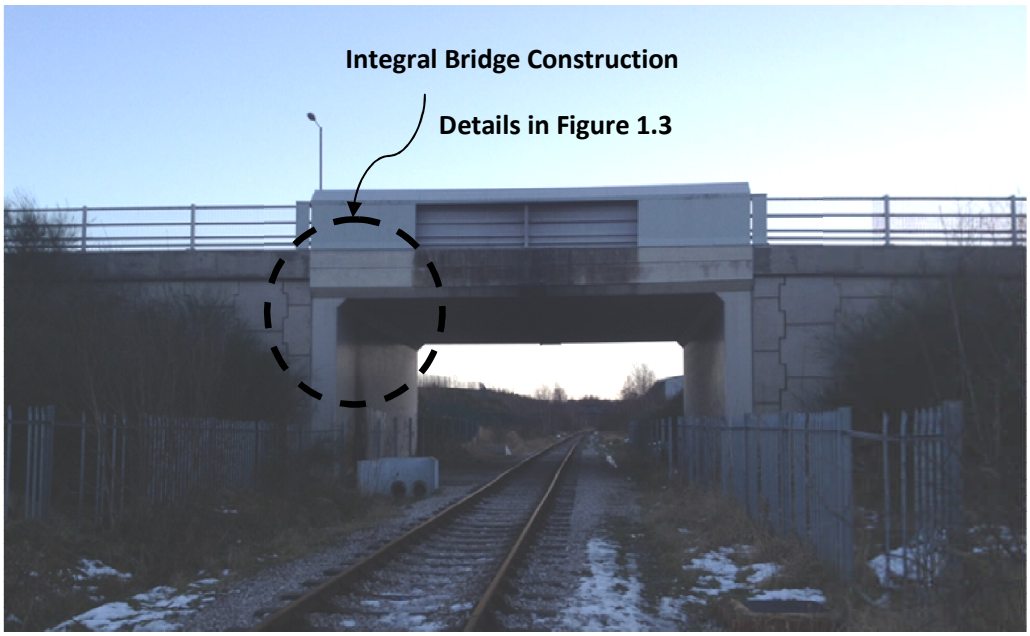

Figure 1.2: Single span integral bridge in service located in Middleton, Leeds (John Charles Approach Road Bridge over railway line), United Kingdom.

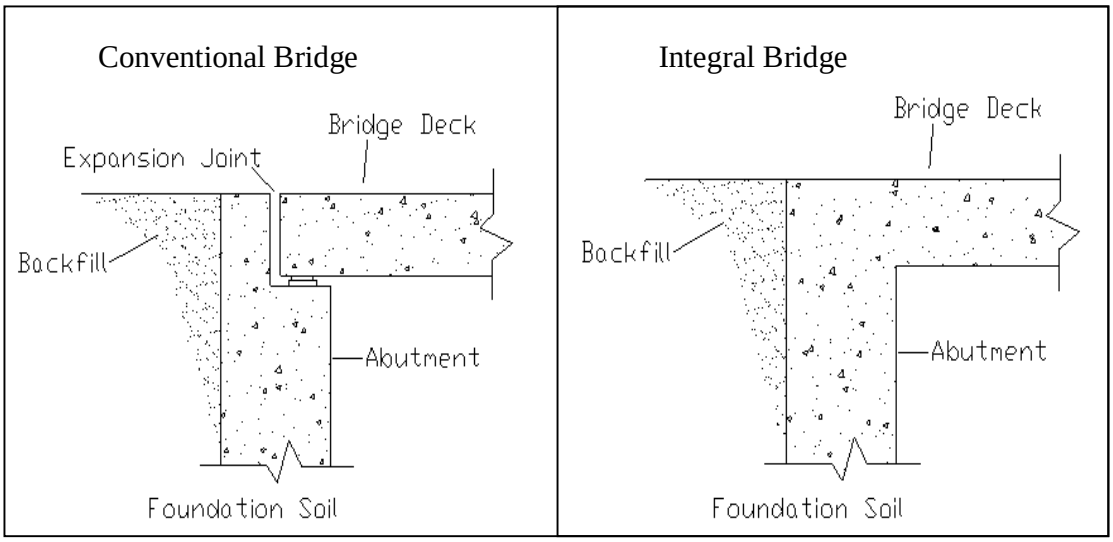

Figure 1.3: Bridge abutment and deck section showing expansion joint construction in conventional bridges and the jointless construction in integral bridges.

Conventional bridges cost more to construct than integral bridges. This is a result of the additional cost in procurement and time to install the expensive expansion joints in the conventional bridges. In owning and operating conventional bridges, the primary concern, other than the higher cost of construction, is the cost of maintaining the expansion joints including the bearing installation that also requires continuing maintenance and replacement (Alampalli and Yannotti, 1998). This also leads to regular disruption to the flow of vehicular traffic. Engineers and clients have identified the maintenance of the expansion joints of conventional bridges as the major cost component in the whole life cost of conventional bridges (Arockiasamy et al., 2004, Dicleli, 2005, Clayton et al., 2006, Faraji et al., 2001, Horvath, 2000).

The integral bridge therefore, is considered an attractive alternative. The bridge deck and the abutment are connected monolithically with a moment resisting connection (Faraji et al., 2001). These bridges are designed to eliminate the need for expansion joints and require little maintenance over time when compared to conventional bridges. Provided the abutment displacement is limited, the integral bridge is generally considered to be more cost effective in construction and maintenance than conventional bridges (Carder and Hayes, 2000, Darley et al., 1998, Davids et al., 2010). As a result, the use of integral bridges has risen in recent years.

1.2. Problem Description

The concept and use of the integral bridge presents challenges that must be accounted for in its design and use. These challenges arise from the monolithic connection that exists between the superstructure and the substructure of the integral bridge. The monolithic connection increases soil-structure interaction. This generates compressive and tensile stresses and strains that may result in soil or structural deformation or failure.

During construction, backfill soils are compacted. Compaction increases the earth pressures within the backfill soil. The backfill soil behind integral bridge abutments is subjected to cyclic loading because of the thermal changes to the bridge deck. Cyclic loading can result in increased earth pressures in the backfill. The integral bridge backfill soil or bridge structure may fail if exposed to excessive earth pressure. Alternatively, cyclic loading can reduce the earth pressures that lead to excessive settlement in the backfill. The bridge abutment wall and foundation structures are subjected to vertical, lateral and rotational loads which cause a range of stress changes, deformations and displacements within the abutment structure, backfill material and foundation soil, making design analysis more complicated than that for a conventional bridge.

The case made for the economic benefits of the use of integral bridges against conventional bridges depends on an extensive scrutiny of the soil-structure interaction as the length of the bridge increases. This has formed the basis of several research studies on integral bridges with some authors and authorities recommending limiting the lengths and heights of the structure (BA42/96, 2003, BD57/01, 2001, Arsoy et al., 2002, Dicleli and Albhaisi, 2004b). Others have recommended changes in the geometric configuration of the structure or the use of granular soils and synthetic materials in construction (White et al., 2010, BA42/96, 2003, Horvath, 2000). However, the concept of the modern integral bridge is relatively new compared to conventional bridges with the first documented construction in 1938 (Burke, 2009). A comprehensive and standardised design and construction guideline generally acceptable to authorities in all countries has not been developed largely due to lack of knowledge of the behaviour of integral bridges. Several countries and authorities have made recommendations for the design and construction of parts of the integral bridge. The challenges presented by the complicated analysis resulting from the soil-structure

interaction still remain the major concern in the integral bridge design, construction and use, for engineers, bridge owners and regulating authorities.

Design and construction of integral bridges are more often dependent on the use of imported materials as backfill. Granular soils with or without reinforcing synthetic materials such as polymeric materials and geocomposites are often recommended for use in backfill construction by engineers (Carder and Card, 1997) as a result of the free draining characteristics of the soils. It is often assumed by design engineers that these materials can be considered to be elastic. These imported materials add to the construction cost. It is also possible to use replacement foundation materials or modify the foundation soils but usually at a significantly higher cost. Consequently, often, the design engineer has to accept the foundation soil on which these bridges and backfill soil are constructed.

Integral bridges can therefore be built on a full spectrum of foundation soils and rocks including clays. Clay soils exhibit characteristics that may adversely affect the behaviour and performance of an integral bridge because of the time dependent response to thermal loading and unloading. Pore pressures may develop in the clays, which can affect the performance of an integral bridge.

The magnitude of the thermal induced loading on integral bridges typically generates small abutment displacements (up to double figure values in millimetres). The effect of this displacement in the backfill and foundation soils on the earth pressures behind the abutment have not been investigated in detail.

Efficient design of integral bridges would be supported by a better understanding of the soil behaviour responding to the soil-structure interaction around the bridge abutment and substructure. This research contributes to the body of knowledge on the soil-structure interaction of the integral bridge by evaluating the impact of thermal loads on the behaviour of the backfill and foundation soils. The foundation soils are assumed to be fully drained or undrained. Undrained means that excess pore pressures can be generated and these do not dissipate during the analysis. Fully drained means that excess pore pressures are not

generated. The backfill soils are assumed to be granular and behave as fully drained materials.

This study was carried out using a two-dimensional (2D) plain strain finite element model. The impact of thermal loading on the backfill and foundation soils was modelled by abutment displacements. It was assumed that the prime cause of these displacements was the expansion/contraction of the bridge deck.

1.3. Research Aims & Objectives

The primary aim of this research is to contribute to the knowledge on the performance of engineered backfill soil materials in integral bridges. This would support better informed decisions by engineers during design, construction and use. The focus is the development of a finite element model that provides a realistic representation of the soil-structure interaction response of the backfill soil to thermal loading.

Data generated was validated against an integral bridge that was instrumented during construction and monitored after construction. The validated model is then used to carry out a parametric study to provide a more revealing insight into the integral bridge soil-structure interaction providing knowledge that would facilitate more informed decisions by engineers.

Plaxis finite element programme was used in developing a functioning model of an instrumented integral bridge. The bridge structure, backfill and foundation soil parameters and geometric configuration, including the thermal effect experienced, were modelled using this software. The in-service performance of the backfill is dependent on the construction process. Therefore, the simulation included modelling the construction process before the thermal loads were applied.

In order to achieve the primary aim of contributing to the knowledge on the performance of engineered backfill soil materials in integral bridges, a number of objectives were identified-

1. A comprehensive literature review on integral bridges and integral bridge soil-structure interaction problems as it relates to the backfill and foundation soil was undertaken to review the concept of the integral bridge, establish the benefits of using integral bridges, identify the issues surrounding integral bridges, establish current practice in integral bridge design and construction and establish research undertaken and the knowledge gaps.

2. A comprehensive finite element model of an integral bridge was developed using an appropriate constitutive soil model capable of generating realistic results within the backfill and foundation soils, closely modelling established backfill soil behaviour from an existing bridge. This meant reviewing relevant soil mechanics concepts applicable to integral bridges, reviewing relevant finite element numerical modelling concepts applicable in developing the model, identifying an appropriate constitutive soil model, identifying an instrumented integral bridge with sufficient data to model the concept of the integral bridge, building a finite element model of an integral bridge soil-structure interaction problem, and comparing the finite element model output with measured site data to validate the model's output and establish realism.

3. The effect of changes in the backfill soil parameters on the earth pressure developed behind the abutment were investigated including the effect of the assumption of fully undrained behaviour and a fully drained behaviour within the fine grained soils in the foundation soils on these changes. In order achieve this it was necessary to identify relevant backfill soil parameters, determine the backfill soil parameter range, establish a simulation plan carry out parametric studies simulations, investigating the effect of changes in the backfill soil parameters on the earth pressure developed behind the abutment and analyse

results to draw conclusions on the performance of the backfill and foundation soils.

4. The effect of the performance of the backfill and foundation soils due to the seasons of construction was investigated. A typical United Kingdom annual temperature pattern was established to determine characteristics of abutment displacements in construction seasons. A parametric study was undertaken to investigate the effect of changes in the seasons of construction, with the assumption of a fully undrained behaviour and a fully drained behaviour in the fine grained soils within the foundation materials. A parametric study was undertaken to investigate the effects of changes in backfill soil parameters. Note that temperature changes due to climate change were not investigated in this study.

5. These studies led to design recommendations for integral bridges.

1.4. Structure of Thesis

The research structure presented in this thesis is illustrated in Figure 1.4. This presents a central core identified using the thick solid line, leading from introducing the concept of the integral bridge, through the abutment displacement, soil-structure interaction, knowledge gap, model development and terminating in the conclusions with consideration of the subjects that influence this core. A literature review was carried out on subjects identified within the oval shapes. Other subjects presented were deduced or created in the course of this research.

The content of this thesis is organised into eight chapters. Chapter 1 introduces the problem addressed in this thesis and presents an overview of the thesis structure. A more detailed insight on integral bridges is presented in Chapter 2. This includes a review of the integral bridge performance, advantages, limitations and challenges that have risen. Details of past

research work and a review of the various solutions proposed to overcome the challenges related to the soil-structure interaction problems are also presented in Chapter 2.

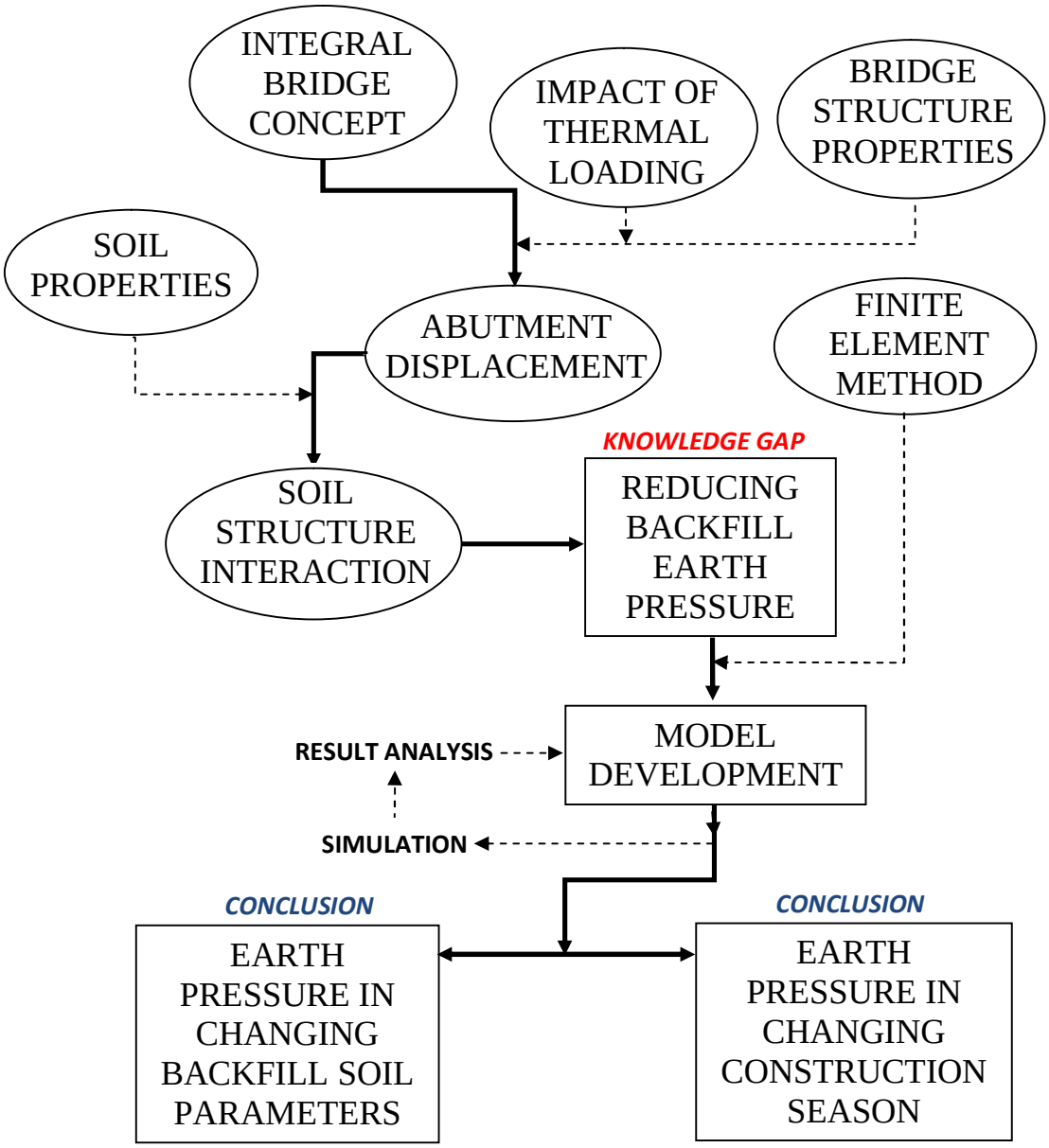

Figure 1.4: Illustration of research structure

The relevant aspects of soil mechanics associated with the stresses and deformation of the backfill and foundation soil as a direct consequence of integral bridge loading is discussed in Chapter 3. Factors affecting the behaviour of backfill and foundation soil during the soil-

structure interaction are highlighted and discussed in this chapter. Constitutive soil models are reviewed.

The numerical modelling method is introduced in Chapter 4. The fundamental principles of the finite element numerical method, the primary research tool for finding the solution to this engineering problem, are described. Plaxis, the finite element software used is also introduced. The relevant software programme applications are described and the validation of the software results is discussed.

Chapter 5 presents the application of the finite element principles in the development of a model integral bridge in Plaxis software. The results generated by the finite element model are primarily validated with the data obtained from an instrumented integral bridge and its site investigation. The findings of evaluating the impact on the behaviour of the backfill soil, of assuming a fully undrained behaviour and a fully drained behaviour in the fine grained soils within the foundation materials, under thermal induced loading are also presented in this chapter.

Parametric study on the backfill soil parameters carried out in the research is presented in Chapter 6. The effect of changes in the backfill soil parameters on the earth pressure behind the abutment is evaluated. The impact of the theoretical cyclic displacement expected against the measured displacement obtained from instrumentation, as well as the assumption of a fully undrained behaviour and a fully drained behaviour in the fine grained soils within the foundation materials, on the earth pressure developed in the backfill soil, are also evaluated. These results are discussed.

Chapter 7 presents the parametric studies on evaluating the impact of the construction seasons, and the assumptions of a fully undrained behaviour and a fully drained behaviour in the fine grained soils within the foundation materials, under thermal induced loading. The findings on the impact of changes in the backfill soil parameter on these assumptions are also presented. The earth pressure developed behind the backfill soil was evaluated in these parametric studies. Chapter 8 summaries the content of this thesis and highlights its contribution and relevance to the engineering design and construction of integral bridges.

Chapter 2 : INTEGRAL BRIDGES

2.1. Introduction

Integral bridges are generally single-span or multiple-span bridges with a continuous deck and jointless connections between the bridge deck and the bridge support. The jointless connection with the bridge deck is primarily composed of abutment supports in a single span bridge or abutment and pier supports in a multi span bridges (Dicleli, 2000a). These supports may be carried on pile foundations that are part of the structure. The integral bridge structures, like most bridges, consist of several components (Chen and Duan, 2000) that interact with each other and with tangible and non tangible components of the host environment, in sustaining a load. The components of an integral bridge structure generally include the bridge deck, abutment and/or pier and/or piles, and approach slab. The tangible components of the environment generally consist of the foundation soil, backfill or construction soil, and road base. The primary non-tangible component of the host environment is the thermal effect on the structure responsible for soil-structure interactions.

The modern integral bridge is a relatively new concept. The first modern integral bridge was built in the United States in 1938 (Burke, 2009). However, integral bridges are gaining popularity and are increasingly being used in different countries. This chapter reviews the advantages and performance of the integral bridge. The limitations of the use of the bridge and the challenges in design and construction are also reviewed. Typical loads an integral bridge structure may be subjected to are highlighted. The characteristic loading of an integral bridge because of the thermal effect and the response of the abutment through varying displacement patterns are discussed. A review of previous research work on the integral bridge is carried out and proposed solutions to solve the challenges of the integral bridge are highlighted.

2.2. Use of Integral Bridges

Bridges have been a feature of human evolution starting with the use of rocks and logs in primitive times (Ryall et al., 2000). Today, modern bridge structures are made from refined engineering materials including steel, concrete, reinforced concrete, timber and composite materials that may include glass or carbon reinforced plastics or any combination of these materials (Ryall et al., 2000).

Primarily as a result of the lower construction and operating costs of integral bridges relative to conventional bridges (Alampalli and Yannotti, 1998), the concept of the integral bridge is increasingly being used as an alternative to conventional bridges for short and medium span crossings. Short and medium spans are bridge spans that result in abutment displacements from thermal actions, which do not cause the backfill soil to fail. Lengths considered acceptable vary between countries and regions. Within the United Kingdom, spans up to 60m are considered acceptable (BA42/96, 2003, BD57/01, 2001). Integral bridges are a preferred option in parts of North America, Europe, and Asia for medium and short span bridges (Civjan et al., 2007).

In 2000, Kunin and Alampalli stated that integral bridges were in use in more than 30 American States and Canadian provinces (Kunin and Alampalli, 2000). By 2004, American transport agencies had constructed over 13,000 integral bridges (Maruri and Petro, 2005). Based on a more recent (2009) survey done in the United States, Paraschos and Amde (2011) identified 41 states in which integral bridges are in use. Integral abutment bridges are becoming more popular in Europe (White et al., 2010) with an increasing percentage of the new bridges constructed being integral bridges (White, 2007). In Finland, 17.6% of bridges built between 2000 and 2004 are integral bridges against 3.6% before 1984 (Kerokoski, 2006). The concept of integral bridges is increasingly being adopted in Asia. Japan completed its first integral bridge in 1996 and South Korea in 2002 (Burke, 2009).

Within the United Kingdom, an increasing percentage of newly constructed bridges are integral bridges. Figure 2.1 presents data from a major United Kingdom steel manufacturer (fabricating majority of the steel works on highway bridges in the United Kingdom), on

steel supplied to bridge types, indicating the percentage of integral bridge construction in the United Kingdom (Iles, 2006). The design and construction requirements for bridges in the United Kingdom, published in a technical document (The Design Manual for Roads and Bridges [DMRB]) that provides mandatory rules and guidance, requires that all highway bridges below 60m in total length, and with skews not exceeding 30°, be designed and constructed as integral bridges (BA42/96, 2003, BD57/01, 2001).

Figure 2.1: Steel manufacturer's data on bridge construction within the UK (Iles, 2006)

2.3. Integral Bridge Problem

During its service life, an integral bridge structure is exposed to loading conditions that result in the development of stresses and strains within and around the structure. The bridge dead load, live load, wind load, and secondary loads responsible for volume changes such as chemical and thermal actions, generate stress in the backfill and foundation soils and the structure. The magnitude of these loads varies depending on the material, size, location, and use of the bridge. Paul et al. (2005) and Lawver et al (2000) showed that the magnitude of the thermal loads on integral bridges are comparable to those caused by live loads. However, loading from thermal action may generate significantly higher stresses up to

failure loads- in excess of 30MPa on concrete structures (Neville, 1995, Neville and Brooks, 1987).

Bridge structures generally expand and contract because of thermal strains, creep, and shrinkage. Such movements have traditionally been accommodated by the provision of expansion joints, roller supports, and expansion bearings (Alampalli and Yannotti, 1998). Without the provision of expansion joints, the effect of secondary loading is more significant. In a single or multi span integral bridge, the superstructure and substructure are monolithically connected. This allows the transmission of the forces resulting from torsion, compression or tension through the abutments or piers to the footings or piles. This causes the superstructure to interact with the substructure, backfill and foundation soil (Dicleli and Erhan, 2008). Integral bridge expansion and contraction has been identified as the primary cause of soil-structure interaction problems between the abutment and the backfill potentially causing settlement of the backfill and increased earth pressure on the abutment.

Movement of the abutment to accommodate the thermal induced expansion of the deck is resisted by the abutment stiffness, mobilised earth pressures in the backfill soil, friction between the abutment walls and backfill soil, friction between the foundation structures and foundation soil, and stiffness of the foundation piles if they are used (Lawver et al., 2000, Knickerbocker et al., 2003). The movement can cause the earth pressure to increase (deck expansion) or reduce (deck contraction. (Arsoy, 2004).

Design for thermal movement is therefore a primary consideration in integral bridge design, and a distinguishing factor from conventional bridge design (thermal movements in conventional bridges are accommodated within the joints). This design consideration should enable the abutments, foundation structure, backfill material and foundation soil to adequately accommodate thermal movements (Nicholson, 1994). A good knowledge of the soil-structure interaction between the soil and the integral bridge structure is required in the design to accommodate thermal movement. This has posed a challenge for engineers in the design of integral bridges (Faraji et al., 2001).

The principal movement causing a change in the backfill earth pressures is the lateral displacement of the abutment walls (Arsoy, 2004, Arsoy et al., 2002, Lawver et al., 2000, Arsoy, 2008) which is caused by the lateral expansion/contraction of the bridge deck. The bridge deck is most vulnerable to temperature variation. This is due to the significantly larger surface area of the bridge deck typically exposed to the shade air temperature (Arsoy, 2008) as illustrated by the shaded area of Figure 2.2. Most of the abutment is covered by the backfill material and foundation soil and is therefore not significantly exposed.

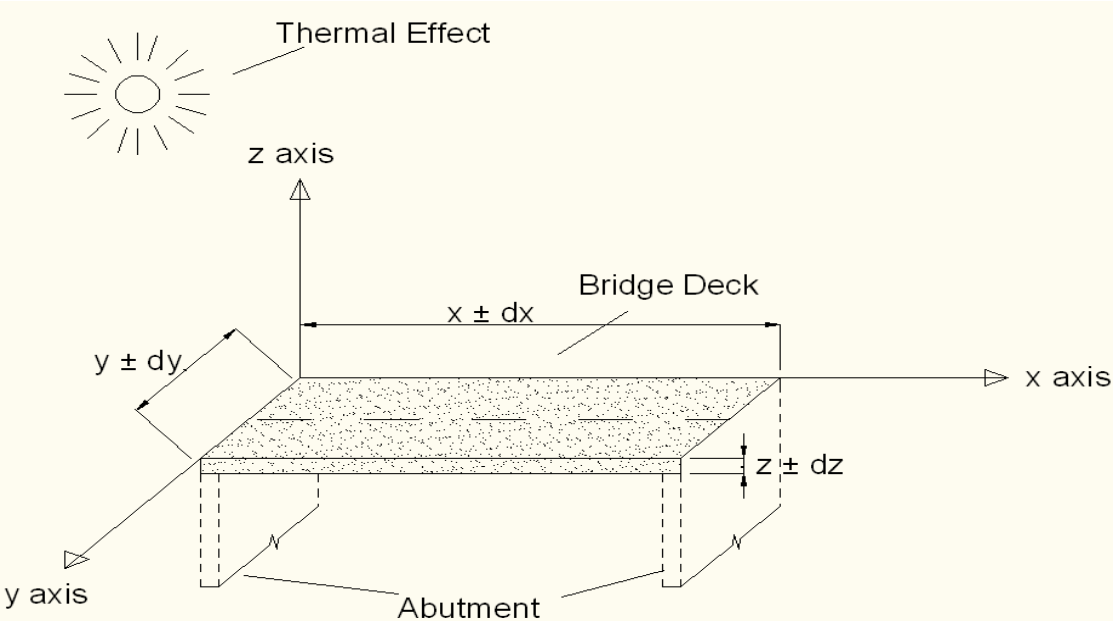

Figure 2.2: Thermal effect (changing temperatures) on integral bridge deck

The deck expands on heating and contracts on cooling. The deck expands and contracts in the x, y, and z axis illustrated in Figure 2.3, where x and y are horizontal (lateral) displacement in the longitudinal and transverse axis respectively, and z is vertical displacement in the vertical axis. The horizontal displacement is restrained by the abutment and backfill soils if the temperature increases. Temperature reduction causes contraction, which is resisted by the abutment only. There are no restraints to vertical expansion of the bridge deck. The transverse horizontal displacement in most bridge designs is not restrained on either side, enabling the deck displacement to occur without restriction.

Displacement of a bridge deck induced by thermal activity in the x, y, and z axis as illustrated in Figure 2.3, is proportional to the length of the deck on the referenced axis. The extent of the displacement of the abutments, caused by the bridge deck, determines the value of the earth pressure experienced within the backfill material located behind the abutment of integral bridge. This relationship consequently introduces restrictions on the length of the bridge deck in order to restrict the changes to the earth pressures, preventing failure of the bridge structure or/and backfill soil.

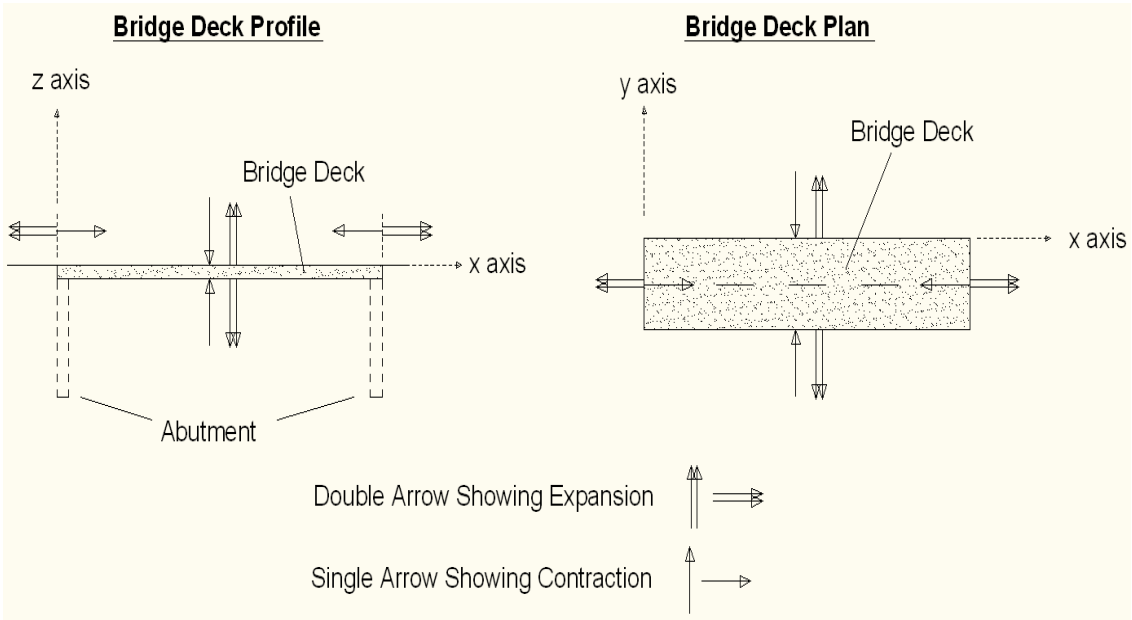

Figure 2.3: Deck expansion, profile & plan

2.4. Performance of Integral Bridges

The concept of the modern integral bridge was developed as early as the 1930s (Burke, 2009, Horvath, 2005). This concept was introduced to the United Kingdom in the last quarter of the 20th century (England et al., 2000). The justification for the construction of bridges without joints is supported by the realization that the joints routinely cause more damage than the stresses the joints were intended to relieve (Burke, 2009).

The lack of joints in integral bridges results in the transfer of moments and displacements through the bridge structure to the backfill and foundation soil. This configuration is generally considered by practicing highway engineers and academics as presenting some advantages over the conventional bridge configuration. Arsoy et al. (2004) summarized the principal advantages of integral bridge to include the following:

- Lower construction costs.
- Lower maintenance costs.
- Improved seismic performance.
- Fewer piles required for foundation support.
- No battered piles required.
- Simple and rapid construction.
- Smooth uninterrupted deck.
- Aesthetically pleasing.
- Improves vehicular riding quality.

The behaviour of integral bridges is influenced by the superstructure and substructure stiffness, the type of foundation, the nature of the foundation and abutment connection details, the soil properties, and the connection between the approach slab and the deck system (Arockiasamy and Sivajumar, 2005).

Research results have shown that backfill materials currently used in integral bridges, can potentially accommodate horizontal displacements resulting from thermal effect in a bridge length range of up to 120m for steel integral bridges, and up to 260m for concrete integral bridges, depending on the climatic conditions (Dicleli and Albhaisi, 2004b). In spite of their susceptibility to increasing stress due to thermal variation, integral bridges have been found to perform well.

Tilly (1994) compared modern integral bridges built in the United States within the last 20 years to the date of the publication and noted that in that time there certainly would have been expansion joint failures in conventional bridges. In a survey carried out on 39 state or

provincial transportation agencies in the United States and Canada on the performance rating of integral bridges, the results indicated that most of the respondents rated the performances as “good” or “excellent” (Kunin and Alampalli, 2000).

The cost of constructing an integral bridge is reduced by eliminating the expansion joints and bearings. The long term operating cost is also reduced because of eliminating joint maintenance and bearing replacement cost. Potential savings can be made from the construction of a single row of vertical piles against the conventional bridge pile foundation configuration which consists of two or more rows of vertical and/or battered piles (Burke, 1996). Generally, less piles are required in integral bridge construction, adding further savings in construction duration and cost (Arsoy et al., 2004). Eliminating the expansion joints and bearings installation in the construction process, and the constructing of fewer piles, enables a shorter construction time and a smooth bridge deck surface without the expansion gaps.

2.4.1. Bridge Loading

Component parts of the integral bridge structure, and the tangible component parts of the host environment, are constantly subjected to loading through the life of the bridge structure. “The predominant loads on bridges are gravity loads due to self-weight and those of moving traffic… Other loads include those due to wind, earthquakes, snow, temperature, and construction…” (Ryall et al., 2000). These loads have similar effect on bridges with or without joints (Nicholson, 1994). Consequently, in the design of all bridges, the effect of these loadings must be accommodated. However, in the design of integral bridges, an additional factor, considered relatively insignificant in other bridges, is prominent. This is the thermal effect on the structure.

Factors that may be responsible for some significant loading on an integral bridge within its life span include:

- Bridge self weight
- Vehicular load (Stationary, Movement, Collision, Breaking)
- Other live loads (Pedestrians, Animals)
- Precipitation (Rain, Snow/Ice)
- Submerged uplift loading (Buoyancy)
- Flow loading (Wind, Water)
- High/low water level (Scouring)
- Bridge settlement under loading
- Differential settlement of foundation
- Differential settlement of abutment backfill
- Volume change in bridge structure (Thermal action, Shrinkage, Creep, Chemical action)

2.4.2. Abutment Displacement

Displacements of the integral bridge abutment occur in a number of ways. Lawver et al. (2000) in an extended study and monitoring of an integral bridge observed that abutment movement to accommodate thermal expansion was predominantly through horizontal translation. Studies by Darley et al. (1998) confirmed that movement of the abutment base was accommodated by sliding and deformation with tilting and translating. Charles et al. (1998) identified two forms of movement in the abutment displacement; the rigid body motion which consists of translational and rotational motions, and bending deflections. Figure 2.4 illustrates the abutment rotation showing rotation angle. Figure 2.5 illustrates abutment-bending deformation showing change in deflection angle within the abutment structure. Figure 2.6 illustrates abutment horizontal translation showing horizontal displacement at the base and the top of the abutment. These forms of abutment displacements may simultaneously occur within the same integral bridge structure.

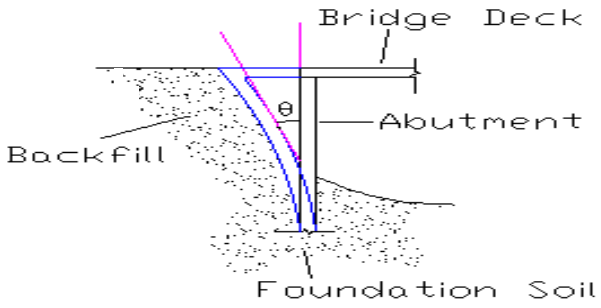

Figure 2.4: Abutment rotation showing rotation at abutment base

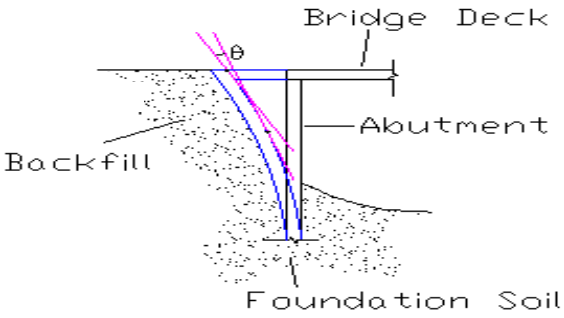

Figure 2.5: Abutment bending deformation indicating different tangents along abutment wall.

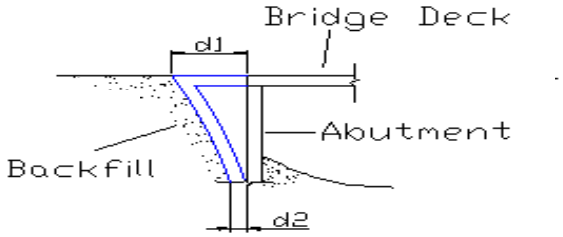

Figure 2.6: Abutment horizontal translation showing displacement of abutment wall at the base and top of the wall

Due to the bridge deck loading at the top and the foundation restraint at the bottom, rotational motion is more predominant as the height of the abutment increases (Horvath, 2005). These movements increase with the magnitude of perturbations at the top of the abutment wall, the number of strain cycles, and the density of the backfill material (Charles et al., 1998).

Abutment displacements result in soil-structure interactions that lead to changes in earth pressure. The impact of abutment displacements on an integral bridge structure also contributes significantly to the load bearing capabilities of the structure. Dicleli and Erhan

(2010) revealed that backfill soil and bridge structure interaction, as a result of abutment movement, has a significant effect on the magnitude of the live load moments in the components of integral bridges. Backfill compaction tend to increase the abutment moment and shear force while reducing the pile moment and shear force (Dicleli and Erhan, 2010).

Earlier studies by Dicleli and Erhan (2008) showed that the soil-structure interaction as a result of the abutment displacement, has a significant effect on the live load distribution factor for the abutments on integral bridges, consequently having an impact on design considerations.

2.4.2.1. Abutment Displacement Resistance

Abutment displacement in an integral bridge in service occurs within the host environment, which predominantly consists of soil mass. Huang et al. (2005) in the study of a pile supported integral bridge, observed a steady increase in the average pile curvature over time under thermal induced abutment displacement. This study suggests possible increase in resistance to displacements by the soil mass. Figure 2.7 illustrates the resistance to abutment movement.

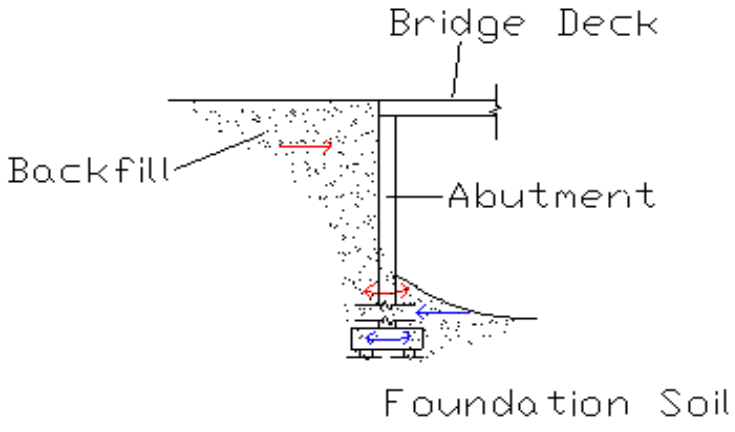

→ Backfill Earth pressure behind the abutment
← Backfill Earth pressure in front of the abutment
↔ Wall friction between the abutment and the soil
↔ Friction between the foundation structures and the soil

Figure 2.7: Movement resistance

The displacement of the abutment is resisted within the soil mass by the backfill earth pressure behind the abutment, backfill earth pressure in front of the abutment, friction between the abutment walls and the soil, and friction between the foundation structures and the soil.

2.5. Thermal Effect

Bridge structure exposure to temperature changes result in expansion and contraction of the structural members (Moorty and Roeder, 1992). In a conventional bridge, these changes in dimension are accommodated by the joints. In an integral bridge, the effect of expansion and contraction of the members are accommodated by the bridge structure, as there are no joints.

The structural temperature of the bridge is influenced by the ambient temperature and changes in the daily temperature cycle, the thermal properties of the structure, solar radiation, precipitation, wind speed, and other environmental and weather conditions (Arsoy, 2008). The daily temperature variation with higher temperatures in the day, tend to result in an abutment displacement pattern that is primarily cyclic. The thermal effect on an integral bridge structure is prominent and predominantly responsible for the soil-structure interaction (Zordan et al., 2011).

Results from studies carried out by Paul et al. (2005) indicate that thermally induced superstructure stresses and shear forces in integral bridges, are comparable in magnitude to those caused by live load. Lawver et al (2000) confirmed this from in situ observations. The thermal effect on an integral bridge may also lead to a uniform temperature change across the structure, which will result in an appreciable change to the bridge deck length. However, where the change in temperature is sudden, this may result in a thermal gradient across the structure introducing stress differences within the structure profile and potential bending (Barr et al., 2005).

The effects of temperature differentials across a structure are often neglected in design. A uniform temperature distribution is often assumed (Paul et al., 2005). This is known as the Effective Bridge Temperature (EBT). In a preliminary study carried out by Paul et al (2005) from a structural perspective, the effects of a temperature gradient versus uniform temperature changes were evaluated. The results of the study showed that the gradient effect was not significant thus validating the use of a constant superstructure temperature through the cross section of a structure (Paul et al., 2005).

Integral bridges have been subjected to extreme temperature variations during service in regions such as Northern Europe, Canada, Northern United States, and Northern Asia. Integral bridges in these regions experience an average daily temperature range and a wider average seasonal temperature range. The upper and lower temperature limits recorded in the United Kingdom are -26.1°C in January 1982 and 38.5°C in August 2003 (Met.Office, 2012).

2.6. Earth Pressure

Temperature induced abutment displacement results in the soil-structure interaction that leads to variation in earth pressure behind the abutment. The thermal induced abutment displacement can result in earth pressures as low as the active pressure, or as high as the passive pressure, possibly resulting in failure (Arsoy et al., 1999). Experiments conducted by several authors (Terzaghi, 1936a, Rowe, 1954, Sherif et al., 1982, Thomson and Lutenegger, 1998) show that the deformation mode and the magnitude of deformation may affect the magnitude and distribution of the earth pressure developed behind the abutment.

Increase in the amplitude of the displacements and the number of cycles results in an increase in the lateral earth pressure but at a decreasing rate (Charles et al., 1998). The increase in earth pressure resulting from the displacement of the abutment and the soil-structure interaction, if appropriately managed, enhances the loading performance of integral bridges. Arsoy (2004), referring to earth pressure behind the integral bridge abutment noted that although the earth pressures are detrimental for the substructure of a

bridge, they are of benefit to the superstructure because they reduce the bending moments caused by the dead loads and live loads in the bridge girders.

There are various theories for the maximum and minimum lateral earth pressures. The Coulomb theory and Rankine theory are two earth pressure theories widely used in geotechnical engineering. These are often referred to as classical earth pressure theories (Sivakugan, 2010). The Rankine theory is however, less complex than the Coulomb theory. The logarithmic spiral earth pressure theory is less widely used compared to the Rankine and Coulomb theories because of its complexity (Duncan and Mokwa, 2001). Alternative earth pressure theories and other solutions in evaluating displacement dependent earth pressures have also been developed and published by several authors (Kumar and Rao, 1997, Soubra, 2000, Zhu and Qian, 2000, Chang, 1997, Zhang et al., 1998),

2.7. Design, Construction & Performance Challenge

The elimination of joints in the integral bridge presents advantages that make it generally preferable to most engineers and bridge owners in short and medium span bridges. However, this presents other challenges as well. Zordan et al. (2011) wrote that it would be rather naive to consider this kind of structure as maintenance free. The integral bridge concept must consequently accommodate the displacements between superstructure and soil caused by seasonal fluctuations of air temperatures (Zordan et al., 2011).

The challenges arising from applying the concept of integral bridge in bridge design are mostly related to the soil-structure interaction (Kunin and Alampalli, 2000, Arockiasamy et al., 2004). Kim and Laman (2012) in an analysis of the actual in situ measurements obtained at four short to medium length integral bridges, observed that all measurements demonstrate that integral bridge response is cyclical, highly nonlinear, and irreversible over time.

2.7.1. Integral Bridge Limitations

Compared to conventional bridges, the behaviour of an integral bridge is more significantly influenced by the environmental conditions, predominantly the thermal effect. The actual temperature conditions, the resultant soil-structure interaction and the reaction of the soil behind the abutment, is a major uncertainty in integral bridge analysis and design (Faraji et al., 2001, Zordan et al., 2011). This introduces further limitations in the design considerations of an integral bridge (Huang et al., 2008).

There is currently no generally acceptable design standards established for integral bridges (Dicleli and Albhaisi, 2004c, Dicleli and Erhan, 2010, Kim and Laman, 2010). Publication by Greimann et al. (1983) showed that 28 United States Highway Agencies designed and constructed integral bridges without established standards. In the United Kingdom, other than recommendations for bridge type under 60m length and 30^{o} skew being constructed as integral bridges within abutment displacement limits, there are no specific rules set out for integral bridges in the design manual for roads and bridges (BA42/96, 2003, BD57/01, 2001). This lack of set standards introduces an additional risk factor in the design and construction procedure.

Skewed integral bridges tend to rotate when subjected to cyclic changes in earth pressures on the abutment as a result of the cyclic temperature changes (Hoppe and Gomez, 1996, Arsoy et al., 1999). The soil-structure interaction as a result of the abutment displacement tends to result in loss of backfill soil material displaced behind the abutment (Lawver et al., 2000). This may result in irregular surfaces or subsidence behind the abutment. Other causes of irregular surfaces and subsidence as identified by Briaud et al (1997) and Arduino and Macari (1998), include compression of fill material, settlement of natural soil under the embankment, poor construction practice, traffic loads, poor drainage, poor fill material and erosion of fill material. This ultimately affects the performance of the bridge structure and the road embankment.

Temperature induced lateral displacements of an integral bridge deck are proportional to the length of the deck. The ability of the approach fill, the soil mass directly affected by the impact of the displacement, and the abutment supporting piles, to accommodate the lateral

displacement of the abutment without distress, is a significant factor in determining the maximum possible integral bridge length the backfill soil may support (Arsoy et al., 2002). Dicleli and Albhaisi (2004b) wrote that expectations on integral bridge lengths were subject to different materials and climates. Consequently, integral bridges can only be used within acceptable length limits. However, the length limit is not clearly established ((Burke, 1996, Soltani and Kukreti, 1996, Wassermann and Walker, 1996) cited in (Arsoy et al., 1999)). GangaRao et al. (1996) cited in Arsoy et al. (1999) determined that integral bridges are suitable if the expected temperature induced movement at each abutment is less than 51 mm (2 in.). The United Kingdom Department of Transport limits this displacement to ±20mm (BA42/96, 2003).

Thermal-induced repeated expansion and contraction of the bridge deck result in cyclic straining of the deck. Integral bridges exert cyclic loading induced by these cyclic strains on the soil behind the abutment (Springman and Norrish, 1994), and soil around the substructure and the foundation. Cyclic loading in integral bridges cause a change in lateral earth pressures behind the abutment. Shear failure and settlement have been attributed to maximum passive and active earth pressures (Card and Carder, 1993, England and Dunstan, 1994, Springman et al., 1996, England et al., 2000, Carder et al., 2002).

Cyclic lateral load tests carried out by Arsoy et al. (2002) supports the findings that stresses in an integral bridge abutment will increase as the resistance to lateral displacement increases. Piles supporting the integral abutments may be subjected to high stresses as a result of cyclic expansion and contraction of the bridge superstructure. These stresses can cause formation of plastic hinges in the piles and may reduce their axial load capacities (Yang et al., 1985).

Dicleli and Albhaisi (2004c) observed that the height of the abutment affects the performance of the bridge by having a direct effect on the intensity and distribution of the backfill pressure, when subjected to loading. In active conditions, the maximum tensile stress is obtained at the top of the abutment. Tensile stress in the soil can create a crack along soil-wall interface reducing the friction on the wall and leading to increased stress if the tension crack is filled with water.

High quality granular backfill materials have been recommended by engineers for use to minimize the risk of problems associated with settlement occurring. In integral bridges, this has been found to increase the risk of developing passive earth pressure within the backfill material (Carder and Card, 1997).

The timeline of the bridge construction affects the behaviour of integral bridges. This is as a result of the temperature dependent properties of the different materials used in the construction of integral bridges with particular reference to concrete (Kim and Laman, 2010) and steel. These materials are influenced by the constantly changing environmental temperature which is time dependent (Arsoy, 2008). The impacts of time dependent factors are experienced in consolidation, cyclic loading, changes in environmental conditions, physical and chemical changes within material composition over time, shrinkage, and creep.

2.7.2. Design & Construction Challenge

As a result of the significant impact of temperature, there is a need for a careful evaluation of the effect of temperature on the structure which is the origin of the soil-structure interaction (Zordan et al., 2011). An efficient design therefore requires an accurate forecast of extreme temperatures through the life of the structure. However, in current analysis and design practice, this relationship is often neglected (Dicleli, 2000b).

As part of the recommendations for integral bridge design within some jurisdictions, integral bridges with skews less than 30^{o} may be designed and constructed (Burke, 2009, White, 2007). This recommendation results from the tendency of the structure to rotate due to the soil-structure interaction. However, the magnitude of the soil-structure interaction effect depends on the temperature variation within a specific bridge location and the length of the structure. This raises the question of design efficiency in generic guidelines.

The timeline of the bridge construction and operating life affects the behaviour of integral bridges. Factors affected include the consolidation process, the cyclic loading pattern of the soil, and changes in environmental and structural conditions. These factors highlights the

significance of analyzing the long-term behaviour of integral bridges beyond the construction time (Pugasap et al., 2009).

The stiffness of an integral bridge superstructure is significantly higher than the stiffness of the approach fill and abutment supporting piles, such that the magnitude of the temperature induced lateral displacement of the bridge superstructure is often unaffected by the stiffness of these resisting structures (Arsoy et al., 2002). This implies that the backfill material completely accommodates the displacements of the abutments. Carder and Card (1997) also found that the degree of compaction of the backfill affects the lateral earth pressures within the backfill.

It is generally acknowledged that the development of high earth pressure is a major problem in integral bridge design. While the value of the passive earth pressure within the backfill can be estimated using several theories, Cole and Rollins (2006), in a review of passive earth pressure analysis, acknowledged the uncertainty inherent in the analysis of passive force subjected to cyclic loading.

Earth pressure magnitude at a point in a soil is achieved by multiplying the vertical effective stress by earth pressure coefficient. This approach, when adopted for abutment wall will result in an earth pressure that varies linearly if the earth pressure coefficient is assumed constant with depth. However, experiments have shown that the earth pressure behind the abutment wall of an integral bridge is not linear ((Wassermann and Walker, 1996) cited in Arsoy (2004)), suggesting that the earth pressure coefficient varies with depth.

2.8. Summary of Previous Research

Research has been carried out on the different components of the integral bridge, mainly the piles, bridge structure, and supporting soil. These have been mostly carried out through field instrumentation of the structure and measurement of environmental parameters, laboratory testing, and modelling.

A significant effect of the soil-structure interaction is the development of earth pressure behind the integral bridge abutment wall. Limited investigations have been carried out on this development. Investigations carried out have been mainly laboratory-based tests (Springman et al., 1996, Ng et al., 1998, England et al., 2000, Xu and Bloodworth, 2006). Limited field monitoring has also been carried out on the earth pressure (Darley et al., 1996, Darley et al., 1998, Barker and Carder, 2000, Barker and Carder, 2001).

In general, there has been limited research carried out on integral bridges through the field instrumentation and monitoring. It has been difficult to obtain conclusive evidence on integral bridge performance under thermal induced loading from field instrumentation and monitoring. This is as a result of the long monitoring periods required to observe the effects of seasonal thermal cycling (Bloodworth et al., 2012). The summary of previous research carried out on integral bridges presented in this section, show that no information is available from research carried out through instrumentation on all component parts of the bridge simultaneously. These also show that in modelling, the effects of the foundation soil, backfill and bridge structure have not been simultaneously evaluated within a single model.

2.8.1. Field Instrumentation and Monitoring

Field instrumentation and monitoring of the integral bridge generally present in situ results conveying the performance data of the integral bridge structure, soil, and environmental conditions. A summary of integral bridge instrumentation is given below.

Kamel et al. (1996) evaluated the performance of the concrete piles on a two span continuous composite steel girder integral bridge in southwest Omaha, Nebraska. The study did not evaluate the bridge deck, abutment or soil. Hoppe and Gomez (1996) evaluated the earth pressures behind the abutment and approach pavement settlement on a steel girder bridge with semi integral abutments in Rockingham Country, Virginia. Hoppe and Gomez (1996) did not consider the structure.

Girton et al. (1991b) measured the air and bridge temperature at the Boone River Bridge (four span) in central Iowa, and the Maple river Bridge (three span) in northwest Iowa. This study also measured the bridge longitudinal movement and abutment pile strains, but did not evaluate the soil displacements or pressures.

Other field instrumentation include; the Haavistonjoki Bridge, Finland (Kerokoski and Laaksonen, 2005); the U.S. 101 - Painter Street Overpass (PSO) bridge, in Rio Dell, California (Goel, 1997); Bridge 55555 in Rochester, Minnesota (Huang et al., 2005); a composite integral bridge structure with concrete I-girders in Pennsylvania (Fennema et al., 2005); Kii Bridge over the Ohia Stream in Kahuku, on the island of Oahu, Hawaii (Ooi et al., 2010b); and a composite bridge built over Leduan in Northern Sweden (Petursson et al., 2011). These measured only a limited number of relevant integral bridge components.

2.8.2. Numerical Analysis

Numerical methods are popular research methods widely used in the analysis of integral bridge problems. Several studies have been done using this method of analysis generating useful results. Some studies carried out on the integral bridge using the numerical method are listed below.

- Dicleli and Albhaisi investigated the effects of clay stiffness around piles, pile size and orientation, pile connection to abutment, abutment height, and bridge size on the performance of integral bridges during thermal loading using a finite element analysis software SAP2000 (Dicleli and Albhaisi, 2004b, Dicleli and Albhaisi, 2004a, Dicleli and Albhaisi, 2005).
- Zhao et al. (2011) investigated the seismic behaviour of an integral bridge in Tennessee by considering the soil-structure interaction around the piles and behind the abutments, using a commercially available finite element software SAP2000.
- Abendroth and Greimann (2005) investigated the effects of loose versus dense sand behind the abutment and the stiffness of the soil around the piles when different vertical temperature distributions are applied over the depth of the superstructure, using a 3D Finite element software ((Abendroth and Greimann, 2005) cited in (Ooi et al., 2010b)).

- Civjan et al. (2007) investigated the effects of backfill properties, foundation soil properties, and pile restraint on bridge distortion and pile moments during thermal loading lateral springs, using a 2D and 3D finite element program.
- Arockiasamy et al. (2004) investigated the effect of the degree of compaction of sand in predrilled holes, depth of predrilled holes, having and not having predrilled holes, water table elevation, soil type around pile and pile orientation on the displacements, moments and shear force in H-piles supporting integral bridges subjected to thermal loading, using a finite element software SAP 2000.
- Zordan et al. (2011) conducted a parametric study assessing the expected structural response of the Isola della Scala Bridge in Verona, Italy, using a 2D simplified finite element model.
- Arsoy et al. (1999) investigated the effects of the approach fill on pile stresses, abutment type, magnitude of thermal movement on the lateral resistance contribution of the abutment relative to the piles, and magnitude of the thermal induced lateral movement and the extent of settlement in the fill behind the abutment, using 2D finite elements.
- Kamel et al. (1996) evaluated the effect of relative compaction, strength, soil type, pile type, pile stiffness, and type of pile head fixity on the lateral stiffness lateral springs, using a numerical software LPILE.
- Khan (2004) investigated the seismic behaviour of single span integral bridges with varying skews, using finite element software.
- Faraji et al. (2001) studied the effect of different soil conditions behind abutment and around piles, using a 3D finite element software.
- England et al. (2000) investigated the effects of different backfill stiffness, backfill density, bridge lengths, bridge completion seasons during thermal cyclic loading on the settlement profile and wall reaction, using a numerical software QSand.
- Khodair and Hassiotis (2005) evaluated the effect of varying steel sleeve diameters surrounding a single H-pile on pile axial stress and displacements, and on the earth pressure on the steel sleeve during thermal loading, using a finite element software ABAQUS.
- Wood and Nash evaluated the effects of backfill strength, stiffness and dilation angle, and abutment flexural stiffness on the earth pressure during thermal

expansion for an integral bridge on spread footings, using a finite difference method software FLAC (Wood and Nash, 2000, Wood, 2004).

- Knickerbocker et al. (2005) investigated the effect of skew angles under various thermal gradients in girders on deflections and pile moments, using a finite element analysis software.

2.8.3. Other Studies

Springman et al. (1996) investigated the behaviour of integral bridges under cyclic temperatures using a centrifuge model. The result showed that the cyclic temperatures cause horizontal displacements within the backfill soil behind the abutments.

Ng et al. (1998) carried out centrifuge model tests, and numerical modelling of an integral bridge abutment simulating the expansion and contraction of the bridge deck. The results showed significant settlements behind the abutment from soil densification, strain ratchetting, horizontal sliding, and a rocking motion of the abutment.

Tsang et al. (2002) investigated the escalation of earth pressures behind the abutment of integral bridges with full height abutments under cyclic temperature changes using a 1 to 6 scale model wall retaining Leighton Buzzard sand. The results indicated that two distinct mechanisms are responsible; flow mechanism relating mainly to the large wall rotations; and arch mechanism relating mainly to the small wall rotations. These mechanisms were dictated by the change in length due to the thermal effect on the bridge deck.

Dicleli and Albhaisi (2005) presented an analytical approach in predicting the limit of an acceptable length of integral bridges built on cohesive soils. They found that the maximum acceptable length is affected by the stiffness of the bridge deck and soils, abutment height, as well as the properties and orientation of the piles (Dicleli and Albhaisi, 2005).

Shamsabadi et al. (2007) used the limit-equilibrium method with a modified hyperbolic soil stress strain behaviour to estimate the abutment nonlinear force displacement capacity as a function of wall displacement and soil backfill properties.

2.9. Proposed Solutions

Horvath (2005) observed that the traditional research approach into finding solutions for the integral bridge problems have been focused on the issue of the earth pressure behind the abutment and in the more recent research efforts, subsidence on the bridge approach. The major problem of the integral bridge has been identified to be the soil-structure interaction. Solutions have been proposed to remedy this problem most notably the use of low stiffness materials, use of highly compressible and elastic materials such as polymeric and geocomposite materials (Carder and Card, 1997), and a restriction to the length of the integral bridge. Xu et al. (2007) showed that a build-up of lateral earth pressure behind embedded integral abutments in clay, over many daily and annual cycle, is not expected. An efficient determination of a safe length is dependent on the ability of the backfill material and foundation soil to accommodate the lateral abutment displacements without distress.

Several highway agencies have accepted the design and use of integral bridges with varying limits on lengths considered safe. The Finnish bridge design guideline recommends the maximum expanding length to be accommodated by an abutment in normal traffic conditions be 35m, limiting the maximum bridge length to 70m (Kerokoski, 2006, Nilsson, 2008). A fixed length limit of up to 180m (600ft) has been adopted by the Federal Highway Administration ("Integral" 1980) (Girton et al., 1991a). In the United Kingdom, the Highway Agency recommends that bridges up to 60m be designed as integral bridges. Some authors including Tilly (1994), observed that current allowance for thermal effects in integral bridge design may be excessive. This is attributed to a lack of understanding of the soil-structure interaction, implying that improvements can be achieved.

Dicleli (2000a) proposed a design method including analysis at each construction phase, and a correlation between the temperature variation and the magnitude of earth pressure. This was to analyse the construction process of the integral bridges in stages, taking into account the prevailing conditions at the time and the long-term behaviour of the bridges beyond the construction time (Pugasap et al., 2009). Studies on integral bridges have highlighted the importance of a stage construction analysis in integral bridge design (Ooi et al., 2010a).

Stress build up have been observed in the integral bridge abutment and backfill. Efforts to minimize passive earth pressure development in the backfill of an integral bridges as summarized by (Burke, 2009) seem to focus mainly on embankment, and bridge geometric and structural rearrangement. It has been recommended that piles should be oriented to accommodate bending predominantly around the weak axis (Girton et al., 1991a, Arsoy et al., 2002, Ooi et al., 2010b). Dicleli and Albhaisi (2004c) recommended the use of non compacted backfill and limiting the abutment height to 4m to minimize the stress build up in the backfill.

Loss of backfill material has been identified as a problem associated with the soil-structure interactions. Lawver et al. (2000) recommended more attention be paid to backfill plan in integral bridges in an effort to minimise or completely eliminate the loss of backfill material around the abutment.

As a result of the abutment displacements mostly induced by thermal activities, more emphasis is placed on the efficiency of the construction materials for improved performance. Compacted granular material is often recommended for use as backfill material. However, the report by Carder and Card (1997) revealed that studies have shown compacted granular material promotes increased earth pressure during thermal strain. This finding emphasises the need for a more cautious application of compacted granular backfill for integral bridges.

Arsoy et al. (2002) suggested that concrete piles may not appear to be a suitable choice for the support of an integral bridge as cracks that develop within the concrete pile structure from cyclic lateral loading, progressively worsen with increasing cycles, thus significantly reducing its load bearing capacity. These findings consequently promoted steel integral bridges instead. However, in consideration of the bridge deck, concrete performs better in encouraging greater bridge spans (Dicleli and Albhaisi, 2004b).

2.10. Summary

Kim and Laman (2012) recognized that integral bridges are now a routine construction and design of choice for many departments of transport as bridges are replaced, or new roadways constructed. However, in spite of the known challenges and proposed solutions, current design specifications do not provide a clearly defined or comprehensive guideline on analysis procedures (Arockiasamy and Sivajumar, 2005). The traditions of managing integral bridge design and construction challenge differ from country to country, leading to different technical solutions for the same problem (White et al., 2010, Kunin and Alampalli, 2000).

The response of the structure to a given set of forces has also been found to depend on the geometry, materials, soil and structure configuration, soil interaction, and construction details of the individual system (White et al., 2010). Knowledge of the performance of the bridge obtained through the actual performance of functioning bridges to support design and analysis methodology is limited. Kim and Laman (2012) noted that the current design and analysis methodologies have not matured substantially because of lack of available long-term field data.

Modelling provides a useful alternative to data obtained from bridge instrumentation and monitoring. Consequently, several researchers have carried out modelling of the different parts of the bridge independently in an attempt to better appreciate the performance of the parts being modelled. While these attempts have generated useful results, the full impact of the part and the entire structure interdependence is lacking. Few complete bridge modelling have been performed.

In summary, the primary challenge encountered in the design and construction of integral bridges arises from the limited understanding of the soil-structure interaction behaviour in response to the thermal induced lateral displacement of the abutment. A better understanding of this behaviour requires the long-term instrumentation of bridges for field data, and the development of models for research based on information obtained from the field data, to obtain new knowledge from the findings.

Chapter 3 : BACKFILL & FOUNDATION SOIL BEHAVIOR

3.1. Introduction

The major problem of the integral bridge is a geotechnical problem associated with the soil-structure interaction of the bridge abutment and the retained soil. In service, an integral bridge structure is subjected to loading from numerous sources, as discussed in Section 2.3.1. These loads contribute to the soil-structure interaction. However, the primary loading of interest in the integral bridge is the thermal induced cyclic loading of the abutment which, in part, is responsible for the behaviour of backfill soil behind the abutment.

Problems that may arise from this interaction as acknowledged by several authors can result in one or more of the following conditions; subsidence of the approach road structure, failure of the soil in increasing compressive or tensile strain, failure of the bridge structure. This chapter highlights the characteristics of the backfill and foundation soil applicable to the soil-structure interaction. The principles behind the soil deformation and the stresses generated consequently in accommodating the displacement of the abutment walls is reviewed in this chapter.

3.2. Soil-Structure Interaction

Several researchers have concluded that the complex soil-structure relationship in integral bridges constitutes the major challenge to engineers in designing and predicting the behaviour of integral bridges in use (Spyrakos and Loannidis, 2003). The post construction flaws of integral bridges are fundamentally of a geotechnical nature, not structural (Horvath, 2005). Faraji et al. (2001) wrote that a major uncertainty in the analysis of integral abutment bridges is the reaction of the soil behind the abutment, next to the foundation piles, and described the handling of the soil-structure interaction in the analysis of integral abutment bridge as problematic.

Several of the challenges associated with the integral bridge design can be ascribed to the attempt of managing the effect of the soil-structure interaction caused by the abutment displacement, or the attempt of controlling the abutment displacement that cause the soil-structure interaction. Two significant consequences of the displacement induced soil-structure interaction have been identified. These are the development of increasing earth pressure behind the abutment in the backfill and irregular surface or subsidence of the bridge approach surface (Arsoy, 2004, kang et al., 2008, Charles et al., 1998, Horvath, 2005).

Studies carried out by authors including Springman et al. (1996), Card and Carder (1993), England & Dunstan (1994) revealed that due to the soil-structure interaction of the backfill soil and abutment structure, the lateral earth pressure behind the abutment is likely to increase progressively with time. This results from the observation that at the end of each annual thermal cycle, there is often an accumulated displacement of the abutment away from the retained soil (Horvath, 2005). While this phenomenon persists after each annual cycle, the displacement experienced by the deck and exerted on the abutment remains constant. This creates a situation in which the provisional space occupied by the soil particles, available to accommodate displacement is shortened while the displacement remains constant thus progressively increasing pressure.

3.3. Construction Soil

Soil is a non-homogeneous mix with a wide range of physical properties. McNally (1998) described soil material as being composed of a diverse lot that includes weathered rock and boiler ash, whose only common characteristic is that they are relatively easy to dig. Invariably, soil possesses numerous characteristics. The integral bridge foundation is normally set in soil, and free draining granular soil is the predominant material recommended and used in the backfill construction. Some of the numerous characteristics of soil components may enhance the efficient performance of the integral bridge while others may simply be less complimentary.

Engineers often specify the backfill material in construction to harness more of the beneficial characteristics of the specified material. Soil materials with granular and cohesive properties, have been recommended for use as backfill construction material by engineers. In the United Kingdom, the Highways Agency identifies several materials with qualities acceptable for use as backfill in bridge abutments (BD30/87, 1987).

Soils that meet the design requirements often have to be imported. However, in most cases, it is not practical to change or pre-determine the soil types that make up the foundation soil. Engineers often have to work with the foundation soil as found, only making amendments to the uppermost surface. As a result of this, information on the behaviour of the backfill soil in response to the characteristics of the foundation soil is a vital tool in the design process, thus contributing to the knowledge required in improving the efficiency of integral bridge design and long term performance.

Natural soil is made up of a collection of particles consisting of weathered, decomposed and broken down rocks, and organic matter with voids. Natural soil particles range in sizes from the finest identified as clays, through to significantly larger size boulders. The voids may contain liquids or gasses. Thus, natural soil can be saturated, dry or partially saturated if the voids contain both liquids and gasses. Engineering construction materials are often devoid of organic matter. Consequently, the behaviour of construction soil is dependent on the presence and percentage composition of soil particle sizes, liquids and gasses within the soil mass. However, soil materials consisting of predominantly clay, fall within the poor quality backfill material soil type and is not often recommended for use in integral bridge construction (BD30/87, 1987).

3.4. Factors Affecting Soil Behaviour

In predicting the behaviour of soil, knowledge of the soil's ability to accommodate stress with strains under loading, is required. The response of a soil element to stress depends on a number of primary factors. These factors, include the soil phase relationship (composition of solids, liquids and gasses in a soil mass) , the stress ratio, the total stress, effective stress

and pore water pressure, the time duration of loading, the stiffness, the elasticity, the stress history, soil component reaction (chemical, magnetic, electrical), and temperature.

Factors that affect the behaviour of backfill materials and foundation soils may be classified as state dependent factors or material dependent factors (Atkinson, 2007). The state dependent factors are governed by the historic and present state of the total stress, effective stress and pore pressure. The material dependent factors are governed by the nature of the material content. Carder and Card (2000) identified other factors that can be considered as secondary factors affecting the behaviour of all soils under cyclic loading (the characteristic loading pattern of the integral bridge). Many of the factors listed are interdependent on the others and are controlled by the primary factors identified above (Carder and Hayes, 2000). The factors identified by Carder and Card (2000) are;

- The magnitude and rate of shear strain or soil displacement
- The frequency and amplitude of the loading
- The degree of saturation of the soil
- The rate of pore water dissipation during loading
- The initial state of stress in the soil
- The number of loading cycles.

3.4.1. Stress & Stress Ratio

Stress in the soil is a measure of the force acting on a defined unit area and strength is the ability to resist shear. The strength of the soil is a measure of the maximum shear stress that can be generated by the soil. In dry soils, the normal stresses applied to the soil are borne only by the soil particles in contact with each other. However, in saturated soils, the normal stresses applied to the soil are borne by the soil particles in contact with each other (soil skeleton) as the effective stress and the pore water as pore water pressure. Soil is a frictional material and thus the strength increases with increasing normal stress confining the particles. The stress ratio (the ratio of shear stress to normal stress) is therefore a major factor in the strength determination. Consequently, soil stresses and stress ratio affect the behaviour of soil.

$$\tan\boldsymbol{\phi}_m = \tau/\sigma \qquad \text{..... (3.1)}$$

Where $\boldsymbol{\phi}_m$ is the mobilized angle of shearing resistance, τ is the shear stress and σ is the normal stress.

The shear strength of water is zero. The soil particles thus generate the shear stress to bear the loading mainly from inter-particle friction. The soil particles also generate some additional strength from the interlocking of the soil particles and light cementing bonds. The component of the total normal stress applied to the soil may be calculated through the principle of effective stress equation (Equation 3.2) (Terzaghi, 1936b, Terzaghi and Peck, 1967). The effective stress controls the volume and strength of the soil (Powrie, 2004). In hydrostatic conditions, Equation 3.3 applies.

$$\boldsymbol{\sigma}' = \boldsymbol{\sigma} - u \qquad \text{..... (3.2)}$$

$$\boldsymbol{\sigma}' = \gamma z - \gamma_w(z - h) \qquad \text{..... (3.3)}$$

Where $\boldsymbol{\sigma}'$ is the effective stress, $\boldsymbol{\sigma}$ is the total normal stress, u is the pore water pressure, γ is the unit weight of soil, z is the depth of the soil element, γ_w is the unit weight of water, h is the depth of the water table.

Shear stress is proportional to the magnitude of shear strain. This implies that larger strains that may be generated from a longer integral bridge (with higher magnitude of cyclic movement), will result in a higher magnitude of shear stress within the backfill soil. Patterns of typical strength-strain relationship in soil loading have been identified. When subjected to strain, dense or stiff soils may develop peak strength at about 1% strain, and critical strength in the order of 10% strain. Loose and soft soils do not develop peak strengths but do develop critical strengths. Clayey soils develop residual strength much in excess of 10% strain. However for soils with no significant clay content, strains in excess of 10% maintain the critical strength value (Atkinson, 2007).

The analysis of the stress effect in soil elements within a soil mass is complex. This is primarily because of the non homogeneous nature of soils, the geometric configuration of

the loading area and the relative position of the soil elements within the soil mass. Loading in the soil causes deformation and displacement of soil elements. Therefore, the analysis of stress within a soil element is independent of the stress experienced in the fixed position the soil element occupied before loading as the element may be displaced. Within any soil mass, the stress effect varies from one point in the soil to the next.

3.4.2. Stress Path

The behaviour of soil material is history and path dependent (Atkinson et al., 1986). The stress and strain history and the current state of stress and strain changes are a major factor in determining the behaviour of the soil. The stress path method for design proposed by Davis and Poulos (1968) and Lambe (1964) presents a more accurate representation of the stress-strain state of selected element in the in situ soil for measurements of stress-strain parameters, enabling predictions that closely replicate the actual behaviour of the soil (Atkinson et al., 1986).

Equations for stress path plots using s and t axis;

$$\delta s = \tfrac{1}{2} (\delta \boldsymbol{\sigma}_1 + \delta \boldsymbol{\sigma}_3) \quad \text{..... (3.4)}$$

$$\delta t = \tfrac{1}{2} (\delta \boldsymbol{\sigma}_1 - \delta \boldsymbol{\sigma}_3) \quad \text{..... (3.5)}$$

$$\delta t' = \delta t \quad \text{..... (3.6)}$$

$$\delta s' = \delta s - \delta u \quad \text{..... (3.7)}$$

Equations for stress path plots using p and q axis;

$$\delta p = 1/3 (\delta \boldsymbol{\sigma}_a + 2 \delta \boldsymbol{\sigma}_r) \quad \text{..... (3.8)}$$

$$\delta q = \delta \boldsymbol{\sigma}_a - \delta \boldsymbol{\sigma}_r \quad \text{..... (3.9)}$$

$$\delta q' = \delta q \quad \text{..... (3.10)}$$

$$\delta p' = \delta p - \delta u \quad \text{..... (3.11)}$$

The development of finite element methods and the advancement of computing technology have led to a more affordable and reliable application of the stress part method in analysis (Atkinson et al., 1986). Stress paths plots may be presented with respect to total and effective axial and radial stress, or major and minor principal stress. The shear and volumetric effect in the soil is more appropriately presented using the axis q and p (Atkinson, 2007) or s and t. The stress paths s and t, or q and p, are plotted using Equations 3.4 - 3.7 and 3.8 - 3.11 respectively. A typical stress path direction plotted using the p and q axis is shown in Figure 3.1, plotted with slopes of either $\delta\boldsymbol{\sigma}_r = 0$ or $\delta\boldsymbol{\sigma}_a = 0$.

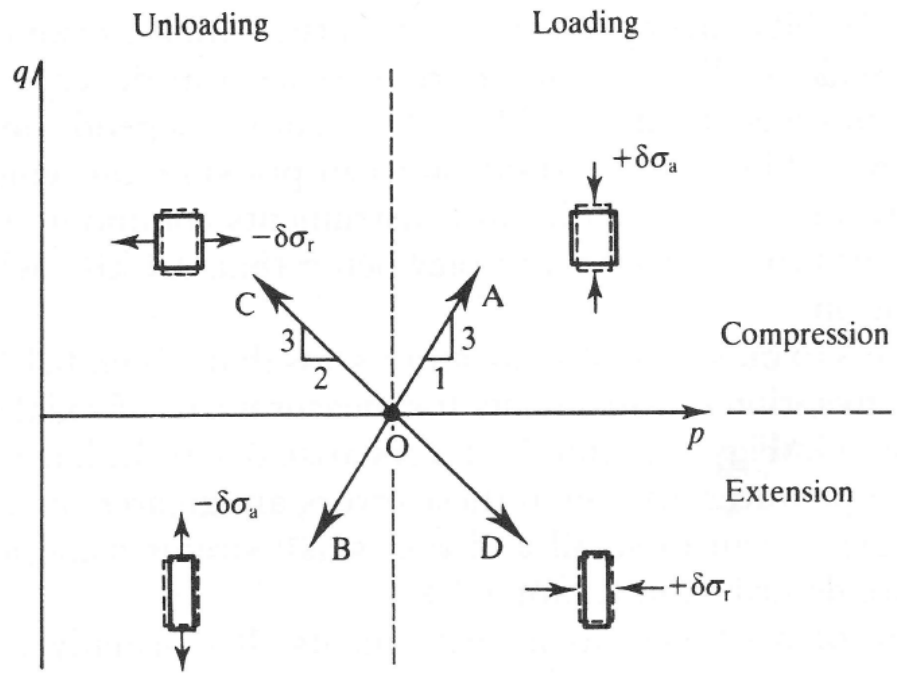

Figure 3.1: Typical Stress Path from Triaxial Test. Modified (Atkinson, 2007).

3.4.3. Soil Phase Relationship

Soil is a complex three phase material consisting of gasses, liquids and solids which participate in a number of different processes that control the physical behaviour of the soil (Richards and Peth, 2009). The phase relationship is a measure of the volumes of air, water, or solid content in a soil mass. The different phases present different characteristics when subjected to loading.

The void ratio, specific volume, and porosity are a measure of the phase relationship presenting the efficiency of solid particles packed together (Powrie, 2004). The percentage of constitution of the different phases in a soil mass is relevant because a combination of the characteristics of the independent phases result in variations to the values of the soil parameters, and consequently affects the general behaviour of a soil mass.

3.4.4. Particle Sizes, Shapes & Grading

The mechanical properties of soil (that constitute the soil strength and stiffness) depend on the nature of the soil grains that constitute the soil mass. This is also dependent on the soil particle sizes, shapes, and grading. Figure 3.2 shows the range of soil particle sizes.

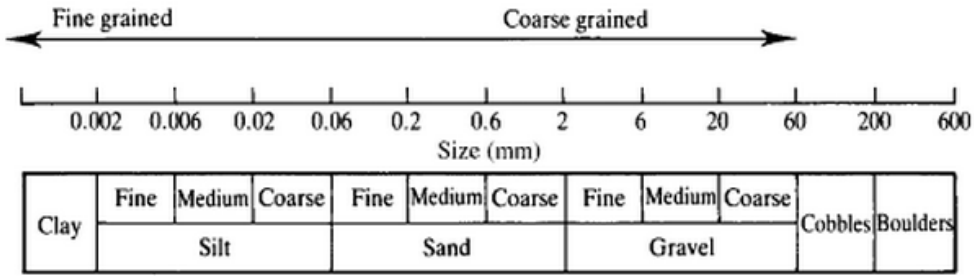

Figure 3.2: Soil particle size range. Modified (Atkinson, 2007).

A typical soil mass consist of a large range of particle sizes. The distribution of particle sizes within the soil mass is represented by the grading curve. The soil particles also consist of varying shapes. However a general description of the clay particle grains can be said to be usually plate like while those of silt, sand, and gravel are more rotund (Atkinson, 2007).

Powrie (2004) found that there is an approximate relationship between particle size and toughness. These findings therefore establish a relationship between the frequency distribution of the particle sizes contained in the soil and the general toughness of the soil mass. The frequency distribution also affects the porosity of the soil mass hence a measure of its permeability.

3.4.5. Soil Permeability

The nature of the soil grains within a soil mass determines the soil permeability. It is established that the major feature distinguishing a granular soil from a cohesive soil thus introducing differences in their behaviour is the permeability. The permeability of soil is largely dependent on the sizes of the soil particles and the particle size distribution.

Research carried out by Montoro and Francisca (2010) related the influence of viscosity ratio, specific surface of particles, soil fabric and particle fluid interaction on hydraulic conductivity to the effective particle diameter and soil void ratio. Where the flow of water through the saturated soil does not affect the structure, permeability calculation is as shown in Equation 3.12 (Terzaghi and Peck, 1967). Equation 3.13 is the Darcy's law equation.

$$K = k\frac{\gamma_w}{\mu} \qquad \text{..... (3.12)}$$

$$v = K\,i \qquad \text{..... (3.13)}$$

Where v is the discharge velocity, K is the coefficient of permeability or hydraulic conductivity, k is the permeability, μ is the viscosity, γ_w is the unit weight of water, i is the hydraulic gradient.

Permeability is a primary factor in determining the choice of modelling a soil mass in static analysis as drained or undrained. Drained analysis is carried out using the effective stresses and pore pressure. Pore pressure is in equilibrium and can be found from the ambient water pressure, which, for hydrostatic conditions, can be based on the water table. In undrained analysis, pore pressure changes and there is no change in water content. In a fully saturated soil undrained analysis, there is no change in volume. In practice, drained or undrained analysis depends on the rate of loading against the rate of drainage within the soil.

3.4.6. Stiffness & Elasticity

The stiffness of the backfill soil is an important factor affecting the behaviour of soil. Predicting ground movements and possible solutions to soil-structure interaction problems

is supported by a knowledge of the soil stiffness (Atkinson, 2007). Stiffness is the quality of the soil that measures the ratio of the incremental stress to incremental strain thus relating the deformation of the soil to the loading applied. Stiffness variation in soil under loading can be large. Lehane et al. (1999) reported that the stiffness of siliceous cohesionless material increases as density increases and void ratio reduces.

Under cyclic loading and abutment displacement of an integral bridge structure, excessive deformation (straining) from stress may lead to the collapse of the structure or failure of the backfill or foundation soil. Simulation results as demonstrated by Wang and Shih (2007) show that reduced deformation in the backfill soil is essential in preventing collapse. During the cyclic displacement of an integral bridge abutment, relatively small displacements occur within the backfill soil. The resulting deformation of the abutment is relatively small. However, repeated deformation because of cyclic loading may result in failure. An ideal construction material would deform on straining and recover when the strain is relieved, without sustaining permanent damage, thus preventing cumulative deformation as a result of the cyclic loading.

Figure 3.3 highlight three regions of strains where the stiffness behaviour is different. In the region before the soil first yields, the stiffness is relatively constant with a linear stress strain relationship. Strains are usually in the order of 0.001%. Strains experienced around the state boundary surface, usually greater than 1%, exhibit elasto-plastic behaviour. Between this strain range, the stiffness changes considerably and the behaviour is non-linear (Atkinson, 2007). The stiffness of the soil may also be affected by other factors including the previous direction of loading, the degree of ageing, the angularity of the deposits, the anisotropy, and the shearing mode to which the material is subjected (Lehane et al., 1999).

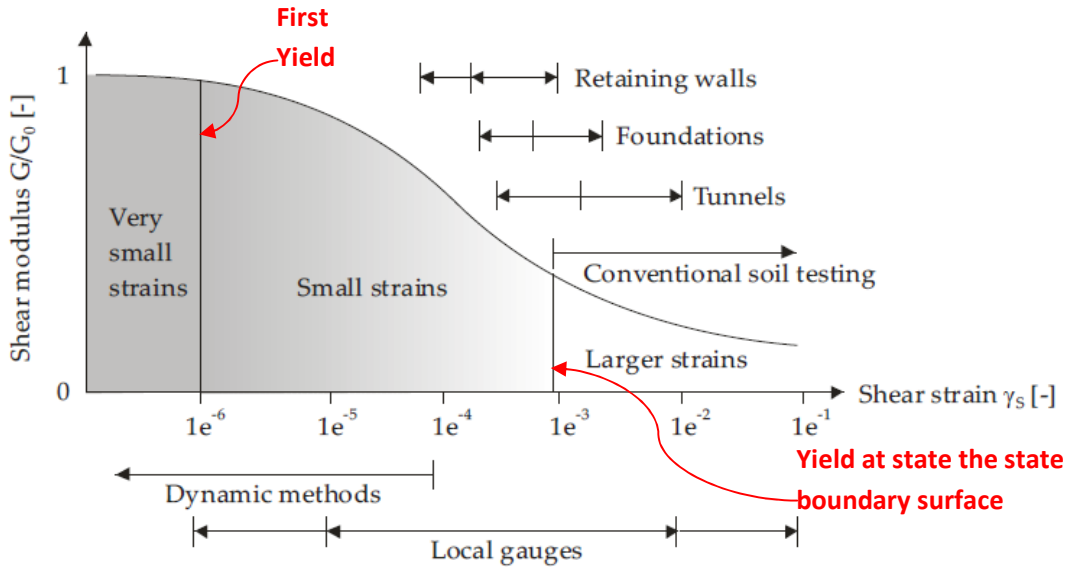

Figure 3.3: Characteristics of soil stiffness across three distinct regions showing structure strain range and measurements. Modified from Atkinson and Sallfors (1991) cited in Plaxis Manual (PLAXIS, 2010a).

3.4.7. Pore Pressure Changes

During soil loading, because of the displacement and rearrangement of soil particles, volume change occurs if a soil is partially saturated or pore pressures are allowed to dissipate. From Equation 3.2, where the pore pressure remains constant, the change in total stress is equal to the change in effective stress. However, where volume change is restricted as a result of restrictions in seepage and the rate at which the load is applied, the pore pressure will change (Atkinson, 2007).

The excess pore pressure is the difference between the pore pressure introduced as a result of the loading and the initial pore pressure. Soil loading is considered fully drained when no excess pore pressure is realised as a result of the loading, and fully undrained when there is no dissipation of excess pore pressure during loading. Consolidation is the process of dissipation of the excess pore pressure through time.

The relationship between the rate of change in soil volume V, change in stress σ', change in pore pressure u, and change in time t, defining the drained and undrained loading is

illustrated in Figure 3.4. The development of excess pore pressure is of critical importance in determining the behaviour of the soil. It has been found to be responsible for liquefaction in granular soil under seismic and cyclic loading (Hazirbaba and Rathje, 2009, Hazirbaba et al., 2011, Wang et al., 2010). Studies on the effect of seasonal ratcheting on clays as a consequence of changing pore pressures have illustrated the relevance of considering this effect on the behaviour of clays (Take and Bolton, 2011).

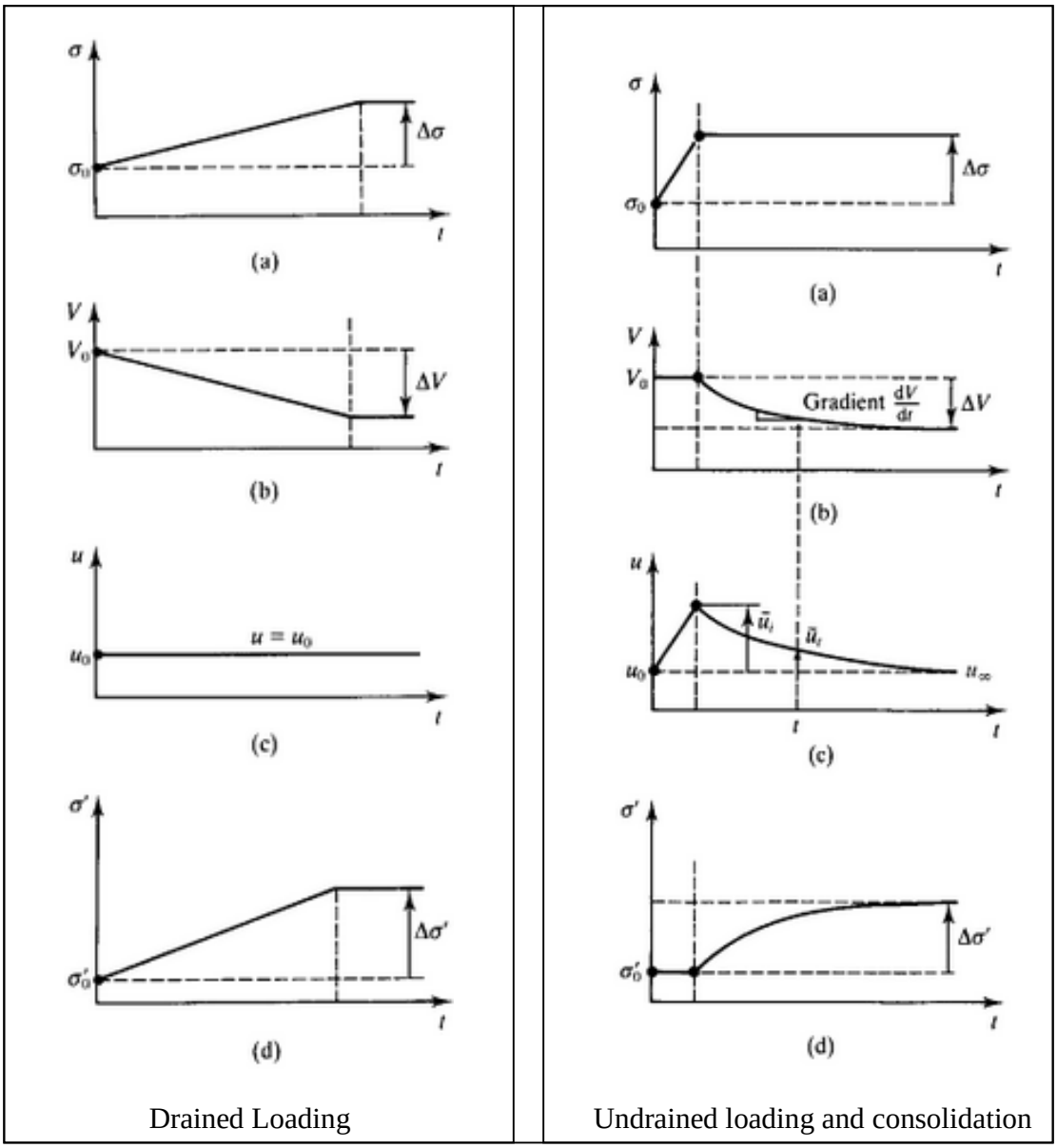

Figure 3.4: Characteristics of drained and undrained loading.
Modified (Atkinson, 2007).

3.4.8. Other Soil Parameters

Soil parameters reflect the composition of the soil and the structure of the soil. They indicate the expected behaviour of the soil. They may be measured insitu, in the laboratory with samples, or by estimation from the description of the soil using predetermined classification from historic data. Soil parameters may depend on the nature of the soil (shape, size, Atterberg limit), identified as material parameters, or on the state of the soil (water content, void ratio, stress history) - most accurately measured in undisturbed samples, identified as state dependent parameters (Atkinson, 2007).

It is appreciable that backfill materials are characteristically disturbed material because of the construction process introducing some change in their natural state dependent parameters. However, foundation materials are often largely undisturbed. Soil composition varies from any specific point to the very next in the field and from one sample to another. These differences give rise to different results on measurement of these parameters. This leads to soil being considered as a spatially variable material such that parameters are often based on a statistical assessment.

3.5. Loading

Integral bridges are subjected to similar loading forces experienced by conventional bridge structures. In addition, the integral bridge structure is subjected to a predominantly lateral and cyclic loading pattern, induced by the thermal expansion and contraction of the bridge deck. Erken & Ulker (2007) observed that failure can occur more readily under cyclic loading in fine grained soils (silt and clay) with low plasticity. Cyclic loading in undrained conditions leads to a reduction in shear strength. The reduction depends on the number of cycles and shear stress amplitude.

Densification occurs in soil when subjected to cyclic loading. Application of cyclic loading results in a reduction of volume due to shear. This volume reduction is less in fine grained soils. The densification is independent of the applied hydrostatic pressure (Pande and

Zienkiewicz, 1982). The impact of cyclic loading on the integral bridge backfill and foundation soil is considered in this section.

3.5.1. Granular Soils

Carder and Hayes (2000) reviewed the behaviour of granular soils by considering the typical behaviour under simple loading conditions. Granular soils are typically recommended as integral bridge backfill materials. The behaviour of the backfill soil immediately behind the abutment of an integral bridge is largely dependent on the strain-controlled behaviour of the backfill material due to the lateral displacement of the integral bridge abutment. The foundation soil sustaining the backfill soil is also subjected to the loading effect of the lateral abutment displacement. However, unlike the backfill soil, the behaviour of the foundation soil is largely dependent on the stress-controlled behaviour of the granular soil. An evaluation of a simple loading condition carried out through stress-controlled and strain controlled loading is presented below.

3.5.1.1. Stress Controlled Loading

In a model with stress-controlled loading, where constant stress is applied in cyclic loading, recoverable and non-recoverable shear strain is experienced. The magnitude of recoverable strain remains fairly constant while the non recoverable strain diminishes with increasing number of cycles (see Figure 3.5). The magnitude of non-recoverable strain resulting from an individual cycle is dependent on the stress applied. Where failure is excluded, increasing the number of loading cycle results in an increased cumulative magnitude of non recoverable strain, up to equilibrium (Carder and Hayes, 2000).

At equilibrium, the material is considered to be in a resilient condition where the recoverable strain is significantly larger than the non-recoverable strain. The resilient strain experienced (shown in Figure 3.5) is largely recoverable. Reduced stress in resilient condition only reduces the magnitude of the resilient strain with no non-recoverable strain. However, increased stress introduces additional non-recoverable strain that will reduce with increasing cycle until failure is reached or an increased stress resilient condition. Carder

and Hayes (2000) reported that in the cyclic loading of a granular material, immediately on starting unloading, there is a sudden increase in the stiffness of the material that progressively decreases as unloading continues. Figure 3.6 show the effect of stress reversal on stiffness.

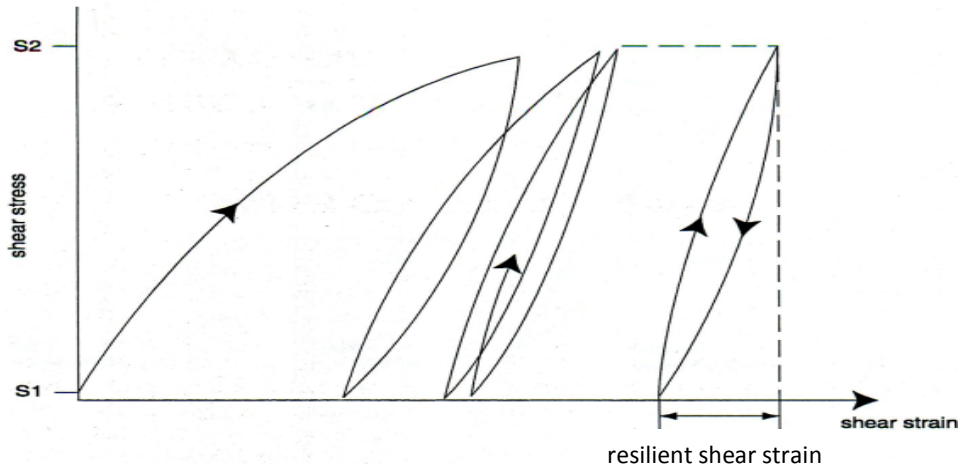

Figure 3.5: Granular Soil Constant Stress Cycle Loading (Resilient Shear Strain) Modified (Carder and Hayes, 2000).

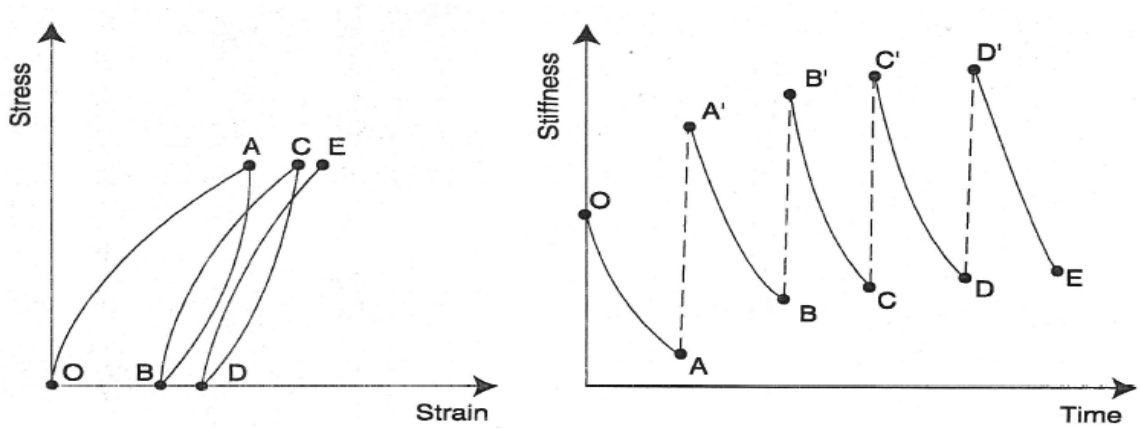

Figure 3.6: Effect of stress reversal on stiffness. Modified (Carder and Hayes, 2000).

3.5.1.2. Strain Controlled Loading

In a model with strain controlled loading, where there is straining on either ends of a neutral position, comparatively high stiffness develops at the centre of the cycle. The

stiffness is observed to increase dramatically on strain reversal before decreasing during continued loading. Figure 3.7 shows the result of cyclic strained controlled loading.

With increasing number of cycles, the area enclosed by the stress strain loop reduces while the stress increases and the material readily accommodate a deformation range within the established strain loop. However, any strain increment will encounter high resistance. Strain-controlled loading appropriately represents the loading of the backfill material behind the integral bridge abutment, as the backfill loading is dependent on the displacement of the abutment controlled by the bridge deck expansion. The abutment displacement is largely unaffected by the stiffness of the resisting structures (i.e. backfill and foundation materials) (Arsoy et al., 2002).

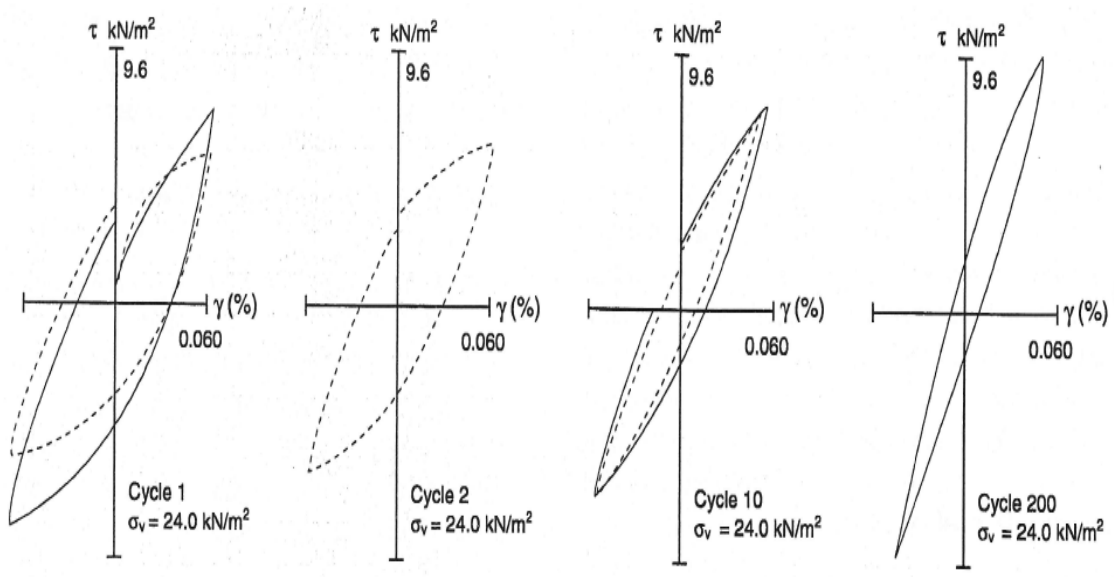

Figure 3.7: Granular Soil Constant Strain Cycle Loading.
Modified (Carder and Hayes, 2000).

3.5.2. Cohesive Soils

Cyclic loading may introduce excess pore pressure that reduces the effective stress in cohesive backfill materials. Dissipation of the excess pore pressure will lead to settlement. The extent of settlement that can occur during cyclic loading depends on the magnitude of excess pore pressure generated and the rate of dissipation. Dissipation is controlled by the

permeability of the soil. Carder and Hayes (2000) illustrated the behaviour of clay under undrained cyclic loading in Figure 3.8.

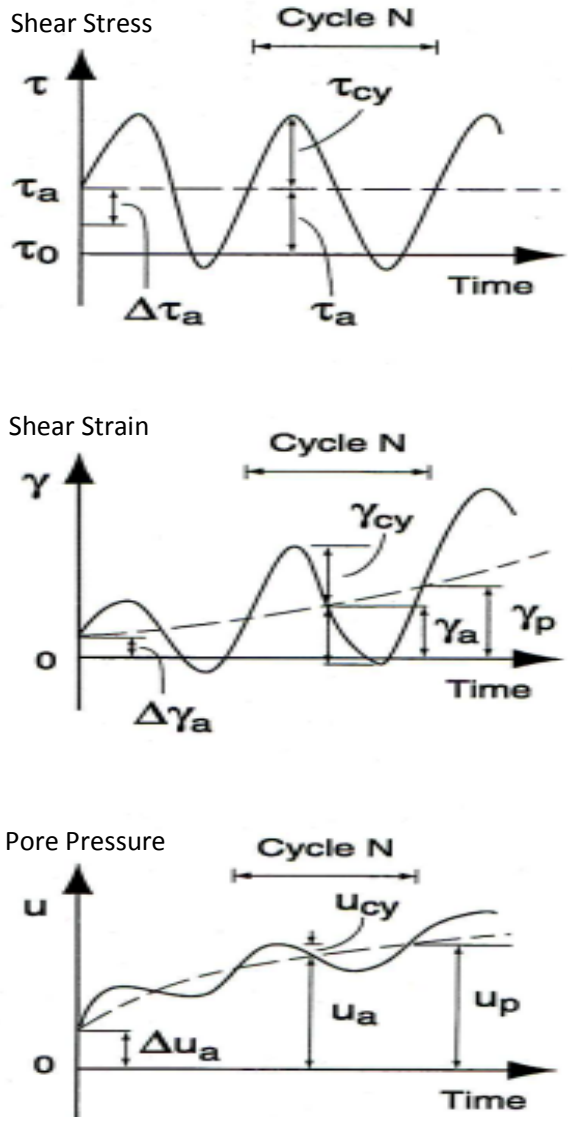

Figure 3.8: Behaviour of clay under undrained cyclic loading condition. Modified (Carder and Hayes, 2000).

The illustration shows that an increment in shear stress generates a corresponding increment in strain and pore pressure. Repeated cycle of stress will generate a pore pressure and strain with cyclic and average value that increase with number of cycles. The pore pressure at the end of the cycle is known as the permanent pore pressure (Carder and Hayes, 2000).

In an integral bridge cohesive backfill or foundation soil, partial drainage may occur due to the relatively slow rate of loading over time. In general, as the number of cycles increases under constant loading, strain amplitude increases, effective stress reduces and pore pressure increases. Yasuhara (1991), however, showed that in normally consolidated clays predominantly under undrained loading conditions where only partial drainage is experienced within a loading cycle, the rate of drainage in subsequent cycles increases with increasing number of loading cycles.

3.5.3. Soil Failure

Mechanical characteristics of soil under loading include a lack of significant capacity to resist tension and a limited capacity to resist high compression up to failure in both cases. Soil is known to fail in tension, shear, barrelling or barrelling and shear. The structural strength of the soil is primarily a measure of the soil's ability to resist sliding along internal planes within the soil mass. This ability is the soil's shear strength.

Several failure criteria have been developed and used in the analysis of soil failure. This includes the Mohr Coulomb criterion (Mohr, 1900, Nadai, 1950, Schweiger, 1994, Woodward, 1997, Kumar, 1998, Tachibana et al., 2007, Labuz and Zang, 2012), Drucker-Prager criterion (Drucker and Prager, 1952, Schweiger, 1994), Hoek-Brown criterion (Hoek and Brown, 1980, Hoek, 1990, Kumar, 1998), Lade-Duncan criterion (Woodward, 1997, Tachibana et al., 2007), Von Mises criterion (von Mises, 1913, Tachibana et al., 2007). Their strengths and weaknesses have been highlighted in numerous publications in which these criteria have been discussed. The Mohr Coulomb failure criterion is a popular criterion used in the analysis of soil strength. Failure in the Mohr Coulomb criterion occurs when the Mohr circle touches the failure line defined by Equation 3.14.

$$\tau' = c' + \sigma' \tan \boldsymbol{\phi}' \qquad \text{(3.14)}$$

Failure is achieved at the point of maximum shear strength. Failure in integral bridge backfill may develop at maximum active or passive earth pressure. In passive mode, failure may be observed to occur in the backfill soil in the form of compressive cracks or shear. In

this mode the displacement from top to bottom of the abutment decreases while the soil resistance increases (Wang and Shih, 2007). In active mode failure may be observed in the form of tensile cracks or excessive settlement.

3.6. Soil Models

The composition of soil is complex and differs across the entire soil mass. This presents a challenge in studying and understanding the behaviour of a soil mass. Knowledge of the nature and behaviour of the soil in loading, deformation, and failure around an integral bridge can be acquired by measurements taken off the integral bridge site. This approach presents many challenges, is expensive, not practical, and the measured results would be peculiar to the circumstances surrounding the particular bridge. However, certain characteristics of soil behaviour, considered relevant to an event, may be replicated using a simplified approach considered a model of the specified soil characteristic. A model is a creation done to be representative of the actual. Dutta and Roy (2002) highlights the importance of accurately modelling soil behaviour in integral bridge analysis.

Soil behaviour may be modelled by a set of mathematical equations, designed to generate outputs that replicate an expected behaviour the soil would generate. Soil models are intended to isolate those elements that significantly influence the soil behaviour for intensive study with less emphasis on features considered irrelevant within the circumstance (Wood, 1990). Wood (1990) classified soil models according to the purpose served. These were; illustration model - illustrating soil behaviour, in which case a simplified but overall picture of the soil is given; and predictive model - predicting soil behaviour, in which case the behaviour of the soil elements in a particular prototype is expected to be closely matched by the model (Wood, 1990).

3.6.1. Modelling

Problems in geotechnical engineering typically originate from changes in stresses, and are centred around stability analysis where the emphasis is on yield with relatively large

deformations, or collapse of the structure, and on soil deformation analysis which is concerned with the stiffness of the soil mass under loading with relatively small deformations (Wood, 1990). Models attempt to idealize the reality of these analyses, without which these behaviours would be too complex to analyse.

Understanding the behaviour of in-situ soil subjected to loading has advanced remarkably within the last century. As a result of these gains in knowledge, more complex soil models, aimed at reflecting more accurately the current understanding of the behaviour of soil have been developed. Research findings, documented in published literature, by several authors such as Collins (2005) and Kelln et al. (2008) have highlighted inadequacies that have been observed in simpler models, thus recommending the use of more complex models in analysis. Many of the more recent models are extremely complex and require several soil parameters that are, in many cases, commercially not practical to acquire (Collins, 2005, Kelln et al., 2008).

Real soil behaviour is predominantly based on a nonlinear stress strain relationship. Kondner (1963) suggested that a hyperbola represents to a high degree of accuracy the nonlinear stress strain behaviour of both sand and clay. However, in a stress strain relationship, a soil material subjected to varying level of stress may experience one or more of linear elastic straining, non-linear elastic straining, yield, elasto-plastic straining, hardening, softening, and failure. Soil models are designed to emphasis these relationships with a set of specific considerations and assumptions. Analysis carried out by Jardine et al. (1986) concluded that, although linear elasticity often used for its simplicity, is a convenient tool that may be used in expressing measurements of soil stiffness, where the non-linear nature of soils is not accounted for, soil-structure interaction computations and the interpretation of field measurements may be misleading.

Numerical and analytical soil models may be designed to simulate soil behaviour as can be accurately mathematically expressed (Potts and Zdravkovic, 1999). The accuracy of predicting soil behaviour through these models depends on how appropriate the models used are in reflecting the relevant characteristics within the circumstance. The stress strain relationship of a typical soil material subjected to loading under linear elastic straining, non

linear elastic straining, yield, elasto-plastic straining, hardening and softening straining, and failure conditions, are presented under the elastic, plastic and elasto-plastic models below. However, a popular validation approach to the predictive abilities of the model used in a given circumstance is the comparison of the model's output with measured values on real structures under similar circumstance.

3.6.2. Modelling Elastic Behaviour

In an elastic model, soil is assumed to be strained on loading and recover completely from any deformation and strains caused by the loading during unloading, irrespective of the number of times the loading and unloading process is carried out. Elastic models may be linear or nonlinear. Figure 3.9 shows the stress-strain relationship of a linear and nonlinear material. The principle of elasticity holds within this model provided the stresses in the soil do not exceed yield stress or failure.

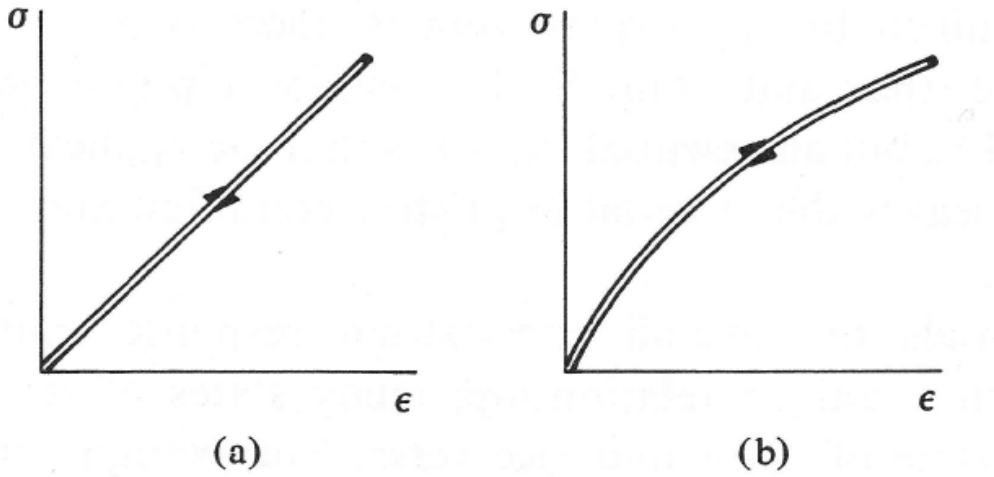

Figure 3.9: Typical elastic stress strain relationship:
(a) Linear; (b) Non-linear. Modified (Wood, 1990).

While changes in the effective stress govern the behaviour of soil, it is useful to describe the elastic response of the soil in terms of the changes in the total stress (Wood, 1990). The stress-strain behaviour for an ideal isotropic soil-like material is given by the generalized form of Hooke's law (Atkinson and Bransby, 1978). In terms of the principal stress and strain in axial symmetry where the intermediate and minor principal stresses are equal, the

equation can be written as shown in Equations 3.15 and 3.16. These equations demonstrate that in an isotropic elastic soil, with an established constant of proportionality, increment of shear strain $\delta\varepsilon_s$, corresponds with increment of deviator stress $\delta q'$, and increment of volumetric strain $\delta\varepsilon_v$, corresponds with increment in mean stress $\delta p'$.

True elasticity in soil behaviour is unlikely to occur under static loading conditions but may be observed under dynamic loading conditions and especially with cohesive soil (Glanville et al., 1952). However, calculations from elastic soil models with judiciously selected elastic parameters may be used in the prediction of soil behaviour with a reasonable degree of accuracy (Powrie, 2004).

$$\delta\varepsilon_v = (1 / K')\, \delta p' \qquad \ldots\ldots\ldots\ldots\ldots (3.15)$$

$$\delta\varepsilon_s = (1 / 3G')\, \delta q' \qquad \ldots\ldots\ldots\ldots\ldots (3.16)$$

$$K' = (1 / 3)\, E' / (1 - 2\nu') \qquad \ldots\ldots\ldots\ldots\ldots (3.17)$$

$$G' = (1 / 2)\, E' / (1 + \nu') \qquad \ldots\ldots\ldots\ldots\ldots (3.18)$$

Where K' is the bulk modulus, G' is the shear modulus, E' and ν' are the Young's modulus and Poisson's ratio appropriate for changes of effective stress.

3.6.3. Modelling Plastic Behaviour

In the plastic phase of a model, deformations and strains incurred on loading are not recovered when unloading. Plastic strain is irreversible. The three essential features that apply in the theory of plasticity are yielding of the material, hardening, and flow (Atkinson and Bransby, 1978). These features are described by the yield function, the hardening law, and the flow rule (Hill, 1958). Where perfect plasticity is assumed, the yield function is equal to failure. Plasticity theory in the hardening law presents the relationship between the change in yield stress and the change in plastic strain. The flow rule in the plasticity theory is the relationship between the failure envelope and the direction of the vector of the plastic strain (Craig, 2004, Atkinson, 2007). Figure 3.10 show the behaviour of an ideal perfectly plastic material.

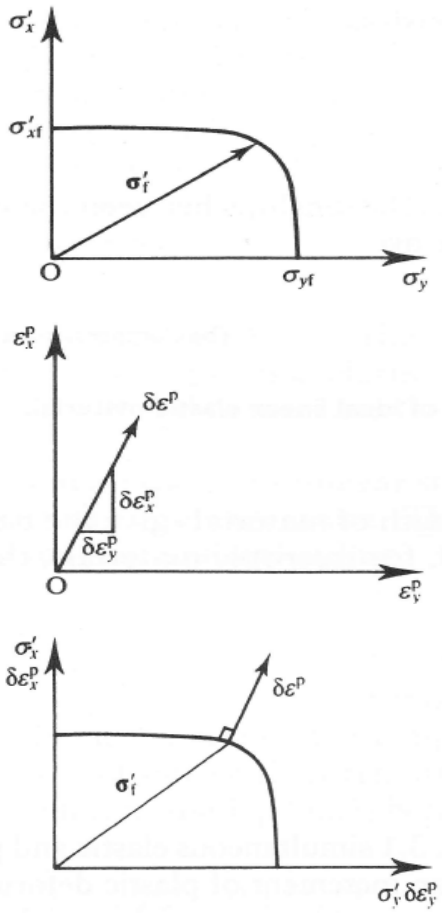

Figure 3.10: Ideal Perfectly Plastic Material Flow Rule:
(a) Stress yield limit (failure envelope); (b) Plastic strain of material;
(c) Flow rule illustration (yield & strain). Modified (Atkinson, 2007).

Loading in excess of the yield stress will result in plastic straining in the soil (Figure 3.10b). Varying combination of stresses defined by the axis in Figure 3.10a may achieve failure defining the failure envelope (curve in Figure 3.10a). Normality conditions apply in a perfectly plastic material where the vector of plastic strain is normal to the failure envelope (Figure 3.10c). In a perfect state of plasticity, soil is assumed to deform continuously without any load increment and change in volume giving rise to a plastic flow. This state is defined by an application of the ultimate load and indefinite increment of strain.

3.6.3.1. Elastic Perfectly Plastic Model

The basic principle behind the Elastic Perfectly Plastic model is the modelling of the combined elastic and plastic property in a soil occurring non-concurrently within the model, where the plastic strains (Y' to Y'') succeed the elastic strains at failure. Yield accounts for failure in this model. Increasing effective stress generates increasing elastic strain. At ultimate effective stress, failure occurs and the strain becomes plastic. Unloading (Y'' to U) will recover the elastic straining without the plastic straining as shown in Figure 3.11. Subsequent reloading will introduce a new yield point at a different cumulative strain. The ultimate effective stress remains unchanged. This model commonly adopts the Mohr Coulomb failure criterion and is appropriate in modelling an approximate and general behaviour of a soil under loading.

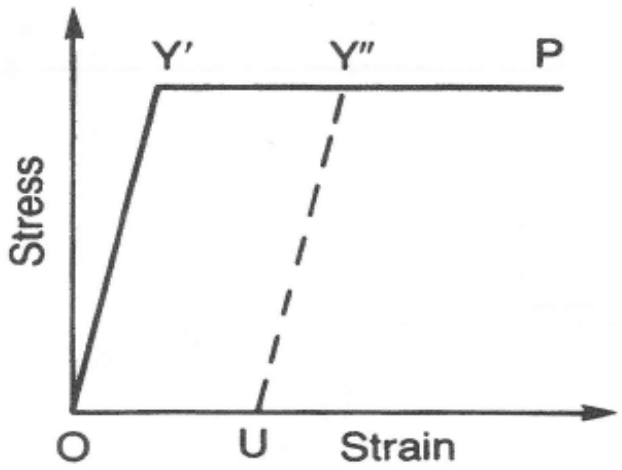

Figure 3.11: Illustration of elastic-perfectly plastic stress strain relationship. Modified (Craig, 2004).

3.6.3.2. Elasto-Plastic Model

Soil exhibits some elastic and/or plastic properties at various stages of loading. Predominantly, most soils typically exhibit a combination of elastic and plastic straining during the unloading of an applied load. The magnitude of either is dependent on the nature of the soil and the properties of the load applied. In accurately modelling the behaviour of

soil, the elastic and plastic properties are combined in soil models considered suitable in modelling the appropriate soil characteristics.

The elasto-plastic model accounts for a combined elastic and plastic property in a soil occurring concurrently. Figure 3.12 illustrates the stress strain behaviour of the elasto-plastic model. Elasto-plastic behaviour is experienced during loading from Y_1 to Y_2. If the material is unloaded at Y_2, elastic strain is recovered but plastic strain O_1 to O_2 is lost. The cycle continues on reloading from O_2 through Y_2 to Y_3. The material behaves elastically when re-loaded and unloaded within the new yield stress limit O_2 to Y_2. The yield stress changes from Y_1 to Y_3 and beyond as the loading increases.

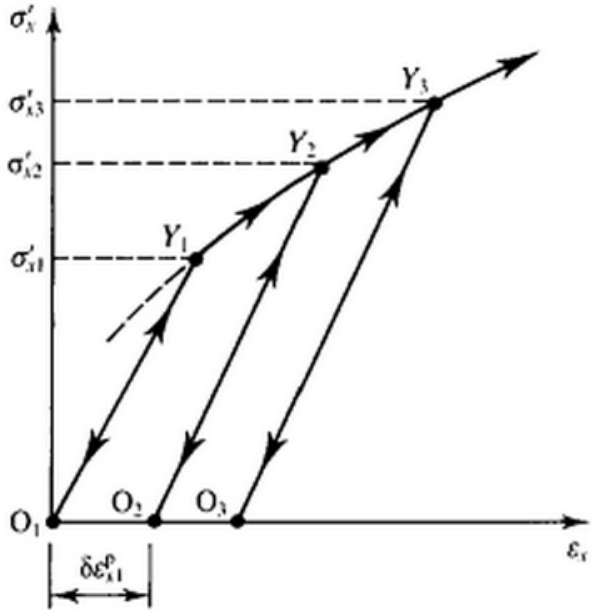

Figure 3.12: Illustration of elasto-plastic stress strain relationship. Modified (Atkinson, 2007).

3.6.3.2.1. Hardening & Softening

Strain hardening and softening is a characteristic of the elasto-plastic model. The increase in yield point from A to B in Figure 3.13 is called hardening and the relationship that exist between the increase in yield stress and the plastic straining is known as the hardening law (Atkinson, 2007). Yielding and straining in the elasto-plastic model may cause softening

where a peak stress has been realized, in which case the yield stress value will be decreasing (Figure 3.14).

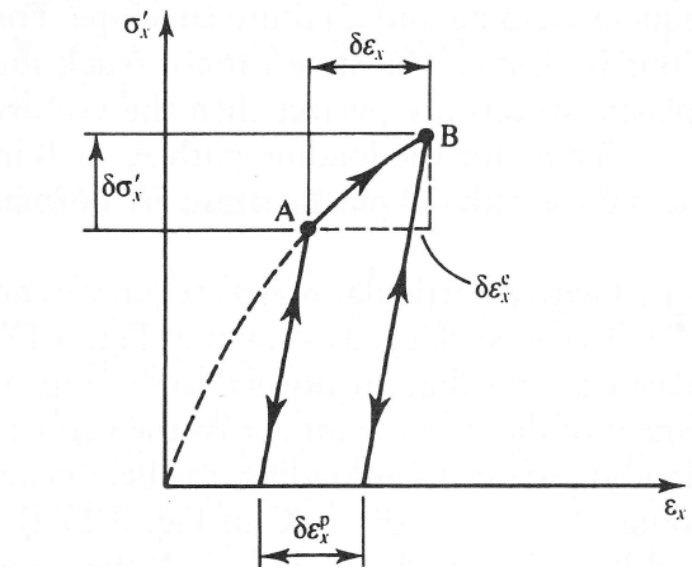

Figure 3.13: Strain hardening (Atkinson, 2007).

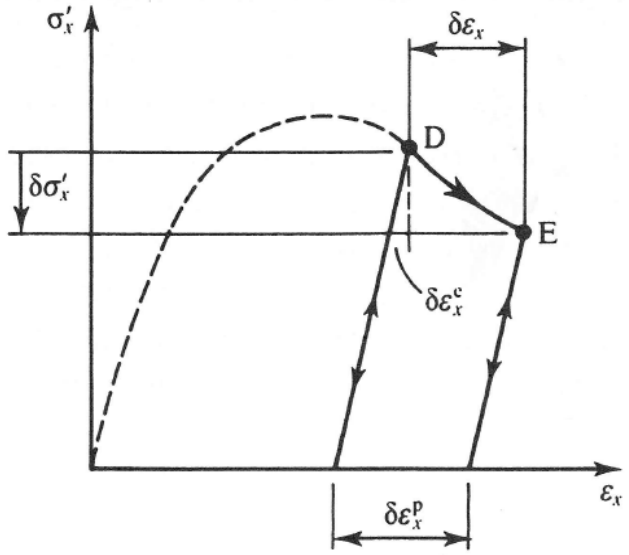

Figure 3.14: Strain softening (Atkinson, 2007).

There are two types of hardening. Hardening from shear strain and hardening from compression. Hardening from shear strain is associated with plastic shear strain while hardening from compression is associated with plastic volumetric strain.

3.7. Summary

A review of the concept of the integral bridge, challenges originating from this concept, proposed solutions, and a summary of the research effort on the integral bridge was carried out in Chapter 2. Chapter 3 reviewed the impact of this concept affecting the behaviour of the backfill and foundation soil. The integral bridge presents advantages that make it preferable. Complications however arise from the concept of the integral bridge in application thus introducing constraints in its use.

Fully understanding the behaviour of the soil subjected to soil-structure interaction in response to the thermal effect on the structure, and the nature of the complications that arise, have been challenging to engineers and academics alike. Generally acceptable design and construction guidelines have not been developed. This is evidently, in part, due to a lack of sufficient information and knowledge that may be required in the development of guidelines for the design and construction of the integral bridge, as is standard practice in most engineering events.

Research has been carried out on the earth pressure developed behind the abutment, considered a primary problem in integral bridges. The result of these studies have shown that change in the values of the backfill soil parameters affect the development of earth pressure within the backfill soil (Wood and Nash, 2000). As a result of the characteristics of soil, the season in which the bridge is constructed affects the development of earth pressure. Studies carried out on the impact of the season of construction on integral bridge performance determined that the effect was not significant and therefore may not be taken into consideration (England et al., 2000). However, in studying the earth pressures developed, these studies did not take into consideration the indispensable effect of the foundation soil on which these structures are constructed.

The development of excess pore pressure is known to have a significant impact on the known behaviour of soil. While the backfill soil is often engineered soil, mostly granular in nature with a little possibility of developing excess pore pressure, the foundation soil is more often cohesive and presents a significantly higher probability of developing excess pore pressure. The impact of the excess pore pressure developed within the foundation soil

as a result of the thermal induced abutment displacement, on the earth pressure behind the abutment within the backfill soil, has not been investigated.

This knowledge is sought primarily by developing a model of an instrumented integral bridge to simulate realistic earth pressure results obtained from the thermal induced backfill soil loading. The impact of the excess pore pressure in the foundation soil, as a result of the thermal-induced abutment displacement, on the development of earth pressure behind the abutment, is then evaluated through the assumptions of fully undrained and fully drained fine grained soils within the foundation materials under loading. This is evaluated as:

- Applicable to the impact of changes in the backfill soil parameters.
- Applicable to the impact of changes in the season of construction.
- Applicable to the impact of changes in the backfill soil parameters in changing construction seasons.

Chapter 4 : NUMERICAL MODELLING

4.1. Introduction

Modelling is an indispensable tool in today's world with the expectation of more efficiency in engineering outputs using leaner resources. Burland (1987) presented the view that geotechnical engineering practice involves three parts. These parts are interlinked and supported by experience consisting of empiricism and precedent. Two of the three parts are; the ground profile established from site investigation, and the soil behaviour established from soil testing. The third part is modelling which entails an application of the knowledge obtained in the other two parts to guide the final decision making process of the engineer.

Engineering events may be modelled using equations. These equations increase in complexity as the quantity of variables taken into consideration increase. Accuracy is also improved as more relevant variables are taken into consideration within these equations. Solving these highly complex equations may be a laborious and time demanding process, fraught with possibilities of error, and may not achieve a solution. However, the numerical method of analysis consistently provides solutions to these complex equations, albeit the solutions are approximate solutions and are achieved through a tedious calculation process (Ford, 1999). Solutions obtained from relatively complicated models of problems, using the numerical method of analysis, are reputed to have a high degree of accuracy where appropriately applied. The principles through which these solutions are achieved are briefly described in this chapter.

4.2. Numerical Method Approach

Potts and Zdravkovic (1999) noted that for an exact theoretical solution to a geotechnical engineering problem, the requirements of equilibrium, compatibility, material behaviour and boundary conditions in forces and displacements must be satisfied. An evaluation of

the methods of analysis showed that the numerical method of analysis satisfy these conditions (Potts and Zdravkovic, 1999).

It has been established that the numerical method of analysis is a powerful tool and a more flexible method in the analysis of problems represented by complex equations, such as may be encountered in geotechnical engineering problems (Ford, 1999, Potts and Zdravkovic, 1999, Cundall and Strack, 1979).

4.2.1. Numerical Method Options

The availability of affordable digital personal computers with increasing capabilities of performing otherwise tedious calculations in record time has encouraged the development and use of advanced numerical methods in routine engineering analysis. Popular numerical methods of analysis developed include the finite element method, the finite difference method, the boundary element method, and the discrete element method. Many variations of these methods with the same fundamental principles are also in use.

The discrete element method (DEM) initiated by Cundall and Strack (1979) is a numerical method of analysis capable of simulating the motion and interactions of individual particles (Kalala and Moys, 2004, Magnier and Donze, 1998). The discrete element method is based on particle interaction modelling, at the moment of contact, defined by particle contact conditions in which finite motions including displacements and rotation of the particle are considered (Reddy, 1993). Elements collide and rebound at the point of contact and its trajectory can be calculated by integrating Newton's law with a knowledge of the geometry, the direction and velocity of the approaching elements, the boundary conditions, and the forces at collision (Richards et al., 2004). It is more suited to problems exhibiting strong discontinuity in material and geometric properties (Mohammadi, 2003) and involving transient dynamics terminating in a state of rest among the particles (Munjiza, 2004). Discrete element numerical analysis method has been used in finding solutions to problems in geotechnical engineering analysis (Richards et al., 2004, Villard et al., 2009a, Chen et al., 2011) but is currently limited because of the time and computing capacity needed to analyse all but the simplest problems.

The boundary element method (BEM) or boundary integral method solves problems formulated as equivalent boundary integral equations. The Boundary integral equation is regarded as an explicit solution to the governing partial differential equation. This is generally obtainable in linear partial differential equation. As a result, the boundary element method is unable to accurately solve non-linear problems when compared to other numerical methods (Katsikadelis and Nerantzaki, 1999). It is, however, an efficient option of numerical analysis where linear problems are encountered.

The finite difference method (FDM) uses a topologically square network of lines to construct the discretisation of partial differential equations. This approach in analysing problems, is a potential bottleneck when applied to complex geometries in multiple dimensions (Peiro and Sherwin, 2005). The constraints encountered as a result of using this approach, motivated the use of the integral forms of the partial differential equations and consequently the development of other numerical methods such as the finite element method (Peiro and Sherwin, 2005). The finite difference method is reputed to be easily implemented over regularly shaped or rectangular form type of geometry.

The finite element method (FEM) solves partial differential equations with values at specific points identified as nodes. The fundamental principle is to discretise a domain into a discrete number of elements known as finite elements and solve for the unknown values at the nodes (Zienkiewicz et al., 1977). The nodes connect the finite elements within a domain and form a mesh. The finite element method is capable of solving most properly defined continuum problems.

4.2.2. Numerical Method Summary

Variations in results among numerical methods, that are considered suitable for a specific type of problem, have been generally adjudged to be minimal (Fang et al., 2002, Marfurt, 1984, Katsikadelis and Nerantzaki, 1999) with arguments about one's advantage over another largely dependent on the exact definition of the referenced process (Zienkiewicz et al., 1977). Different numerical methods suited for a given type of problem may provide acceptable solutions to the problem using their various approaches. However, the choice of

the most appropriate method to apply in any given circumstance is dependent on the nature of the problem in consideration, and a recognition of the advantages and disadvantages of a numerical method's approach over another within the said circumstance (Zienkiewicz et al., 1977).

In solving similar problems, the finite element method has been consistently rated generally equal to the finite difference method or better in output (Marfurt, 1984, Simpson and Clement, 2003). Results of the studies carried out by Fang et al. (2002) on a two point boundary value problem, indicated that the finite element method had a slight advantage in accuracy over other methods investigated especially the finite difference method.

The discrete element method was developed for materials exhibiting discontinuities thus limiting its application on cohesive soils. As highlighted above, solutions to non-linear problems as may be encountered in natural soil loading are challenging using the boundary element method. Using the finite element method, complex non-linear equations and problems with complex geometries, can be solved as analytical solution forms are not required (Zienkiewicz et al., 1977) as is the case in the boundary element or the finite difference method. A review of the fundamental principles of the finite element method as applicable in geotechnical engineering problems, highlights its robustness in dealing with problems that may be defined through complex equations, have finite boundary conditions, and act as a continuum (Potts and Zdravkovic, 1999). The finite element application is capable of solving problems with complex geometries, complex restraints, and complex loading conditions. Its ability to deal with several complex equations in a continuum makes it advantageous in simulating events such as a soil-structure interaction problem with relatively small displacement.

The characteristic of the finite element method as identified above, coupled with a computer-aided execution of the calculation analysis in successive stages, is ideally suited to simulate the integral bridge construction and abutment displacement sequence and closely replicate the behaviours of the soil materials within these sequences. The finite element method is used in this research.

4.3. Finite Element Approach

The finite element method finds approximate solutions to partial differential and integral equations. This method derives solutions of problems in a given domain and provides the approximate values of variables only at discrete number of points in a domain (Desai and Abel, 1972). It is based on the principle of dividing a given domain into smaller domains known as finite elements (Reddy, 1993). Figure 4.1 shows the discretisation of an irregular shaped object into finite elements.

The fundamental idea behind the finite element method is to find solutions to a complicated problem by replacing it with a simpler problem generating an approximate solution rather than the exact solution (Rao, 2005). The finite element method of analysis over time has been a popular application in finding solutions to geotechnical engineering problems. It was identified by Britto and Gunn (1987) as the most commonly used numerical method in geotechnical engineering applications and by Reddy (2004) as one of the most commonly used methods for practical engineering problems.

Known properties of a typical finite element within the domain are acquired. Functions that approximate the distribution of the actual displacement over each finite element are chosen. This process is achieved through a mathematical formulation of the physical process. The resulting equation is known as the “element equation” (Reddy, 1993). The unknown value of the displacement functions are the displacement at the nodal points (Desai and Abel, 1972). This equation is unique to and must be developed for each type or class of element within the domain.

In the finite element method, problems dependent on time are solved in two stages. In the first stage, the differential equations are approximated by the finite element method to achieve ordinary differential equations in time. The next stage involves these equations being solved to obtain algebraic equations that are then resolved to obtain the values at the nodes (Reddy, 1993).

The element equations are subject to boundary conditions that introduces a unique identity and a solution to each case. The approximate solution to the problem in the given domain is

obtained by assembling the properties of the finite elements in a meaningful way. The assembly is based on the assumption that the solution considered is continuous at the inter-element boundaries controlled by the nodes (Reddy, 1993).

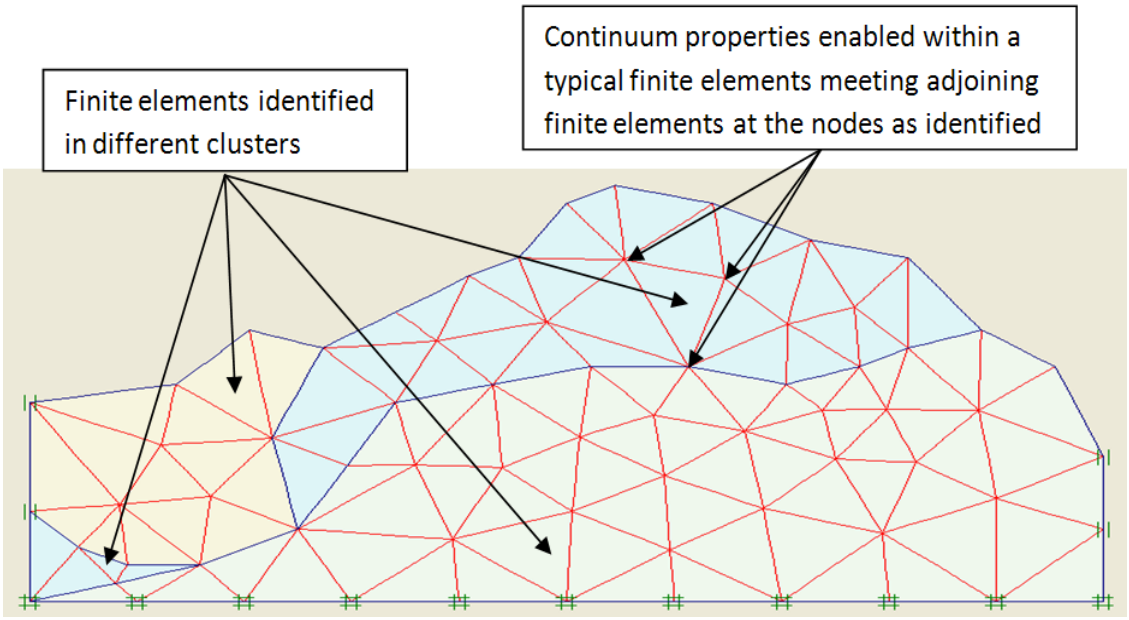

Figure 4.1: Finite element discretisation of an irregular shape modelling a soil mass with cluster representing different soil types

In the finite element method, it is possible to improve the accuracy of the approximate solution. The degree of accuracy is based on the number of finite elements defined within a domain. This arises from the principle that the approximate solution converges to the actual solution as the number of finite elements tends to infinity. Consequently, the global error (total finite element error) converges to zero (Reddy, 1993).

4.3.1. Discretisation

The primary step in the finite element approach is to quantify and define an approximate geometry of the problem. The quantified geometry makes up the domain in consideration. The domain is subdivided into a mesh of finite elements, a process known as discretisation. The finite elements consequently constitute a cluster of smaller discrete regions that make up the domain (Reddy, 1993, Desai and Christian, 1977).

In a two dimensional domain, the finite elements are often triangular or quadrilateral in shape. The finite elements are separated by nodal lines and the intersection of these nodal lines is called nodal point (Desai and Christian, 1977). Finite elements are considered to be interconnected at nodal points also known simply as nodes. In a finite element with straight sides, the nodes make up the corners. The geometry of the nodes is identified by the coordinates within the geometry of the domain (Potts and Zdravkovic, 1999). The finite elements may be uniform resulting in a uniform mesh or otherwise, in a non-uniform mesh.

Discretisation presents the advantage of allowing "accurate representation of complex geometries and inclusion of dissimilar materials" and "accurate representation of the solution within each element to bring out local effect" (Reddy, 1993). Accuracy of the finite element results depend on an accurate representation of the geometry. Discretisation also presents the advantage of controlling the number of finite elements within a domain. In the finite element method, the number of finite elements within the domain controls the degree of accuracy.

4.3.2. Primary Variable Approximation

The finite element approach includes the selection of a primary variable such as displacement or stress. The rule of how the variable should vary over the finite element must be established. In a displacement primary variable selection, the primary unknown quantity is the displacement, which varies through the domain. Other variables including the stress are treated as secondary quantity and can be obtained through their representative relationships with the displacement values.

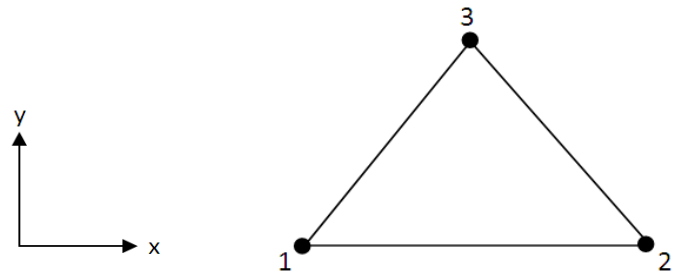

Figure 4.2: Typical three node finite element.

$$u=a_1+a_2x+a_3y \quad \text{…….. (4.1)}$$

$$v= b_1+b_2x+b_3y \quad \text{…….. (4.2)}$$

The constants in Equations 4.1 and 4.2 are expressed in terms of the individual nodes to generate the nodal displacement equation.

The variation of displacements within the finite elements must satisfy the condition of compatibility. In a two-dimensional plane strain analysis, displacement within the domain is characterized by two global displacements that may be represented as u in the horizontal (x) axis and v in the vertical (y) axis. The finite element axial displacement components are assumed to vary over the domain by equations in a polynomial form as presented in Equations 4.1 and 4.2 where the order of the polynomial is dependent on the number of the nodes within the element. The nodal displacement equations for the nodes of the three node finite element in Figure 4.2 are expressed as shown in Equations 4.3 - 4.8.

$$u_1=a_1+a_2x_1+a_3y_1 \quad \text{…….. (4.3)}$$

$$u_2=a_1+a_2x_2+a_3y_2 \quad \text{…….. (4.4)}$$

$$u_3=a_1+a_2x_3+a_3y_3 \quad \text{…….. (4.5)}$$

$$v_1= b_1+b_2x_1+b_3y_1 \quad \text{…….. (4.6)}$$

$$v_2= b_1+b_2x_2+b_3y_2 \quad \text{…….. (4.7)}$$

$$v_3= b_1+b_2x_3+b_3y_3 \quad \text{…….. (4.8)}$$

The simultaneous equations are solved for the constants $a_1, a_2, a_3, b_1, b_2, b_3$, in terms of the displacements at the nodes to obtain Equation 4.9 where $[N]$ is defined as the matrix of shape functions and the number of nodes in the element is n.

$$\begin{Bmatrix} u \\ v \end{Bmatrix} = [N].\{u_1,\ u_2, \ldots\ldots,\ u_n,\ v_1,\ v_2, \ldots\ldots,\ v_n\}^T = [N].\begin{Bmatrix} u \\ v \end{Bmatrix}_{nodes} \quad \text{…….. (4.9)}$$

Accuracy of the finite element depends on the nature of the primary variable approximation and on the size of the finite element. As the numbers and therefore the sizes of the elements

within a domain change, the displacement approximation must have continuity within the displacement domain in order to avoid voids or overlaps occurring; be capable of representing rigid body movements; and be capable of representing constant strain rates (Potts and Zdravkovic, 1999).

Variations of unknown displacements within a finite element are defined in terms of the displacement at the nodes. Consequently, displacement within the domain is determined by displacements at the nodes that satisfy compatibility conditions within adjoining finite elements.

4.3.3. Equations

Functions that represent the distribution of the displacement over each finite element are assembled into an element equation. This equation governs the deformation of the finite element in a loading analysis. A typical element equation primarily satisfies the conditions of equilibrium, compatibility and material constitutive behaviour. Changes in displacements u and v in a plane strain analysis are assumed to be represented as follows:

$$\{\Delta d\} = \begin{Bmatrix}\Delta u \\ \Delta v\end{Bmatrix} = [N]\begin{Bmatrix}\Delta u \\ \Delta v\end{Bmatrix}_n = [N]\{\Delta d\}_n \quad \text{…….. (4.10)}$$

Strains corresponding to the displacements u and v on the x and y axes respectively in plane strain analyses are represented by:

$$\Delta\varepsilon_x = -\frac{\partial(\Delta u)}{\partial x} \quad \text{…….. (4.11)}$$

$$\Delta\varepsilon_y = -\frac{\partial(\Delta v)}{\partial y} \quad \text{…….. (4.12)}$$

$$\Delta\gamma_{xy} = -\frac{\partial(\Delta u)}{\partial y} - \frac{\partial(\Delta v)}{\partial x} \quad \text{…….. (4.13)}$$

$$\Delta\varepsilon_z = \Delta\gamma_{xz} = \Delta\gamma_{zy} = 0 \quad \text{…….. (4.14)}$$

$$\{\Delta\varepsilon\}^T = \left\{\Delta\varepsilon_x \ \Delta\varepsilon_y \ \Delta\gamma_{xy} \ \Delta\varepsilon_z\right\}^T \quad \text{…….. (4.15)}$$

Strains across the finite elements can be expressed in terms of the nodal displacements by a combination of Equations 4.10 - 4.15 and is given by Equation 4.16 where $[B]$ is a matrix that contains derivatives of the shape functions and $\{\Delta d\}_n$ is the nodal displacement for the finite element.

$$\{\Delta\varepsilon\} = [B]\{\Delta d\}_n \qquad \text{…….. (4.16)}$$

The constitutive model representing the behaviour of the material can be expressed in terms of stress strain relationship given in Equation 4.17 where $[D]$ is the constitutive matrix in a two dimensional plane strain analysis and $\{\Delta\sigma\}^T = [\Delta\sigma_x \ \Delta\sigma_y \ \Delta\sigma_{xy} \ \Delta\sigma_z]$.

$$\{\Delta\sigma\} = [D]\{\Delta\varepsilon\} \qquad \text{…….. (4.17)}$$

For a linear elastic material, $[D]$ takes the form presented in Equation 4.18 where υ is Poisson's ratio and E is Young's modulus (Potts and Zdravkovic, 1999).

$$\frac{E}{(1+\upsilon)}\begin{bmatrix} (1-\upsilon) & \upsilon & \upsilon & 0 & 0 & 0 \\ \upsilon & (1-\upsilon) & \upsilon & 0 & 0 & 0 \\ \upsilon & \upsilon & (1-\upsilon) & 0 & 0 & 0 \\ 0 & 0 & 0 & (1/2-\upsilon) & 0 & 0 \\ 0 & 0 & 0 & 0 & (1/2-\upsilon) & 0 \\ 0 & 0 & 0 & 0 & 0 & (1/2-\upsilon) \end{bmatrix}$$

…….. (4.18)

The principle of minimum potential energy states that the static equilibrium position of a loaded linear elastic body is responsible for minimizing the total potential energy. This principal is the basis for determining the element equation for linear elastic material. The total potential energy (E) of a body is defined as the strain energy (w) or work done within the material less the work done by the applied loads (L) on the material. The principal of minimum potential energy equilibrium equation is expressed in Equation 4.19.

$$\delta\Delta E = \delta\Delta W - \delta\Delta L = 0 \qquad \text{…….. (4.19)}$$

The strain energy (ΔW) is defined in Equation 4.20 where integrations are over the volume of the body represented by Vol.

$$\Delta W = \frac{1}{2}\int_{Vol}\{\Delta\varepsilon\}^T\{\Delta\sigma\}\,dVol = \frac{1}{2}\int_{Vol}\{\Delta\varepsilon\}^T[D]\{\Delta\varepsilon\}\,dVol \quad \text{... (4.20)}$$

The work done by applied loads (ΔL) consists of work input from body forces and surface tractions and is expressed as shown in Equation 4.21 where; $\{\Delta d\}^T = \{\Delta u, \Delta v\}$ is the displacement vector; $\{\Delta F\}^T = \{\Delta F_x, \Delta F_y\}$ is the body force vector; and $\{\Delta T\}^T = \{\Delta T_x, \Delta T_y\}$ is the surface traction vector. Srf represents the integration over the part of the domain which surface tractions are applied.

$$\Delta L = \int_{Vol}\{\Delta d\}^T\{\Delta F\}\,dVol + \int_{Srf}\{\Delta d\}^T\{\Delta T\}\,dSrf \quad \text{..... (4.21)}$$

A combination of Equations 4.19 - 4.21 gives an equation for the total potential energy of the body and this is expressed as a sum of the potential energies of the contributing elements. The volume integral for this equation is over the volume of the element and the surface integral is over the portion of the element boundary subject to surface traction as shown in Equation 4.22. N is the number of elements.

$$\Delta E = \sum_{i=1}^{N}\left[\frac{1}{2}\int_{Vol}\left(\{\Delta d\}_n^T[B]^T[D][B]\{\Delta d\}_n - 2\{\Delta d\}_n^T[N]^T\{\Delta F\}\right)dVol - \int_{Srf}\{\Delta d\}_n^T[N]\{\Delta T\}\,dSrf\right] \quad \text{..... (4.22)}$$

Equilibrium is achieved by minimizing the potential energy with respect to the incremental nodal displacements over the mesh $\{\Delta d\}_n$ as shown in Equation 4.23.

$$\delta\Delta E = \sum_{i=1}^{N}(\{\delta\Delta d\}_n^T)_i\left[\int_{Vol}[B]^T[D][B]dVol\,\{\Delta d\}_n - \int_{Vol}[N]^T\{\Delta F\}dVol - \int_{Srf}[N]^T\{\Delta T\}\,dSrf\right]_i = 0 \quad \text{..... (4.23)}$$

The expression as shown in Equation 4.23 can be represented in the form of Equation 4.24. $[K_E]$ is the element stiffness matrix and $\{\Delta R_E\}$ is the right hand side load vector.

$$\sum_{i=1}^{N}[K_E]_i(\{\Delta d\}_n)_i = \sum_{i=1}^{N}\{\Delta R_E\} \quad \text{..... (4.24)}$$

$$[K_E] = \int_{vol}[B]^T[D][B]\, dVol \quad \text{..... (4.25)}$$

$$\{\Delta R_E\} = \int_{Vol}[N]^T\{\Delta F\}dVol + \int_{Srf}[N]^T\{\Delta T\}\, dSrf \quad \text{..... (4.26)}$$

The element equation can be summarized into an equation determining and summing the constituent element equations within a finite element in Equation 4.17 (Potts and Zdravkovic, 1999). In order to evaluate the equations of the element stiffness matrix and the right hand side load vector, integration of the equations must be carried out. An evaluation of this form of integration cannot usually be carried out explicitly. Therefore, a numerical approach is adopted for solutions.

$$[K_E]\{\Delta d\}_n = \{\Delta R_E\} \quad \text{..... (4.27)}$$

The number of integration points determines the integration order and the higher the order, the more accurate the result. The number of functions evaluated also depends on the integration point thus demanding higher computing capacity for greater accuracy. It is more convenient to restrict evaluations of stress and strains to integration points as the stiffness matrix is determined by numerical integration, and the element equations are referred to integration points (Potts and Zdravkovic, 1999).

Several numerical integration approaches have been established. However, Potts and Zdravkovic (1999) identified the Gaussian integration scheme as the most commonly used numerical integration scheme. The integration points within the Gaussian integration scheme are identified as the Gauss points. The integration order in this scheme depends on the shape and type of element being used in the analysis.

To achieve solutions to problems within a domain the element equations within that domain are assembled into a global equation where $[K_G]$ is the global stiffness matrix; $\{\Delta d\}_{nG}$ is a vector containing the unknown nodal displacements for the entire finite elements within the domain; and $\{\Delta R_G\}$ is the global right hand side load vector as shown in Equation 4.28.

$$[K_G]\{\Delta d\}_{nG} = \{\Delta R_G\} \qquad \text{…….. (4.28)}$$

The element stiffness matrix is assembled into the global stiffness matrix and the terms are obtained through summing the individual element contribution, while taking into account the degree of freedom or nodal displacement common between elements. The terms of the right hand side load vector are obtained through summing the individual loads acting on each node.

4.3.4. Boundary Conditions

A loaded body or structure will undergo unlimited rigid body motion unless constraints are imposed to keep the body or structure in equilibrium. The boundary conditions are introduced to define a boundary value problem making it possible to achieve a solution in equilibrium.

Two types of boundary conditions, the forced or geometric and the free or natural can be imposed (Rao, 2005, Anandarajah, 2010). A combination of these types of boundary conditions is used in achieving a solution to finite element problems. Boundary conditions are controlled by the loads and displacements that finite elements may be subjected to within the domain.

Loading inputs that include loading conditions, line load, and surcharge pressure, affect the right hand side of the global system of element equation. Loading inputs into the right hand side load vector $\{\Delta R_G\}$ are prescribed as force (Equation 4.28), thus pressure boundary conditions must be expressed as equivalent nodal force to be assembled into the right hand side load vector (Potts and Zdravkovic, 1999).

Displacement boundary conditions and inputs affect the vectors containing unknown nodal displacements$\{\Delta d\}_{nG}$ (Equation 4.28). In analysis, sufficient displacement conditions required in achieving a rigid body mode of deformation such as rotation or translation must be prescribed. In conditions of insufficient displacement, the global stiffness matrix will be singular and the equation cannot be solved.

4.3.5. Solutions

The global equations assembled with the boundary conditions form a large system of simultaneous equations. These simultaneous equations are solved to give the values of the unknown nodal displacements. Several mathematical techniques used in solving a large system of simultaneous equations exist. However, most finite element programs adopt a technique based on Gaussian elimination in the evaluation of a large system of simultaneous equations (Potts and Zdravkovic, 1999).

Secondary quantities such as strain and stress are determined after the primary quantities are determined. A combination of the nodal displacement values obtained in the analysis and equations representing material relationships are evaluated to achieve values of the secondary quantities.

4.3.6. Non-linear theory

In non-linear behaviour, the constitutive matrix [D] is not constant but varies with stress or strain. Consequently, in a non-linear finite element analysis, a technique to accommodate the change in the constitutive matrix must be developed to represent more accurately the behaviour of the material.

The basic strategy developed involves applying the boundary conditions incrementally. The incremental application of the boundary conditions modifies the finite element global equation to take account of the increments and is expressed as shown in Equation 4.29 where $[K_G]^i$ is the incremental global stiffness matrix; $\{\Delta d\}_{nG}{}^i$ is a vector containing

incremental nodal displacements; $\{\Delta R_G\}^i$ is the vector of incremental nodal forces; and i is the increment number.

$$[K_G]^i\{\Delta d\}_{nG}{}^i = \{\Delta R_G\}^i \quad \text{…….. (4.29)}$$

The change in the boundary conditions is applied in a series of increments during the analysis, and for each increment, Equation 4.29 must be solved. As a result of the non-linear constitutive behaviour, the incremental global stiffness matrix will be based on the current increment stress and strain levels thus varying over the loading process. This implies that the element stiffness matrix within a specific increment depends on the stress and strains determined at the preceding increment.

A cumulative result of the increments after the final increment presents a solution to a non-linear problem. Several different techniques have been developed to accommodate the change in the constitutive matrix including the tangent stiffness method, the visco-plastic method, and the modified Newton-Raphson method (Potts and Zdravkovic, 1999).

4.3.7. Stress Analysis

Stresses in soil are analysed in terms of either the total stress or the effective stress and pore pressure. The relationship that exists between the total stresses, effective stress, and pore pressure is expressed in the principal of effective stress. Equation 4.30 is the principal of effective stress equation where $\{\Delta\sigma\}$ is the total stress, $\{\Delta\sigma'\}$ is the effective stress and $\{\Delta\sigma_f\}$ is the pore pressure. Equation 4.32 represents a fully drained analysis.

$$\{\Delta\sigma\} = \{\Delta\sigma'\} + \{\Delta\sigma_f\} \quad \text{…….. (4.30)}$$

$$\{\Delta\sigma_f\} = \{\Delta p_f \ \Delta p_f \ \Delta p_f \ 0 \ 0 \ 0\}^T \quad \text{…….. (4.31)}$$

$$\{\Delta\sigma\} = \{\Delta\sigma'\} \quad \text{…….. (4.32)}$$

In undrained analysis, the solid and fluid phase deform together thus on the larger scale the strains in the solid and fluid are assumed to be equal. The stress component in Equation 4.30 is equated to strain through the equation defining material constitutive behaviour in Equation 4.17 to give Equations 4.33 and 4.34. Substituting Equations 4.17, 4.33 and 4.34 into Equation 4.30 results in Equation 4.35 where $[D]$ is the constitutive matrix in terms of total stress; $[D']$ is in terms of effective stress; and $[D_f]$ in terms of pore pressure.

$$\{\Delta\sigma'\} = [D']\{\Delta\varepsilon\} \qquad \text{…….. (4.33)}$$

$$\{\Delta\sigma_f\} = [D_f]\{\Delta\varepsilon\} \qquad \text{…….. (4.34)}$$

$$[D] = [D'] + [D_f] \qquad \text{…….. (4.35)}$$

However, $[D_f]$ is related to the bulk modulus of the pore fluid K_f. In a two phase fluid such as may occur in a partially saturated soil, $[D_f]$ can be presented as shown in Equation 4.36 where K_e, the equivalent bulk modulus of pore fluid, is a constant, 1_3 is a 3x3 matrix of 1s, and 0_3 is a 3x3 null matrix.

K_f is related to K_e as presented in Equation 4.37 where n is the soil porosity, and for saturated material, Equation 4.38 (Naylor, 1974) apply. Consequently, in the consideration of effective stress, pore pressure, and total stress, instead of specifying $[D]$ in a finite element analysis, a direct combination of the pore fluid equivalent bulk modulus K_e and the constitutive matrix in terms of effective stress $[D']$ is specified for analysis. K_e is used in calculating the change in pore pressure values from Equation 4.39 where Δp_f is an increment in pore pressure and $\Delta\varepsilon_v$ is the volumetric strain.

$$[D_f] = K_e \begin{bmatrix} 1_3 & 0_3 \\ 0_3 & 0_3 \end{bmatrix} \qquad \text{…….. (4.36)}$$

$$K_e = \frac{K_f}{n} \qquad \text{…….. (4.37)}$$

$$K_e = K_f \qquad \text{…….. (4.38)}$$

$$\Delta\varepsilon_v = \frac{\Delta p_f}{K_e} \qquad \text{…….. (4.39)}$$

4.3.8. Soil-Structure Interaction

Most problems in geotechnical engineering would involve some interaction between soil and structure. Typical soil and typical structure materials characteristically have different properties that lead to significantly different constitutive behaviour. In soil-structure interactions problem with sufficient displacements, relative movement occur with respect to the soil and the structure.

Continuum within the elements and compatibility of displacements prevents relative displacement of elements at common nodes and consequently soil-structure interaction behaviour. To accommodate this constraint, interface elements are used to model the soil-structure boundary (Boulon and Nova, 1990, Viladkar et al., 1994). The interface element presents the ability to vary the constitutive behaviour of the interface and allow differential movement of the adjoining elements (Potts and Zdravkovic, 1999).

Several methods have been proposed for the analysis of interface properties including the use of thin continuum elements, use of linkage elements, hybrid method where the soil and structure are modelled separately and linked through constraint equations for compatibility, and use of special joint element with zero or finite thickness (Potts and Zdravkovic, 1999).

4.4. Finite Element Software

The principles of the finite element method have been adopted in the development of numerous computer software programs for commercial purposes or private use. The commercially available finite element software have the added advantage of being more widely used by professionals and academics, and consequently more independently tested in its application. The rapidly growing list of commercially available finite element software include the general application type of finite element software such as ABAQUS that may be adopted for use in most engineering problems (ABAQUS, 2000), as well as more specialized type of finite element software such as SAP2000 for structural engineering analysis and Plaxis for geotechnical engineering analysis.

The general application software is a useful tool in the analysis of engineering problems that cut across different fields of engineering. However, these software are least specialized in some specific application when compared to other specialized software. They are less flexible than the more specialized software in direct application over a specific problem and may therefore require the development of other specialized codes. This usually would require an extensive validation process, demanding time and resources to build confidence for its use. The general application software are often less suitable than a specialized software in solving practical problems within such specific fields.

Several specialized geotechnical engineering software have also been developed including, Frew by Oasys Limited, Arup Group, UK, SVSoild by soil vision systems Ltd, Canada, Plaxis 2D by Plaxis bv, Netherlands (Smadi, 2012). However, Plaxis is a popular software that has featured as an effective tool in the analysis of many geotechnical engineering problems. It has the advantage of being one of the oldest commercially available geotechnical finite element software, having been in development and use since 1987 (Brinkgrene et al., 2008).

Plaxis finite element software program has been extensively used for geotechnical engineering analysis, providing valid results in academic research. Several articles published on geotechnical engineering research identify Plaxis as the finite element software used in analysis. It has been used in seeking solutions to several geotechnical problems and research studies including problems in soil-structure interaction, consolidation, and slope stability analysis (Abusharar et al., 2009, Demir et al., 2009, Lovisa et al., 2010, Tan, 2008, Hammouri et al., 2008, Howard and Warren, 2009, Gong and Zhao, 2009, Cui and Zhou, 2009).

4.4.1. Plaxis Software

The Plaxis code incorporates models of structural behaviour and soil that can be used to simulate the behaviour of soil and soil-structure interaction. The software is specially equipped with programs designed to model the constitutive relationships that can be used in

simulating non-linear and time-dependent behaviour of soils (PLAXIS, 2010b). Plaxis software is also equipped with special procedures in dealing with hydrostatic and non-hydrostatic pore pressures as characterized by soil.

Plaxis has been used extensively to generate high quality research outputs that have been found to closely match results obtained using other analytical approach as was demonstrated in the slope stability analysis by (Hammouri et al., 2008). Results from Plaxis have also been found to closely match results obtained using laboratory based approach as demonstrated in the study of the behaviour of geotextile-reinforced sand bed by (Lovisa et al., 2010), and results obtained from actual measurements taken on site as demonstrated in the modelling of an instrumented flexible pavement by Howard and Warren (2009) .

The finite element analysis in this research is carried out using the Plaxis code and its soil models. Plaxis 2D version 9.0 used in this research offers soil model options including linear elastic and perfectly plastic soil behaviour, and variants of the hyperbolic soil model behaviour.

4.4.2. Plaxis Soil Models

Soil modelling using the finite element approach consists of a set of mathematical equations, integrated into the finite element software code, to generate outputs that replicate the expected behaviour a soil with specific characteristics would generate. These equations take into consideration parameters that significantly influence some specific behaviour of the soil, under specific conditions, to generate an expected output.

Several types of soil models are available with increasing complexities or simplicity. An increase in the complexity or simplicity of the soil model will certainly change the cost of analysis but may not generate a more relevant result. Therefore, the relevant characteristics of the soil type and the governing features and parameters are carefully considered in order to determine a suitable soil model.

Soils behaviour is generally non-linear under loading. However, specific characteristic behaviours of soil may be modelled using linear or non-linear models under simulated loading. Plaxis uses a number of soil models offering several levels of sophistication in modelling the behaviour of soil. The Plaxis Mohr Coulomb model can be generally considered as a first order approximation for soil behaviour and can be used for a quick assessment in modelling. A review of the Mohr Coulomb model as constituted in Plaxis 2D version 9.0 is presented in Section 4.4.2.2 below.

Undrained behaviour in Plaxis may be modelled using the undrained effective stress analysis or the undrained total stress analysis. The undrained effective stress analysis considers the effective stress and pore pressure distinctively in analysis. This enables undrained analysis to be executed with effective stress input parameters. The undrained total stress analysis requires undrained parameters in analysis and generates outputs in total stress (PLAXIS, 2010a).

4.4.2.1. Soil Model Review

The Plaxis code supports a number of soil models including the elastic perfectly plastic Mohr Coulomb soil model and other more sophisticated models that highlight different properties of soil and models several other characteristics. The behaviour of these models is controlled by parameters that identify specific characteristics, and the governing equations designed to relate these parameters in a certain way.

Soil parameters required in analysis within the Plaxis soil models include: Young modulus, E, Axial stress / axial strain in uniaxial compression or extension test where radial stress is constant ($d\boldsymbol{\sigma}_a / d\varepsilon_{a)}$; Secant modulus at 50% of the material strength, E_{50}^{ref} (Secant stiffness in standard drained triaxial test); Oedometer modulus, E_{oed}^{ref}; Unloading and reloading stiffness, E_{ur}^{ref}; Poisson's ratio, v, Radial strain / axial strain in uniaxial compression or extension test where radial stress is constant ($- d\varepsilon_r/d\varepsilon_a$); Poisson's ratio for unloading, v'_{ur}; Angle of internal friction, $\boldsymbol{\phi}'$; Cohesion, c'; Dilatancy, ψ; Power for stress-level dependency of stiffness, m; Initial void ratio, e_{int}; Reference shear modulus at very small strain, G_0^{ref}; Threshold shear strain, $\gamma_{0.7}$; Modified compression index, λ^*; Modified swelling index, κ^*;

Modified creep index, μ*; Cam clay compression index, λ; Cam clay swelling index, κ; Slope of critical state line, M (PLAXIS, 2010a, PLAXIS, 2010b).

These soil models in Plaxis are designed to simulate various characteristics of the soil. The Mohr Coulomb model simulates elastic and perfectly plastic soils behaviour, with a fixed yield value at which the soil exhibits a perfectly plastic behaviour, and before which the behaviour is assumed perfectly elastic.

The hardening soil model is designed to model the elasto-plastic behaviour of soils with decreasing stiffness, irreversible plastic straining under loading, and a shifting yield value below which the behaviour is perfectly elastic in unloading and reloading. The Hardening Soil model with small strain stiffness is developed based on the Hardening soil model and performs accordingly but is in addition enhanced to capture the soil behaviour at infinitesimal strains.

The Soft Soil Creep (Time dependent behaviour) model is an elasto-plastic model designed to capture the special features of soft soil secondary (time dependent) compression. The Soft Soil model is an elasto-plastic model designed to simulate the behaviour of soft soils. The Modified Cam-Clay model is an elasto-plastic model based on the modified cam-clay soil model principle as developed by (Roscoe and Burland, 1968) cited in (Anandarajah, 2010).

A review of the composition of the Modified Cam-Clay soil model highlights its shortcomings in analysing problems involving cyclic loading. The integral bridge abutment backfill material is subjected to cyclic loading. Consequently, the behaviour of the backfill soil materials and loading pattern in an integral bridge model may not be accurately modelled using the modified Cam-Clay soil model.

Integral bridge backfill and foundation materials typically include soils not classified as soft soils. A basic feature of the Soft Soil models is the linear stress dependency of stiffness. This feature may not be applicable in modelling the varying material types that constitute the integral bridge backfill and foundation soils. As a result, the behaviour of the backfill

soil materials in an integral bridge model may not be accurately modelled using the Soft Soil and the Soft Soil Creep model.

The Mohr Coulomb model does not take into consideration irrecoverable soil deformation on loading under the yield stress value. The model only assumes perfectly plastic straining at the yield stress value. The Mohr Coulomb model is consequently not suitable in accurately modelling the soil properties of the materials surrounding a typical integral bridge.

The Hardening Soil model and the Hardening Soil model with small strain stiffness are models based on the same principles. However, the Hardening Soil model with small strain stiffness is enhanced to capture soil behaviour at infinitesimal strains. The Hardening Soil model with small strain stiffness requires inputs resulting from very small strain values (usually in the order of 0.001%) and cannot be realistically observed or measured in the loading of an integral bridge. Strains generated from an integral bridge loading typically occur within the range of the retaining walls and foundations limits illustrated in Figure 3.3.

The limitations associated with sourcing of the model parameter values for modelling in a post construction analysis also limits the flexible use of several relevant models in simulation. The Hardening Soil model as formulated by Plaxis, within this research, is considered the best model for simulating the relevant features of the soil behaviour, originating from a combination of different soil types subjected to cyclic loading. The combination of soil parameters that constitute the soil model equations account for the characteristics considered relevant in determining the soil behaviour, and consequently most realistically model the features these soil combination may exhibit as a continuum. The Hardening Soil model is therefore used in developing the integral bridge soil models and modelling the behaviour under loading. The parameters values required by the Hardening Soil model, within the context of this research are available. A review of the Hardening soil model as constituted in Plaxis 2D version 9.0 is presented in Section 4.4.2.3.

4.4.2.2. Mohr Coulomb Model (Perfect plasticity)

The Mohr Coulomb model in Plaxis is a material soil model designed to simulate an elastic perfectly plastic behaviour. The onset of plasticity is identified by a fixed yield boundary. Values of stress below the fixed yield value result in perfect elastic behaviour and reversible strains. Strains and strain rates are made up of the elastic and plastic components as shown in Figure 4.3. Plasticity in this model is defined by the Mohr Coulomb failure criteria. The Mohr Coulomb failure criteria can be defined as shown in Equations 4.40 and 4.41.

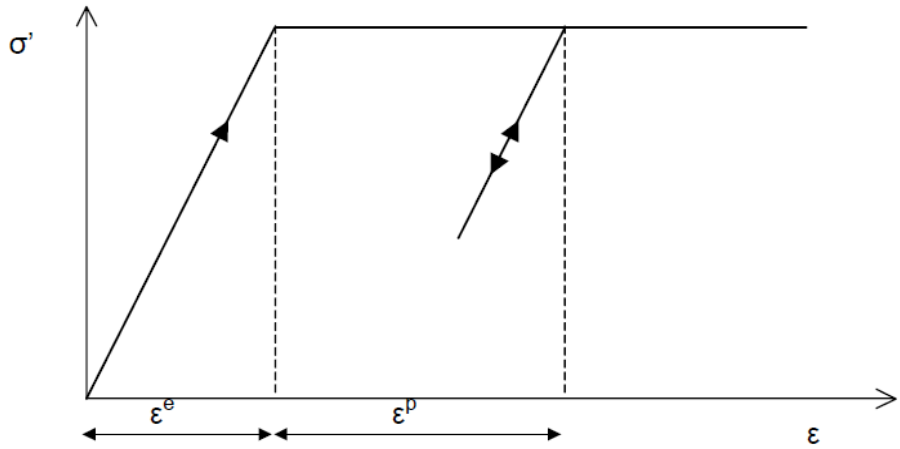

Figure 4.3: Stress strain representation of an elastic perfectly plastic model (PLAXIS, 2010a).

$$\tau = c' + \sigma' \tan \phi' \quad \text{..... (4.40)}$$

$$\frac{1}{2}(\sigma'_2 - \sigma'_3) = \frac{1}{2}(\sigma'_2 + \sigma'_3)\sin\phi' + c' \cos\phi' \quad \text{..... (4.41)}$$

The failure criteria can be represented by the six functions presented in Equations 4.42 - 4.47 when formulated with respect to the principal stresses. The condition in which all the functions are zero presented together represent a hexagonal cone in principal stress space as shown in Figure 4.4.

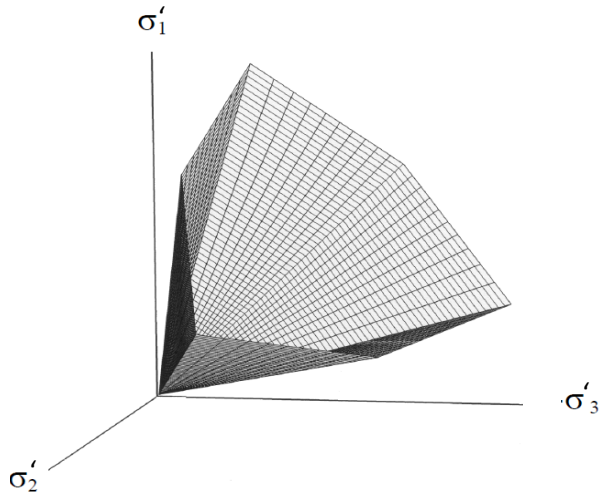

Figure 4.4: Mohr-Coulomb failure surface in principal stress space where c = 0. Modified (PLAXIS, 2010a).

$$f_{1a} = \frac{1}{2}(\sigma'_2 - \sigma'_3) + \frac{1}{2}(\sigma'_2 + \sigma'_3)sin\phi' - c'\,cos\phi' \leq 0 \quad \text{..... (4.42)}$$

$$f_{1b} = \frac{1}{2}(\sigma'_3 - \sigma'_2) + \frac{1}{2}(\sigma'_3 + \sigma'_2)sin\phi' - c'\,cos\phi' \leq 0 \quad \text{..... (4.43)}$$

$$f_{2a} = \frac{1}{2}(\sigma'_3 - \sigma'_1) + \frac{1}{2}(\sigma'_3 + \sigma'_1)sin\phi' - c'\,cos\phi' \leq 0 \quad \text{..... (4.44)}$$

$$f_{2b} = \frac{1}{2}(\sigma'_1 - \sigma'_3) + \frac{1}{2}(\sigma'_1 + \sigma'_3)sin\phi' - c'\,cos\phi' \leq 0 \quad \text{..... (4.45)}$$

$$f_{3a} = \frac{1}{2}(\sigma'_1 - \sigma'_2) + \frac{1}{2}(\sigma'_1 + \sigma'_2)sin\phi' - c'\,cos\phi' \leq 0 \quad \text{..... (4.46)}$$

$$f_{3b} = \frac{1}{2}(\sigma'_2 - \sigma'_1) + \frac{1}{2}(\sigma'_2 + \sigma'_1)sin\phi' - c'\,cos\phi' \leq 0 \quad \text{..... (4.47)}$$

The basic parameters of the Mohr Coulomb model in Plaxis include; Angle of dilatancy, ψ in degrees; Angle of internal friction, $\boldsymbol{\phi}'$ in degrees; Cohesion, c' in kN/m^2; Poisson's ratio, v'; and Young's modulus, E in kN/m^2. Alternative stiffness parameters within this model include; Oedometer modulus, E_{oed}; and Shear modulus, G (Shear stress / Shear strain). Relationship between the oedometer modulus and Young modulus is presented in Equation 4.48. Equation 4.49 is the relationship between shear modulus and Young's Modulus.

$$E_{oed} = \frac{(1 - \nu')\,E'}{(1 - 2\nu')(1 + \nu')} \quad \text{..... (4.48)}$$

$$G = \frac{E'}{2(1 + \nu')} \quad \text{..... (4.49)}$$

4.4.2.3. Hardening Soil Model (Elasto-plastic)

When subjected to loading, soil shows decreasing stiffness and develops irreversible strain. The Hardening Soil model in Plaxis is designed to capture these soil properties. It simulates the elasto-plastic behaviour of soils. The yield surface in this model is not fixed in the principal stress space, changing as a result of plastic straining.

The Hardening Soil model Plaxis code is designed to simulate the behaviour of soft soils and stiff soil (Schanz and Vermeer, 1998). This model supersedes the popular hyperbolic material model (Duncan and Chang, 1970, Kondner, 1963) by introducing soil dilatancy and a yield cap (PLAXIS, 2010a). Features of this model includes a hyperbolic stress strain relationship, dilatancy, stress dependent stiffness according to a power law, plastic straining due to primary deviatoric loading, plastic straining due to compression, elastic unloading and reloading, observed yield cap, and failure according to the Mohr Coulomb model.

The Hardening Soil model is based on the hyperbolic relationship between vertical strain and deviatoric stress in a primary triaxial loading. In a standard drained triaxial test, the curves can be described by Equation 4.50 where the deviatoric stress q, is less than that at failure, q_f, and ε_1 is the strain.

$$\varepsilon_1 = \frac{q}{E_i - (E_i q / q_a)} \quad \text{..... (4.50)}$$

The asymptotic value of the shear strength is q_a and E_i is the initial stiffness. E_i and E_{50} are related by Equation 4.51. This relationship is graphically represented in Figure 4.5. E_{50} is the confining stress dependent stiffness modulus, dependent on stress for primary

loading and can be derived by Equation 4.52 with E_{50}^{ref} being a reference stiffness modulus corresponding to the reference confining pressure p^{ref}, and m being the power that defines the amount of stress dependency. p^{ref} has a default value equal to a hundred stress units.

Equations 4.53 and 4.54 respectively define the deviatoric stress at failure and the asymptotic value of the shear strength. q_f is derived from the Mohr Coulomb failure criterion. Where q is equal to q_f, the failure criterion is satisfied and the stress strain relationship becomes perfectly plastic. In Plaxis, the ratio between q_f and q_a is given by the failure ratio R_f with a default value of 0.9 (see Figure 4.5).

$$E_i = \frac{2E_{50}}{2-R_f} \qquad \text{…….. (4.51)}$$

$$E_{50} = E_{50}^{ref}\left(\frac{c'\cos\phi' - \sigma'_3\sin\phi'}{c'\cos\phi' + p^{ref}\sin\phi'}\right)^m \qquad \text{…….. (4.52)}$$

$$q_f = (c'\cot\phi' - \sigma'_3)\frac{2\sin\phi'}{1-\sin\phi'} \qquad \text{…….. (4.53)}$$

$$q_a = \frac{q_f}{R_f} \qquad \text{…….. (4.54)}$$

E_{50}^{ref} in Equation 4.52 is substituted by E_{ur}^{ref} to describe the relationship for the stress dependent stiffness modulus, E_{ur} for unloading and reloading as shown in Equation 4.55. E_{ur}^{ref} is the referenced Young's modulus for unloading and reloading corresponding to the reference pressure, p^{ref}.

$$E_{ur} = E_{ur}^{ref}\left(\frac{c'\cos\phi' - \sigma'_3\sin\phi'}{c'\cos\phi' + p^{ref}\sin\phi'}\right)^m \qquad \text{…….. (4.55)}$$

$$E_{oed} = E_{oed}^{ref}\left(\frac{c'\cos\phi' - \frac{\sigma'_3}{K_0^{NC}}\sin\phi'}{c'\cos\phi' + p^{ref}\sin\phi'}\right)^m \qquad \text{…….. (4.56)}$$

In Plaxis E_{ur}^{ref} is set to $3E_{50}^{ref}$ by default. The relationship between E_{oed}^{ref} and E_{oed} is defined by Equation 4.56. E_{oed}^{ref} is the referenced tangent stiffness modulus corresponding to the reference pressure, p^{ref}.

The basic parameters for the Plaxis Hardening Soil model include: Cohesion, c' in kN/m^2; Angle of internal friction, ϕ' in degrees; Angle of dilatancy, ψ in degrees, Secant stiffness in standard drained triaxial test, E_{50}^{ref} in kN/m^2; Tangent stiffness for primary oedometer loading, E_{oed}^{ref} in kN/m^2; Unloading and reloading stiffness, E_{ur}^{ref} in kN/m^2; Power of stress level stiffness dependency, m. Alternative stiffness parameters include; Compression index, C_c; Swelling index C_s; Initial void ratio e_{init}.

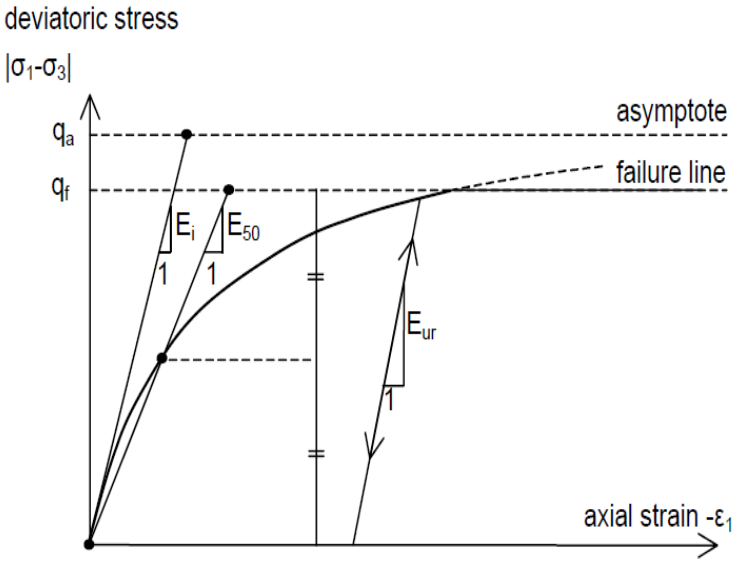

Figure 4.5: Hyperbolic stress strain relationship. Modified (PLAXIS, 2010a).

Plaxis Hardening soil model is capable of effectively modelling a combination of soft and stiff soil behaviour as may be found constituting the foundation and backfill soil of an integral bridge. It is therefore used in developing a model of an instrumented integral bridge identified for this study. Undrained behaviour is modelled using Plaxis undrained effective stress analysis in the Hardening Soil model.

4.4.3. Plaxis Structure Modelling

Structures and structural behaviour may be modelled in Plaxis by the use of either one of or any combination of plates, hinges and rotation springs, tunnels, node to node anchor and fixed end anchor. See Plaxis reference manual for more details (PLAXIS, 2010b). The choice of the structure model to be used in modelling is significantly dependent on the characteristics of the effect of the structure on the soil that is relevant in the modelling.

The presence and effect of these structural members in the analysis can be controlled. This implies that structures or parts of structures can be introduced or eliminated gradually in successive phases of analysis to simulate construction processes. Structural model used in this research include the plates, hinges, and node to node anchor.

The node to node anchor is a two node elastic spring element that models the ties between two points. This spring element is allocated a constant spring normal stiffness that can be subjected to tensile and compressive forces. The maximum forces that this element may be subjected to can be introduced to simulate maximum capacity beyond which failure occurs (PLAXIS, 2010b).

Plates are used to model the effects on the soil of relatively slender structures with significant flexural rigidity and normal stiffness. The structural geometry of plates in not replicated in Plaxis but the influence of the structure on the soil is simulated. Plates are represented in Plaxis by a line. Hinges and rotation spring is a plate connection that prevents continuous rotation of linking plates at the point of connection thus acting like a hinge at point of connection (PLAXIS, 2010b).

4.5. Validation

Validating a model is not an attempt to provide a general seal of approval but is rather more of an indication of the level of confidence in the model's behaviour for a clearly defined purpose under specific conditions (Greenberger et al. (1976) cited in Ford (1999)). A

consequence of the use of modern computers in modelling is the increasing difficulty in validating and verifying the outputs of these complex analyses for confidence in their reliability. Several validation tests that may be used in modelling exist. Ford (1999) identified five of these tests as prominent among the others. These are; Verification test- where test is rerun in a completely independent manner from the original test run; Face validity test- where the test results are simply evaluated on how realistic and sensible they appear to be; Historical behaviour test- where the results generated by the model of a recorded case are comparable to the results that were recorded; Extreme behaviour test- where extreme conditions are tested to see if the model's results are plausible; Detailed model check test- where more detailed models are used to verify components of the results.

Replicating the historical behaviour by a model is one of the most common and important test and arguably the most convincing. Within the scope of this research, validation test carried out other than the replicating historical behaviour test, include the face validity test and the verification test as described by Ford (1999).

4.5.1. Modelling Errors

Reliable finite element simulation results primarily depend on an application of the right approach to modelling while limiting error that may also be cumulative. Errors within the finite element simulation arise from several contributing factors that can be generally grouped under the three segments that contribute to modelling. These are the data input factor, the computing input factor and the human input factor.

The data input factor error is controlled by values that may be measured or perceived. This includes the geometry definition, the material information and the environmental information. The certainty of the definition of the geometry and the value of the material and environmental information gathered, together with the use of all the relevant input parameter components in modelling is a prerequisite for a reliable modelling result.

The computing unit introduces computing input factor error. This error may be cumulative in the course of an analysis and may become substantial. It is affected mainly by the

capacity and capabilities of the computer used in the analysis. The human input factor error is directly attributed to the errors introduced by the human operator of the model. This may range from the conscious choices made in the cause of the simulation to the unconscious omissions that adversely affect the accuracy of the outputs.

A primary characteristic of modelling is the simplification of actual events. Consequently, several assumptions are made. It is vital to critically analyse these assumptions to verify that they predominantly reflect the actual circumstance being modelled as accurately as possible in order to generate useful results.

4.5.2. Simulation Steps

A successful simulation process generally complies with a defined pattern commencing with the case assessment, and a series of implementations, evaluations and reviews. The process typically starts with a problem review where the aim of the modelling process is determined. A review of the available data and software capability/flexibility is considered in determining the approach necessary to achieve the aim of the model. The model is setup accordingly and tested in order to appreciate the pattern of results generated.

The model may be calibrated or validated by adjusting the approach or parameters with flexibilities to refine the outputs. The model is then used for the purpose it was designed for and the results are analysed for its sensible representation of reality. Figure 4.6 show a flow chart inspired from a presentation by Wicks (2011). The chart summaries the steps of modelling also discussed in details by Ford (1999).

The preceding steps identified within the flow chart are usually reviewed at the decision points. Ford (1999) acknowledged the iterative, trial and error process, built up in steps of increasing complexities, involved in setting up a model capable of replicating the observed behaviour of a system.

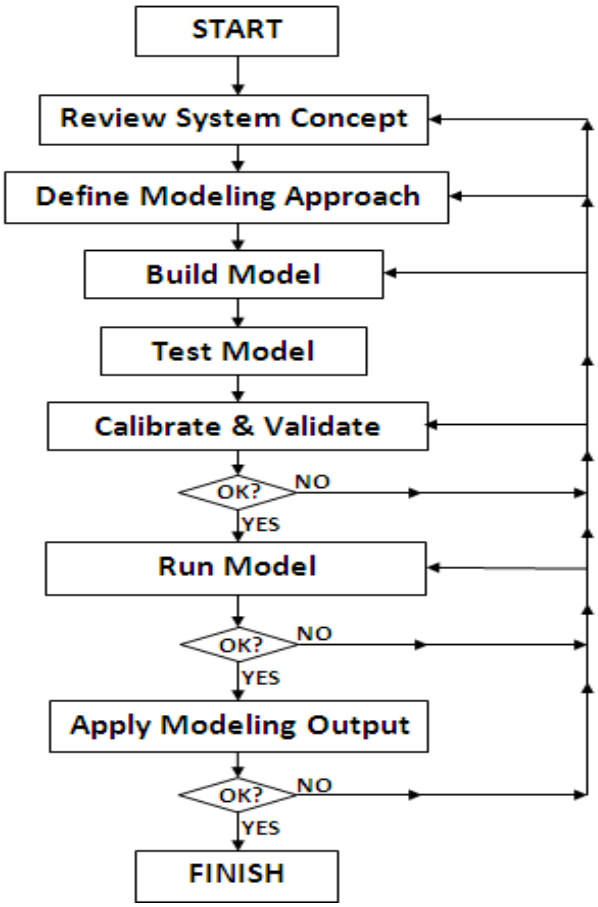

Figure 4.6: Modelling flow chart.

4.5.3. Validation Conclusion

Models are based on simplification of complex systems for the primary reason of appreciating specific characteristics. Models therefore exclude factors considered least relevant and focus on the interaction of factors considered relevant. Consequently, the characteristic of modelling is to generate results without the impact of certain factors otherwise present in real cases. Modelling therefore generates little more than a useful and illuminating support base towards understanding a real case, and should be considered accordingly. Perhaps the most important fact in a modelling simulation is that the perceived accuracy and validity of the results are dependent on how the result is to be used.

A review of published literature on analysis of soil behaviour in geotechnical engineering reveals an increasingly large number of successful studies carried out using the finite

element method. Studies using the finite element method on integral bridge have been carried out by authors including (Civjan et al., 2007) - in evaluating the integral bridge structure, (Khodair and Hassiotis, 2005) - in soil pile interaction, and (Pugasap et al., 2009) - in predicting soil pressure. Results generated using the finite element models were found to be similar to results measured by other conventional methods.

4.6. Summary

This chapter briefly described the numerical method and its application in analysis. A brief description of the more commonly used numerical methods was presented. The fundamental principle of the finite element method approach adopted in this research was highlighted. An overview of computer software - Plaxis, based on the finite element method, was also presented together with details of the relevant Plaxis software's structure and soil model applications. The validation of the modelling output was discussed.

Implementation of the principles of the finite element method as discussed in this chapter is reported in the next chapter. The process of modelling of an integral bridge and the simulation of the backfill loading is also presented in the next chapter. The results of the modelling outputs are validated using the principles discussed in this chapter.

Chapter 5 : INTEGRAL BRIDGE MODEL DEVELOPMENT

5.1. Introduction

The process of modelling an integral bridge presents several challenges, ranging through the choices of parameters to use in the analysis, to the appropriate approach to be adopted for simulation. It is important to generate a model that is as realistic as possible. In order to achieve this, a number of assumptions have to be made in relation to the soil properties, the constitutive model, the geological profile, and modelling of the construction processes.

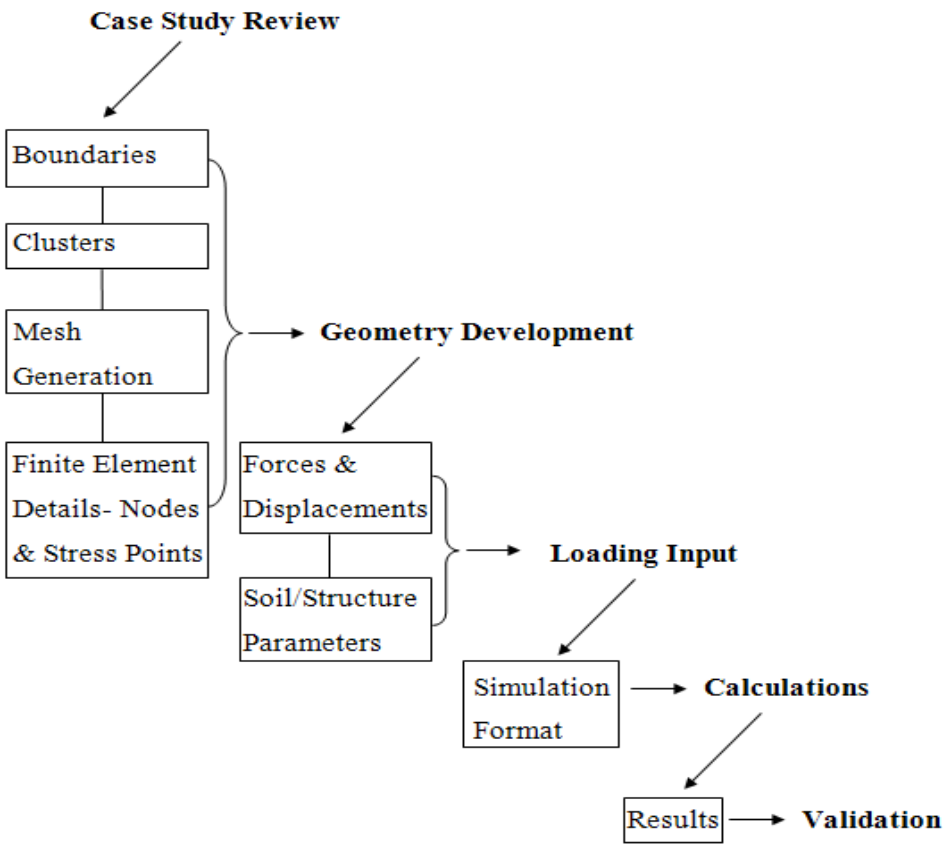

Figure 5.1: Illustration showing summary of model development flow

This chapter describes the process of developing a model integral bridge. The model development was achieved through the computer-aided application of the numerical

method using the finite element approach. This was implemented using the parameters of the structural members, and the parameters of the foundation and construction soil materials taken from a case study bridge. Abutment displacement in response to thermal loading was applied to establish the earth pressure response within the backfill soil. Figure 5.1 presents the path followed and the subjects considered in the development of this finite element model, starting at the case study review and ending at validation.

The problems encountered in the process of generating a realistic model are highlighted. The thought process and the principles behind the solution to these problems through the stages of the model development, construction and abutment displacement simulation are presented. Results generated by subjecting the model backfill soil to a similar loading process as in the actual bridge are presented. Validation of the output is discussed. The bridge structure, backfill and foundation soils are modelled using Plaxis finite element software (Plaxis 2D, Version 9.0).

5.2. Typical Integral Bridge Case Study

To provide a revised design guideline for long jointless (integral) bridges, the Finnish Road Administration commissioned research within the Institute of Earth and Foundation Structures in Tampere University of Technology (TUT) under the title "Jointless Bridge–Soil Interaction" 2002–2008. The research included the long-term field tests of the Haavistonjoki Bridge commencing in 2003 to 2008 (Nilsson, 2008, Kerokoski, 2006). The eastern abutment and deck of this bridge were instrumented during construction. Figure 5.2 show a picture of the Haavistonjoki Bridge. Figure 5.3 presents an illustration of the eastern abutment of this bridge section.

The Haavistonjoki Bridge is an integral bridge located along the Tampere–Jyväskylä highway in Finland. It is a 3 span slab bridge with a total span length of 50m and a total bridge width of 11m. An abutment height of 2.5m and thickness of 1.2m was constructed at the eastern end of the bridge span to support the bridge deck. Two pile columns, with a diameter of 710mm each, resting on rock were used as intermediate supports to the bridge

deck and abutment (see T3 and T4 in Figure 5.3). This bridge was constructed and instrumented in the summer of 2003.

Figure 5.2: Photograph of the Haavistonjoki Bridge after construction (Kerokoski, 2006)

The Haavistonjoki Bridge was built above an existing ground surface that consists of clayey silt to a depth of 5m at the location of the then proposed bridge eastern abutment. Below the clayey silt at this location is a thin layer of clay with a thickness of approximately 1m, and below that a 3.5m deep moraine layer beneath the clay. Beneath the moraine layer, rock is encountered. The bridge deck was built well above the existing ground surface requiring extensive backfilling. The backfill material consists of well compacted crushed rock to a fill height of approximately 5m above the existing ground level at the location of the eastern abutment. The ground water level was not observed but estimated (Kerokoski, 2006).

A total of 191 gauges were installed during the construction of the bridge to measure the performance of the bridge over time. Results obtained from the gauges included measurements of the bridge deck temperature, eastern abutment displacement, and earth

pressure. Figures 5.4 and 5.6 show a picture of some instruments attached to the bridge during construction. These results were used in developing a bridge model.

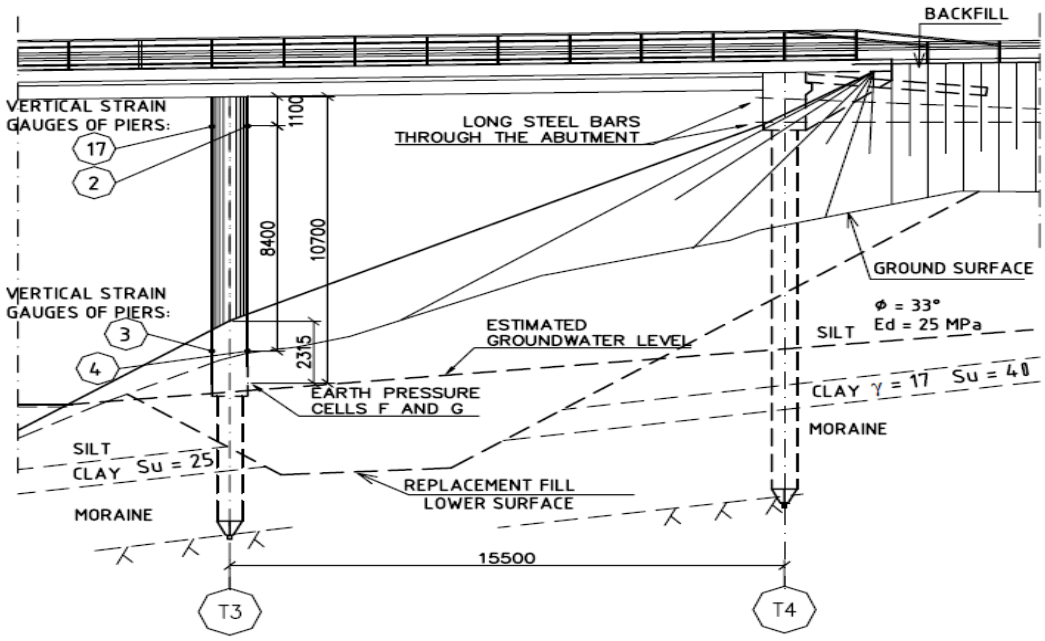

Figure 5.3: Technical illustration of the bridge deck cross section showing, the eastern abutment and pile (Kerokoski, 2006)

Figure 5.4: Bridge abutments showing laser distance-meter equipment and protruding end of steel bars (Kerokoski, 2006)

The changes in bridge length were measured by installing laser distance-meter equipment between the opposing abutments. Abutment displacements were measured using ten long steel bars installed at three levels through the eastern abutment (see Figure 5.3 and Figure 5.4).

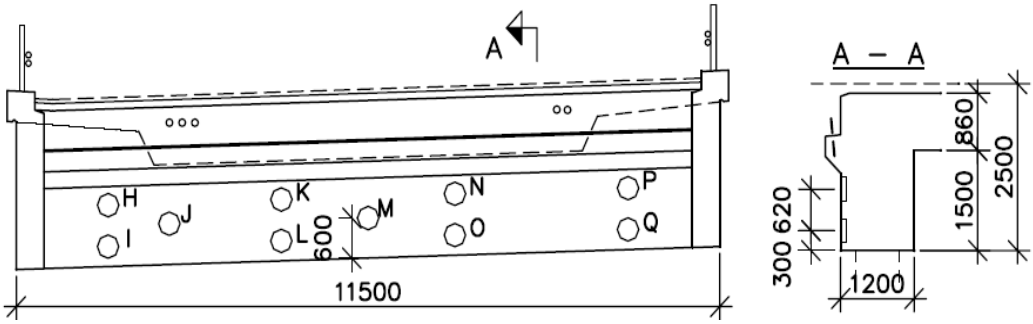

Figure 5.5: Technical illustration of bridge abutment section showing location of earth pressure cells (Kerokoski, 2006)

Figure 5.6: Photograph of bridge abutment showing location of earth pressure cells (Kerokoski, 2006)

Temperature gauges were installed within the deck slab, in the soil near the abutment piles, and within the backfill soil behind the abutments. Earth pressure cells embedded in the

concrete abutment were installed on the outer surface of the abutment wall behind the abutment and in contact with the backfill soil. These were used to measure the earth pressures developed in the backfill soil at the interface between the abutment and the backfill soil. The earth pressure cell locations are presented in Figures 5.5 and 5.6.

The graphs in Figures 5.7 and 5.8 were generated with information obtained from the measurement of the bridge performance over time. Figures 5.3 and 5.5 provide the relevant location codes used in Figures 5.7 and 5.8. Figure 5.7 shows the deck temperature and the recorded earth pressure from individual earth pressure cells at the abutment plotted against time (recorded dates). Figure 5.8 shows the displacement at the eastern abutment plotted against time (recorded dates).

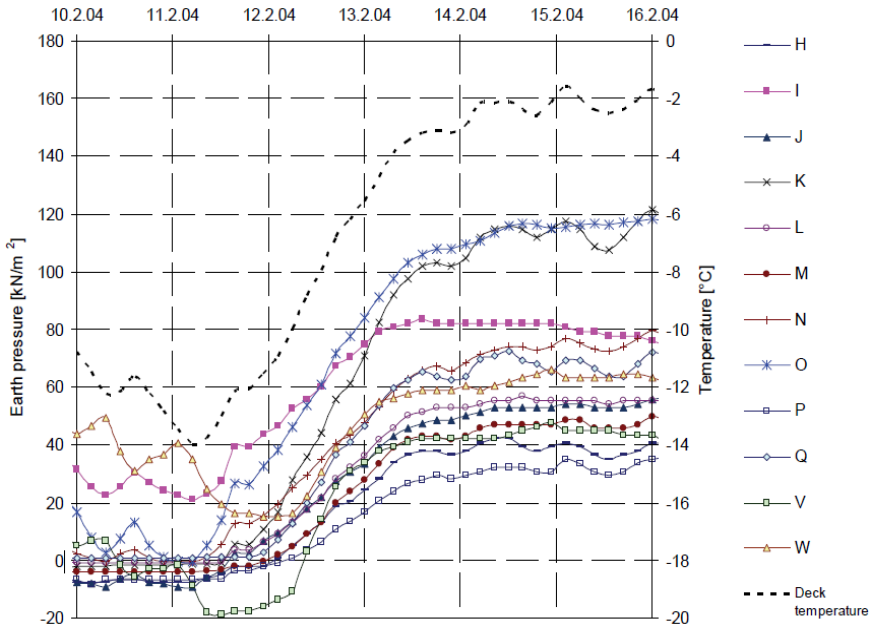

Figure 5.7: Graph of earth pressure and deck temperature against time (date) (Kerokoski, 2006)

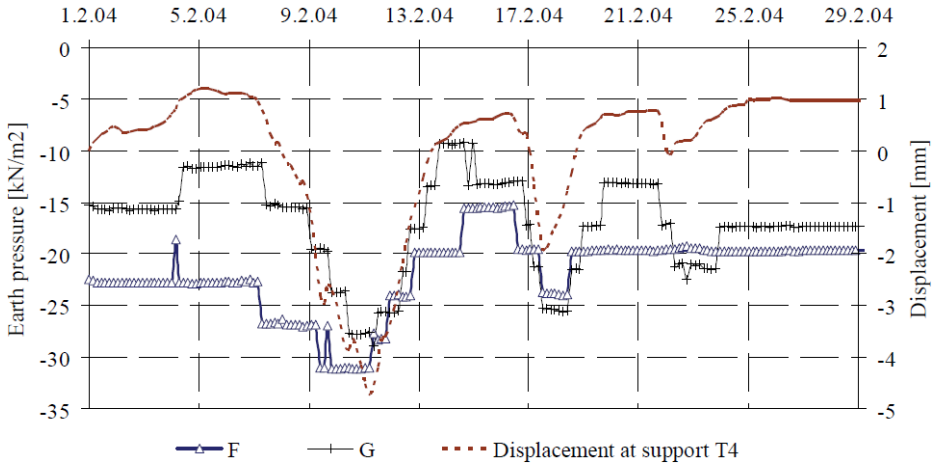

Figure 5.8: Graph of displacement against time (date) at abutment (Kerokoski, 2006)

The geometric and material properties of the bridge structure, foundation soils, and backfill soil used in developing the model integral bridge were taken from the published information about the Haavistonjoki Bridge (Nilsson, 2008, Kerokoski, 2006) highlighted in this section. The finite element model developed and used in this study was modelled after the eastern abutment of the Haavistonjoki Bridge. The temperature and the thermal induced eastern abutment displacement measured on site were used in developing the model abutment displacement. This information was used in simulating the integral bridge construction and thermal induced abutment displacement through time. Details of these are presented in Sections 5.3, 5.4 and 5.5.

5.3. Model Development

Construction of a typical integral bridge structure as described in Section 5.2 consists of several components including the foundation soil, backfill soil, bridge deck, and bridge abutment. The thermal induced displacement of an integral bridge abutment model therefore requires a complex system that considers several component models working together to sustain loads (see Figure 5.9). This section presents the process of creating the component models and the conditions under which they function as a unit. This includes developing a model of the integral bridge structure that consists of the geometric and material properties of the Haavistonjoki bridge abutment, deck, and piles as described in

Section 5.2. Models of the construction soils and the foundation soils are also required. The model of the construction soils consists of the geometric and material properties of the backfill and excavation fill material of the Haavistonjoki bridge, while the model of the foundation soils consist of the geological profile and material properties of the different foundation soil materials.

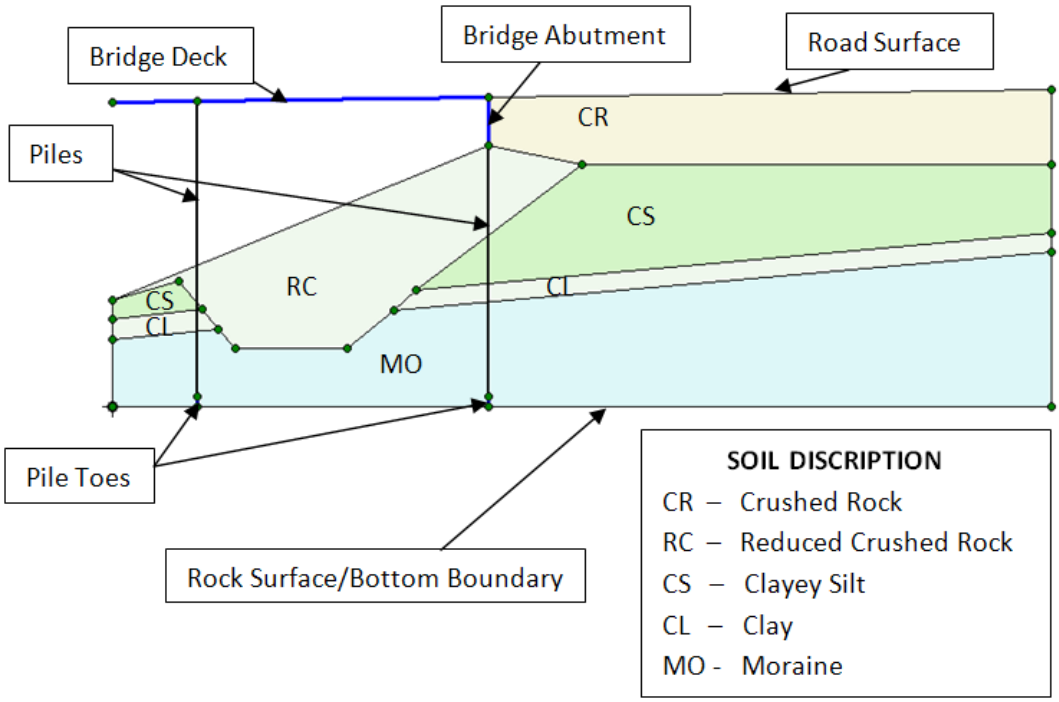

Figure 5.9: Component models that constitute the integral bridge model

5.3.1. Components Model Development

The development of the component models that make up the bridge structure, the foundation soil and the construction soils are presented in this section. Other than the geometric and material properties of these component models as published (Nilsson, 2008, Kerokoski, 2006, Kerokoski and Laaksonen, 2005), a number of other considerations affect the development of the model. These include the assumptions made in the process of developing the models and details of the finite elements and conditions of operation.

5.3.1.1. Geometry

Information obtained from the publications (Nilsson, 2008, Kerokoski, 2006, Kerokoski and Laaksonen, 2005) on the components of the Haavistonjoki Bridge include the relative positioning of the soil components and the structural members of the bridge. The relative positioning was modelled as published. Detailed information about the soil profile and the general geometric measurements of the cross section of the bridge on site as illustrated in Figure 5.3 were obtained from site investigation data (Nilsson, 2008, Kerokoski, 2006).

Different finite element clusters defined the different soil types. A cluster is a defined area marked out by boundaries within the finite element domain. In Plaxis, the cluster is defined by a closed loop of different lines within which the finite elements may be assigned certain properties to simulate the behaviour of the soil in the enclosed section (PLAXIS, 2010b).

The base of the model was modelling the interface between the rock and the soil with the rock being rigid. It was assumed that there would be no vertical displacement to the soil particles at this interface. The ground water table on the site was not measured (Kerokoski, 2006) but estimated at 9.5m below the finished road level in the model. The construction involved excavation through three different soil types. The excavated soil materials were replaced with a fill material. A soil cluster cutting across these three materials defining the geometry of the excavation was established to accommodate the properties of the replacement fill material. Details of the simulation process that describes the construction modelling are explained in Section 5.4.

The structural components were modelled using plates and node to node anchors within the Plaxis code (PLAXIS, 2010b). A brief description of these components and their application are presented in Section 4.4.3. An abutment height of 2.5m and thickness of 1.2m was modelled using a plate. The bridge deck was modelled using a different plate with model thickness of 0.86m (see Section A–A in Figure 5.5). Pile support for the abutment was modelled using node to node anchors. The bridge deck was positioned above the existing ground surface requiring a backfill height of approximately 5m at the abutment location. The abutment rested directly on the model pile foundation. The bottom of the

model pile columns were fixed to the base of the model at a location to simulate piles rooted in rock as shown in Figure 5.27 (b). Details of the parameters assigned to these component models are presented in Section 5.3.1.4.

5.3.1.2. Finite Element Boundaries

The fixed base, the surface of the soil and the vertical boundaries, define the external boundaries of the finite element domain, created to model the integral bridge. Figure 5.10 show the boundaries. The vertical boundaries (right and left boundaries) are established at locations within the soil mass where boundaries do not actually exist. These boundaries are established on the sides that have a relatively infinite soil boundary, to provide solutions to the loading simulation of these soils. Each of these four external boundaries identified in Figure 5.10 is subject to boundary conditions. The boundary displacement conditions are presented below and the process through which the external boundaries are established is also presented.

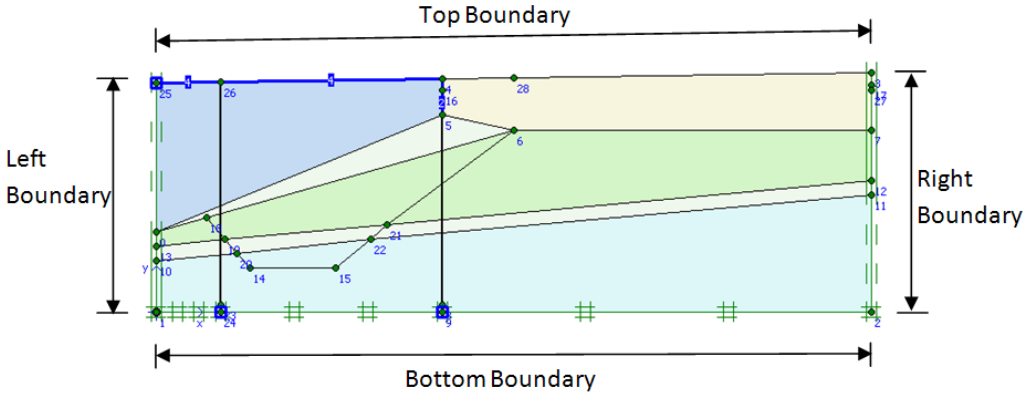

Figure 5.10: External geometric boundaries of the integral bridge finite element model

5.3.1.2.1. Boundary Conditions

The finite element nodes at the external boundaries of the left and right sides of the model were fixed horizontally but were not restrained vertically. The finite element nodes at the external boundaries of the bottom of the model, representing the rock surface were fixed

vertically and horizontally. The finite element nodes at the external boundaries of the top sides of the model were not restrained vertically and horizontally.

5.3.1.2.2. Loading Effect on Boundary

The external boundaries must be established to enable realistic solutions for the problem. These external boundaries within which all finite element clusters and applications are contained may be forced or natural. Natural boundaries are defined by the existing geometry or conditions of the real event. However, in cases that consist of relatively infinite boundaries, artificial boundaries must be set to define the domain. These artificial boundaries are forced boundaries that do not exist in reality and are set by the user primarily to enable a quantifiable definition of the problem. Consequently, forced boundaries affect the accuracy of the model.

The primary factor responsible for the accuracy of a finite element model with forced boundaries is the positioning of these boundaries. The positioning of the forced boundaries may generate forces or displacements that are reflected back into the model by the boundaries in locations where they do not exist. Reflective forces or displacements are caused where the forces or displacement imposed are restricted or altered within its natural range or limits, acting on the principles of Newton's third law of motion. However, within a soil mass, the impact of an imposed force or displacement exerted at a referenced position diminishes with increasing distance from that position. The range within which this impact can be appreciated and measured is defined in this research as the impact influence zone.

Ideally, the forced boundaries (in this case the vertical boundaries on the left and right sides in Figure 5.10) should be set at infinity to ensure that the boundaries do not influence the analysis in anyway. This is not feasible within the principles of the finite element approach and therefore forced boundaries must be set.

A solution is to model a relatively large area, setting the boundaries a significant distance away from the location of the imposed force or displacement, exceeding the region of the impact influence zone. However, extensive analytical details of the model would be lost

within the spread of the finite element nodes and stress points in the relatively vast space that will be introduced thus having an effect on the accuracy. Finer finite element mesh in these circumstances to capture these details may cost exceedingly more in time and resources, and will generate less analytical detail than defining a relatively smaller area for the problem using the same resources. Therefore, a balance between the cost of analysis and the effect on the model's accuracy has to be achieved in locating the forced external boundaries. In this study, the forced external boundaries were positioned where the effect from the model loading is diminished, and satisfactory details of the analysis were preserved for review.

The soil loading in this model is caused by the horizontal displacement of the top of the abutment. This is modelled as a prescribed lateral displacement on the abutment at the location of the fixed joint between the bridge deck and abutment to ensure that all the structural properties of the bridge during the abutment displacement (including the bending moments), are accurately modelled. Analysis to define the impact influence zone of this displacement within the domain was carried out. This was done by comparing simulation results of no abutment displacement (establishing the default), maximum abutment displacement away from the backfill soil, and maximum abutment displacement towards the backfill soil, to reveal an approximate boundary area that would define the limit of the impact influence zone on the model behaviour as a result of these displacements.

Figure 5.11 shows the effective mean stress contour results of the model subjected to maximum abutment displacement away from the backfill soil, and maximum abutment displacement into the backfill soil. Point A and B in Figure 5.11 identify abutment displacement away from and into the backfill soil respectively. The dotted vertical line across the models in Figure 5.11 towards the right external boundary indicates the region (towards the right) beyond which an insignificant amount of change is experienced as a result of the displacements experienced by the abutment. This region is defined as the limit of the impact influence zone on the right external boundary.

To determine appropriate locations for the forced boundaries, the results of modelling the resultant stresses developed within the backfill soil due to the abutment displacements were

compared with the forced boundaries at various locations. Results of simulations carried out with the right vertical external boundary beyond the dotted vertical line (towards the right) in the direction away from the abutment displacement location, were compared to the results of the simulation carried out with the right vertical external boundary at the dotted vertical line (considered the limit of the impact influence zone). These results were found to be similar. However, an appreciable difference was increasingly found where the results of the simulation carried out establishing the right side vertical external boundary at the dotted vertical line, were compared with the results of simulations carried out with the right vertical external boundary nearer to the abutment than the dotted line.

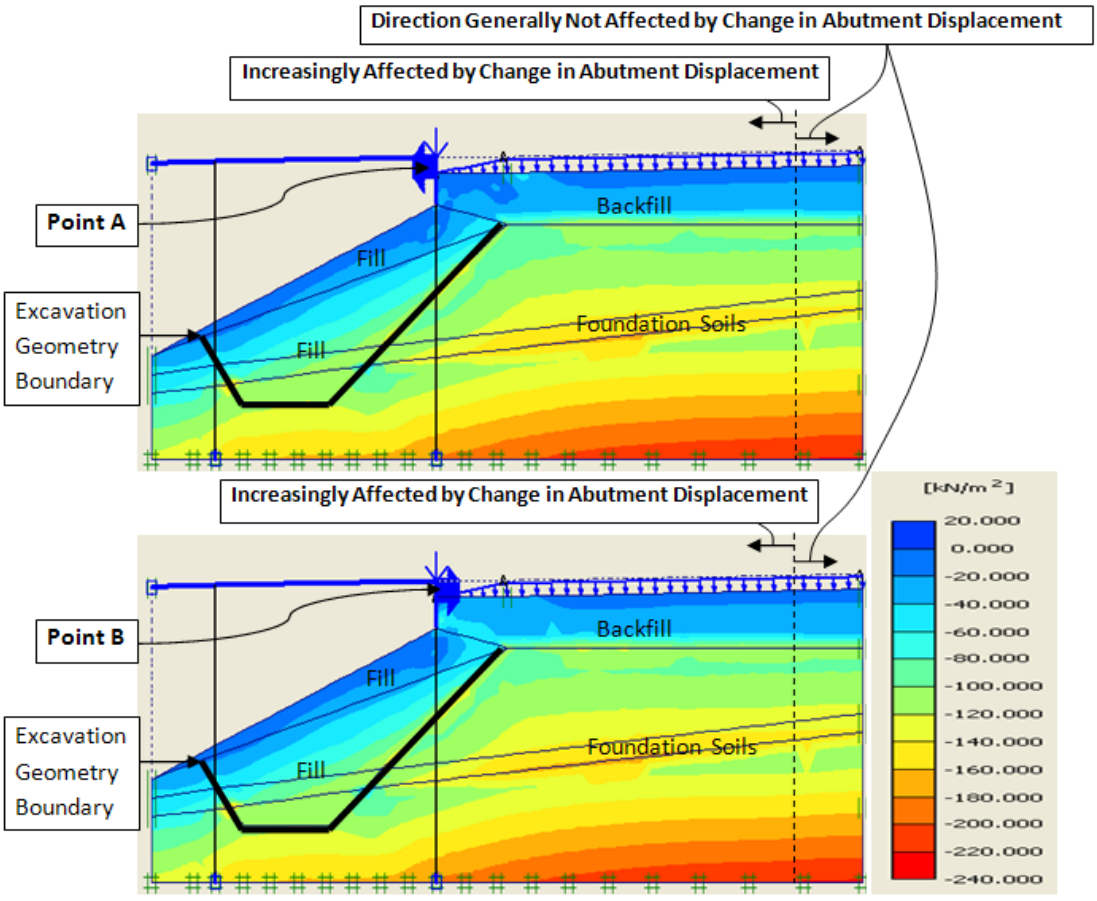

Figure 5.11: Impact of maximum displacement into and away from backfill on mean stress compared, showing little effect to the right hand boundary

This indicates that establishing the right vertical external boundary at any location beyond the dotted vertical line to the right will generate similar results within the backfill soil. The

right vertical external boundary was therefore established at a location immediately beyond the dotted vertical line. Stresses developed as a result of the abutment displacement within the backfill were little affected by the location of the left vertical external boundary when the boundary was established beyond the limit of the excavation geometry to the left, highlighted in Figure 5.11 (Excavation Geometry Boundary). Consequently, the location of the vertical left external boundary, positioned to accommodate the excavation geometry was considered appropriate.

5.3.1.3. Finite Element Details

There are two finite element types incorporated into the Plaxis code; the 6 node triangular element, and the 15 node triangular elements. The 6 node element has 6 finite element nodes and 3 Gaussian integration points within the element. The 15 node element has 15 finite element nodes and 12 Gaussian integration points within its element as shown in Figures 5.12 and 5.13.

The 15 node element requires more computing capacity than the 6 node element but provides a more accurate simulation result. This is because a fourth order interpolation is used for displacement calculation in the 15 node element against the second order interpolation used in the 6 node element. See Plaxis reference manual for more details (PLAXIS, 2010b). Stresses and strains calculated at the 12 Gaussian integration points (stress points) in the 15 node element have also been found to provide reliable results (Nagtegaal et al., 1974, Sloan and Randolph, 1982). The 15 node element was used in developing the integral bridge model for analysis.

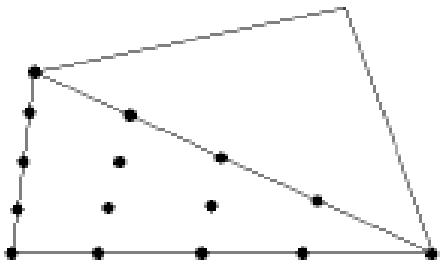

Figure 5.12: Location of nodes within a 15 node triangular element (PLAXIS, 2010b)

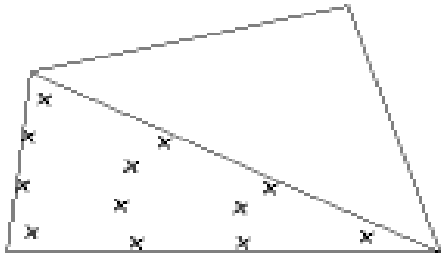

Figure 5.13: Location of stress points within a 15 node triangular element (PLAXIS, 2010b)

5.3.1.4. Parameters

The integral bridge material model consists of the structural components and the soil component. The structural components are made up of the bridge deck, abutment, pile and pile toe structure models. The soil components are made up of soil model types including the backfill material soil model (crushed rock), construction fill material soil model (reduced crushed rock) and foundation material soil models (clayey silt soil, moraine soil and clay soil).

5.3.1.4.1. Structure Components

Plaxis models the effect of the structural components of the instrumented bridge (including the concrete reinforcements) on the soil models. Information on the reinforcement details were not provide in the publication and are therefore not modelled. Details of the bridge structure, pile toe and pile properties used are presented in Tables 5.1 and 5.2. Most of the geometric and material properties of the structural components were obtained from the publications (Nilsson, 2008, Kerokoski, 2006). However, some values of the parameters of the structure component's material required in modelling the behaviour of these components were not provided in the published data. Consequently, typical parameters of these materials were assumed in the modelling. The bridge was built of reinforced concrete. Parameters for reinforced concrete not provided in the publication were obtained from published data on concrete and reinforced concrete properties (Neville, 1995, Neville and Brooks, 1987, Mindess et al., 2002, Kerokoski, 2006, Reynolds et al., 2008).

Name	Type	EA kN/m	EI kN m^2/m	w kN/m^3	v
Abutment Wall	Elastic	**3.960 x 10^8**	**4.752 x 10^7**	**28.800**	**0.2**
Bridge Deck	Elastic	**1.650 x 10^8**	**3.438 x 10^6**	**12**	**0.2**
Pile Toe	Elastic	**1.188 x 10^7**	**3.742 x 10^5**	**4.750**	**0.2**

Table 5.1: Bridge Structures and Pile Toe Material properties

Name	Type	EA kN/m	$L_{spacing}$ m
Pile	Elastic	**1.188 x 10^7**	**5.50**

Table 5.2: Pile Material properties

A Young's Modulus of 30GPa, unit weight (w) of 24kN/m^3 and Poisson's ratio (v) of 0.2 was assumed for the bridge and pile structures. As a result of the bridge deck cross section shape (Figure 5.5), an average effective bridge deck thickness of 0.5m was assumed for the purpose of calculating the flexural rigidity (bending stiffness) EI and axial stiffness EA. A pile axial stiffness value calculated from a concrete pile diameter of 710mm was used. A calculated out of plane pile spacing (identified as $L_{spacing}$ in Plaxis software), of 5.5m was also used for the pile support. Foundation pile were designed as compression piles and are therefore modelled using node to node anchor which enables compressive and tensile stiffness. This feature in Plaxis models abutment supports only and does not interact with the foundation soil. The structural members of the model were simulated as materials exhibiting linear elastic properties.

5.3.1.4.2. Soil Components

Soil parameters required and the values used in modelling the soil behaviour using Plaxis Hardening Soil model are presented in Table 5.3 (PLAXIS, 2010a, PLAXIS, 2010b). The stiffness, cohesion, friction angle, dilatancy and the unit weight parameters are the primary

parameters used in this studies. The values of these parameters were obtained from the bridge site investigation (Kerokoski, 2006, Kerokoski and Laaksonen, 2005). Where the values of these parameters were not published from the bridge site investigation, typical parameters for the backfill and foundation soil type as published by several authors (Bowles, 1997, Bakker et al., 2006, Bell, 2000, Bowles, 1984, Chou and Bobet, 2002, McNally, 1998, Parsons, 1992, Steele and Snowdon, 1996, Smith et al., 2001) were used. Plaxis Hardening Soil model requires other soil parameters. These other parameters were not provided by the publication. Values of some of these parameters are also not readily obtainable in practice. However, Plaxis software provides default values for these parameters.

Published data obtained from the actual bridge site did not include the permeability values of the backfill and construction fill material, or the permeability values of the different foundation soil types. This implies that some assumed values must be used to satisfy the conditions required within the finite element equations. The accuracy of a model is improved where a limited number of assumptions are made. However, the permeability parameter within the soil model provides information required in modelling the consolidation behaviour, which exist between fully drained and fully undrained behaviour within the foundation material. An informed decision was therefore made on the choice of simulating the soil models as exhibiting either drained or undrained characteristics, when subjected to loading. This was to establish the respective limits within which the soil behaviour is expected fall. The decision to model the materials as drained or undrained was supported by the permeability equations obtained from Darcy's law and the displacement rates established from the thermal loading on the integral bridge abutment.

Darcy's law relates the discharge of fluid through a porous medium such as soil to the permeability as expressed in Equations 5.1 and 5.2. A factor in this equation is the hydraulic conductivity with the units of velocity. This is a measure of the rate of flow through an area. In soil mechanics, granular or highly porous soil materials such as crushed rock and moraine typically have hydraulic conductivity values in excess of 10^{-2}m/s and clayey silt material typically have hydraulic conductivity values below 10^{-8}m/s (Zhang, 2006, Murthy, 2003).

Hardening Soil Model Parameters						
Soil Parameter	Units	Crushed Rock	Reduced Crushed Rock	Clayey Silt	Clay	Moraine
$\boldsymbol{\phi}$	^{o}	45	42	33	25	45
c	kN/m^2	0	0	1	2	0
ψ	^{o}	8	5	0	0	4
E_{50}^{ref}	MN/m^2	80	29.7	9.3	4	80
E_{oed}^{ref}	kN/m^2	E_{50}^{ref}	E_{50}^{ref}	E_{50}^{ref}	E_{50}^{ref}	E_{50}^{ref}
E_{ur}^{ref}	kN/m^2	3 x E_{50}^{ref}	3 x E_{50}^{ref}	3 x E_{50}^{ref}	3 x E_{50}^{ref}	3 x E_{50}^{ref}
γ_{sat}	kN/m^3	19-23	22	18	18	23
γ_{unsat}	kN/m^3	18-22	20	17	16	23
k_x	m/day	0	0	0	0	0
k_y	m/day	0	0	0	0	0
c_k	-	10^{15}	10^{15}	10^{15}	10^{15}	10^{15}
Rayleigh alpha	-	0	0	0	0	0
Rayleigh beta	-	0	0	0	0	0
Dilatancy cut-off	-	Not Activated	Not Activated	Not Activated	Not Activated	Not Activated
m	-	0.5	0.5	0.5	0.5	0.5
C_c	-	-	-	-	-	-
C_s	-	-	-	-	-	-
e_{init}	-	0.5	0.5	0.5	0.5	0.5
v_{ur}	-	0.2	0.2	0.2	0.2	0.2
p^{ref}	kN/m^2	100	100	100	100	100
K_0^{nc}		1-sin $\boldsymbol{\phi}$	1-sin $\boldsymbol{\phi}$	1-sin $\boldsymbol{\phi}$	1-sin $\boldsymbol{\phi}$	1-sin $\boldsymbol{\phi}$
$c_{increment}$	kN/m^3	0	0	0	0	0
y_{ref}	m	0	0	0	0	0
R_f	-	0.9	0.9	0.9	0.9	0.9
Tensile Strength	kN/m^2	0	0	0	0	0
Interface Strength	-	Rigid	Rigid	Rigid	Rigid	Rigid

Table 5.3: Soil Material properties

A preliminary finite element simulation of the thermal induced abutment displacement of the model integral bridge, subjected to a typical daily temperature variation of up to 10^{o}C/day (FMI, 2012), that may be experienced within the regional location of the Haavistonjoki Bridge in Finland, generated maximum displacement rate of approximately 10^{-6}m/s at Point A in Figure 5.14 and approximately 10^{-7}m/s in the clay layer at Point B.

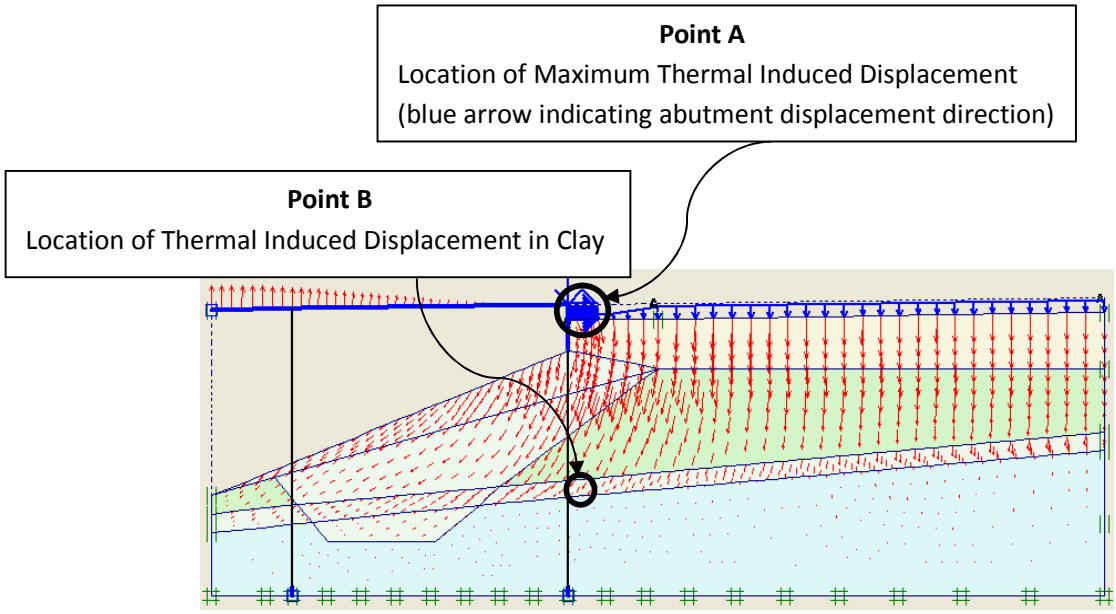

Figure 5.14: Finite element simulation of total displacements within the bridge as a result of the thermal induced abutment displacements recorded

In a soil mass subjected to loading, the build up of excess pore pressure is dependent on the ease at which water displaced as a result of the loading may flow through soil (seepage). Where there is restriction to this flow, excess pore pressure develops. This is largely dependent on the permeability of the mass. Where other factors are constant (same fluid within the same medium), permeability may be directly related to hydraulic conductivity (Equation 5.2).

An indication of the ease of flow through the clay soil medium was obtained where the hydraulic conductivity of clay was compared to the displacement experienced within the clay medium in the model. The results showed that the hydraulic conductivity value of a typical clay soil was less than the displacement rate experienced within the clay soil in the simulation. Furthermore, displacements experienced within the soil mass may result in plastic straining and reduced pore spaces.

This information suggests restricted drainage and a build up of pore pressure. The typical hydraulic conductivity values of the other soil materials used in the modelling were also compared with the displacement rates experienced within these materials in the simulation.

The results showed that the hydraulic conductivity values of these materials significantly exceeded the displacement rates experienced within these materials in the simulation. This suggests free draining and no build up of pore pressures within these materials.

$$q = KiA \qquad \text{…….. (5.1)}$$

$$K = k\frac{\rho g}{\mu} \qquad \text{…….. (5.2)}$$

Where q is the discharge; K is the hydraulic conductivity measured in m/s; i is the hydraulic gradient; A is the cross-sectional area of flow; k is the intrinsic permeability; ρ is the fluid density; μ is the fluid viscosity; g is the gravitational acceleration.

Comparing the typical hydraulic conductivity of the materials to the displacements experienced within these same materials in the model suggests a remote possibility of an increase in pore pressure in the crushed rock, reduced crushed rock and moraine materials. Consequently, the crushed rock, reduced crushed rock and moraine materials were considered more likely to exhibit drained characteristics when subjected to loading under these conditions. These materials were modelled as drained. However, material consisting of clay may exhibit undrained characteristics when subjected to loading under these conditions. Consequently, clayey silt and clay materials were modelled as undrained. Details of type of modelling (drained or undrained) used in simulating loading within the soil models are presented under ‘Initial’ column of ‘Model (Type)’ in Table 5.4 Section 5.6.1.

5.3.1.5. Nodes & Stress Points

The finite element method generates results at the specific locations of the nodes and the stress points. These locations are identified in the Plaxis model before calculation. The measured abutment displacement as a result of the thermal induced expansion and

contraction of the bridge deck occurs at the contact point between the bridge deck and the abutment. This contact point is the location of the maximum thermal induced abutment displacement (see Figure 5.15). Figure 5.16 show the location of the earth pressure cells within the finite element model.

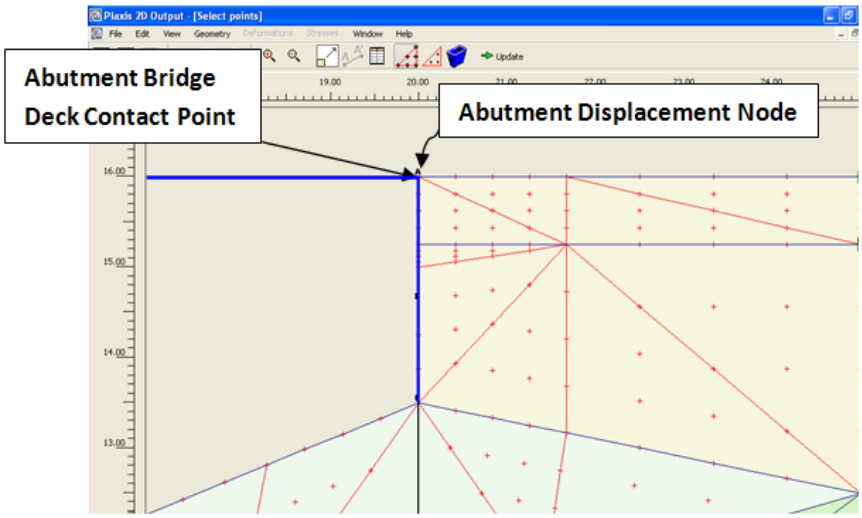

Figure 5.15: Location of the abutment and bridge deck intersection and the abutment displacement node in the model

The intersection of the plate modelling the abutment and the plate modelling the bridge deck, models the jointless link of the integral bridge. These plates are structurally linked with a fixed joint. The recorded abutment displacement caused by the thermal induced expansion and contraction of the bridge deck is measured at the “Abutment Bridge Deck Contact Point.” This point is identified in Figure 5.15. At this location, the maximum displacement of the bridge deck is accurately accounted for. The abutment displacement node is therefore selected at this contact point to effectively model and monitor the abutment displacements during the loading simulation of the integral bridge model.

On the instrumented bridge, earth pressure cells were placed behind the abutment to measure the earth pressure developed as a result of the abutment displacement. The location of the earth pressure cells is illustrated in Figure 5.16 (b) (a magnified section A-A in Figure 5.5). Stress points, identified in Figure 5.16 (a), measuring the calculated earth

pressure within the model were selected at similar locations within the model also identifying the upper and lower earth pressure cell positions.

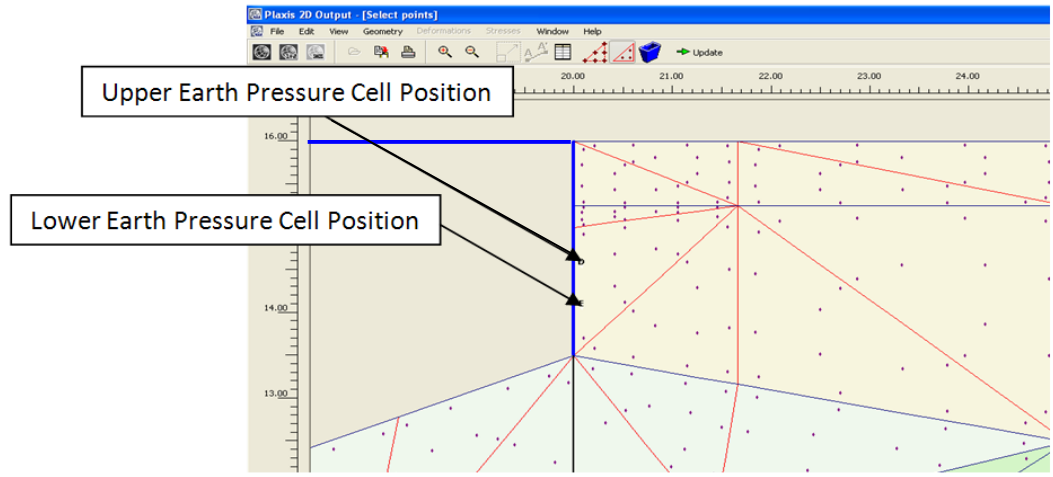

(a) Upper and lower stress point position modelling the earth pressure cell position in the bridge

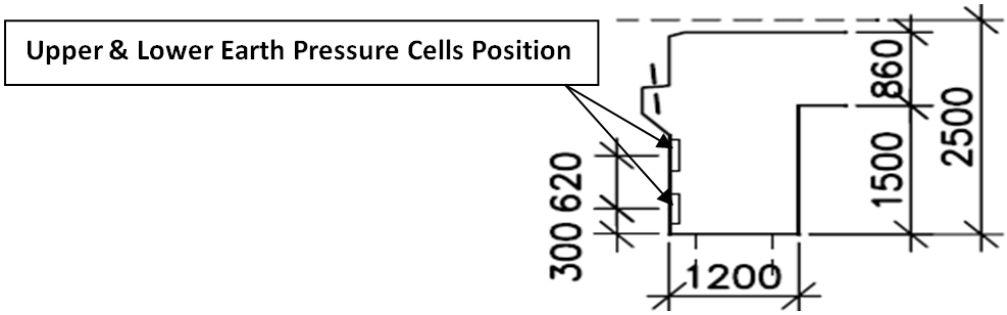

(b) Section showing the relative position of upper and lower earth pressure cells on the Haavistonjoki Bridge abutment. See Figure 5.4. Modified (Kerokoski, 2006).

Figure 5.16: Section of model abutment (a); Illustration showing the cross section of the abutment and the location of the earth pressure cells (b)

5.3.2. Loading Modelling

The thermal induced expansion and contraction of the bridge deck results in the horizontal displacement of the upper end of the abutment structure, causing the abutment to deform. This was modelled by the introduction of a prescribed horizontal displacement to the upper section of the model abutment. The resultant horizontal displacement is modelled through the structural properties of the abutment. The model abutment displacement was measured at the contact point between the abutment and bridge deck (Figure 5.15) by the nodal horizontal displacement. Integral bridge abutment displacements are small. This reduces the magnitude of earth pressure developed. Modelling the interface between the soil and the structure further reduces the magnitude of the earth pressure developed. Consequently, to simulate the maximum possible values of earth pressures that may be developed from the magnitude of abutment displacements used within the model, interface properties were not activated in this parametric study.

However, modelling of the abutment displacement pattern presented challenges, some of which was solved by modelling other components of the bridge as applied load. This section presents the process of creating the components of the model that were modelled as applied load. The properties of the finite element modelling approach, the abutment displacements, and the soil-structure interaction that necessitated this modelling approach are discussed.

5.3.2.1. Road & Approach Slab Structure

The completed integral bridge and backfill soil construction consist of the bridge approach made up of the road embankment (road structure) and approach slab. The locations of the road structure and approach slab within the model are labelled (Label 1 & Label 2 in Figure 5.17). The 5m long approach slab was constructed with a hinge joint connection to the abutment. The bottom of the approach slab was located at a depth of 0.8m below the finished road level (Kerokoski, 2006). The thickness of the approach slab was assumed to be the thickness of a typical bridge slab, 0.2m (Chen and Duan, 2000).

In modelling the bridge, the upper section of the backfill that models the road structure should consist of component models that account for the behaviour of an approach road structure including an approach slab. The different material properties of the soil and structure components required in developing the road structure model, as well as modelling of the soil-structure interaction of these component models had to be dealt with in a variety of ways. Several constraints were encountered in this process. The solutions to these constraints used in the final model development are presented.

An option considered was modelling the approach slab section and the road structure only sections (see Label 2 in Figure 5.17) using separate plates (Plaxis provision for modelling structures). Using this option, the principal of continuity in a finite element analysis ensures a bond between the plates modelling the road structure only section and the approach slab located at one end of the approach slab span (Location B in Figure 5.18). This principle also ensures a bond between the plates modelling the approach slab and the plate modelling the abutment (Location A in Figure 5.18). Consequently, a moment or a hinge would have to be introduced as a result of the plate to plate contacts that exist between the abutment and the approach slab, and between the approach slab and the road structure.

The properties of the road structure and approach slab contact point are not accurately represented by a hinge joint, or by sustaining a structural moment as would be the case at these contact points if plates model the approach slab and road structures. There is also a potential to develop differential settlement in the backfill soil under these structures which will not be appropriately accounted for. As a result of the characteristics of the plate to plate link in Plaxis, this option will not model the road structure, approach slab, and abutment contact point accurately. This option underestimates the calculated vertical stresses under loading and hence the earth pressure in the backfill soil.

Another option considered involves modelling the properties of the road pavement using the soil material model. Unlike the previous approach illustrated in Figure 5.18 where the materials within the approach slab span are treated as a unit and modelled as a plate, this approach separates the approach slab span unit into soil and structure. This includes the use of a plate to model the approach slab as it is made up of a different material property type

from soils as modelled in Plaxis (Figure 5.19). The approach slab positioned behind the abutment (see Approach Slab in Figure 5.17 and Figure 5.19) is modelled within the road structure and backfill soil material.

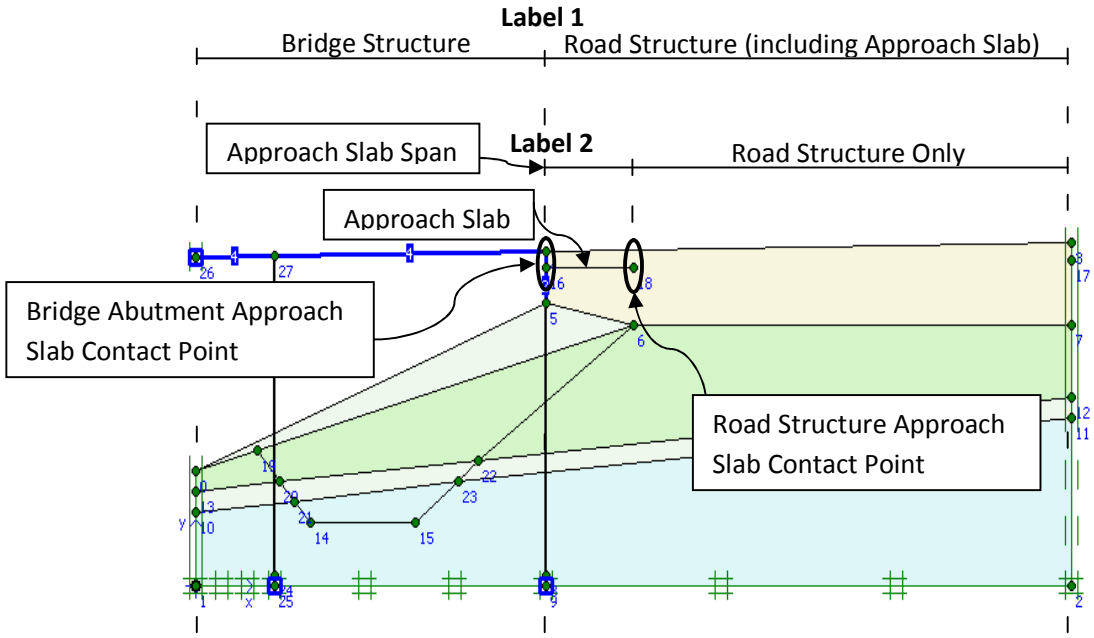

Figure 5.17: Road structure section of bridge model showing road structure, approach slab and abutment contact point

Using the Plaxis software code in this modelling option would require superimposing the properties of the approach slab structure (through the plate) on the location within the soil where the plate is positioned. This is because in Plaxis finite element modelling, plates are superimposed on a continuum and consequently overlap the soil (PLAXIS, 2010b). The immediate impact of this is the absence of the dimensioning of the approach slab within the soil model as plates are not assigned 2D properties in Plaxis (see Approach Slab modelled using plate in Figure 5.17). The other shortcoming is that the weight of the approach slab structure is superimposed on the weight of the soil within the same location thus increasing dramatically the total material weight at that location. This option exaggerates the calculated earth pressure in the backfill soil.

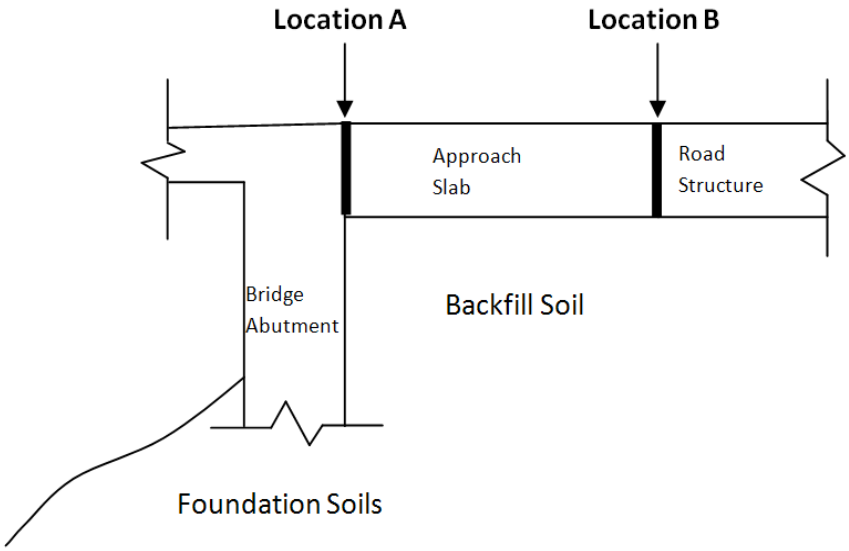

Figure 5.18: Illustration of road structure and integral bridge structure link

Having encountered these constraints, a review of the modelling approach was considered. The primary problem of the integral bridge is known to originate from the soil-structure interaction between the bridge abutment structure and the backfill/foundation soil. In a parametric study of the integral bridge backfill performance subjected to thermal induced abutment displacements, detail information on the composition of the road structure and its characteristic behaviour may be considered less relevant. However, the road structure will contribute to the loading of the backfill and foundation soil. This effect is considered relevant in modelling the backfill soil behaviour.

The road structure and approach slab was therefore modelled as a load sustained by the backfill soil and abutment. These weight effects are simulated as distributed and point loads on the backfill soil and abutment structure. Loading is not a material model hence eliminates the constraints posed by material models and their properties. The loading also acts within locations that material properties are considered least important in the model. The loads act at the level of the bottom of the road structure and approach slab within the backfill soil (Level A in Figure 5.20), and the contact point of the bottom of the approach slab on the abutment structure (Point A in Figure 5.20). The distributed loads act within the backfill at the level of the bottom of the road structure and approach slab. The point load acts at the contact point of the bottom of the approach slab on the abutment structure. The road structure only (Label 2 in Figure 5.17) is modelled as a uniformly distributed load

spanning across its width while the approach slab is modelled as triangular distributed load and a point load.

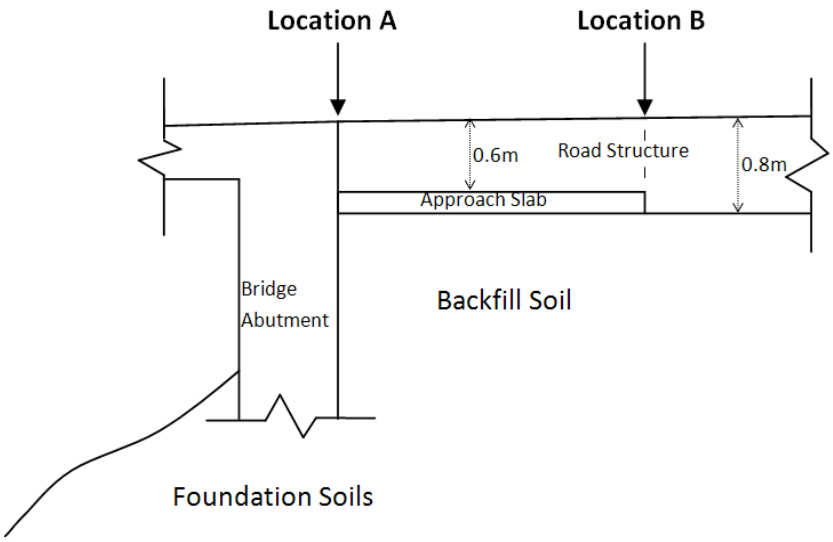

Figure 5.19: Illustration of approach slab road structure and integral bridge structure link

The triangular distributed load is the loading experienced within the backfill soil beneath the approach slab. The soil fully supports the weight of the approach slab at the approach slab and road structure contact point (see Location B in Figure 5.18 and Point B in Figure 5.20). The magnitude of the triangular distributed load at Point B is 18.6kN/m. At the approach slab abutment contact point, the abutment fully supports these weights because the approach slab is structurally linked to the abutment at this end (see Location A in Figure 5.18 and Point A in Figure 5.20). The road structure at the approach slab span is consequently modelled using a triangular distributed load and a point load, thus incorporating half of the weight of the approach slab distributed as experienced within the backfill soil and the other half fully supported by the abutment (see Figure 5.20). The magnitude of the point load at Point A is 46.5kN

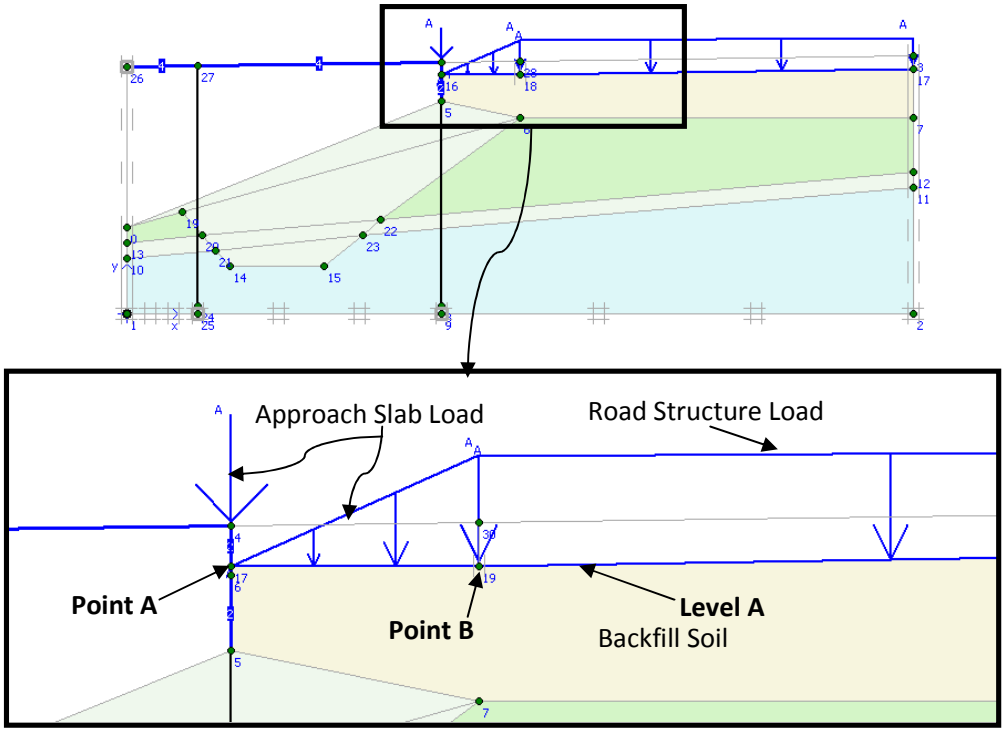

Figure 5.20: Location of distributed load modelling road structure and approach slab within backfill soil and abutment structure

The unit weight of road pavement structure (including the wearing course, base course and sub base) was not provided. This was assumed to be 23kN/m^3 (Glanville et al., 1952, McNally, 1998). The representative unit weight of the abutment, deck and approach slab was assumed to be the typical unit weight of reinforced concrete. The average thickness of road structure at the road structure only section was assumed to be 0.8m. The total thickness of the road structure at the approach slab span is 0.8m including an approach slab thickness of 0.2m.

5.3.2.2. Approach Slab Span Displacement

The earth pressure immediately behind the abutment is significantly affected by the loading pattern the backfill soil experiences as a result of the abutment displacement. Consequently, modelling the realistic behaviour of a constructed integral bridge requires in addition to the other load information, detailed information on the loading pattern the backfill soil is

subjected to as a result of the impact of the abutment displacements transmitted through the approach slab.

The approach slab is joined to the abutment (see Region A in Figure 5.21) and therefore experiences similar lateral displacements as the bridge abutment during thermal induced displacements. During the abutment displacements, the approach slab slides within the soil. Other than across the length of the approach slab, the lateral impact of the slide is limited to the region immediately around the end of the approach slab (see Region B in Figure 5.21). The road surface immediately above the end of the approach slab (Point B in Figure 5.21) typically experiences no appreciable displacement as a result of the thermal induced abutment displacement.

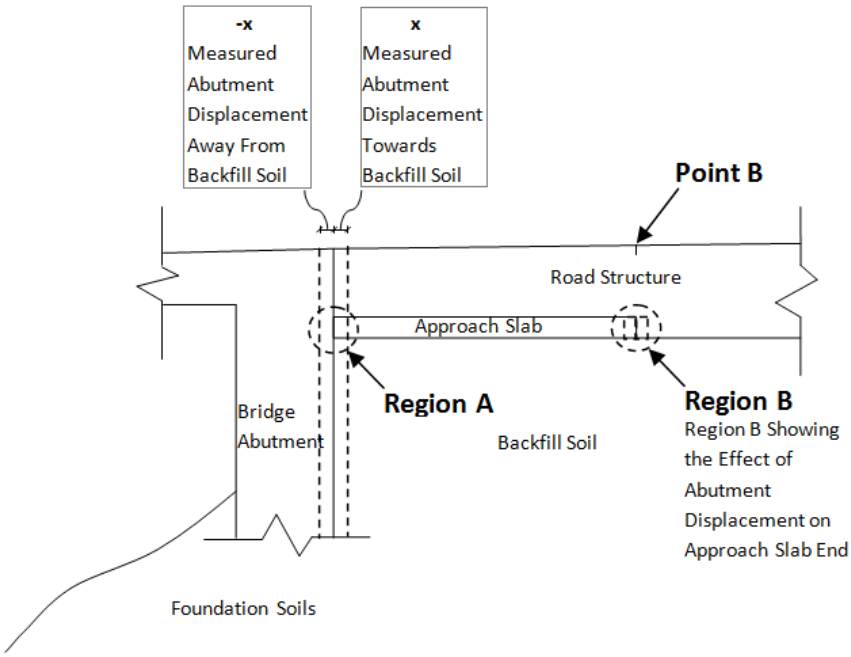

Figure 5.21: Illustration of approach slab displacement behind the abutment

Under these circumstances, a significant part of the displacement impact from the lateral displacement of the abutment is absorbed by the backfill soil beneath the approach slab. This implies that the effect of the lateral displacement diminishes away from the abutment (beyond Region B in Figure 5.21). This detail is important because in a finite element modelling approach (where the continuity conditions apply) the lateral displacements of the nodes simulating the impact of the abutment lateral displacements may not appropriately

model the actual conditions on site. The impact significantly affects the vertical stresses calculated immediately behind the abutment and hence the earth pressures at this location.

As a result of the continuity conditions of the finite element approach, the entire span of the road structure surface is uniformly affected by the impact of a displacement within the same cluster (where dealing with similar material) during the simulation of the lateral displacement of the model abutment (Dim. A in Figure 5.22 indicates the impact range). In reality, this impact is primarily experienced by sections of the road structure built above the approach slab (see Dim. B in Figure 5.22) as described above. Immediately beyond the approach slab the impact of this movement rapidly diminishes.

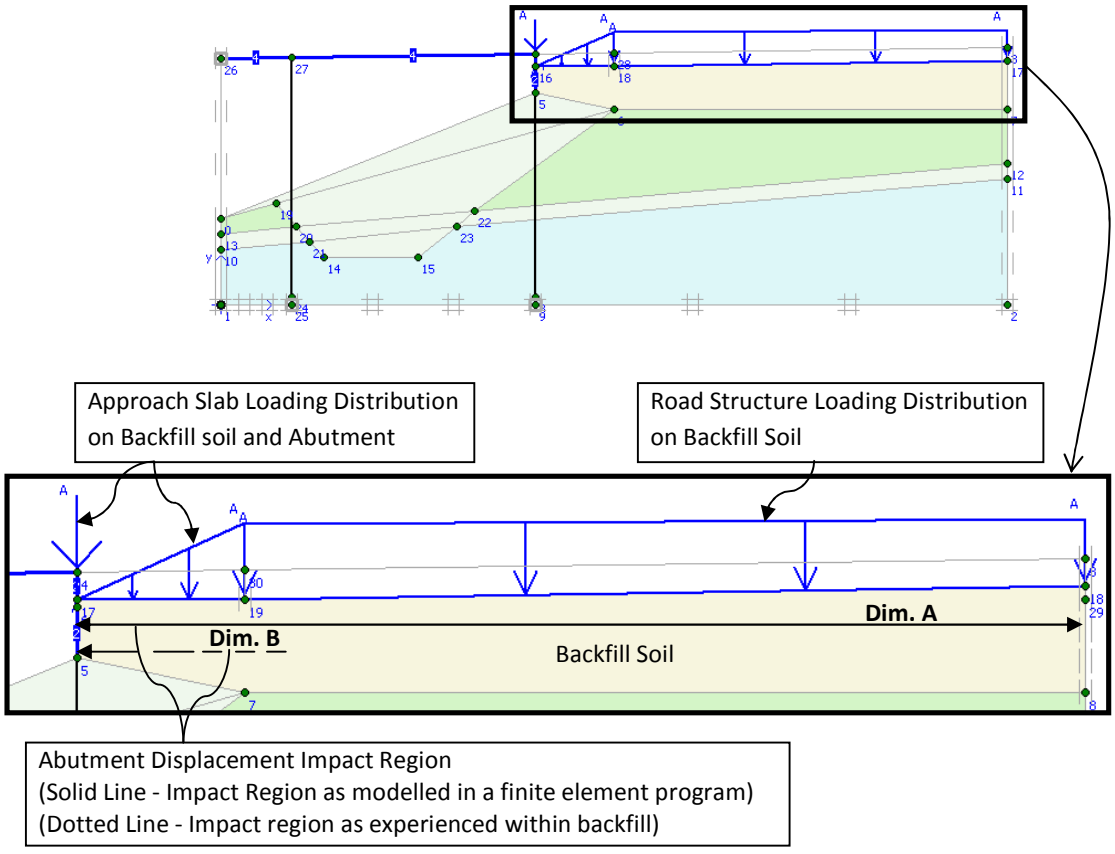

Figure 5.22: Road structure modelling and abutment displacement impact region on backfill soil

Figure 5.24 presents an illustration of the backfill loading pattern, considering the loading distribution on the backfill soil only as highlighted in the enlarged section of Figure 5.22. Figure 5.24 illustrates the comparative effect of introducing lateral displacement restriction.

Figure 5.23 illustrates the displacements as modelled using the finite element approach, without displacement restrictions. Case A, B and C show the backfill loading distribution pattern; where no abutment displacement is experienced (Case A), where abutment displacement away from the backfill soil is experienced (Case B), and abutment displacement into the backfill soil (Case C). The extent of displacement is indicated by the dotted vertical (dimension) lines to the left identified as' –x' for displacement away from the backfill soil and 'x' for displacement towards the backfill soil (see Figure 5.21 for –x and x).

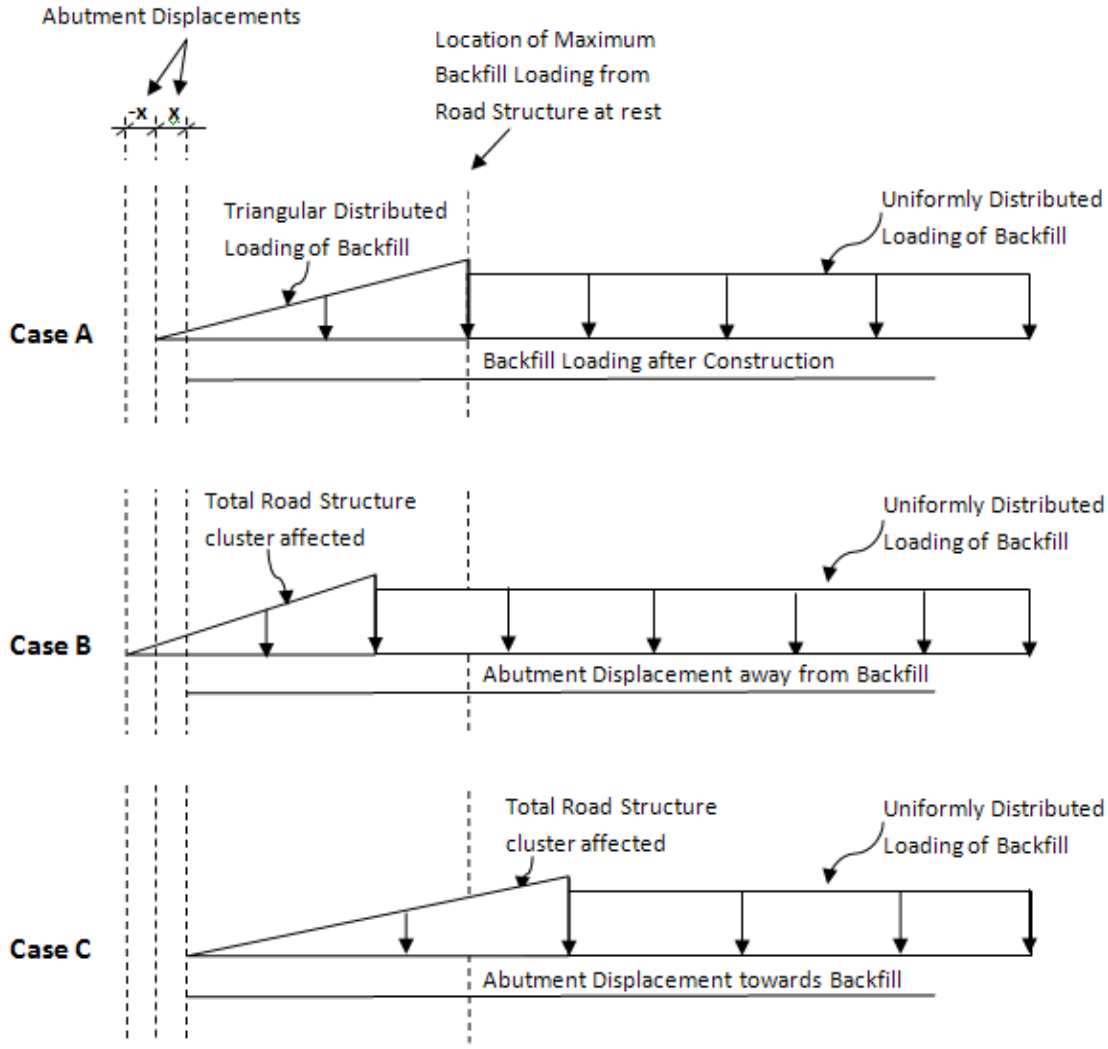

Figure 5.23: Unrestricted approach slab and road structure displacement impact on backfill soil under distributed load modelling the bridge approach of the road structure

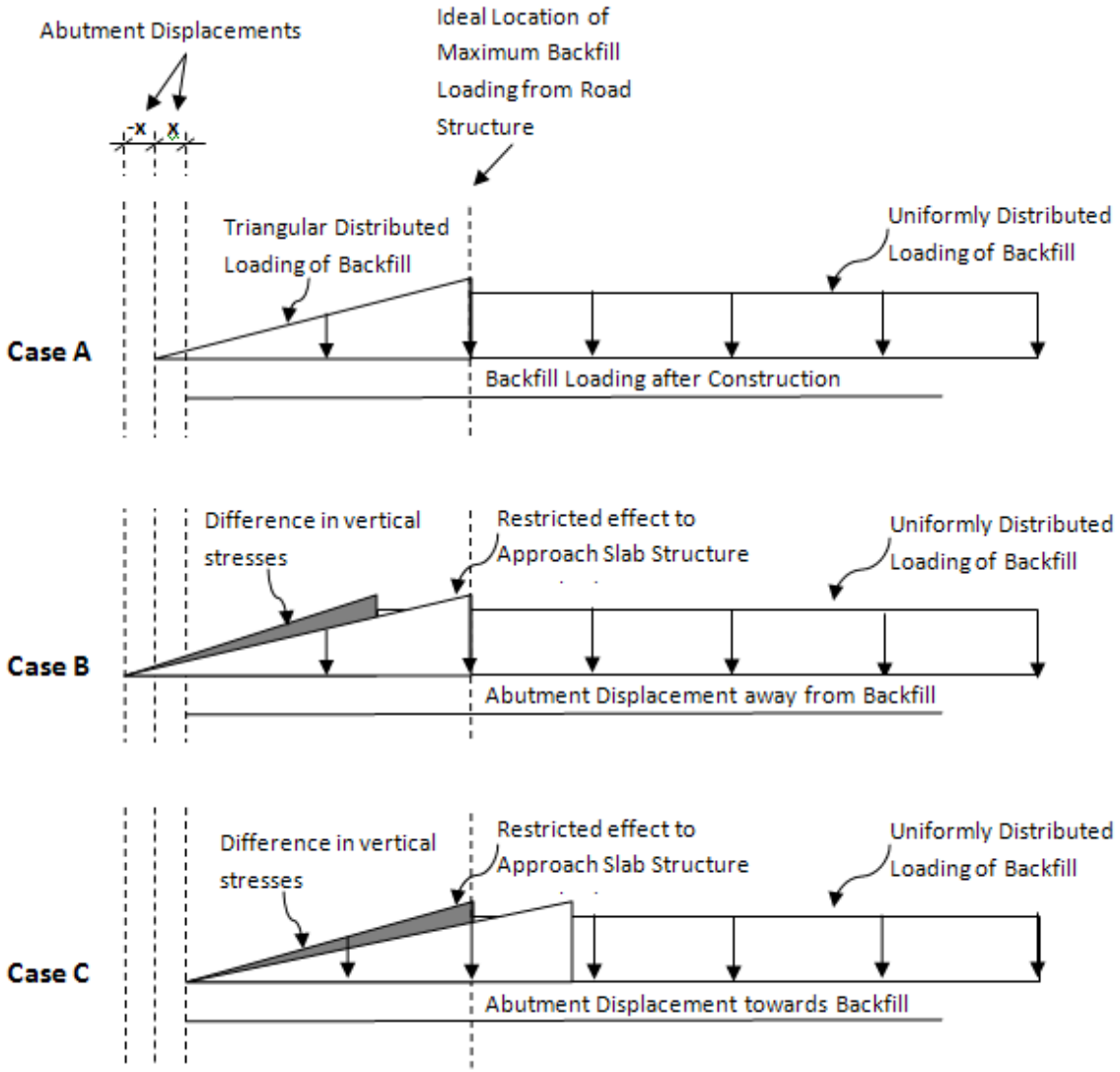

Figure 5.24: Comparative approach slab and road structure displacement impact on backfill soil under distributed load modelling the bridge approach of road structure

Considering the reduction in load sustained by the backfill soil under the approach slab in the direction towards the abutment (represented by the converging sides of the triangular distributed loading towards Point A in Figure 5.20), slight changes in lateral displacement may result in a significant percentage change in the approach slab loading impact experienced within the backfill soil. Consequently, modelling the impact of the entire road structure length experiencing the horizontal displacements (as enforced by the continuity conditions of the finite element approach in a cluster - indicated by the triangular loading labelled 'Total Road Structure cluster affected' in Case B and C in Figure 5.23), against

modelling the same impact with restrictions applied to the approach slab displacement impact (to significantly diminish the effect beyond the end of the approach slab span - indicated by the triangular loading 'Restricted effect to Approach Slab Structure' in Case B and C in Figure 5.24), result in differences in the vertical stresses and the earth pressure experienced behind the abutment (see shaded section of Case B and C in Figure 5.24).

Case B illustrates the restricted impact compared with the simply applied finite element approach in the abutment displacement away from the backfill soil. Case C illustrates the same comparison as Case B but in abutment displacement towards the backfill soil. Without the application of the loading impact restriction within the backfill soil, the abutment displacements result in exaggerating the earth pressure experienced in abutment displacement away from the backfill and under estimating the earth pressure experienced in abutment displacement towards the backfill. This difference is highlighted by the shaded section of the triangular loading in Case B and Case C of Figure 5.24.

To account for this development and model the restriction, horizontal displacements at the finite element node identifying the road structure approach slab contact point (Region B in Figure 5.21) is restricted allowing vertical displacements only (Point B in Figure 5.20). This restriction applies to this singular node only. All other nodes around this road structure approach slab contact point node are not restricted. Being the node that directly transmit the impact of the lateral displacements, this largely confines the effect of the approach slab span loading displacements to the approach slab span section, and limits the effect of the lateral approach slab displacement to the location identified by Region B in Figure 5.21. This closely models the loading effect in the backfill soil at the road structure approach slab contact point and the loading effect of the approach slab span section on the backfill soil.

5.4. Simulation

The simulation process using the finite element approach involves several steps as follows:

- A geometrical representation of the bridge site.
- Assigning properties to the component parts of the model.

- Defining an appropriate finite element mesh.
- Modelling the construction sequence
- Modelling the operational aspects of thermal loading.

Geometric representation of the bridge site was carried out in a model developed using Plaxis 2D version 9.0 software. The bridge and soil properties of the instrumented bridge described in Section 5.2 were assigned to the component parts of the model. Mesh sensitivity analysis showed that the coarse finite element mesh in Plaxis was adequate for this parametric study. This was generated across all clusters of the model (see Figure 5.25). Modelling the construction sequence and the operational aspects of thermal loading are presented in this section.

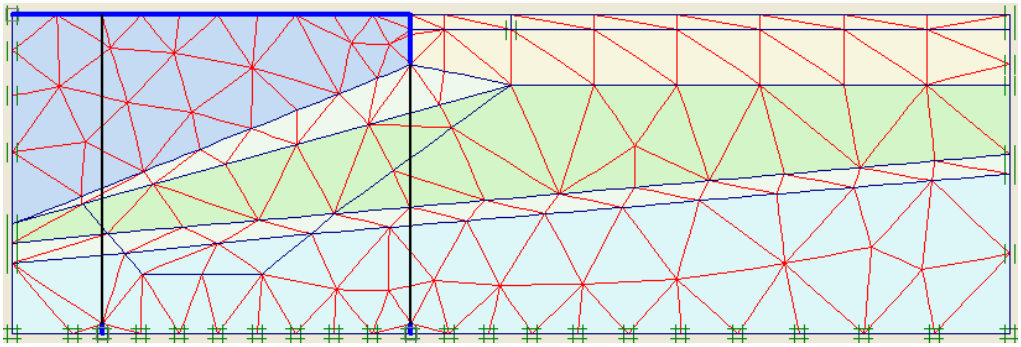

Figure 5.25: Finite element mesh of the bridge model

Finite element simulation using Plaxis 2D Version 9.0 is based on a two dimensional plane strain analysis. Figure 5.26 presents an illustration of a 2D plain strain mesh within a 3D object. An elastoplastic analysis was undertaken to evaluate the impact of thermal induced bridge deck expansion and contraction on the abutment. Two conditions were assumed during loading simulation on the soil models. These include a condition in which no excess pore pressures were generated in the foundation soils during loading, and a condition in which excess pore pressures were generated within the fine grained soils of the foundation materials resulting from the rate of the thermal induced soil loading (i.e. foundation material soils with clay).

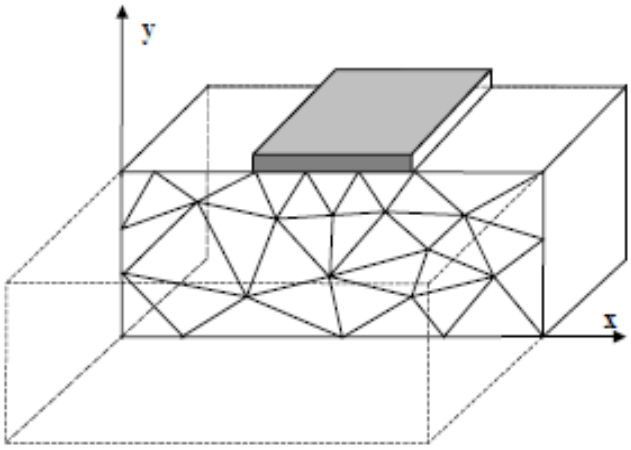

Figure 5.26: Illustration of 2D plane strain mesh (PLAXIS, 2010b)

The components of the models were simulated in four stages (Figure 5.27). This process includes modelling the bridge and backfill construction process from the original site conditions before construction, and up to the integral bridge abutment displacement. The first stage was to simulate the original geotechnical soil profile (Figure 5.27(a)); the second the earth works and foundation construction of the bridge (Figure 5.27(b)); the third the bridge deck and approach embankment construction (Figure 5.27(c)); and the fourth the abutment displacement into and away from the backfill soil (Figure 5.27(d)).

Component models created in Plaxis may be activated and deactivated during the calculation phases. This process was used in simulating the construction process and defining the sequence of events. Activation or deactivation introduces or removes the properties assigned to these component models within the cluster. The cluster representing the area beneath the model bridge deck and above the sloping construction fill surface (Space in Figure 5.28) is also not activated as this represents a space subject to atmospheric conditions only.

The initial condition models the preconstruction state of the site (Figure 5.27(a)). In the sequences of simulation, the initial step of the finite element calculation involves generating the initial stresses within the preconstruction soil materials. This is achieved in the simulation by introducing gravity loading to the finite elements modelling the preconstruction soil. Gravity loading introduces displacement within the soil model as

stress is generated. The stresses are retained as the initial stresses while the displacements are reversed. This provides a soil model free of displacement inputs but with initial stresses.

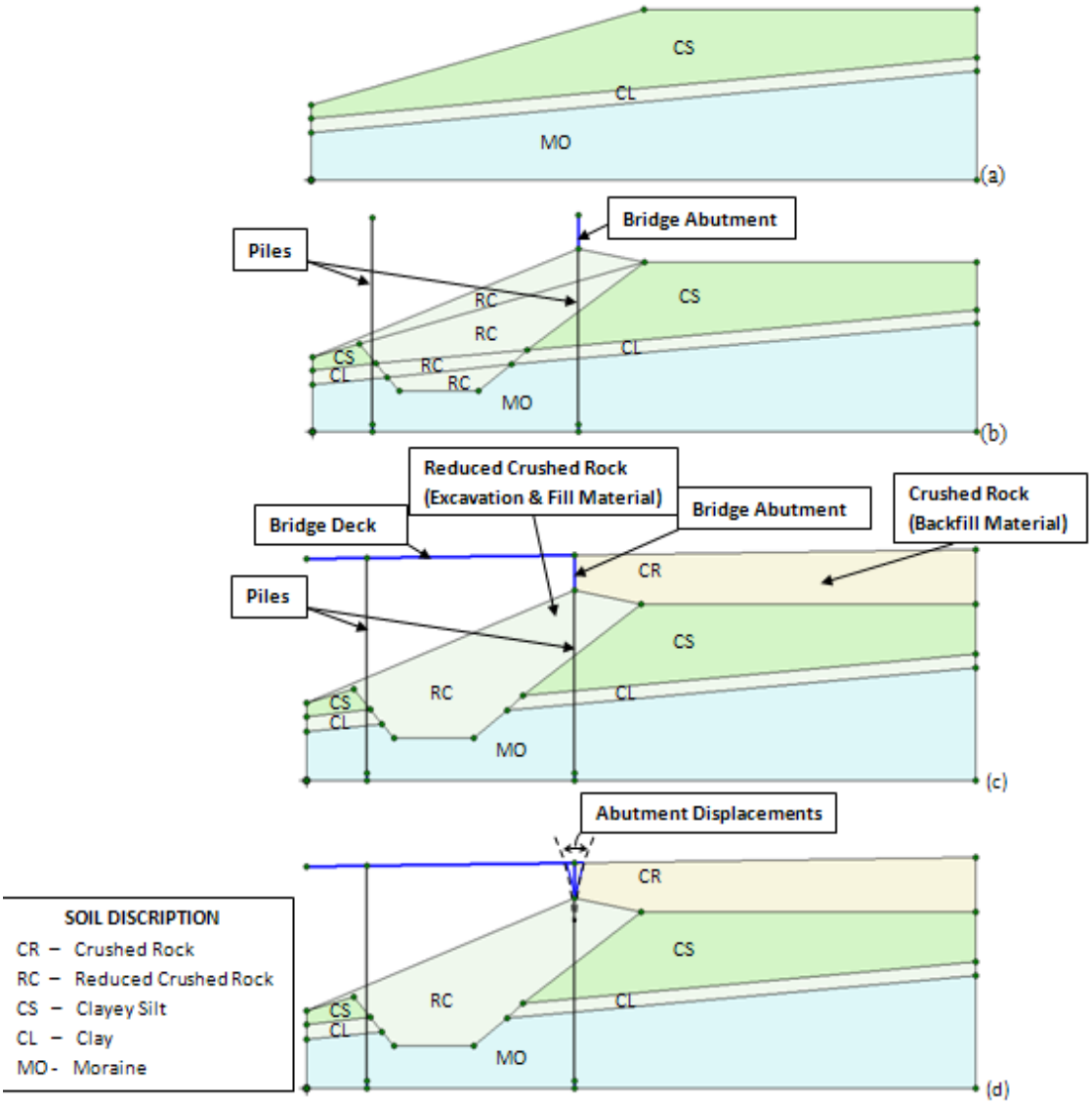

Figure 5.27: Model simulation; (a) Existing profile before construction; (b) Construction of bridge abutment, pile structures, and replacement fill materials in the construction phase; (c) Finished construction soil profile and bridge; (d) Abutment displacements

The next steps in the sequence of the simulation involved activating the soil clusters to simulate mass earth works construction and deactivating those clusters to simulate excavations. This was done by first deactivating the preconstruction material (Figure

5.27(a)) and then replacing with fill material identified in the area labelled RC in Figure 5.27(b). The cluster labelled CR in Figure 5.27(c) was then activated to simulate backfill soil construction. The construction simulation of structural members was also achieved by activating the presence of these members in the sequence of pile toe and piles, abutment (Figure 5.27(b)), and finally the bridge deck (Figure 5.27(c)). These processes of activation and deactivation were carried out in separate phases of calculations that follow the sequence in which these processes occur on the construction site during construction. This procedure models the history of the foundation soil and the stresses the foundation and construction materials were subjected to during the construction process. Finite element meshes within the clusters are illustrated in Figure 5.28.

The impact of the temperature change on an integral bridge structure is measured by the lateral displacement of the abutment within the recorded time. The abutment displacements recorded at the bridge site against time were used in simulating the thermal induced abutment displacement. The phases of calculation simulating the abutment displacement do so by simulating prescribed lateral displacement to the abutment in sequence (defined by the recorded time). This process simulates the soil-structure interaction between the abutment and the backfill soil.

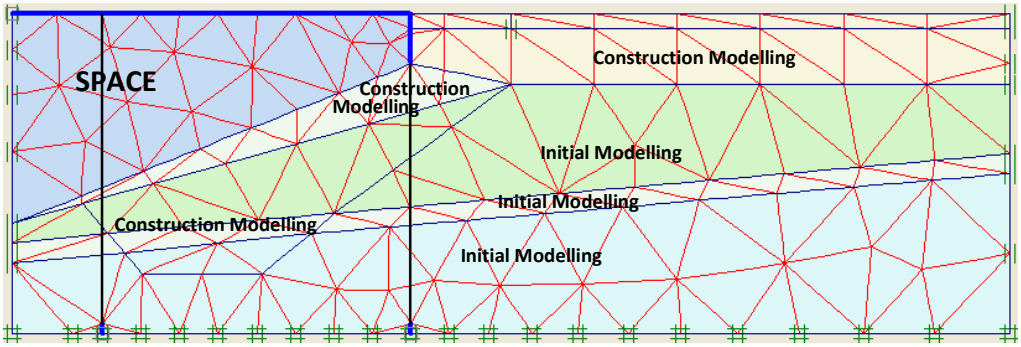

Figure 5.28: Finite element mesh of the bridge model highlighting clusters indicating initial steps and construction steps during the model development

Modelling and evaluating the impact of the thermal induced cyclic lateral displacement on the integral bridge structure and backfill soil is dependent on data that relates the corresponding values of temperature, abutment displacement, and earth pressure to time.

The abutment displacement simulation was limited to a time frame within which data relating these corresponding values on the Haavistonjoki Bridge was published

5.4.1. Load Model Simulation

The distributed and point load representing the road structure and the approach slab were activated to simulate the construction of the roadway after the bridge and backfill construction calculation phases. However, the soil cluster modelling the location of the road and approach slab structure at the upper section of the backfill soil cluster is not activated (see Road Structure in Figure 5.29(b)). This is because the cluster was replaced by the distributed load (see same location in Figure 5.29(a)) imposed on the backfill soil which models the road structure and approach slab loading impact on the backfill soil instead.

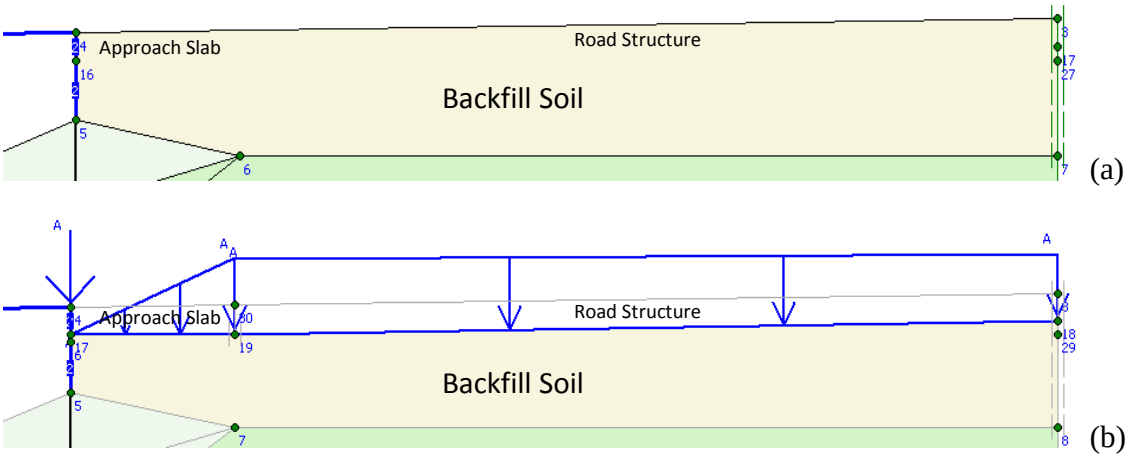

Figure 5.29: Modelling the road structure with distributed load.

5.4.2. Thermal Effect & Abutment Displacement

The predominant and most relevant effect of thermal changes in the functioning of an integral bridge is the expansion and contraction of the bridge deck. The magnitude of this expansion and contraction is largely dependent on the effective bridge temperature (EBT). The EBT of a bridge is controlled by several factors including the thermal conductivity of the various materials that make up the bridge, the sun's intensity and shades obstructing the

sun's radiation, wind effect, precipitation volume, and other environmental conditions and factors the bridge deck may be subjected to.

The actual displacement of the abutment as measured on site, is affected by several other factors other than the EBT. These other factors include the bridge abutment properties, the abutment foundation structure, the foundation soil properties and the backfill soil properties. At the Haavistonjoki Bridge site, the eastern abutment displacement is also affected by the prevailing circumstances of these conditions at the western abutment.

Theoretically, the thermal induced dimension change in a structural member that accounts for the linear displacement experienced at one end is a product of the coefficient of thermal expansion, the change in temperature and the length of the structure accounting for the change. This relationship is expressed in Equation 5.3 where ΔL is the change in length, α is the coefficient of thermal expansion, Δt is the change in temperature and L is the length (bridge deck length). However, calculating the actual change in abutment displacement on any integral bridge site is more complicated and certainly not obtained from the product of the coefficient of thermal expansion, temperature change and length of the bridge deck alone. This is because the influence of other factors that affect the displacement of the abutment some of which exhibit a non linear stress strain relationship such as the backfill and foundation soil. However, it has been found that the stiffness of an integral bridge superstructure is significantly higher than the stiffness of the backfill and abutment supporting piles such that the temperature induced abutment displacement is primarily controlled by the bridge structure behaviour (Arsoy et al., 2002) which is predominantly linear. Equation 5.3 is a simple relationship to predict the lateral displacement at the abutment based on the coefficient of expansion of the bridge deck. In practice, this cannot be used because of the factors related to EBT.

$$\Delta L = \alpha \, \Delta t \, L \qquad \text{…….. (5.3)}$$

The alternative was to use the published data and develop a linear relationship by comparing several recorded temperatures at specific times and the corresponding recorded

displacement. It was found that the displacement (measured in this case as change from a referenced point) of the eastern abutment may be approximated to a displacement pattern defined by Equation 5.4.

$$CL=1.712 + 0.458Ct \qquad \text{…….. (5.4)}$$

Equation 5.4 was obtained using the data obtained from the bridge site (Kerokoski, 2006) to create a simple linear regression for temperature and displacement data as shown in Figure 5.30. This equation is used as the model displacement for the integral bridge abutment in this study. In Equation 5.4, CL is the current length of the change in abutment displacement relative to the referenced abutment displacement position in mm, Ct is the current temperature in ^{o}C, 1.712 and 0.458 are the regression constants. Equation 5.4 sets an abutment displacement of 0mm to occur at a corresponding temperature of approximately -3.74^{o}C. This is the reference point for this equation.

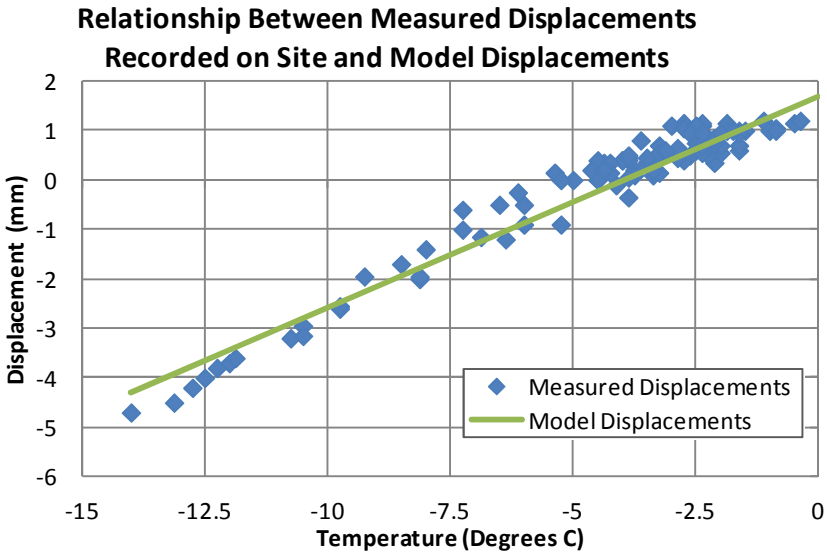

Figure 5.30: Graph of displacement against temperature showing the relationship between Equation 5.4 and the abutment displacement measured on site

5.5. Results

Results obtained in the process of modelling the thermal induced loading of the bridge are presented under the headings of abutment displacement, temperature controlled displacement, and earth pressure.

Imposed displacements in Plaxis are presented in Section 5.5.1. Abutment displacement results obtained through Equation 5.4 are presented in Section 5.5.2. The results of the earth pressure behind the abutment calculated within the model as a result of simulating the abutment displacement pattern recorded at the bridge site is presented in Section 5.5.3.

5.5.1. Abutment Displacement

Data presenting recorded values of the earth pressure, temperature and the eastern abutment displacement was presented from the 10th to the 16th of February 2004 (Kerokoski, 2006, Kerokoski and Laaksonen, 2005).

Figure 5.31 shows the abutment displacement output as modelled within Plaxis software (simulated displacement in Figure 5.31). These displacements were generated from inputs into Plaxis of the measured displacement on site as published (measured displacement in Figure 5.31). The result of the abutment displacement within the time frame that presents sufficient information for replicating the behaviour of the bridge in Plaxis is superimposed on the recorded displacements measured on site (across the month). Results within the section of the displacement against time graph indicating the 10th to the 16th of February 2004 are compared. The results show the output from the software closely modelling the measured displacement recorded on site. Output from the finite element software, Plaxis, approximates the displacements to the nearest tenth of a millimetre within the first millimetre and to the nearest millimetre after the first millimetre. Abutment displacement simulation is carried out using a 6 hourly interval input of measured displacement.

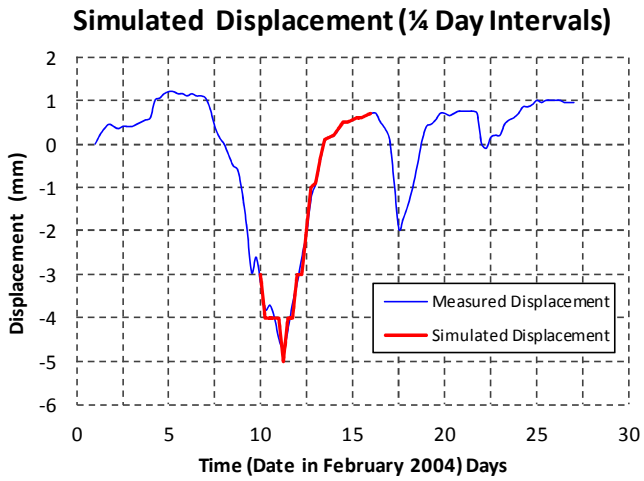

Figure 5.31: Plaxis simulated 6 hourly data input abutment displacement from 10th to 16th February 2004 superimposed on displacements recorded on site

5.5.2. Temperature Controlled Displacement

The previous section presented the results of the abutment displacement output generated from an input of the measured abutment displacement in Plaxis. This section presents the results of the abutment displacements model generated by Equation 5.4. In both sections, the results are compared with the measured displacement to indicate the accuracy of the outputs.

The displacement result generated by Equation 5.4 and the measured displacement recorded on site are presented in Figure 5.32. This compares the measured abutment displacement on site with the model abutment displacement using Equation 5.4 from the 10th to the 16th of February 2004. The Effective Bridge Temperature (EBT) as recorded on site determines the abutment displacement output using Equation 5.4. The results show the abutment displacement output from Equation 5.4 matches the measured displacement recorded on site.

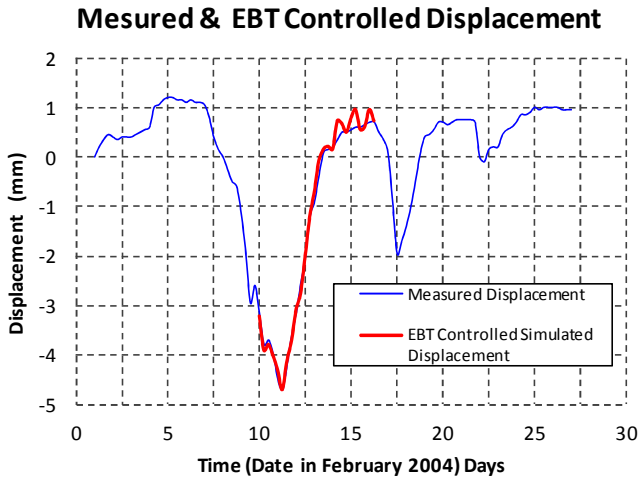

Figure 5.32: Simulated effective bridge temperature (EBT) from the 10th to 16th February 2004 and measured abutment displacement recorded on site from 1st to 27th of February, 2004

5.5.3. Earth Pressure

The average earth pressure from the earth pressure cells installed on the instrumented bridge site was obtained (average of earth pressure results in Figure 5.7). This was compared with the earth pressure results obtained from the displacements inputs in the finite element analysis (simulated displacement in Figure 5.31).

Plaxis 2D executes a two-dimensional plane strain analysis considering information along the bridge length and height whereas the earth pressure cells were positioned at intervals across the bridge width. As a result, the average earth pressures recorded in the earth pressure cells positioned behind the eastern abutment as shown in Figures 5.5 and 5.6 were used in modelling.

5.5.3.1. Initial & Fully Drained Models

Thermal loading is slow enough to prevent excess pore pressures developing in the granular materials. However, in the fine grained materials it is possible that some excess pore pressures will develop the amount depending on the permeability of the soils and the rate of

loading. It is highly likely that these soils will be partially drained. Rather than attempting to predict the actual excess pore pressure, two extremes were considered. These extremes are the fully undrained conditions and the fully drained conditions.

As discussed in Section 5.3.2.4.2, the crushed rock, reduced crushed rock, and moraine soils are more likely to exhibit drained characteristic. These are therefore modelled only under fully drained conditions. However, clayey silt and clay soils may exhibit some undrained characteristic. The clayey silt and clay soil are therefore modelled as fully drained and fully undrained.

From these drainage conditions, two integral bridge models were developed for the parametric studies. The first model simulates the crushed rock, reduced crushed rock, and moraine soil models as fully drained and simulates the clayey silt and clay soil models as fully undrained. This model is identified as the initial model. The second model simulates all the soil models as fully drained. The second model is identified as the fully drained model (see Table 5.4, Section 5.6.1.).

Figure 5.33 shows the simulated average earth pressure values generated from the model using the abutment displacement recorded on site in the initial model (simulated mean) and the average earth pressure values obtained from the earth pressure cells (measured mean) against time.

Figure 5.34 shows the simulated average earth pressure values generated from the model using the abutment displacement recorded on site in the fully drained model (simulated mean) and the average earth pressure values obtained from the earth pressure cells (measured mean) against time. Data generating the measured average earth pressure value curves, identified in Figures 5.33 and 5.34 as the measured mean were obtained from bridge instrumentation.

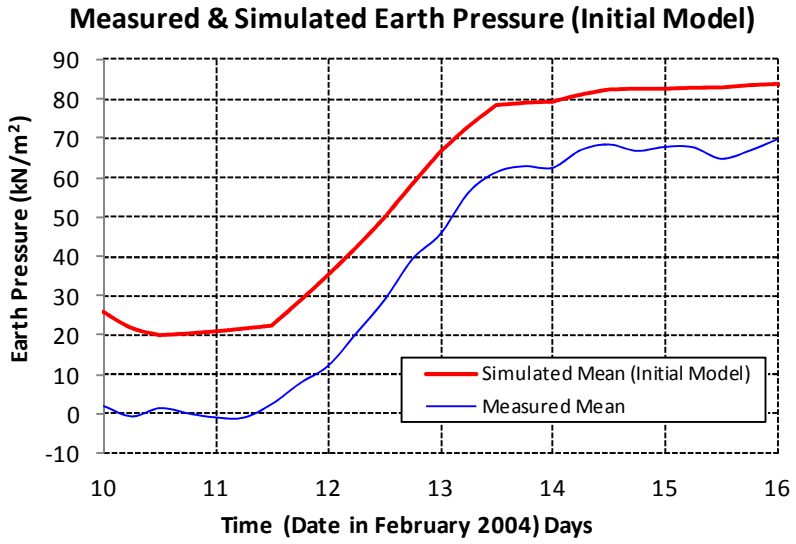

Figure 5.33: Initial model simulated earth pressure values compared with the average earth pressure values of the earth pressure cells measured on site

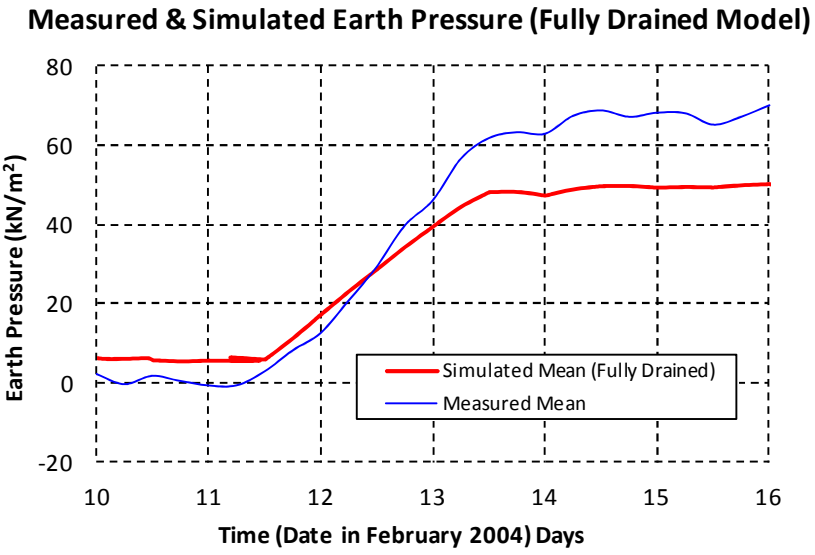

Figure 5.34: Fully drained model simulated earth pressure values compared with the average earth pressure values of the earth pressure cells measured on site.

The measured mean curve and the initial model have a relative response that appears similar in the general trend and pattern of behaviour as well as the earth pressure range. However, the values of the earth pressure differ (Figure 5.33).

5.6. Validation

Simulation outputs of the bridge model may be validated through replicating the historical behaviour, face validity test, and the verification test as described by Ford (1999). Details of these tests are presented in Section 4.5. The instrumentation of the bridge provided earth pressure values and the corresponding abutment displacement values, bridge temperature values, and the recorded time.

The historical behaviour test was used in validating the earth pressure values developed by the model bridge. The verification test was used in validating the EBT controlled eastern abutment displacement model as well as the finite element method approach and software output. The results as obtained in all cases satisfy the face validity test as they appear to be within reasonable and acceptable limits. Validation of these various components of the model using these methods improves confidence in the model developed for this research. This process is discussed in this section.

5.6.1. Historical Behaviour Test

Stress points selected in the integral bridge model at similar locations of the earth pressure cells groups (Figure 5.16) measured the earth pressure developed in the model during the loading simulation. Figures 5.33 and 5.34 compares the average earth pressure measured on site to the predicted average earth pressure.

It can be observed that the earth pressure developed and measured on site on the 10th of February 2004 is lower than the earth pressure values simulated from the models at a time modelling the same day (Figure 5.33 and 5.34). The relative changes in earth pressures are similar. The initial difference may be attributed to a few factors. The history of the existing soil is a factor that may possibly be responsible for the difference between the predicted results and the measured results from the bridge site. The actual time of construction may have been different from that used in the prediction. The installation of the earth pressure cells could have affected the earth pressures acting on the cells.

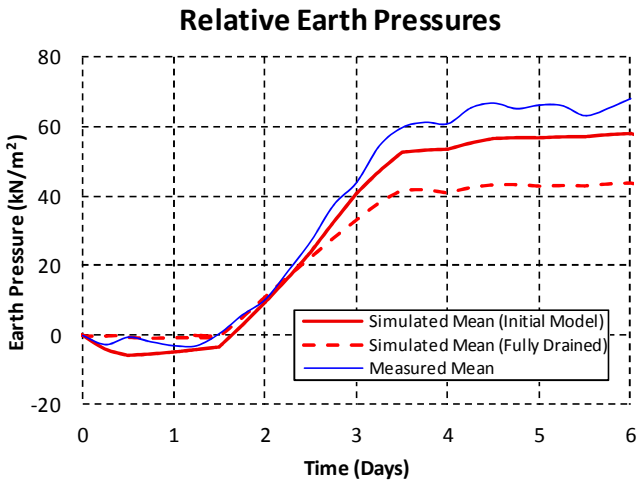

Figure 5.35: Relative earth pressures developed in the initial model and fully drained model compared to the relative earth pressures measured on site

The validation is reported relative to the 10th February in time. Figure 5.35 presents the relative earth pressure results comparing the earth pressure values from the initial model simulation result, the fully drained model simulation result, and the measured values obtained from the bridge site.

In modelling, certain parameters within the event being modelled may be uncertain. There may also be variations in the recorded values of parameters and the actual parameters. This may result in variations between the modelled behaviour and the actual behaviour. These values may be adjusted within the probable range of error, to obtain acceptable results (Ford, 1999). Typically, within a specific soil mass, soil parameters may vary slightly from one point to another. Measured soil parameters may be different from the in situ values because the stress path of the test procedure is different from the in situ stress path. The extent of variation may depend partly on the nature and style, and possibly time (as in the case of the integral bridge) of obtaining the measurements.

The backfill stiffness value is considered the primary parameter of concern on the instrumented bridge construction site because of the sensitive response of granular material stiffness values to compaction (Leong et al., 2006, Modoni et al., 2010). The stiffness measurement is traditionally taken before the completion of the construction process as part of the site investigation or material testing for design and construction. However, the

mobilised stiffness may differ because the laboratory compaction is different from the in situ compaction leading to different densities and the construction process can cause further changes in density and therefore stiffness. Consequently, the stiffness parameter of the model was varied to reflect the variation of stiffness that may arise from material compaction. A series of stiffness values was assumed in several simulations of the integral bridge model generating a series of earth pressure values. The stiffness value providing the best model of the backfill earth pressure was obtained using a statistical approach.

The mean squared error statistical approach (Montgomery and Runger, 2007, Montgomery et al., 2007), expressed in Equation 5.5, and best estimate condition between any two estimates (where E_1 is the best estimate), expressed in Equation 5.6, were adopted in the determination of the best fit to the predicted and measured earth pressures.

$$E = \sum_{i=1}^{n} (y_i - \hat{y}_i)^2 \qquad \text{…….. (5.5)}$$

$$\frac{E_1}{E_2} < 1 \qquad \text{…….. (5.6)}$$

E is the mean square error of the estimator, n is the number of variables, y is the estimator and ŷ is the data, E_1 and E_2 are any two estimator's mean square error. Several variations of the stiffness values were considered in both the initial model and the fully drained model. The best model estimate was achieved at a backfill stiffness value of 92.1MN/m^2 against 80MN/m^2 reported in the publication.

The best model estimate of the backfill soil behaviour using a stiffness value in the initial model presented in Figure 5.36, show consistent pattern of behaviour between the mean earth pressures measured on site and the simulated mean earth pressures obtained through the initial model. Figure 5.36 also presents the result of the fully drained model with a stiffness value of 92.1MN/m^2. Variations in the stiffness values of the fully drained model obtained a best fit curve to the actual pattern of the behaviour of the backfill soil at a

significantly higher stiffness value of 107.5MN/m^2. However, the best match of the fully drained model behaviour pattern presented results with obvious variations from the measured backfill soil behaviour when compared with results from the initial model (Figure 5.37).

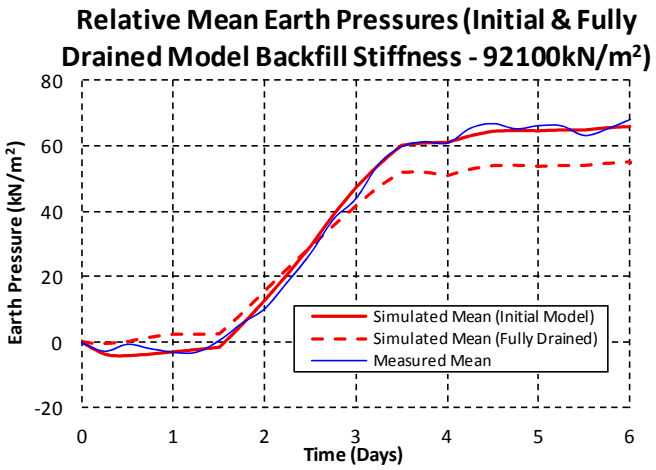

Figure 5.36: Best estimate of the average relative earth pressures measured on site generated through a backfill stiffness value of 92.1MN/m2 in the initial model and the earth pressure generated where subjected to fully drained conditions.

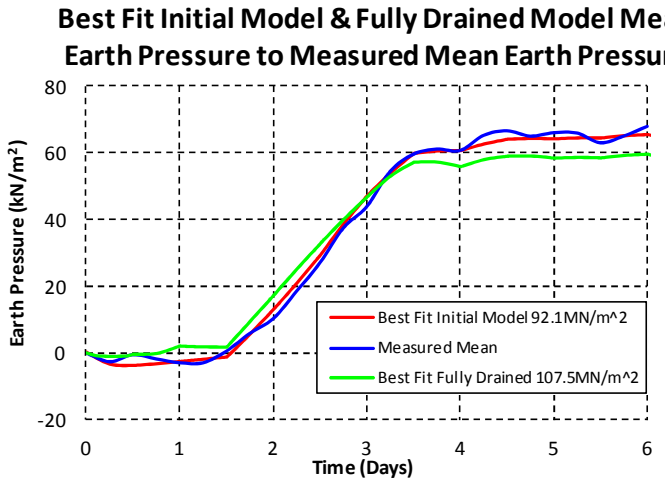

Figure 5.37: Best fit estimates of the average relative earth pressures as measured on site generated through variation of the Initial model and the fully drained model stiffness values.

Variations of the other soil parameters used in modelling (identified in Section 5.3.1.4.2) had an insignificant effect on the pattern of behaviour defined by the stiffness (the insignificant effect of changes in other backfill soil parameters was investigated and reported in Chapter 6). Where the stiffness in the initial model is assumed to be 92.1MN/m^2, Figure 5.36 defines the boundaries within which the earth pressures developed as a result of the drainage state of the soil is expected to exist. This falls within the limits defined by the initial model and the fully drained model.

The results presented in Figure 5.37 show that the actual soil behaviour of the in situ backfill soil after construction may be based on a stiffness value of 92.1MN/m^2, against the preconstruction recorded value of 80MN/m^2, using the initial model. The initial model produce a better fit than the fully drained model suggesting that the soil response was more likely to be partially drained i.e. the stress changes due to the variation in temperatures generated excess pore pressure in the foundation soils. Table 5.4 presents the input values of stiffness, cohesion, friction angle, dilatancy and the unit weight that match the behaviour of the instrumented bridge. Values of the other Hardening Soil model parameter are as presented in Table 5.3. These values (parameters of Table 5.4 and the remaining parameters in Table 5.3) are used as the model soil parameters in Chapters 6 and 7.

Name	**Model (Type)**		γ_{unsat} **kN/m^3**	γ_{sat} **kN/m^3**	E_{50} **kN/m^2**	**c kN/m^2**	ϕ **o**	ψ **o**
	Initial	*Fully Drained*						
Crushed rock	Drained	-	22	23	92,100	0	45	8
	-	*Drained*						
Reduced crush rock	Drained	-	20	22	29,700	0	42	5
	-	*Drained*						
Clayey silt	Undrained	-	17	18	9,300	1	33	0
	-	*Drained*						
Moraine	Drained	-	23	23	80,000	0	45	4
	-	*Drained*						
Clay	Undrained	-	16	18	4,000	2	25	0
	-	*Drained*						

Table 5.4: Soil Material properties

5.6.2. Verification Test (Temperature)

The UK Design Manual For Roads and Bridges (BD37/01, 2001) recommends that for calculating temperature effects, the coefficients of thermal expansion for structural steel and concrete structures may be taken as 12 x 10^{-6}/°C. However, in the case of a thermal induced displacement of an integral bridge abutment, the measured expansion is dependent on several factors as described in Section 5.4.2.

An actual expansion displacement of approximately 5.9mm for a change in temperature of 13.625°C was measured on site at the eastern abutment. The calculated deck expansion value using the coefficient of thermal expansion value (12 x 10^{-6}/°C) as recommended by the UK design manual for roads and bridges (assuming the 50m bridge length) in Equation 5.3, is 8.175mm for a similar temperature change value. This translates to a thermal expansion ratio of 0.72 for the measured abutment displacement length on site to the theoretical expansion length used in design.

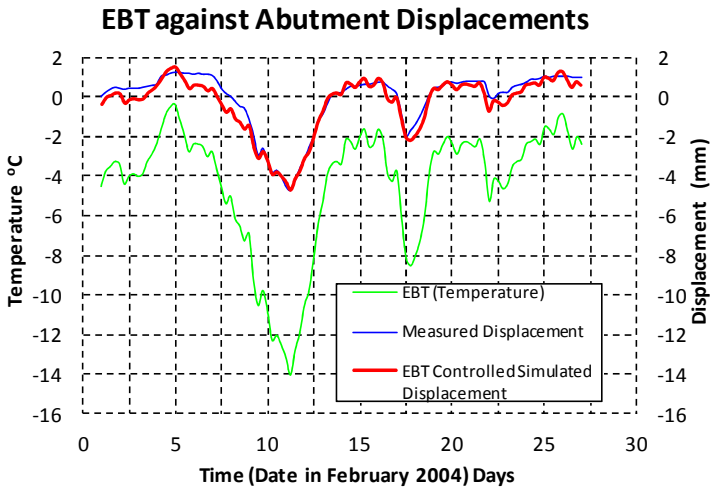

Figure 5.38: EBT with corresponding abutment displacement measured on site and the modelled temperature controlled abutment displacement

Across the life of the bridge, the effective bridge temperature (EBT) of the structure may be subjected to extremes of -26.1°C for minimum temperature and 38.5°C for maximum temperature based on similar extreme shade air temperatures obtained in England (Met.Office, 2012). Subjected to these extreme temperatures, the relationship representing

the effect of the factors affecting abutment displacement is shown in Figure 5.39. The ratio of the simulated eastern abutment displacement length from the EBT controlled abutment displacement model (using Equation 5.4), to the theoretical expansion length used in design (Equation 5.3), on the 50m span instrumented integral bridge across the extreme temperatures is (29.58mm/38.76mm) 0.76.

The result ratio for the abutment displacement temperature model (Equation 5.4) is 0.76 while the result ratio for the theoretical expansion length used in design (Equation 5.3) is 0.72. These two result ratio show reasonable consistency within an error margin of ±6%. This suggests that the EBT controlled eastern abutment displacement model (Equation 5.4) is consistent with the actual behaviour and, by design standards, the error margin of ±6% is acceptable.

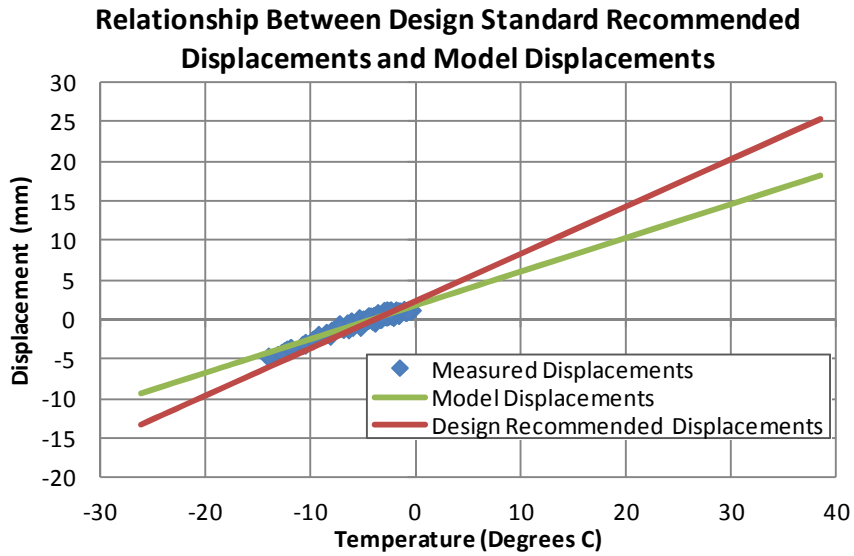

Figure 5.39: Relationship between Equation 5.4 and Equation 5.3 relative to the measured abutment displacement measured on site.

The curves showing the model displacement calculated (using Equation 5.4), the actual displacement measured on site, and the effective bridge temperature (EBT) obtained from site measurements are presented in Figure 5.38. While the displacements calculated from the EBT appear to be sensitive to immediate temperature changes, it closely matches the displacements measured on site that appear to be less sensitive to immediate changes in temperature. Figure 5.39 illustrates the relationship between the model abutment

displacement that accounts for the factors affecting the actual abutment displacement (Equation 5.4), the abutment displacement calculated by design recommendations (Equation 5.3), and the abutment displacement taken from site measurements.

5.6.3. Verification Test (Finite Element Approach)

The verification test identified by Ford (1999) may be used in validating the finite element software approach in the modelling of the earth pressure values developed behind the abutment of an integral bridge. This is done in this study by comparing the output generated using the finite element method approach to the output generated using a different approach in the analysis of earth pressure developed behind the abutment of an integral bridge. Wood and Nash (2000) modelled a simplified version of an integral bridge applying the finite difference numerical method using FLAC 3.3 software in the analysis.

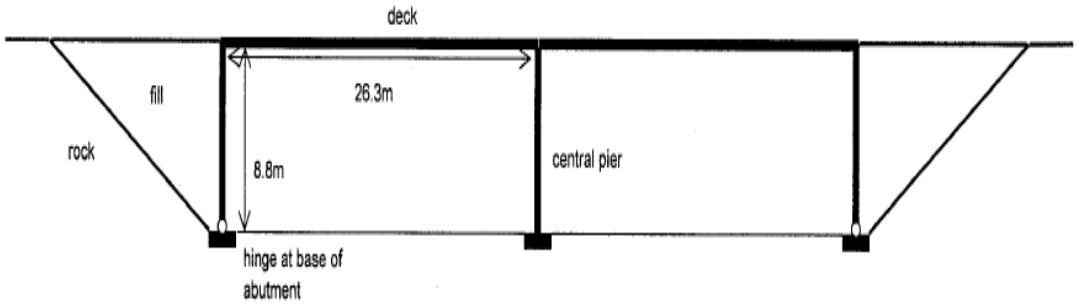

Figure 5.40: Schematic diagram of integral bridge (Wood and Nash, 2000)

A similar integral bridge model was developed using the finite element method. Identical parameters used in the finite difference model development and abutment displacement simulation were also used in developing the model integral bridge, and in simulating the model abutment displacement in Plaxis. The Mohr Coulomb model designed to simulate an elastic perfectly plastic behaviour was used in both analyses to simulate the soil behaviour (Wood and Nash, 2000).

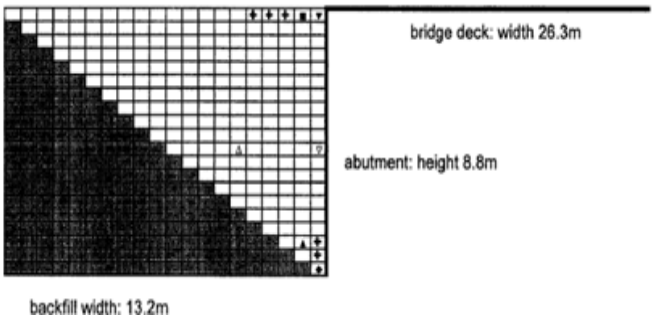

Layout of zones in FLAC software model (Wood and Nash, 2000)

(a)

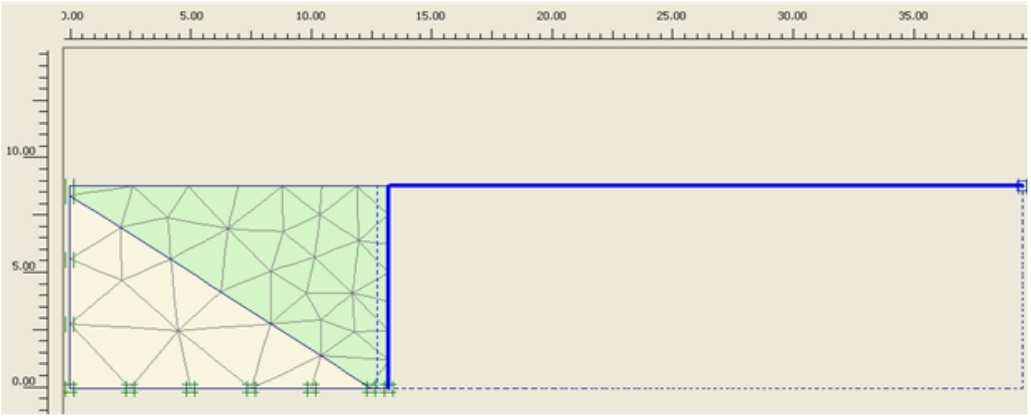

Finite element mesh in Plaxis

(b)

Figure 5.41: Models displaying unite of analysis in FLAC (a) and Plaxis (b)

Values of the soil parameters as used by Wood and Nash (2000) were used in developing the soil model in Plaxis. Similar displacement values to the top of the abutment as published was used in the displacement of the finite element model (Wood and Nash, 2000). Properties of the abutment and deck as defined in the publication was also used (Wood and Nash, 2000). An abutment thickness of 1.2m was assumed. The results obtained using Plaxis finite element software approach compared with the results obtained by Wood and Nash (2000) using the finite difference approach were similar. Modelling details and results are presented in Figures 5.40, 5.41 and 5.42. These results also supports confidence in the approach adopted in the use of Plaxis 2D to develop the component models enabling loading simulations on an integral bridge model.

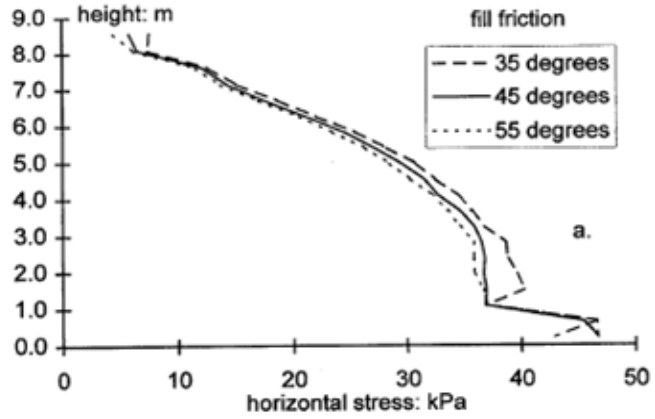

(a)

Horizontal stresses (FLAC 3.3) developed at end of construction using the finite difference method numerical software in analysis

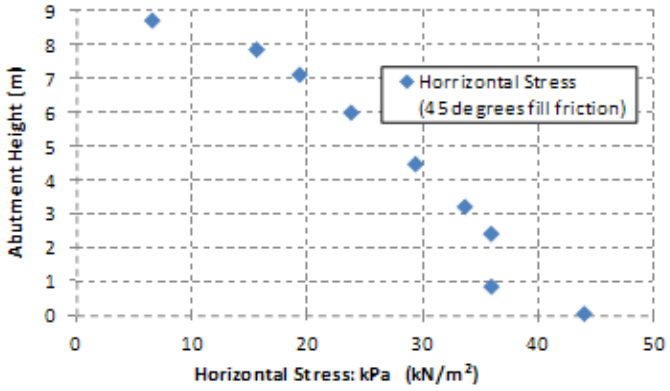

(b)

Horizontal stresses (Plaxis 2D Version 9.0) developed at end of construction using the finite element method numerical software in analysis.

Figure 5.42: Results of horizontal stresses modelling earth pressures in FLAC (a) and Plaxis (b)

5.7. Conclusion

The process of developing an integral bridge model and simulating the abutment displacement and earth pressures developed within the backfill soil of an instrumented integral bridge were presented in this chapter. The relevant details of an instrumented integral bridge required in the successful development of a model was described and the data obtained through the instrumentation of the bridge was presented.

It is appreciated that modelling the abutment displacement and the earth pressures developed as a result of the thermal induced expansion and contraction of the abutment involves several relevant component models. The processes involved in the development and compilation of these component models to function as a unit sustaining common loading in a characteristic manner were highlighted and discussed. Parameters used in the component model development and loading simulation of the backfill soil were obtained from published information providing data on an instrumented integral bridge. Validation of the result outputs generated by these component models was discussed.

Modelling an integral bridge remains a complex undertaking even with advanced finite element numerical method software. It was found that modelling an instrumented bridge presents several challenges not often considered in the process of simply modelling an integral bridge without actual performance data to compare the model output against. These challenges arise from fine details, which may be considered less relevant in the choices made while modelling components of the integral bridge in a soil-structure interaction using the finite element method. However, these challenges are also appreciated to be dependent on the geometric characteristic of the structure as well and therefore care must be taken in appreciating primarily the properties of the structure and soil, and the characteristic of the modelling tool. The principles behind the solutions adopted were discussed.

The results of models featuring fully drained and fully undrained characteristics in the clay foundation soils were compared. Subjected to similar conditions, the fully drained model expectedly developed lower earth pressure values under the displacement controlled integral bridge loading than the initial model. It was found that a relatively minor modification to the backfill stiffness parameter of the fully undrained model generated results that closely matched the actual behaviour of the backfill soil as measured on site. However, with extensive modification to the backfill stiffness parameter of the fully drained model, the best match displayed results with obvious variations from the actual behaviour. It is also appreciated that the foundation soils are not significantly affected by the thermal loading even though they affect the earth pressures. This highlights the

importance of taking into consideration and evaluating the effect of the state of the clay components of foundation soil during loading on the behaviour of the backfill material.

An effective bridge temperature (EBT) abutment displacement model was also developed for use in Chapter 6. The relationships between this temperature model displacement, the actual displacement measured on site, and the UK recommended design standard displacement were highlighted showing that the design predictions are incorrect as they ignore the complex thermal expansion and displacement of the bridge deck and the abutment. However, the ratio between the thermal displacements predicted by the design code and the measured values confirmed by the numerical study suggests a simple way to predict design displacements.

The next chapter presents a parametric study on the backfill soil of an integral bridge. This is carried out by introducing variations to the backfill soil parameter values and analysing the impact of these variations on the earth pressure. The impacts of the state of the foundation soil on the variation of these backfill soil parameters are also evaluated. This analysis is carried out on the integral bridge and soil models that have been developed in this chapter.

Chapter 6 : BACKFILL SOIL PARAMETRIC STUDY

6.1. Introduction

The nature of the backfill soil and its behaviour under loading is predominantly responsible for the magnitude of earth pressure experienced behind the abutment of the integral bridge structure. A characteristic behaviour of a soil mass is predicted through the values of the relevant soil parameters, established to be a measure of the properties that are responsible for the behaviour. During the design process of an integral bridge, the predicted characteristics of the backfill soil obtained from the values of the backfill soil parameters present a reliable indication of the long-term performance of the bridge. Determining the design length of the bridge is based on this information. The choice of backfill material and management of these materials in the construction process is also dependent on this information.

This chapter presents the results of a parametric study carried out to determine the impact that changes in specific backfill soil parameters would have on the earth pressure behind the abutment of an integral bridge. The instrumented integral bridge (discussed in Chapter 5) is used in this study. The bridge model and its measured abutment displacement pattern are used as the primary integral bridge abutment displacement model for this study. However, a supporting abutment displacement pattern based on an assumed EBT is used to develop a cyclic abutment displacement model, theoretically expected from the thermal induced abutment displacement of the integral bridge. The impact of the fully drained and the fully undrained state of the fine grain soils within the foundation material on the behaviour of the backfill soil is taken into consideration in these analyses.

The backfill and foundation soil are modelled using soil parameters obtained from the bridge site investigation. Soil parameters investigated in earlier studies include the stiffness, cohesion, friction angle, dilatancy and the unit weight (Wood and Nash, 2000, Kerokoski

and Laaksonen, 2005, Kerokoski, 2006, Nilsson, 2008). These are the primary parameters investigated in this parametric study. In addition, the effect of change in the Poisson's Ratio is also investigated in Section 6.6.3. However, within a specific soil material type, these parameters exist within some established range. Soil parameter values may vary slightly across similar materials of the same type obtained at different intervals even from the same source or location. The construction process involving the material may also introduce variation within these parameter values. These variations result in changes within the soil properties of similar material type. Relatively large variations may potentially lead to significant changes in the soil behaviour as a result of the largely uncertain effect of the soil-structure interaction. Knowledge obtained from this study would enable a more adequate design, accommodating the effect of these variations that may arise as a result of the material source or construction process.

6.2. Model Soil & Abutment Displacement

The soils and abutment displacement patterns are defined and described in this section. The measured lateral abutment displacement pattern used as the primary model abutment displacement pattern is presented in this section. Details of the cyclic abutment displacement model carried out to support the findings are also presented.

6.2.1. Backfill & Foundation Soil

The backfill soil material parameters obtained from the model soil (generating outputs matching the behaviour of the instrumented bridge backfill - see details in Section 5.61) with a backfill soil stiffness value of 92.1MN/m^2, was used in this parametric study. Details of the instrumented bridge's backfill and foundation soil parameters used in this analysis are presented in Tables 5.3 and 5.4 (see Section 5.6.1). Two parallel models were simulated in which the behaviour of the foundation soil models under loading was altered. This was to evaluate the effect of assuming fully drained and fully undrained fine grain soils behaviour within the foundation material, under thermal induced loading on the behaviour

of the backfill soil. These parallel models identified as the initial model and the fully drained models are as defined in Section 5.5.3.1.

The parametric study required the variation of specific soil parameters of the backfill soil during the loading simulation. While the values of one or more of these soil parameters - stiffness, cohesion, friction angle, dilatancy and the unit weight are altered for each loading simulation, other soil parameters retained a default backfill soil parameter value. These default values are as presented in Table 5.4. This was carried out in order to appreciate the effect of changes to the specific parameter on the backfill soil behaviour. The relationship between the fully saturated bulk density and dry density was maintained in the variation of soil parameters.

6.2.2. Abutment Displacement Pattern

The abutment displacement pattern obtained from the bridge site from the 10th to the 16th day of February 2004 is used as the primary displacement model in this study (see measured displacement in Figure 5.31). However, between these dates (10th to 16th of February, 2004), the abutment displacement recorded does not appear to follow a simple cyclic lateral abutment displacement pattern.

A problem of the integral bridge is the soil-structure interaction associated with the cyclic loading of the backfill soil. Studies carried out by many researchers have shown that cyclic loading in soil result in different soil behaviours. This includes studies by Carder and Hayes (2000) that determined cyclic loading of soils can be characterised in two ways (one way cyclic loading and two way cyclic loading) all resulting in different soil behaviours, both of which may apply during a thermal induced integral bridge abutment loading of the backfill soil. Due to the fact that the abutment displacement pattern measured on the bridge site does not define a cyclic loading pattern, the findings on the impact of change in soil parameter values on the earth pressure using this displacement pattern may require further evaluation accommodating the impact of cyclic loading.

A secondary displacement model option is therefore considered to support the findings that may be established using results obtained from modelling the measured abutment displacement pattern. This option models a typical cyclic abutment displacement pattern established by a cyclic temperature variation. The model simulates a predicted abutment displacement induced by the daily maximum and minimum temperature of the bridge site. The model is based on the instrumented bridge introducing only change to the abutment displacement pattern.

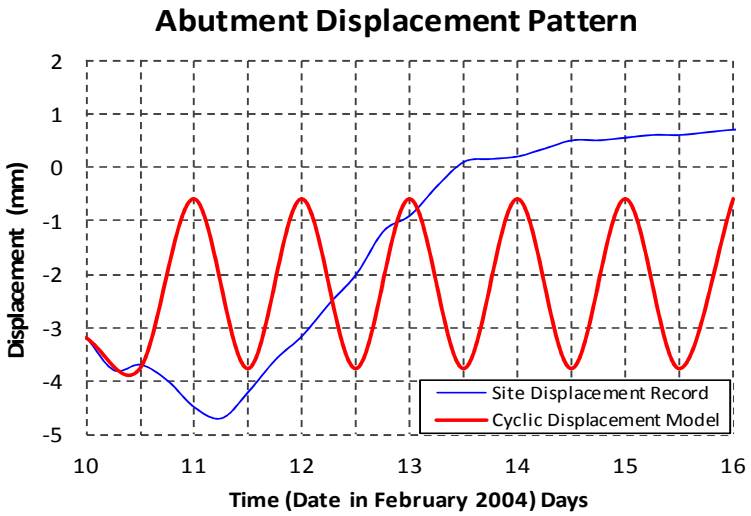

Figure 6.1: Graph showing EBT controlled average daily maximum and minimum temperature at bridge site region (Cyclic Displacement Model) and actual recorded displacement (Site Displacement Record).

The daily average maximum and minimum temperature recorded at the Tampere and Jyväskylä region of Finland, the location of the bridge, on the 10th to the 16th of February 2004, was determined to be approximately -5°C and -12°C respectively. This information obtained from the temperature contour map published by the European Climate Assessment & Dataset (ECA&D) (Klein Tank et al., 2002) for these dates, was used in determining the predicted displacement the bridge structure may have been subjected to based on the average daily maximum and minimum temperature recorded. This was developed from the EBT controlled abutment displacement model (see Equation 5.4) that provided abutment displacement results with high accuracy. Details of the model abutment displacement patterns are presented in Figure 6.1.

6.3. Backfill Soil Parameter Range

The parametric study carried out involves the variation of the model backfill soil (crushed rock) parameters across a specific range. To generate realistic results, the limits and range of the backfill soil parameter were established within limits considered realistic to the specific soil parameter in a typical crushed rock material. Typically, information available on the backfill soil properties of structures of this type are limited (Wood and Nash, 2000). Some information on the typical range of the backfill soil parameters was also provided from the bridge site investigation (Nilsson, 2008, Kerokoski, 2006, Kerokoski and Laaksonen, 2005).

Consequently, the range of typical soil parameter for crushed rock material was obtained from publications by several authors on crushed rock and soil material parameters. The crushed rock backfill soil parameter range established for the purpose of this parametric study are cohesion, 0kPa – 4kPa, unit weight, 18kN/m^3 – 22kN/m^3, friction angle 35^o – 45^o (Bowles, 1997, Bakker et al., 2006, Bell, 2000, Bowles, 1984, Chou and Bobet, 2002, McNally, 1998, Parsons, 1992, Steele and Snowdon, 1996, Smith et al., 2001). The range of the stiffness value of the compacted crushed rock material used in the backfill construction was obtained from the publication (Kerokoski, 2006). The dilatancy angle range was based on the friction angle dilatancy relationship in granular soils (De Josselin De Jong, 1976, Rowe, 1962). The stiffness and dilatancy range are 50MPa – 250MPa, and 0^o – 10^o respectively.

	BACKFILL SOIL PARAMETERS				
	Stiffness	Cohesion	Friction Angle	Dilatancy	Unit Weight
BACKFILL SOIL PARAMATER RANGE	50 MPa	0 kPa	35^o	0^o	18 kN/m^3
	100 MPa	1 kPa	37.5^o	3^o	19 kN/m^3
	150 MPa	2 kPa	40^o	6^o	20 kN/m^3
	200 MPa	3 kPa	42.5^o	8^o	21 kN/m^3
	250 MPa	4 kPa	45^o	10^o	22 kN/m^3

Table 6.1: Model soil backfill parameters

The parametric study involves a wide combination of several parameter values. Within the range of the backfill soil parameters, a number of parameter values considered sufficient to

establish some pattern of behaviour were identified. For each backfill soil parameter, five parameter values including values that define the upper and lower limit and three other values in-between these limits were established. Details of the soil parameters and values identified for this parametric study are presented in Table 6.1.

In reporting the impact of these parametric studies, two types of parametric variation were further identified based on defining each of the five parameters as one of the following; a subject parameter; a variable parameter; or other parameter. The first parametric variation involves defining one parameter as variable parameter and four as other parameter. In this parametric variation, the five values of the variable parameter identified under the backfill soil parameters column in Table 6.1 are simulated with other parameter values retaining the default parameter value as defined in Table 5.4. The second parametric variation involves defining one parameter as subject parameter, one as variable parameter and three as other parameter. In the second parametric variation, for each value of the five subject parameters (a column in Table 6.1), the five variable parameter values (a second column in Table 6.1) are simulated with the three other parameter values retaining the default parameter values (defined in Table 5.4). In both parametric variation types (first and second), the backfill soil parameters identified as the subject, variable and other parameter change until all combinations have been simulated.

These parametric variation combination were simulated using the initial model and again in the parallel fully drained model (see Model (Type) in Table 5.4). In the parameter combination layout within this studies, a number of repetitions could have occurred where the identity of the subject and variable soil parameter in one simulation were interchanged in another. To eliminate the risk of repetition and omissions, a numerical identity was assigned to every simulation option. This process supported a more effective management of the large number of simulations required in this analysis. While the first parametric variation type is enveloped in the second parametric variation type, the first was found to appropriately define the effect of the changes to the values of the variable parameter on the model, therefore presenting an accurate overview of the more detailed simulation combinations carried out in the second.

6.4. Simulation Plan

Simulations on a number of soil parameter combinations was not carried out because of the interrelationships that exist between the friction angle and dilatancy in granular materials, making some combination unrealistic (Bolton, 1986, De Josselin De Jong, 1976). The default soil model parameters include a dilatancy angle of 8^o not sustainable with a friction angle value of 35^o and 37.5^o. This combination may be appreciated in the stiffness against friction angle table (Table 6.3), cohesion against friction angle table (Table 6.7), friction angle against dilatancy table (Table 6.12), dilatancy against friction angle table (Table 6.16), and unit weight against friction angle table (Table 6.20). Other unrealistic combinations exist where friction angle and dilatancy were varied as highlighted in Sections 6.4.3 and 6.4.4. These soil models, indicated in red italic fonts were not taken into consideration in the analysis. The parametric variation involved 396 independent cases. This is because in the parametric variations, the variables are dependent on each other causing repetitions. These simulations were numbered accordingly (See Table 6.2- 6.21).

The format of presenting the simulation plan is explained using the tables in Section 6.4.1. Section 6.4.1 presents the simulation plan where the stiffness parameter is chosen as the subject parameter. Details of the subject parameter (stiffness) are presented within the upper two rows within the tables in this section (Tables 6.2-6.5). In Table 6.2, cohesion is identified as the variable parameter while the remaining parameters not identified as either subject or variable are identified as other parameters. Tables 6.3, 6.4 and 6.5 have friction angle, dilatancy and unit weight respectively identified as the variable parameters. Details of the variable parameters are presented within the first two columns in this section. The value of the subject and variable parameters within each simulation identity is as defined in the row and column of the table while the values of the other parameters are the default values in Table 5.4. This simulation plan presentation format applies in Sections 6.4.2, 6.4.3, 6.4.4 and 6.4.5 for cohesion, friction angle, dilatancy and unit weight respectively.

6.4.1. Stiffness

Simulation layout for stiffness parametric study is presented in Tables 6.2 - 6.5.

		STIFFNESS				
		50 MPa	**100 MPa**	**150 MPa**	**200 MPa**	**250 MPa**
Cohesion (Initial Model)	**0 kPa**	4	123	5	124	6
	1 kPa	139	140	141	142	143
	2 kPa	13	144	14	145	15
	3 kPa	146	147	148	149	150
	4 kPa	16	151	17	152	18
Cohesion (Fully Drained Model)	**0 kPa**	1	121	2	122	3
	1 kPa	125	126	127	128	129
	2 kPa	7	130	8	131	9
	3 kPa	132	133	134	135	136
	4 kPa	10	137	11	138	12

Table 6.2: Stiffness against cohesion

		STIFFNESS				
		50 MPa	**100 MPa**	**150 MPa**	**200 MPa**	**250 MPa**
Friction Angle (Initial Model)	**35°**	*25*	*167*	*26*	*168*	*27*
	37.5°	*169*	*170*	*171*	*172*	*173*
	40°	28	174	29	175	30
	42.5°	176	177	178	179	180
	45°	4	123	5	124	6
Friction Angle (Fully Drained Model)	**35°**	*19*	*153*	*20*	*154*	*21*
	37.5°	*155*	*156*	*157*	*158*	*159*
	40°	22	160	23	161	24
	42.5°	162	163	164	165	166
	45°	1	121	2	122	3

Table 6.3: Stiffness against friction angle

		STIFFNESS				
		50 MPa	**100 MPa**	**150 MPa**	**200 MPa**	**250 MPa**
Dilatancy (Initial Model)	**0°**	37	195	38	196	39
	3°	197	198	199	200	201
	6°	202	203	204	205	206
	8°	4	123	5	124	6
	10°	40	207	41	208	42
Dilatancy (Fully Drained Model)	**0°**	31	181	32	182	33
	3°	183	184	185	186	187
	6°	188	189	190	191	192
	8°	1	121	2	122	3
	10°	34	193	35	194	36

Table 6.4: Stiffness against dilatancy

		STIFFNESS				
		50 MPa	**100 MPa**	**150 MPa**	**200 MPa**	**250 MPa**
Unit Weight (Initial Model)	**18** kN/m^3	49	223	50	224	51
	19 kN/m^3	225	226	227	228	229
	20 kN/m^3	52	230	53	231	54
	21 kN/m^3	232	233	234	235	236
	22 kN/m^3	4	123	5	124	6
Unit Weight (Fully Drained Model)	**18** kN/m^3	43	209	44	210	45
	19 kN/m^3	211	212	213	214	215
	20 kN/m^3	46	216	47	217	48
	21 kN/m^3	218	219	220	221	222
	22 kN/m^3	1	121	2	122	3

Table 6.5: Stiffness against unit weight

6.4.2. Cohesion

Simulation layout for cohesion parametric study is presented in Tables 6.6 - 6.9.

		COHESION				
		0 kPa	**1 kPa**	**2 kPa**	**3 kPa**	**4 kPa**
Stiffness (Initial Model)	**50 MPa**	4	139	13	146	16
	100 MPa	123	140	144	147	151
	150 MPa	5	141	14	148	17
	200 MPa	124	142	145	149	152
	250 MPa	6	143	15	150	18
Stiffness (Fully Drained Model)	**50 MPa**	1	125	7	132	10
	100 MPa	121	126	130	133	137
	150 MPa	2	127	8	134	11
	200 MPa	122	128	131	135	138
	250 MPa	3	129	9	136	12

Table 6.6: Cohesion against stiffness

		COHESION				
		0 kPa	**1 kPa**	**2 kPa**	**3 kPa**	**4 kPa**
Friction Angle (Initial Model)	**35°**	*67*	*255*	*68*	*256*	*69*
	37.5°	*257*	*258*	*259*	*260*	*261*
	40°	70	262	71	263	72
	42.5°	264	265	266	267	268
	45°	58	239	59	240	60
Friction Angle (Fully Drained Model)	**35°**	*61*	*241*	*62*	*242*	*63*
	37.5°	*243*	*244*	*245*	*246*	*247*
	40°	64	248	65	249	66
	42.5°	250	251	252	253	254
	45°	55	237	56	238	57

Table 6.7: Cohesion against friction angle

		COHESION				
		0 kPa	**1 kPa**	**2 kPa**	**3 kPa**	**4 kPa**
Dilatancy (Initial Model)	**0°**	79	283	80	284	81
	3°	285	286	287	288	289
	6°	290	291	292	293	294
	8°	58	239	59	240	60
	10°	82	295	83	296	84
Dilatancy (Fully Drained Model)	**0°**	73	269	74	270	75
	3°	271	272	273	274	275
	6°	276	277	278	279	280
	8°	55	237	56	238	57
	10°	76	281	77	282	78

Table 6.8: Cohesion against dilatancy

		COHESION				
		0 kPa	**1 kPa**	**2 kPa**	**3 kPa**	**4 kPa**
Unit Weight (Initial Model)	**18** kN/m^3	91	311	92	312	93
	19 kN/m^3	313	314	315	316	317
	20 kN/m^3	94	318	95	319	96
	21 kN/m^3	320	321	322	323	324
	22 kN/m^3	58	239	59	240	60
Unit Weight (Fully Drained Model)	**18** kN/m^3	85	297	86	298	87
	19 kN/m^3	299	300	301	302	303
	20 kN/m^3	88	304	89	305	90
	21 kN/m^3	306	307	308	309	310
	22 kN/m^3	55	237	56	238	57

Table 6.9: Cohesion against unit weight

6.4.3. Friction Angle

A dilatancy angle of 6^o may not be sustained with a friction angle value of 35^o, and a dilatancy angle of 10^o may not be sustained with friction angle values of 35^o and 37.5^o as indicated in Table 6.12 (Bolton, 1986, De Josselin De Jong, 1976). Simulation identities reflecting these unrealistic combinations of soil parameters are presented in red italic fonts in the simulation layout for friction angle parametric studies (Tables 6.10 - 6.13).

		FRICTION ANGLE				
		35°	**37.5°**	**40°**	**42.5°**	**45°**
Stiffness (Initial Model)	**50 MPa**	*25*	*169*	28	176	4
	100 MPa	*167*	*170*	174	177	123
	150 MPa	*26*	*171*	29	178	5
	200 MPa	*168*	*172*	175	179	124
	250 MPa	*27*	*173*	30	180	6
Stiffness (Fully Drained Model)	**50 MPa**	*19*	*155*	22	162	1
	100 MPa	*153*	*156*	160	163	121
	150 MPa	*20*	*157*	23	164	2
	200 MPa	*154*	*158*	161	165	122
	250 MPa	*21*	*159*	24	166	3

Table 6.10: Friction angle against stiffness

		FRICTION ANGLE				
		35°	**37.5°**	**40°**	**42.5°**	**45°**
Cohesion (Initial Model)	**0 kPa**	*67*	*257*	70	264	58
	1 kPa	*255*	*258*	262	265	239
	2 kPa	*68*	*259*	71	266	59
	3 kPa	*256*	*260*	263	267	240
	4 kPa	*69*	*261*	72	268	60
Cohesion (Fully Drained Model)	**0 kPa**	*61*	*243*	64	250	55
	1 kPa	*241*	*244*	248	251	237
	2 kPa	*62*	*245*	65	252	56
	3 kPa	*242*	*246*	249	253	238
	4 kPa	*63*	*247*	66	254	57

Table 6.11: Friction angle against cohesion

		FRICTION ANGLE				
		35°	**37.5°**	**40°**	**42.5°**	**45°**
Dilatancy (Initial Model)	**0°**	101	337	102	338	79
	3°	339	340	341	342	285
	6°	*343*	344	345	346	290
	8°	*67*	*257*	70	264	58
	10°	*103*	*347*	104	348	82
Dilatancy (Fully Drained Model)	**0°**	97	325	98	326	73
	3°	327	328	329	330	271
	6°	*331*	332	333	334	276
	8°	*61*	*243*	64	250	55
	10°	*99*	*335*	100	336	76

Table 6.12: Friction angle against dilatancy

		FRICTION ANGLE				
		35°	**37.5°**	**40°**	**42.5°**	**45°**
Unit Weight (Initial Model)	**18** kN/m^3	*109*	*361*	110	362	91
	19 kN/m^3	*363*	*364*	365	366	313
	20 kN/m^3	*111*	*367*	112	368	94
	21 kN/m^3	*369*	*370*	371	372	320
	22 kN/m^3	*67*	*257*	70	264	58
Unit Weight (Fully Drained Model)	**18** kN/m^3	*105*	*349*	106	350	85
	19 kN/m^3	*351*	*352*	353	354	299
	20 kN/m^3	*107*	*355*	108	356	88
	21 kN/m^3	*357*	*358*	359	360	306
	22 kN/m^3	*61*	*243*	64	250	55

Table 6.13: Friction angle against unit weight

6.4.4. Dilatancy

Simulation layout for dilatancy parametric study is presented in Tables 6.14 - 6.17. Dilatancy angles of 6° and 10° may not be sustained with a friction angle value of 35°, and a dilatancy angle of 10° may not be sustained with a friction angle value of 37.5° (Bolton, 1986, De Josselin De Jong, 1976). Simulation identities reflecting these combinations of soil parameters are presented in red italic fonts in the simulation layout for the dilatancy against friction angle parametric studies (Table 6.16).

		DILATANCY				
		0°	**3°**	**6°**	**8°**	**10°**
Stiffness (Initial Model)	**50 MPa**	37	197	202	4	40
	100 MPa	195	198	203	123	207
	150 MPa	38	199	204	5	41
	200 MPa	196	200	205	124	208
	250 MPa	39	201	206	6	42
Stiffness (Fully Drained Model)	**50 MPa**	31	183	188	1	34
	100 MPa	181	184	189	121	193
	150 MPa	32	185	190	2	35
	200 MPa	182	186	191	122	194
	250 MPa	33	187	192	3	36

Table 6.14: Dilatancy against stiffness

		DILATANCY				
		0°	**3°**	**6°**	**8°**	**10°**
Cohesion (Initial Model)	**0 kPa**	79	285	290	58	82
	1 kPa	283	286	291	239	295
	2 kPa	80	287	292	59	83
	3 kPa	284	288	293	240	296
	4 kPa	81	289	294	60	84
Cohesion (Fully Drained Model)	**0 kPa**	73	271	276	55	76
	1 kPa	269	272	277	237	281
	2 kPa	74	273	278	56	77
	3 kPa	270	274	279	238	282
	4 kPa	75	275	280	57	78

Table 6.15: Dilatancy against cohesion

		DILATANCY				
		0°	**3°**	**6°**	**8°**	**10°**
Friction Angle (Initial Model)	**35°**	101	339	*343*	*67*	*103*
	37.5°	337	340	344	*257*	*347*
	40°	102	341	345	70	104
	42.5°	338	342	346	264	348
	45°	79	285	290	58	82
Friction Angle (Fully Drained Model)	**35°**	97	327	*331*	*61*	*99*
	37.5°	325	328	332	*243*	*335*
	40°	98	329	333	64	100
	42.5°	326	330	334	250	336
	45°	73	271	276	55	76

Table 6.16: Dilatancy against friction angle

		DILATANCY				
		0°	**3°**	**6°**	**8°**	**10°**
Unit Weight (Initial Model)	**18** kN/m^3	117	385	386	91	118
	19 kN/m^3	387	388	389	313	390
	20 kN/m^3	119	391	392	94	120
	21 kN/m^3	393	394	395	320	396
	22 kN/m^3	79	285	290	58	82
Unit Weight (Fully Drained Model)	**18** kN/m^3	113	373	374	85	114
	19 kN/m^3	375	376	377	299	378
	20 kN/m^3	115	379	380	88	116
	21 kN/m^3	381	382	383	306	384
	22 kN/m^3	73	271	276	55	76

Table 6.17: Dilatancy against unit weight

6.4.5. Unit Weight

Simulation layout for unit weight parametric studies is presented in Tables 6.18 - 6.21.

		UNIT WEIGHT				
		18 kN/m^3	19 kN/m^3	**20** kN/m^3	**21** kN/m^3	**22** kN/m^3
Stiffness (Initial Model)	**50 MPa**	49	225	52	232	4
	100 MPa	223	226	230	233	123
	150 MPa	50	227	53	234	5
	200 MPa	224	228	231	235	124
	250 MPa	51	229	54	236	6
Stiffness (Fully Drained Model)	**50 MPa**	43	211	46	218	1
	100 MPa	209	212	216	219	121
	150 MPa	44	213	47	220	2
	200 MPa	210	214	217	221	122
	250 MPa	45	215	48	222	3

Table 6.18: Unit Weight against stiffness

		UNIT WEIGHT				
		18 kN/m^3	19 kN/m^3	**20** kN/m^3	**21** kN/m^3	**22** kN/m^3
Cohesion (Initial Model)	**0 kPa**	91	313	94	320	58
	1 kPa	311	314	318	321	239
	2 kPa	92	315	95	322	59
	3 kPa	312	316	319	323	240
	4 kPa	93	317	96	324	60
Cohesion (Fully Drained Model)	**0 kPa**	85	299	88	306	55
	1 kPa	297	300	304	307	237
	2 kPa	86	301	89	308	56
	3 kPa	298	302	305	309	238
	4 kPa	87	303	90	310	57

Table 6.19: Unit Weight against cohesion

		UNIT WEIGHT				
		18 kN/m^3	19 kN/m^3	**20** kN/m^3	**21** kN/m^3	**22** kN/m^3
Friction Angle (Initial Model)	**35^o**	*109*	*363*	*111*	*369*	*67*
	37.5^o	*361*	*364*	*367*	*370*	*257*
	40^o	110	365	112	371	70
	42.5^o	362	366	368	372	264
	45^o	91	313	94	320	58
Friction Angle (Fully Drained Model)	**35^o**	*105*	*351*	*107*	*357*	*61*
	37.5^o	*349*	*352*	*355*	*358*	*243*
	40^o	106	353	108	359	64
	42.5^o	350	354	356	360	250
	45^o	85	299	88	306	55

Table 6.20: Unit Weight against friction angle

		UNIT WEIGHT				
		18 kN/m^3	19 kN/m^3	**20** kN/m^3	**21** kN/m^3	**22** kN/m^3
Dilatancy (Initial Model)	**0^o**	117	387	119	393	79
	3^o	385	388	391	394	285
	6^o	386	389	392	395	290
	8^o	91	313	94	320	58
	10^o	118	390	120	396	82
Dilatancy (Fully Drained Model)	**0^o**	113	375	115	381	73
	3^o	373	376	379	382	271
	6^o	374	377	380	383	276
	8^o	85	299	88	306	55
	10^o	114	378	116	384	76

Table 6.21: Unit Weight against dilatancy

6.5. Soil Parameter Variation & Earth Pressures

Results of the first parametric variation (defined in Section 6.3) showing earth pressure developed during simulation of the abutment displacement are presented in this section. Section 6.5.1 presents the results of the simulation based on the abutment displacements as recorded on site ('Site Displacement Record' curve of Figure 6.1). Section 6.5.2 discusses the results of the simulation from the cyclic abutment displacement model developed ('Cyclic Displacement Model' curve of Figure 6.1).

6.5.1. Measured Abutment Displacement Model

Simulation results of earth pressures developed from modelling the abutment displacement recorded on the site are presented. The results, presented in Figures 6.2 - 6.11, show the impact of change in specific soil parameters across the parameter range as defined in Table 6.1.

Stiffness:

Results showing the impact of simulating changes in the backfill soil stiffness values are presented in Figures 6.2 and 6.3.

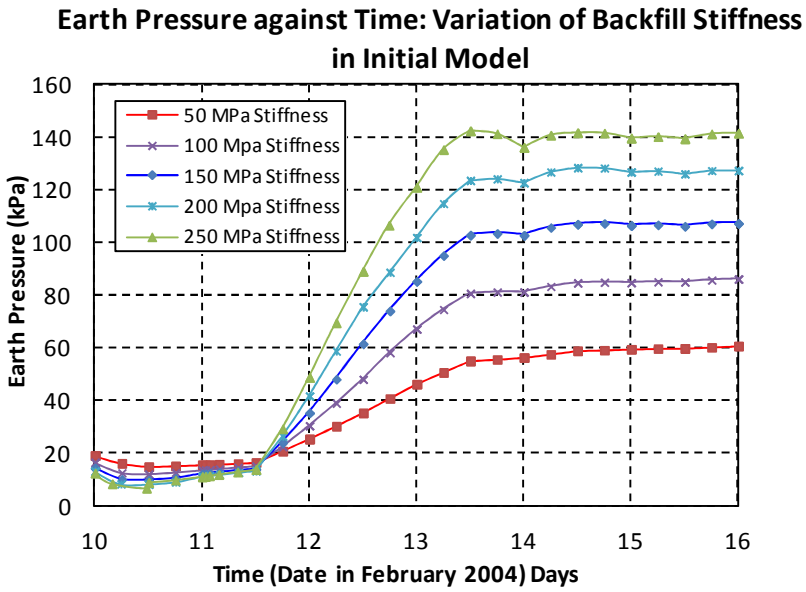

Figure 6.2: Change in backfill stiffness (Initial Model).

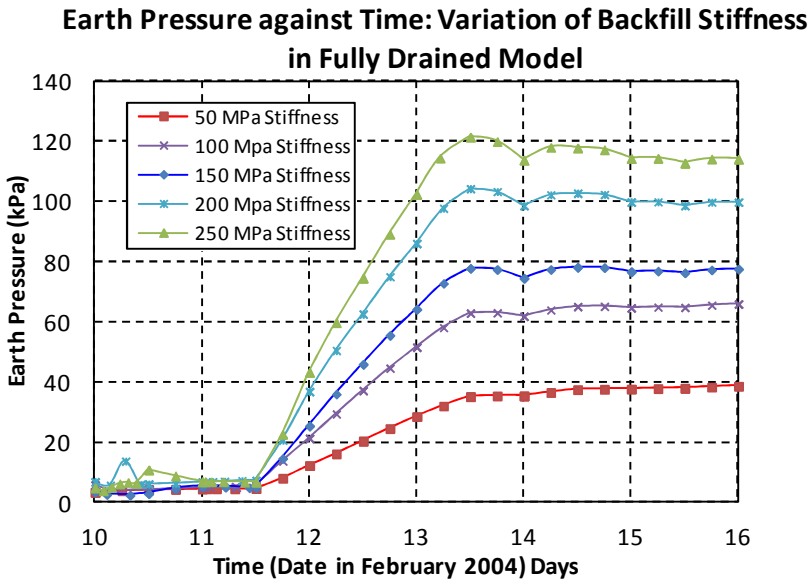

Figure 6.3: Change in backfill stiffness (Fully Drained Model).

Cohesion:

Results showing the impact of simulating changes in the backfill soil cohesion values are presented in Figures 6.4 and 6.5.

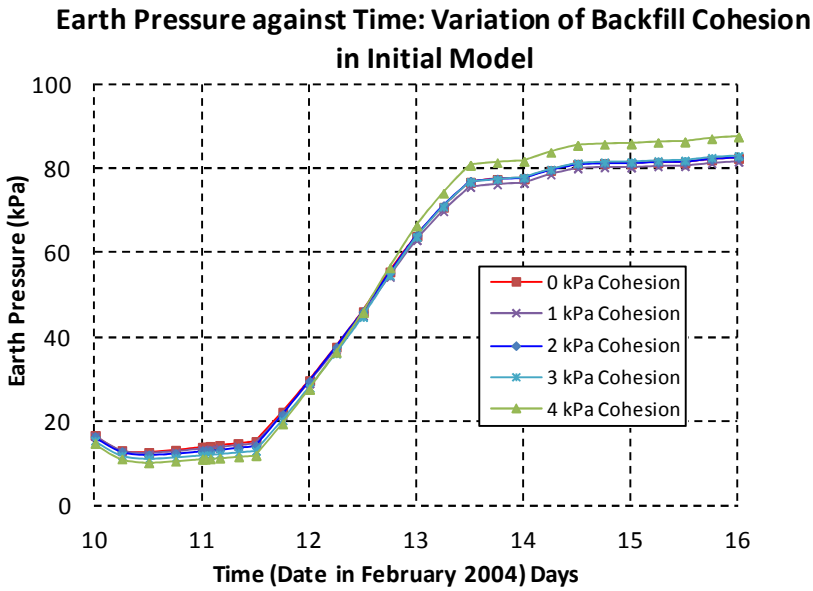

Figure 6.4: Change in backfill cohesion (Initial Model).

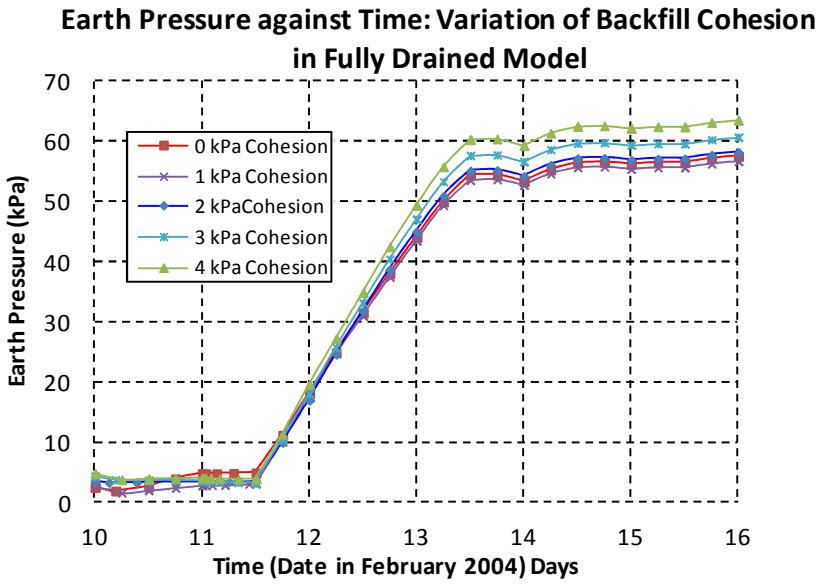

Figure 6.5: Change in backfill cohesion (Fully Drained Model).

Friction angle:

Results showing the impact of simulating changes in the backfill soil friction angle values are presented in Figures 6.6 and 6.7.

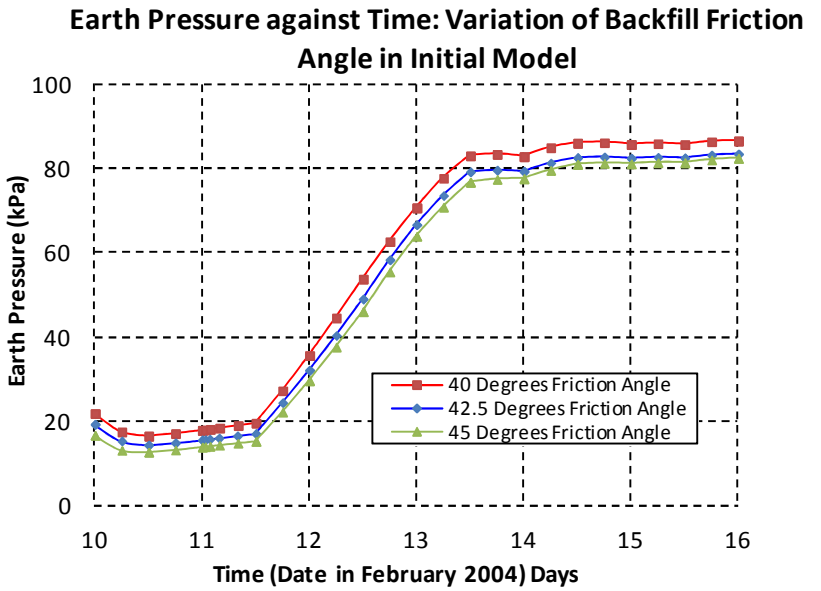

Figure 6.6: Change in backfill friction angle (Initial Model).

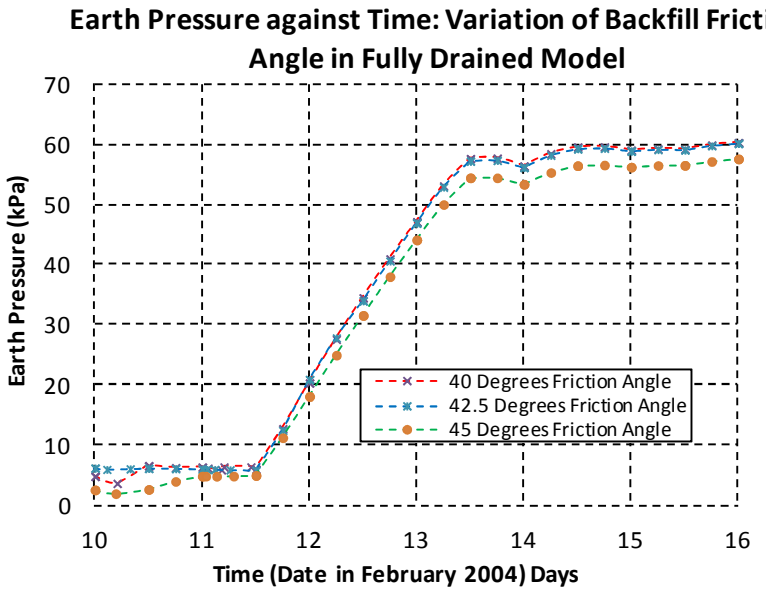

Figure 6.7: Change in backfill friction angle (Fully Drained Model).

Dilatancy:

Results showing the impact of simulating changes in the backfill soil dilatancy values are presented in Figures 6.8 and 6.9.

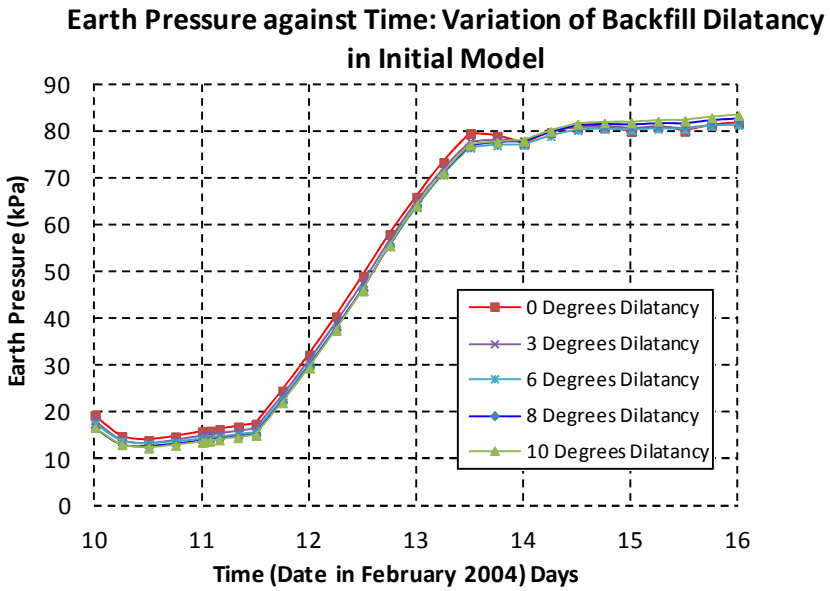

Figure 6.8: Change in backfill dilatancy (Initial Model).

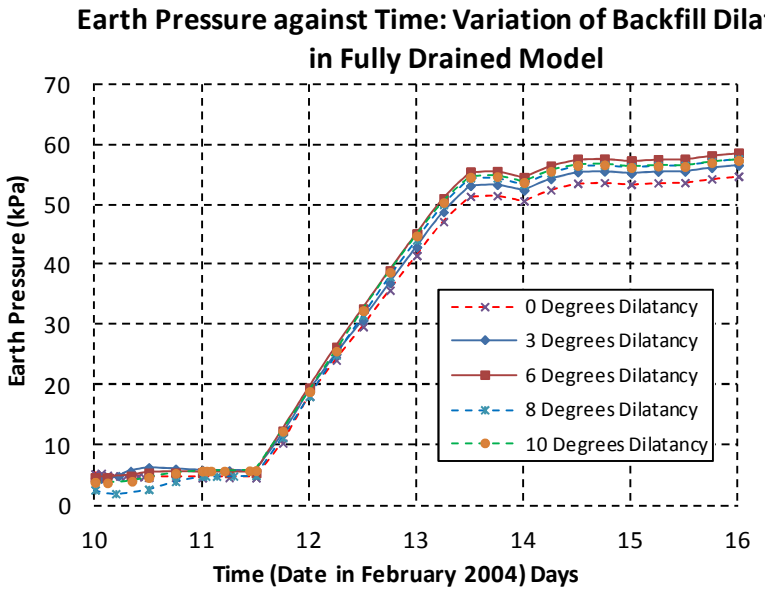

Figure 6.9: Change in backfill dilatancy (Fully Drained Model).

Unit weight:

Results showing the impact of simulating changes in the backfill soil unit weight values are presented in Figures 6.10 and 6.11.

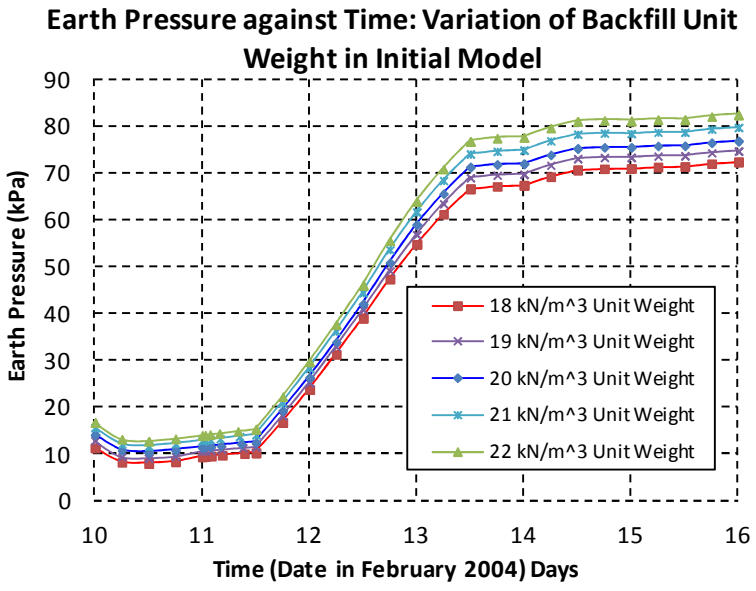

Figure 6.10: Change in backfill unit weight (Initial Model).

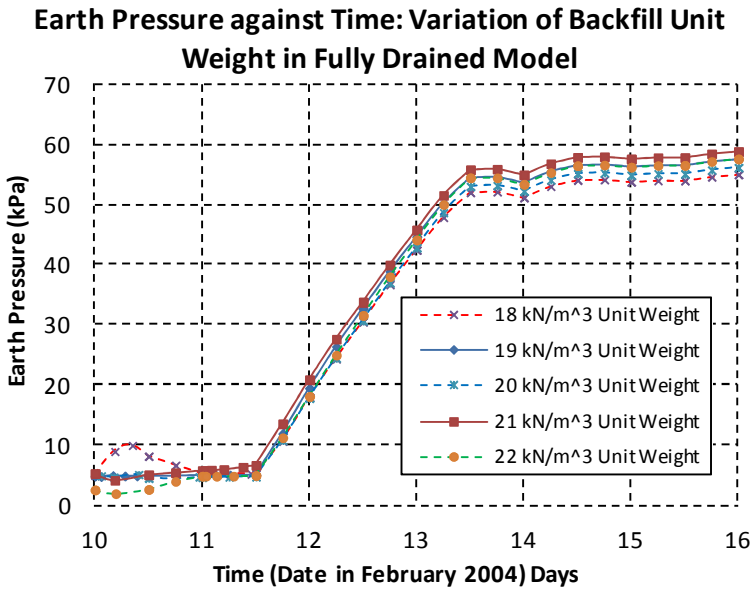

Figure 6.11: Change in backfill unit weight (Fully Drained Model).

6.5.2. Model Abutment Cyclic Displacement

Simulation of a cyclic abutment displacement pattern (secondary displacement model option) was carried out on the initial model and the fully drained model. The results of these simulations presented in Appendix 1 show the impact of the changes to the backfill soil parameters values across the range as defined in Table 6.1 while other parameters of the backfill soil retained the default values defined in Table 5.4.

The magnitude or range of the abutment displacement in the cyclic displacement model is lower than that realised from the measured abutment displacement (see Figure 6.1).

6.6. Analysis &Discussion

Data obtained from simulating the abutment displacements under varying conditions were analysed. The results of these analysis and the implications are discussed in this section.

6.6.1. Measured & Cyclic Displacement

The maximum difference in earth pressure values developed as a result of the changes in backfill soil parameters across the range of a specific backfill soil parameter was quantified (see Figures 6.12 and 6.13). This was to determine the impact of these changes on the magnitude of earth pressure experienced behind the integral bridge abutment. Comparative analyses of these quantities, based on the first parametric variation type (described in Section 6.3), show the relative impact of change in each backfill parameter on the earth pressure.

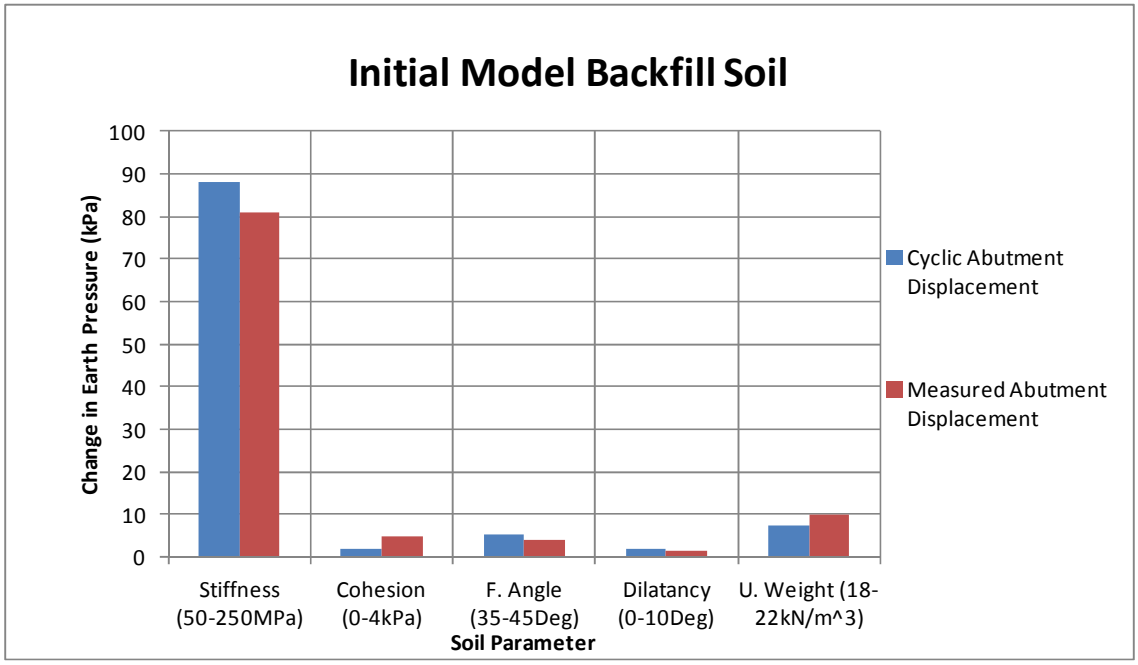

Figure 6.12: Impact of changes in backfill soil (Initial model) parameter within the model crushed rock backfill soil as a result of the model integral bridge abutment displacements.

The results obtained through this process, from simulations based on the measured abutment displacement pattern, and simulations based on an assumed cyclic abutment displacement pattern were directly compared. This was presented as results generated in the initial model and in the fully drained model. In both cases, the results show an emphatic impact on the earth pressure as a result of the change in the stiffness parameter over the impact of the change in other soil parameters.

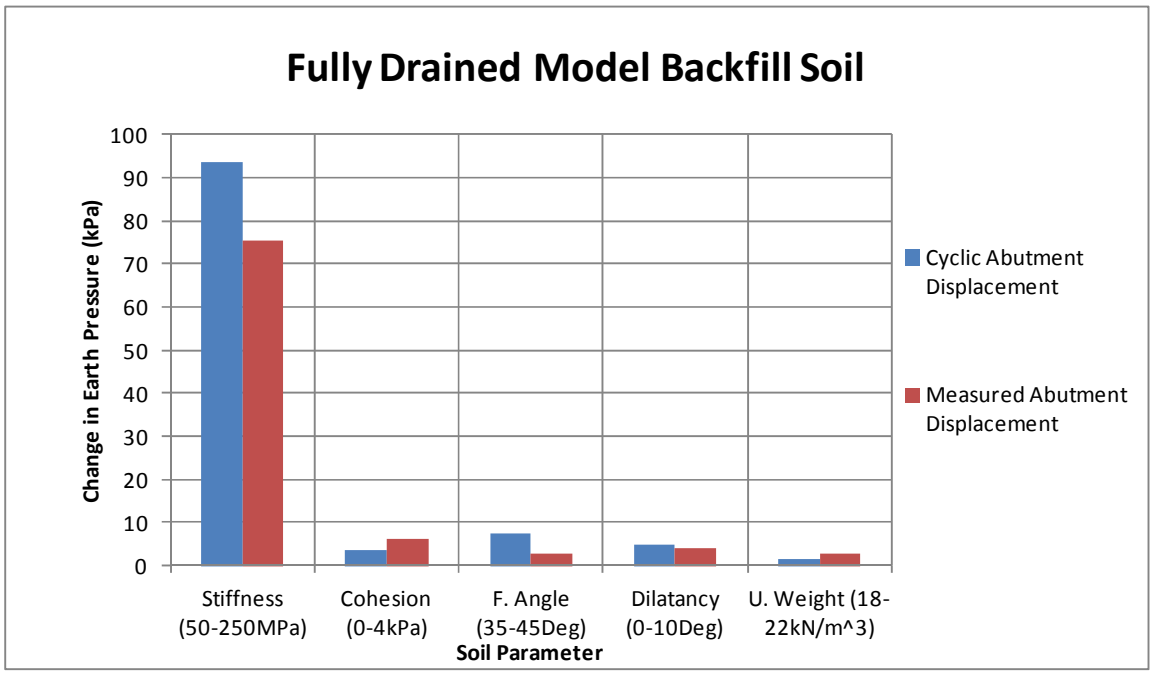

Figure 6.13: Impact of changes in backfill soil (Fully drained model) parameter within the model crushed rock backfill soil as a result of the model integral bridge abutment displacements.

While the magnitude of the model abutment displacement in the cyclic displacement pattern is less than the magnitude of the model abutment displacement in the measured displacement pattern (see Figure 6.1), the change in earth pressure developed from the cyclic abutment displacement range as a result of similar changes in the backfill stiffness parameter is appreciably higher than that generated from the measured abutment displacement. This results support previous findings on the nature of cyclic loading on granular materials as research by Carder and Hayes (Carder and Hayes, 2000) on the integral bridge and as described by several other researchers including Bolton and Steedman (2000) on earth retaining structures (Bolton and Steedman, 1982).

Results generated from the initial model and the fully drained models appear to show a consistent trend of behaviour between the measured and cyclic abutment displacement. However, there is a significantly greater impact as a result of the changes in the unit weight in the initial drained model. The earth pressure ranges developed in the initial model are also found to be lower than that generated in the fully drained model. These suggest

different behaviour pattern as a result of the assumptions on state of the fine grain soils. Further analysis based on the second parametric variation (described in Section 6.3) was carried out to provide more details from the evaluation of the impact of these changes. These analyses considered the simultaneous impact of the changes in the subject and variable parameter on the earth pressures. The results obtained from the second parametric variation type show little variation from the results obtained using the first parametric variation type. These results (from the second parametric variation) confirm the significant impact of change in the backfill stiffness parameter and the relatively insignificant impact of change in the other soil parameters considered in this study. Detailed analyses of the impact of changes in the backfill soil parameters evaluated in the second parametric variation are presented in Sections 6.6.2.

6.6.2. Impact of Change in Backfill Soil Parameters

The impact of change in the backfill soil parameters on the earth pressure developed behind the abutment is evaluated using the bridge model featuring the abutment displacement recorded on the site (see 'Site Displacement Record' curve of Figure 6.1). Results presented show earth pressure plotted against the subject parameters with the variable parameters defining the curves. The results show that some degree of change occurs in the earth pressure values generated within the model as a result of changes in the backfill soil parameters. The results however indicate that change in earth pressure values is predominantly controlled by change in the stiffness value. The results also show that lower earth pressure is developed in the fully drained model when compared to the initial model.

6.6.2.1. Impact of Stiffness

Results evaluating the impact of change in stiffness values are presented in this section. The change in the earth pressure values as a result of the changes in the backfill soil stiffness values is found to be significant irrespective of the changes that occur within the other backfill soil parameter values in the model (see Figures 6.14-6.17). It can be appreciated that the maximum and minimum percentage change in earth pressure value developed as a result of change in stiffness values from 50 to 250MPa, within the initial and the fully

drained model are 220% and 110% respectively . This may be found in Figure 6.16 (“0 Deg. Dilatancy (Fully Drained Model)” curve for maximum change and “0 Deg. Dilatancy (Initial Model)” curve for minimum change). The average percentage change is 161.2%.

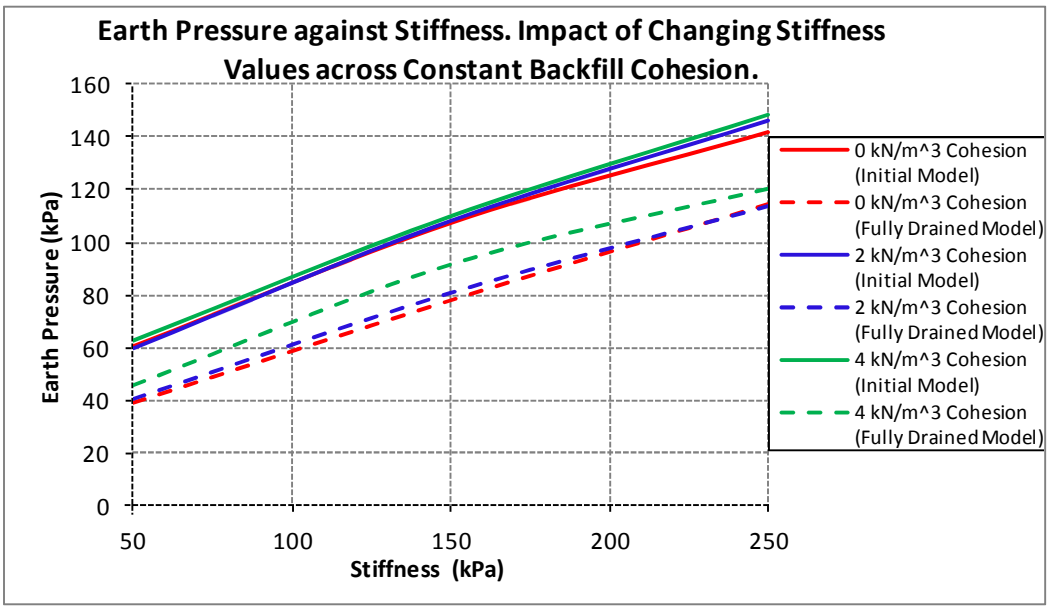

Figure 6.14: Cohesion curves showing impact of changing stiffness values in the model bridge backfill soil at the maximum abutment displacement.

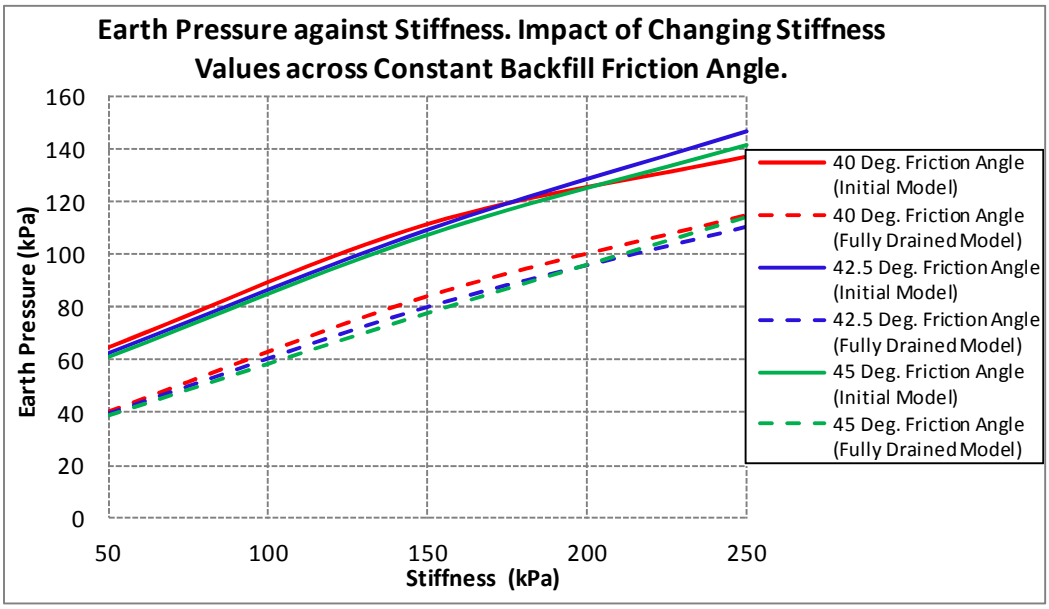

Figure 6.15: Friction angle curves showing impact of changing stiffness values in the model bridge backfill soil at the maximum abutment displacement.

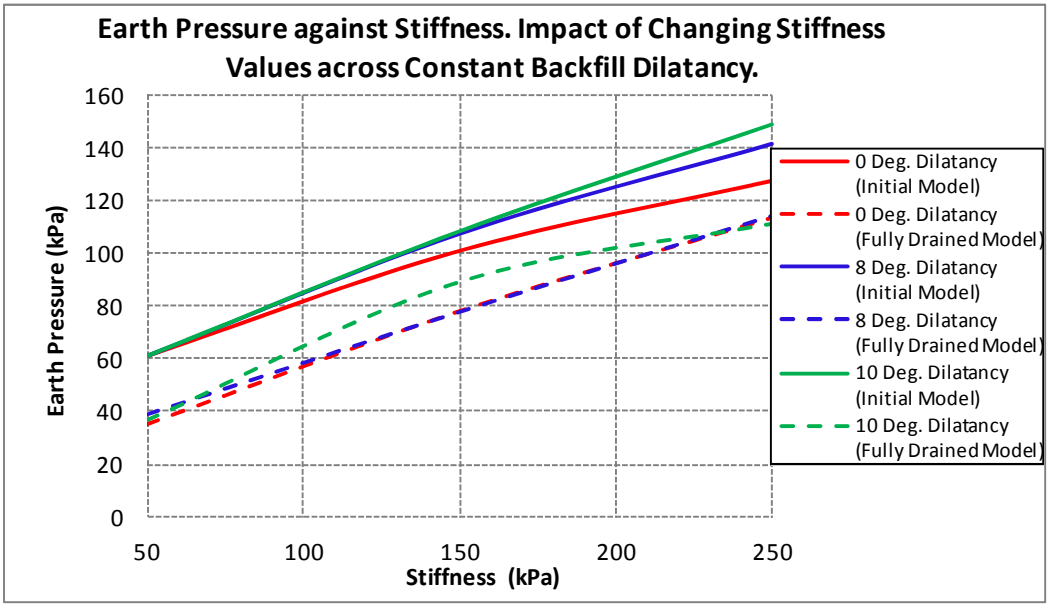

Figure 6.16: Dilatancy curves showing impact of changing stiffness values in the model bridge backfill soil at the maximum abutment displacement.

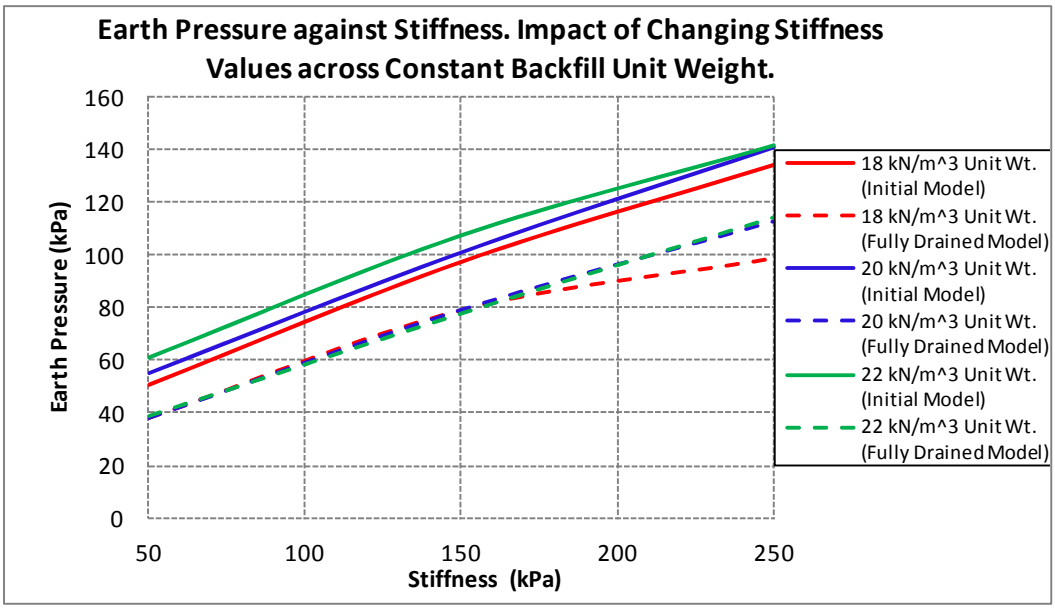

Figure 6.17: Unit weight curves showing impact of changing stiffness values in the model bridge backfill soil at the maximum abutment displacement.

6.6.2.2. Impact of Cohesion

Results evaluating the impact of change in cohesion values are presented in Figures 6.18 - 6.21. In general, there appear to be an increase in the earth pressure values as cohesion value increases across the changes in the soil parameters evaluated. It is also appreciated that the maximum and minimum percentage change in earth pressure developed as a result of the changes in cohesion values from 0 to 4kPa, within the initial and the fully drained model are 22% and 2% respectively. This may be found in Figure 6.19 ("42.5 Deg. Friction Angle (Fully Drained Model)" curve) for maximum and Figure 6.18 ("150MPa Stiffness (Initial Model)" curve) for minimum. The average percentage change is 8.3%.

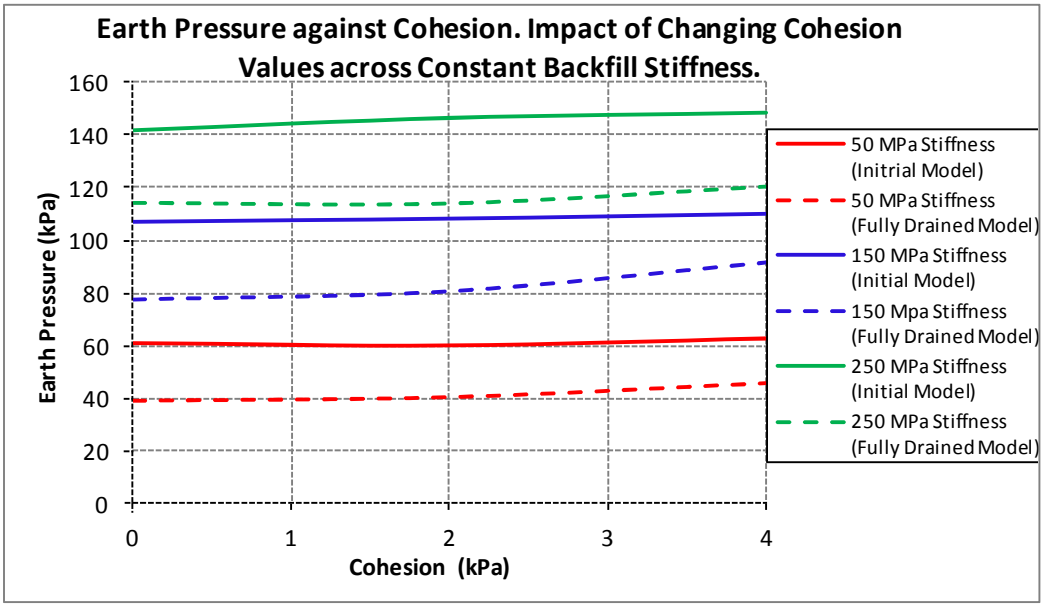

Figure 6.18: Stiffness curves showing impact of changing cohesion values in the model bridge backfill soil at the maximum abutment displacement.

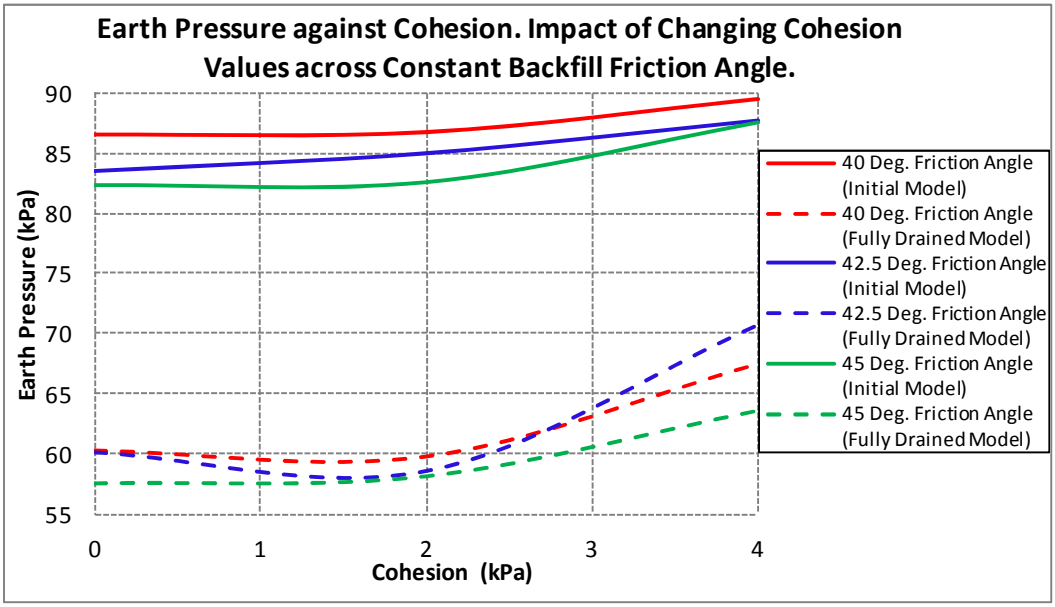

Figure 6.19: Friction angle curves showing impact of changing cohesion values in the model bridge backfill soil at the maximum abutment displacement.

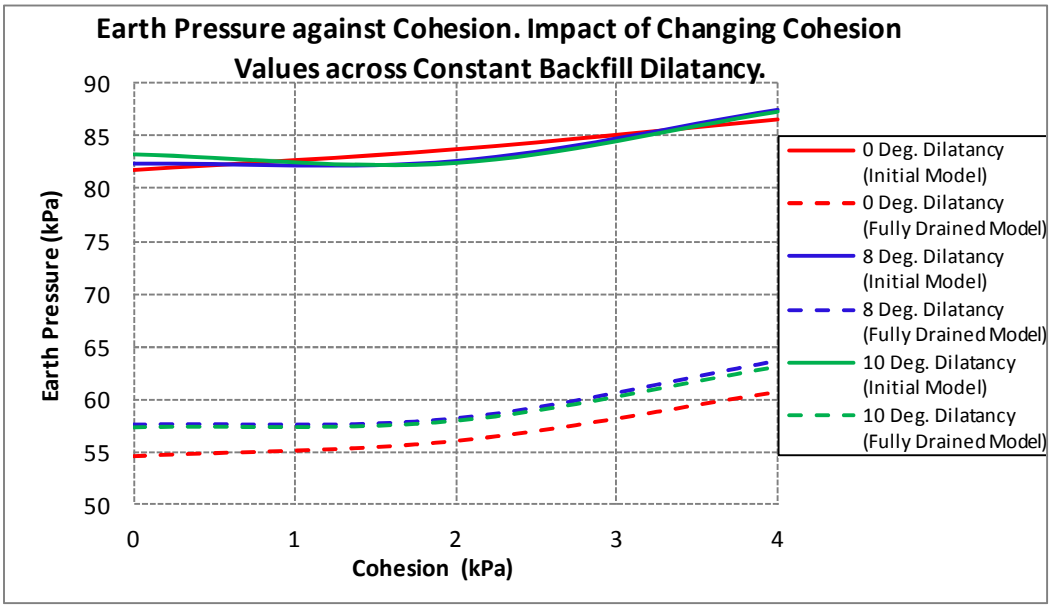

Figure 6.20: Dilatancy curves showing impact of changing cohesion values in the model bridge backfill soil at the maximum abutment displacement.

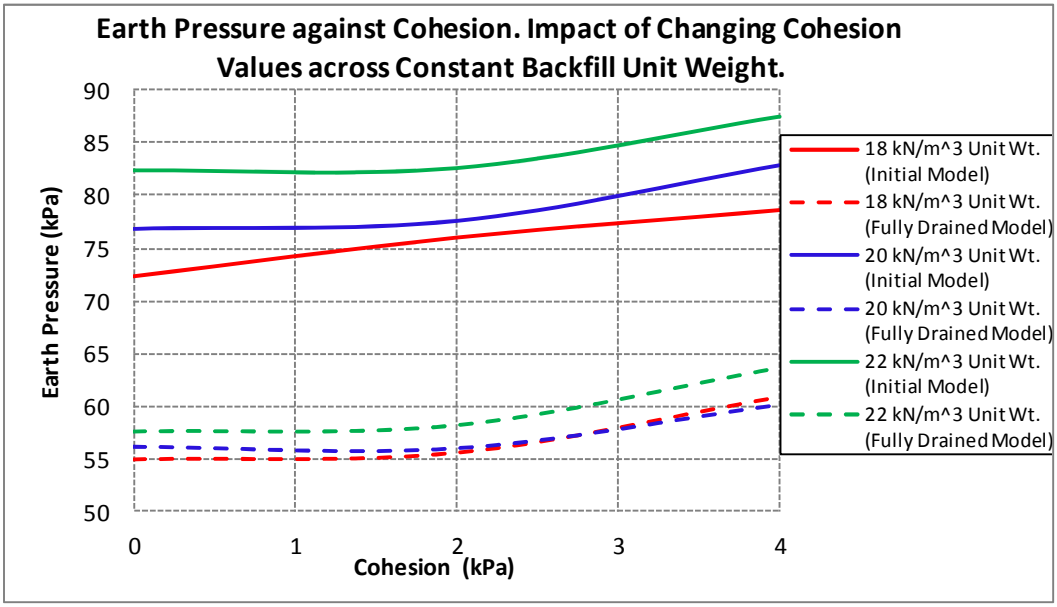

Figure 6.21: Unit weight curves showing impact of changing cohesion values in the model bridge backfill soil at the maximum abutment displacement.

6.6.2.3. Impact of Friction Angle

Results evaluating the Impact of change in the friction angle value of the backfill soil are presented in Figures 6.22 - 6.25. In general, there appear to be a decrease in the earth pressure values as friction angle value increases. It will be appreciated that the maximum and minimum percentage change in earth pressure values developed as a result of the changes in friction angle values from 40^{o} to 45^{o}, within the initial and the fully drained model are 11% and 4% respectively. This may be found in Figure 6.23 ("4kN/m^3 Cohesion (Fully Drained Model)" curve) for maximum and Figure 6.22 ("150MPa Stiffness (Initial Model)" curve) for minimum. The average percentage change is 4.8%.

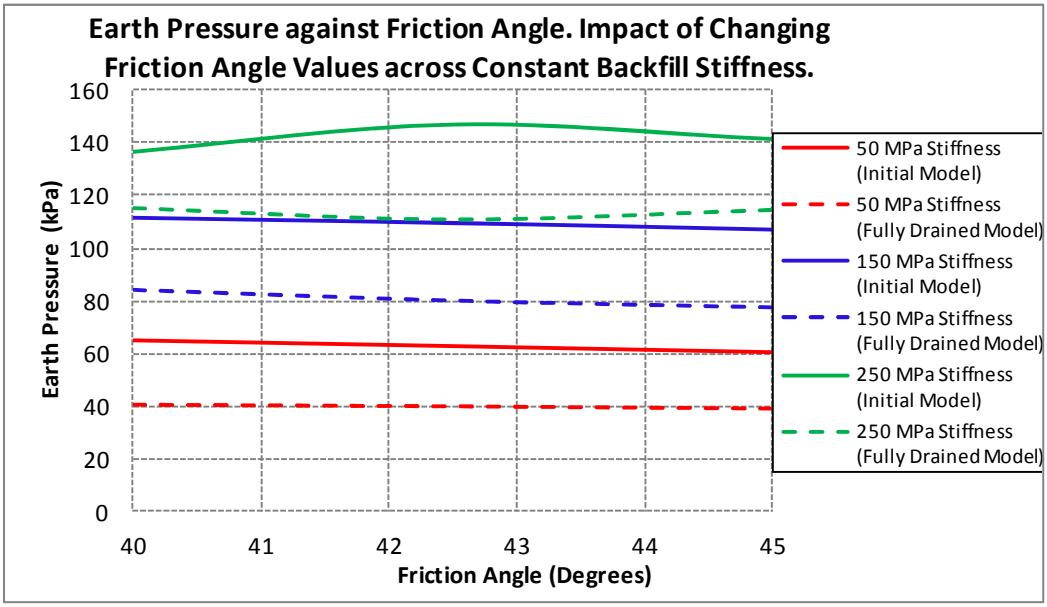

Figure 6.22: Stiffness curves showing impact of changing friction angle values in the model bridge backfill soil at the maximum abutment displacement.

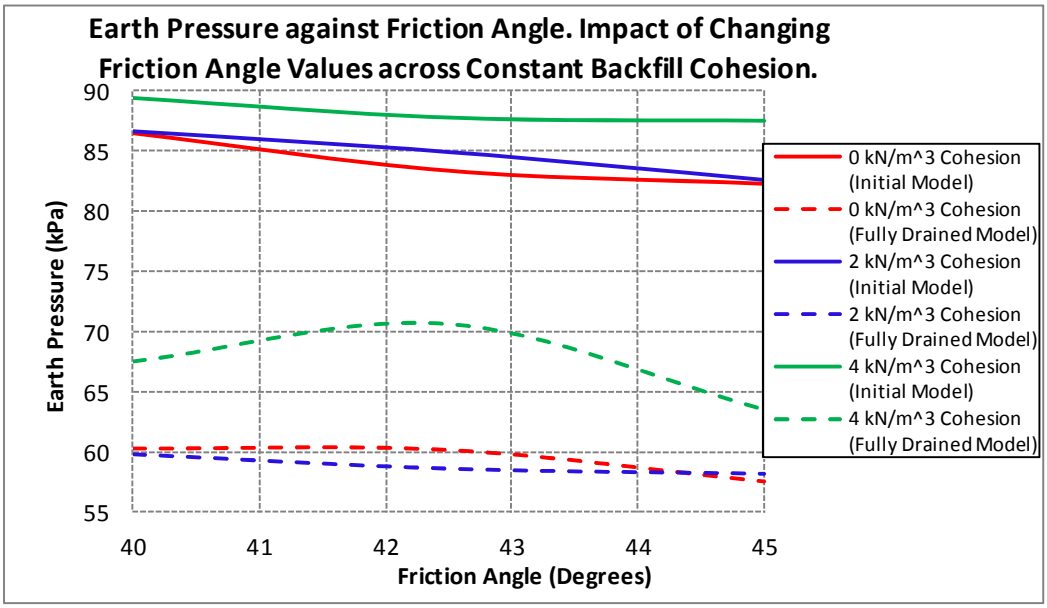

Figure 6.23: Cohesion curves showing impact of changing friction angle values in the model bridge backfill soil at the maximum abutment displacement.

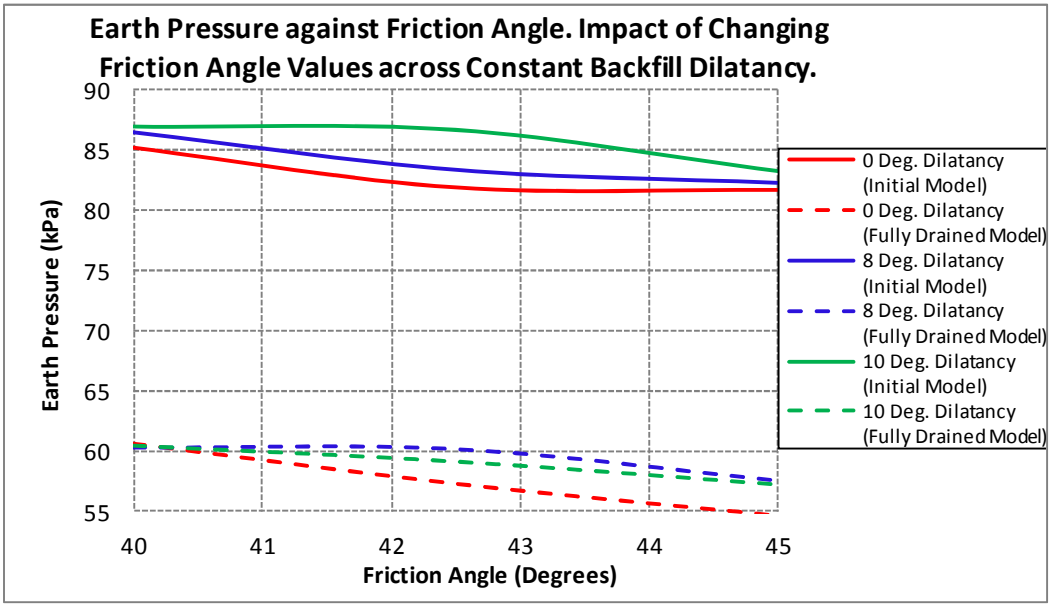

Figure 6.24: Dilatancy curves showing impact of changing friction angle values in the model bridge backfill soil at the maximum abutment displacement.

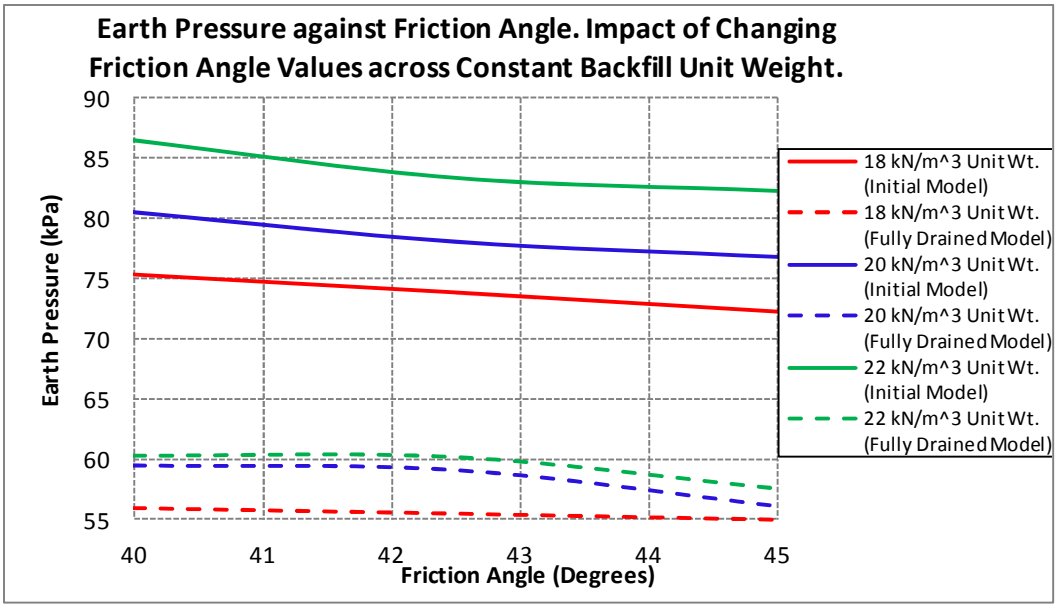

Figure 6.25: Unit weight curves showing impact of changing friction angle values in the model bridge backfill soil at the maximum abutment displacement.

6.6.2.4. Impact of Dilatancy

The results of evaluating the impact of the changes in the value of the backfill soil dilatancy angle are presented in Figures 6.26 - 6.29. The maximum and minimum percentage change in the earth pressure value developed as a result of the changes in dilatancy angle values from 0^o to 10^o, within the initial and the fully drained model are 16% and 1% respectively. The curves showing these changes are presented in Figure 6.26 ("250MPa Stiffness (Initial Model)" curve for maximum and "50MPa Stiffness (Initial Model)" curve for minimum). The average percentage change is 5.2%

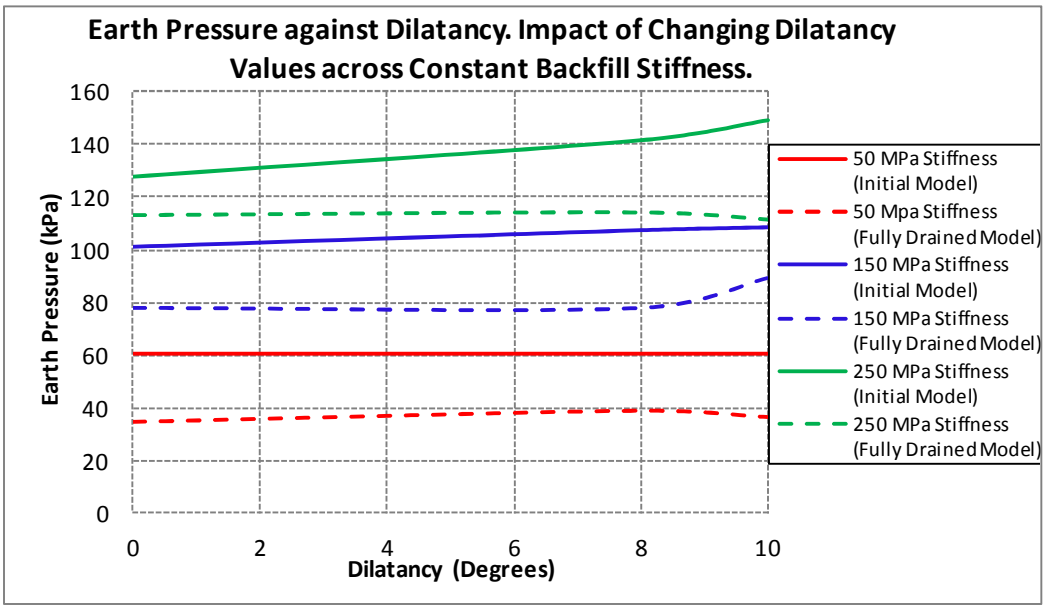

Figure 6.26: Stiffness curves showing impact of changing dilatancy values in the model bridge backfill soil at the maximum abutment displacement.

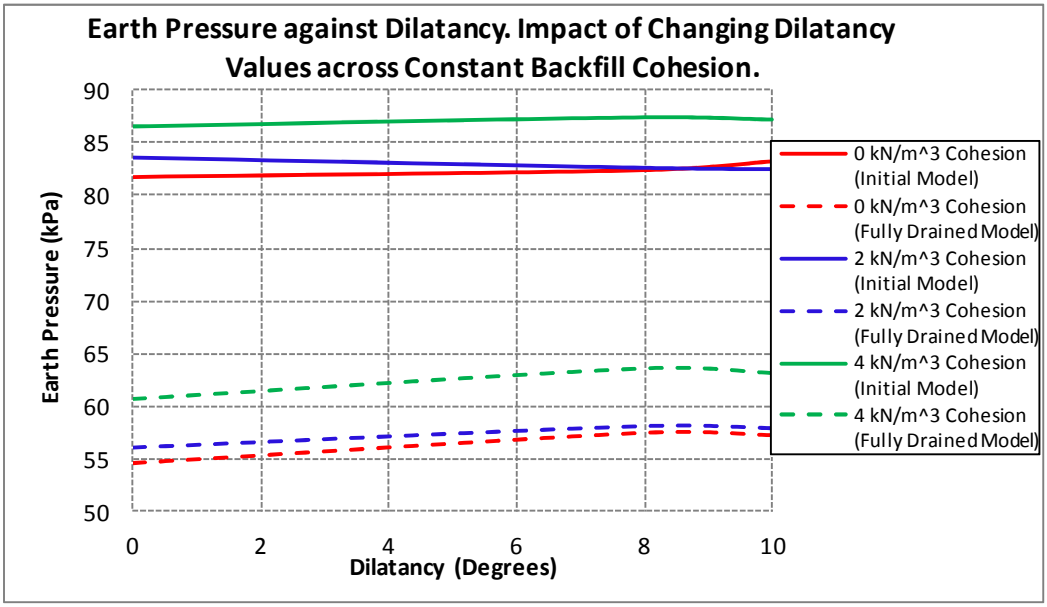

Figure 6.27: Cohesion curves showing impact of changing dilatancy values in the model bridge backfill soil at the maximum abutment displacement.

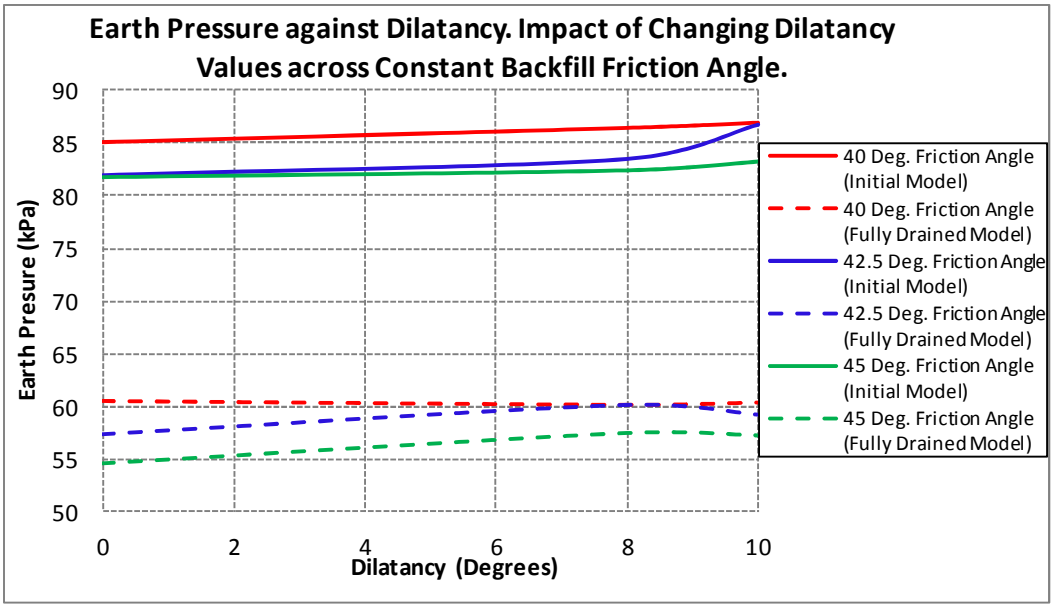

Figure 6.28: Friction angle curves showing impact of changing dilatancy values in the model bridge backfill soil at the maximum abutment displacement.

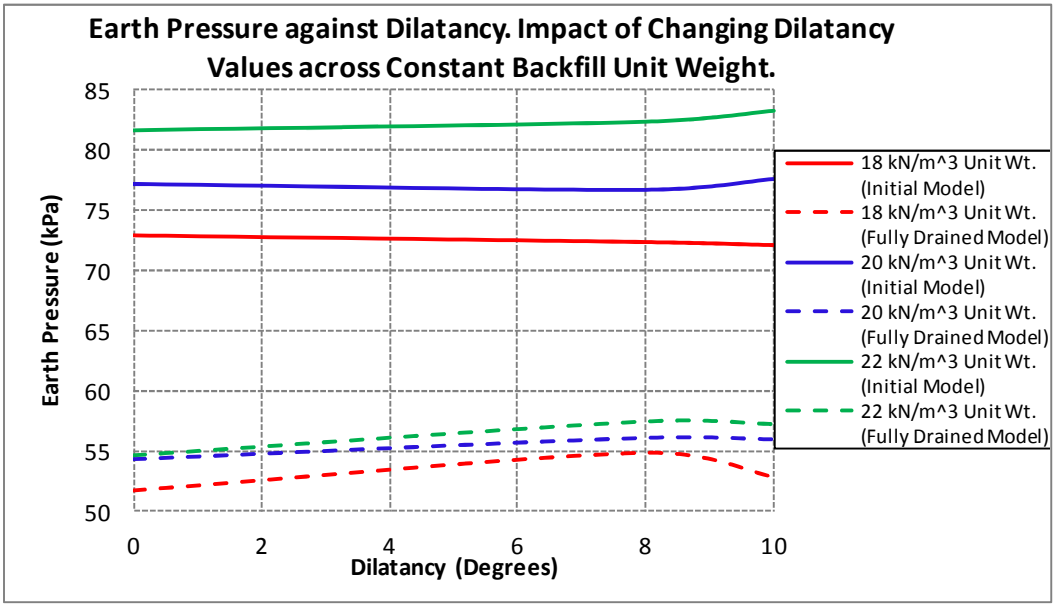

Figure 6.29: Unit weight curves showing impact of changing dilatancy values in the model bridge backfill soil at the maximum abutment displacement.

6.6.2.5. Impact of Unit Weight

The results of evaluating the impact of change in unit weight values within the backfill soil on earth pressure values are presented in Figures 6.30 - 6.33. There appear to be a general increase in the earth pressure values as unit weight value increases across the changes in the backfill soil parameters evaluated. The maximum and minimum percentage change in earth pressure values developed as a result of the changes in unit weight values from 18 to 22kN/m^3, within the initial and the fully drained model are 18% and 1% respectively. This may be found in Figure 6.30 ("50MPa Stiffness (Initial Model)" curve for maximum and "150MPa Stiffness (Fully Drained Model)" curve for minimum). The average percentage change is 8.6%

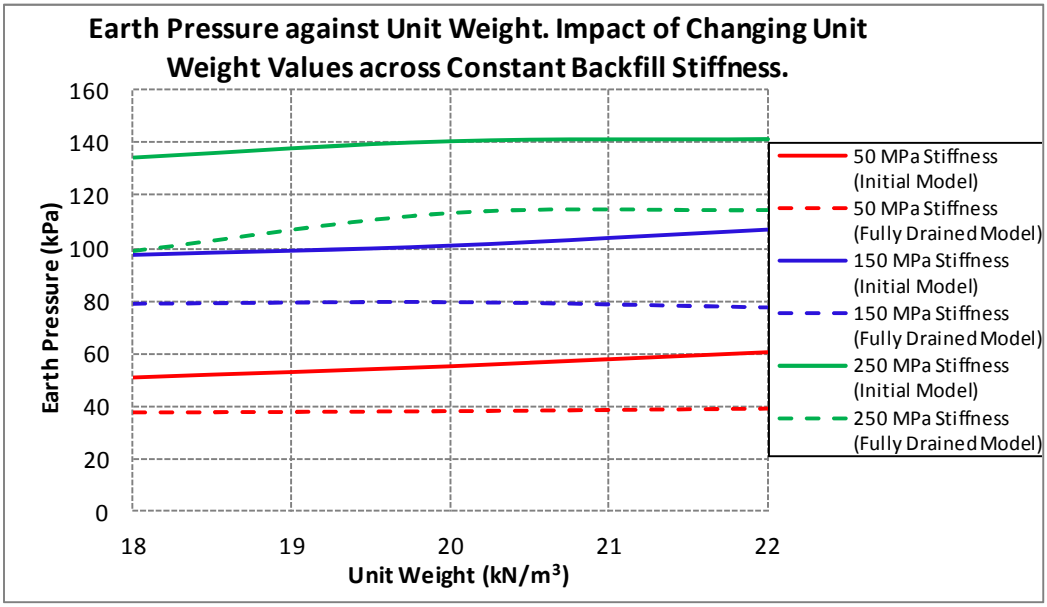

Figure 6.30: Stiffness curves showing impact of changing unit weight values in the model bridge backfill soil at the maximum abutment displacement.

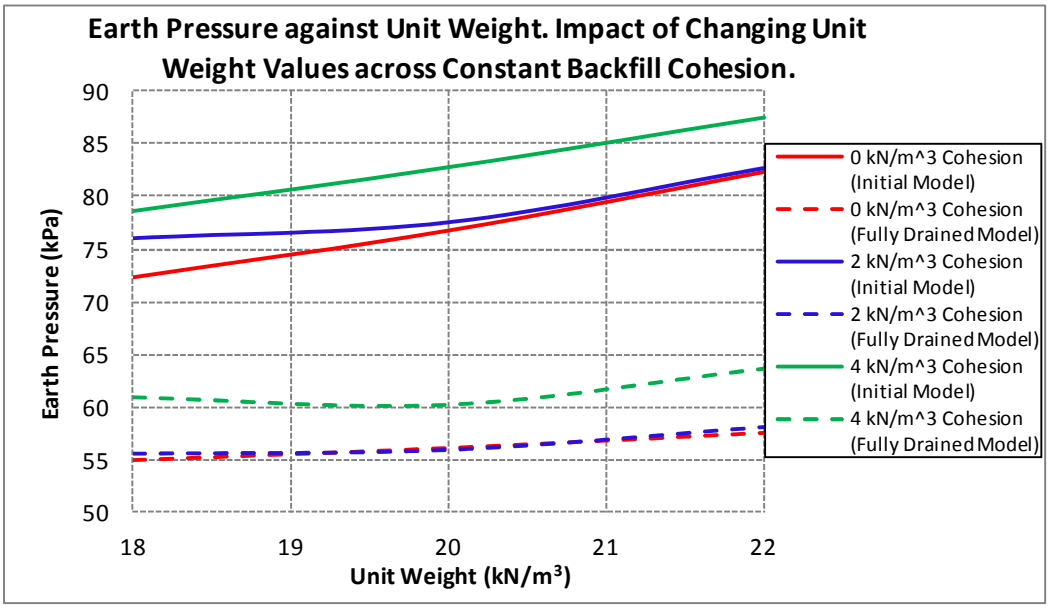

Figure 6.31: Cohesion curves showing impact of changing unit weight values in the model bridge backfill soil at the maximum abutment displacement.

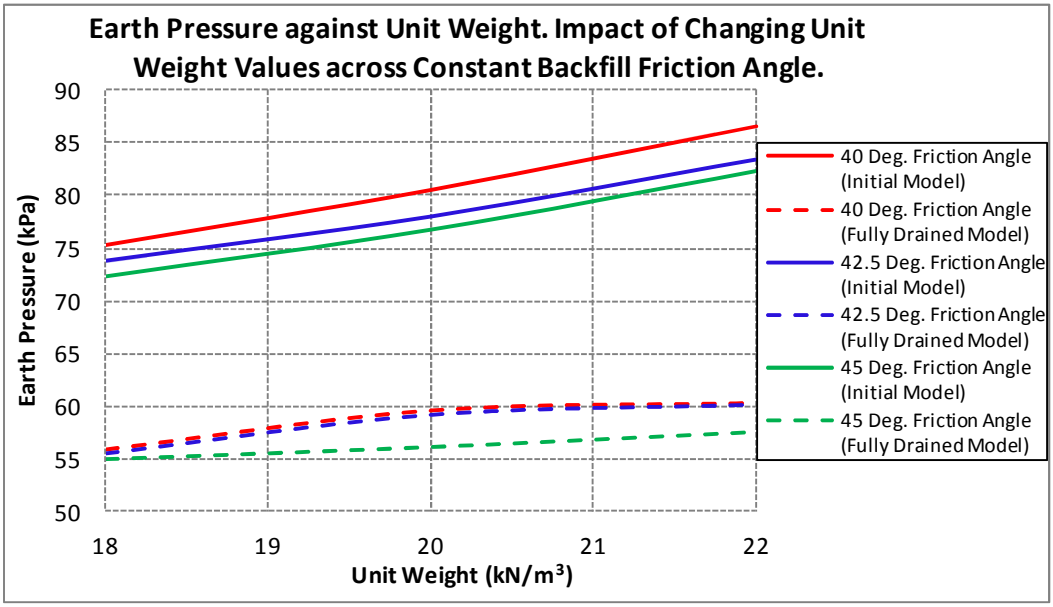

Figure 6.32: Friction angle curves showing impact of changing unit weight values in the model bridge backfill soil at the maximum abutment displacement.

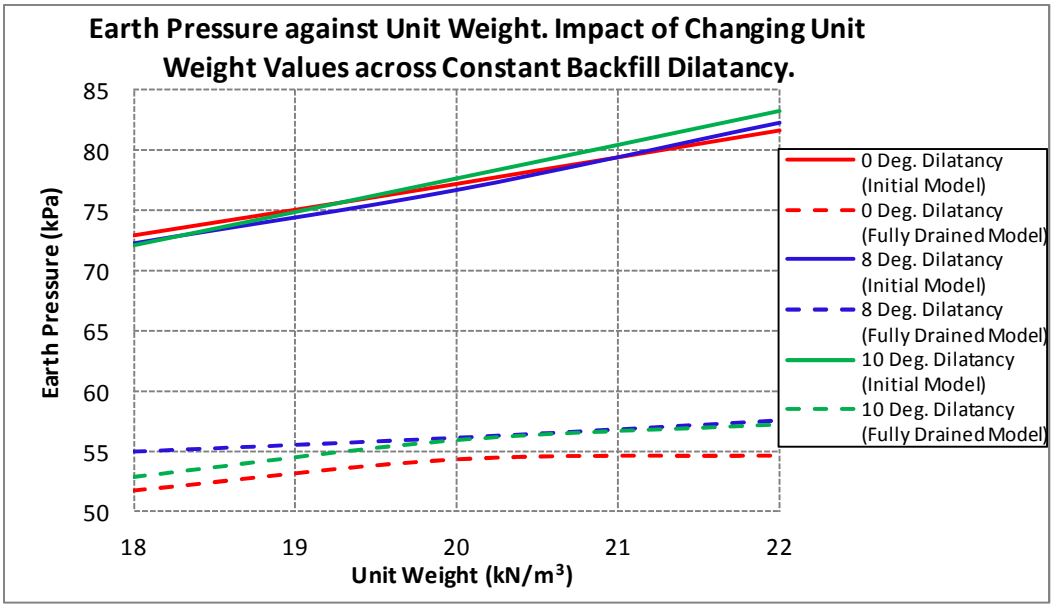

Figure 6.33: Dilatancy curves showing impact of changing unit weight values in the model bridge backfill soil at the maximum abutment displacement.

6.6.3. Impact of Change in Poisson's Ratio

Plaxis Hardening Soil model requires an input of the unloading and reloading Poisson's Ratio parameter. The cyclic loading of the model integral bridge carried out in this study involves the unloading and reloading of the backfill and foundation soil materials. Consequently, a parametric study on the variation of the Poisson's Ratio within this model was carried out to establish the effect of this parameter on the model.

Typical Poisson's Ratio parameter value of soils as found in several publications range from approximately 0.1 to virtually incompressible 0.5 (United States. Federal Highway et al., 1999, Das, 2008). The value of the Poisson's Ratio for the backfill soil material type, crushed rock, range from 0.15 to 0.35 (Ryall et al., 2000). However, for realistic computational results in the Plaxis undrained effective stress analysis, the bulk modulus of water must be appreciably higher than the effective bulk modulus of the soil. This condition is best satisfied with a soil Poisson's Ratio less than 0.35 (PLAXIS, 2010a).

Parametric studies was therefore carried out varying the value of the backfill soil Poisson's Ratio from 0.16 to 0.32. Figures 6.34 and 6.35 present the results showing the impact of simulating changes in the backfill soil Poisson's Ratio in the initial model and in the fully drained model respectively. Results of the cyclic model are presented in Appendix 1.

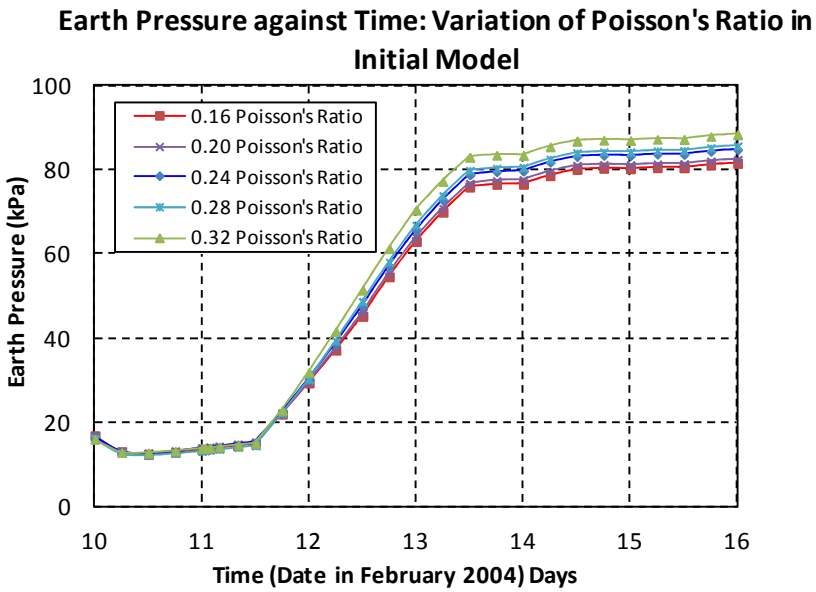

Figure 6.34: Change in Backfill Poisson's Ratio (Initial Model)

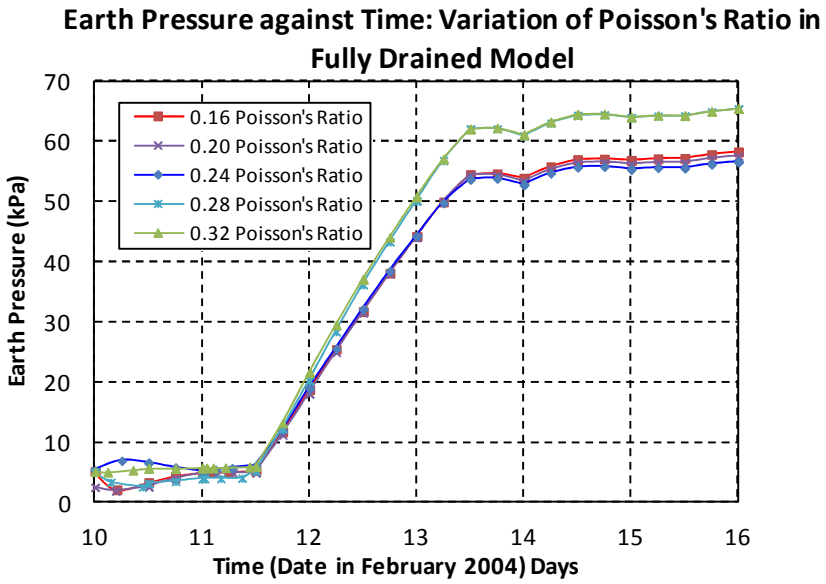

Figure 6.35: Change in Backfill Poisson's Ratio (Fully Drained Model)

Figure 6.36 compare the impact of change in Poisson's Ratio and the impact of change in other soil parameters to the impact of change in the stiffness parameter. The results show a significantly larger impact on the earth pressure values as a result of the change in the stiffness parameter compared to change in the Poisson's Ratio parameter and change in the other soil parameters analysed.

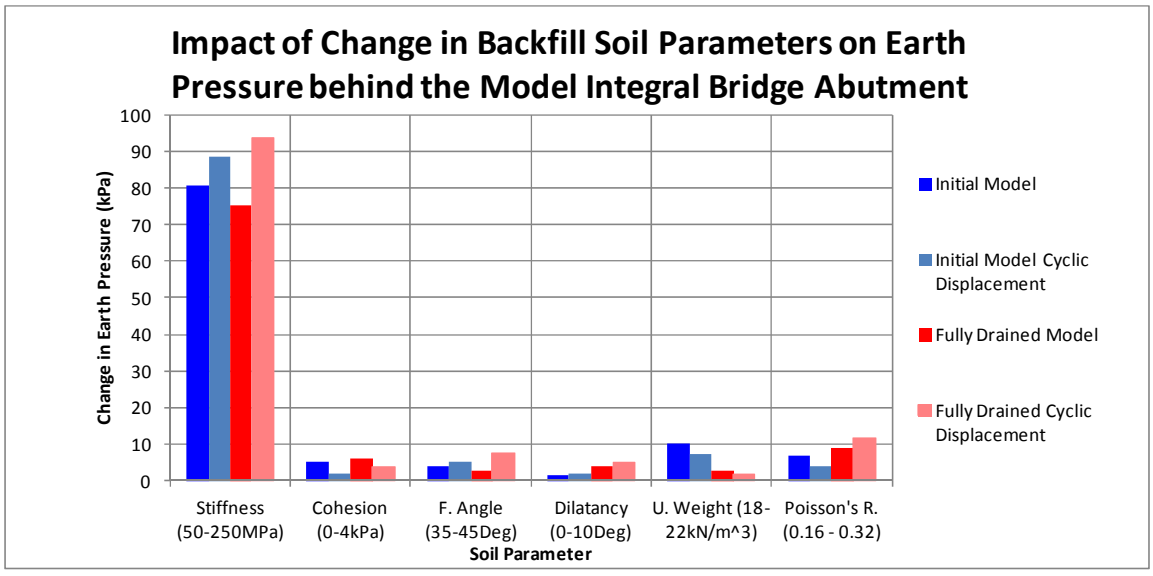

Figure 6.36: Impact of change in backfill soil parameters on earth pressure

6.6.4. Summary

As established in Chapters 2 and 5, several factors affect the magnitude of the lateral abutment displacement. These include the foundation geometry, foundation material type, the bridge structure properties and geometry that may affect the extent to which the abutment may yield in bending and rotation. These factors merge in a relatively complicated combination to affect the earth pressure values. The impact of these combinations on the earth pressure values is unique to each bridge as it largely depends on the combination of the bridge structure properties, and the nature of the bridge site/location. However, the effect of these combinations was not considered in this study as the bridge model developed for this simulation was based on an instrumented bridge, only varying the backfill soil parameters, state of foundation soil under loading, and abutment displacement, to enable a parametric study of the effect of these variations on the model.

The results obtained in this study show that changes in the values of all backfill soil parameters affect to some extent, the magnitude of earth pressure experienced within the backfill soil. There appears to be an increase in the earth pressure values as stiffness, cohesion and unit weight values increases across the changes in the other soil parameters (see Figures 6.14 – 6.21 and Figures 6.30 – 6.33 respectively). There also appear to be a decrease in the earth pressure values as friction angle values increases across the changes in the other soil parameters (see Figures 6.22 – 6.25). These clearly indicate a behaviour trend owing to change in specific backfill soil parameter values. However, the change in earth pressure values recorded as a result of the changes in the cohesion, friction angle, dilatancy and unit weight backfill soil parameters values, are relatively small and predominantly result in an average percentage change of less than 10% to the earth pressure values across the parameter variation range. As a result of the relatively negligible magnitude of change, these slight variations may also be considered to be a product of other factors affecting the magnitude of earth pressure experienced within the backfill soil that have not been taken into consideration in this study. Consequently, the patterns of behaviour attributed to changes in the cohesion, friction angle, dilatancy and unit weight backfill soil parameters, have not been clearly established from this analysis.

However, the impact of changes in the stiffness values on earth pressure is convincing with the relatively large variation in the earth pressure values dependent on these changes. Change in stiffness values within the model crushed rock backfill material may potentially result in an average percentage change in excess of 160% to the earth pressure values across the parameter variation range. This pattern of behaviour was observed in the models where the backfill stiffness parameter value of 50MPa was gradually increased to 250MPa (see Figures 6.14 - 6.17). Changes in the values of other parameters pale in comparison. This suggests that the magnitude of earth pressure developed behind the abutment of an integral bridge as a result of the thermal induced loading is primarily controlled by the relative stiffness of the backfill soil. This result agrees with the conclusions reached by Wood and Nash (2000) in a similar study varying primarily the friction angle against the stiffness, using an elastic perfectly plastic soil model, on a simplified model of an integral bridge, in a numerical model analysis.

The earth pressures developed in the fully drained model was found to be generally lower than the earth pressure developed in the initial model under similar conditions. The range of the earth pressures developed across similar change in backfill soil stiffness parameter was however found to be higher in the fully drained model. There is no clearly defined or established pattern of behaviour sustained in the initial model as well as the fully drained model. This is appreciated through a review of the impact of changes in specific soil parameters between measured and cyclic abutment displacement bar chart in the initial and fully drained models (see Figures 6.12 and 6.13). From inspecting Figures 6.12 and 6.13, it is evident that the earth pressure range in the initial model was not sustained in the fully drained model. The ratio between the measured and cyclic displacements in the initial model was also not sustained in the fully drained model. The impact of changes to the unit weight parameter is only less significant than the impact to the change in stiffness (see Figure 6.12) in the initial model, rather than least significant among all the parameters evaluated (see Figure 6.13) in the fully drained model. These results clearly show appreciable differences suggesting that a different behaviour pattern, hence earth pressure values may be expected in assuming a fully drained or undrained behaviour for fine grained soils during analysis.

6.7. Conclusion

Results of the parametric studies carried out to determine the impact that changes in specific soil parameters within the backfill material have on the earth pressure developed behind the abutment of a model integral bridge, were presented in this chapter. The backfill soil parameters identified for evaluation included the stiffness, cohesion, friction angle, dilatancy and unit weight. Loading simulations defining the pattern of abutment displacement recorded on an instrumented bridge site were carried out. Secondary loading simulations defining an established cyclic loading pattern were also carried out. These loading simulations were carried out varying the values of these parameters within the model backfill soil and varying the state of the foundation soil materials under loading.

Results of the study reported in this chapter suggest that changes in the value of all backfill soil parameters affect to some extent the magnitude of earth pressure experienced within the backfill soil. However, the results indicate that the magnitude of earth pressure developed behind the abutment of an integral bridge as a result of the thermal induced loading is primarily controlled by the change in the stiffness value of the backfill soil, and that changes in other backfill soil parameters have a negligible impact on the earth pressure. These results also indicate that the state of the integral bridge foundation soil under thermal induced loading have an appreciable effect on the behaviour of the backfill soil and the earth pressure values.

A parametric study on the impact of the variation of the backfill soil parameters was considered in this chapter. A parametric study on the impact of the seasons within which the integral bridge is constructed on the earth pressure developed within the backfill soil is considered in the next chapter. The impact of the variation of the stiffness parameter values (now established as being primarily responsible for the magnitude of earth pressure developed) on the season in which the integral bridge structure is completed is also considered in the next chapter. These analyses are carried out evaluating the impact of the state of the foundation soil materials under thermal induced loading.

Chapter 7 : IMPACT OF CONSTRUCTION SEASON

7.1. Introduction

While the integral bridge is significantly affected by temperature changes that are dependent on time and season, the construction process of the bridge structure in practice is generally not influenced by time periods or seasons. As a result, bridge construction activities in most cases occur all year round except in the most extreme of weather conditions. It is appreciated that the four distinct seasons within a typical year in the United Kingdom are associated with clearly different temperature range and weather conditions.

It has been observed through the review of the temperature data and the corresponding displacement pattern of the integral bridge abutment that the nature of the change in temperature defines the characteristics of the displacement experienced on any typical integral bridge. Where rising temperature is responsible for an abutment displacement in a specific direction, falling temperature within the same circumstances on the same bridge structure will be responsible for an abutment displacement in the opposite direction. The patterns of displacements defined by the patterns of temperature change, potentially define a unique pattern of behaviour within the backfill soil.

Through establishing a link between the time or season of construction and the abutment displacement pattern of an integral bridge, abutment displacement simulations are carried out to determine the impact of the construction season. This chapter presents the results of the parametric studies evaluating the impact of the season of construction on the magnitude of earth pressure developed within the backfill soil behind the abutment. The impact of the assumption of fully drained and the fully undrained state of the fine grain soils within the foundation material on the behaviour of the backfill soil is taken into consideration. As a result of the significant impact the variation of the backfill soil stiffness parameter has on the magnitude of earth pressure experienced within the backfill soil (see Chapter 6), the impact of changes in the backfill soil stiffness parameter on the season of construction is

also evaluated. The temperature model is based on a typical United Kingdom annual temperature pattern established in this chapter. The earth warmed by 0.75^{o}C within the last century (Met.Office, 2012) typically resulting in only fractions of a millimetre in abutment displacement. The temperature changes due to daily and seasonal changes are much greater than the temperature change due to climate change. Consequently, the impact of climate change was not considered in this study. However, the predicted increase in temperature will increase the earth pressures as the mean temperature increases.

The resulting abutment displacement is calculated using Equation 5.4 (see Chapter 5) and the coefficient of thermal expansion as recommended for concrete and steel bridges by the UK Design Manual For Roads and Bridges (BD37/01, 2001). A measure of the abutment displacement is as described in Section 5.3.1.5 (Chapter 5). The integral bridge model developed in Chapter 5 including the soil model, bridge and soil geometry and parameters are retained for this study.

7.2. Temperature Record

The UK met office offers arguably the most reliable and most widely used United Kingdom weather data information. Consequently, data used in modelling the possible temperature scenarios to which an integral bridge constructed in the United Kingdom may be subjected to, was obtained from publicly available data published by the UK met office.

The temperature data made available by the UK met office is presented in monthly and annual summaries from data stations located within the counties of the United Kingdom. These can be viewed as summaries for geographical regions within a United Kingdom country, summaries for countries, or summaries for the entire United Kingdom. These data summaries are presented as average and maximum or minimum temperature values. The geographical definition of the boundaries that define the regions is available on the UK met office website (Met.Office, 2012). Extreme case temperature data within the United Kingdom and its regions are also presented.

Extreme temperature data are considered ideal for most engineering design purposes. However, an evaluation of the available data published by the UK Met office show that several regions do not experience the temperatures similar to those identified as extreme in other regions. More critically, colder regions are often colder and warmer regions, warmer. Thus regions that have been subjected to an upper extreme temperature have not been subjected to the lower extreme temperature and vice versa. An annual temperature model made up of extreme temperature values thus present an unrealistic scenario unlikely to occur within the life span of a bridge structure built in any region within the United Kingdom.

Months	**UK Mean Daily Temperature / Month (^{o}C)**		**Temperature Range (^{o}C)**	**Calculated Model Abutment Displacement (mm)**
	Highest Maximum Average Temperature Recorded (England SE / Central S)	Lowest Minimum Average Temperature Recorded (England SE / Central S)		
January	9.9	-5.4	**15.3**	**7.0**
February	10.9	-4.3	**15.2**	**7.0**
March	14.1	-1.2	**15.3**	**7.0**
April	18.2	0.9	**17.3**	**7.9**
May	19.4	4.2	**15.2**	**7.0**
June	23.4	7.4	**16.0**	**7.3**
July	26.1	9.7	**16.4**	**7.5**
August	25.7	9.1	**16.6**	**7.6**
September	22.7	6.7	**16.0**	**7.3**
October	18.6	2.5	**16.1**	**7.4**
November	13.2	-0.2	**13.4**	**6.1**
December	10.4	-2.7	**13.1**	**6.0**

Table 7.1: Highest maximum and lowest minimum average temperature from England South East / Central South region (1910 to 2012). Abutment displacement calculated from Equation 5.4.

Temperature records considered best suited for use in modelling the performance of a typical thermal induced integral bridge abutment displacement within the United Kingdom,

would ideally include maximum and minimum temperature values that have the potential of regularly occurring within the months of the year in any region across the United Kingdom. This temperature record would support the development of a model that more realistically simulates the performance of an integral bridge under realistic United Kingdom climatic conditions. Through a review of the United Kingdom temperature data set, the average temperature data (average maximum and minimum) was found to present high and low temperature values with the greatest probability of occurring within the months of the year across the regions in the United Kingdom.

England South East / Central South was identified as the region with the most extreme cases of maximum and minimum average temperature data. The maximum and minimum temperature averages from 1910 to 2012 within this region, was identified for use in the modelling. The temperature data obtained within this region was considered the best available recorded data for a number of reasons. Primarily, it affords a wider temperature range and therefore a greater calculated abutment displacement and more significant earth pressure values for evaluation, while the calculated abutment displacement for the bridge model remained within the integral bridge abutment displacement limit of ±20mm defined by the United Kingdom design of integral bridges manual (BA42/96, 2003).

Temperature data across all regions of the United Kingdom also showed that the temperature average values from the England South East / Central South were attained or exceeded in all other United Kingdom regions over the duration within which records have been published (1910 – 2012). Consequently, maximum and minimum average temperature data obtained from the England South East / Central South region is considered suitable as being representative of the United Kingdom. This is supported by a publication of temperature records in Britain by Webb and Meaden (Webb and Meaden, 2000). These maximum and minimum averages (shown in Table 7.1) were used in establishing a typical temperature pattern over the course of a year.

7.3. Displacement & Construction Season

The conventional construction process of an integral bridge requires a full construction or placement of the abutments before the construction or placement of the bridge deck. During the construction process, when the abutment is fully erected before the deck is constructed, the abutment may be considered to be at a relative neutral horizontal position - without any forces or displacement input from the deck. Lateral abutment displacement or lateral forces from the bridge deck as a result of the thermal expansion and contraction of the bridge deck can only occur when the deck is structurally linked to the abutments. On construction completion, before the effect of thermal displacement is experienced, the change in bridge deck length or relative abutment displacement is 0mm. In modelling the construction seasons, the effect of thermal variation on the integral bridge structures is assumed elastic. Abutment displacement is assumed to be strain controlled because the stiffness of the bridge super structure is significantly higher than the stiffness of the materials resisting the abutment displacement (Arsoy et al., 2002).

The direction of the abutment displacement, with respect to the backfill soil, depends on the nature of the temperature change. A temperature change resulting in rising temperatures will lead to a bridge deck expansion. The expansion of the bridge deck results in abutment displacement away from the bridge deck and into the backfill. A temperature change resulting in falling temperatures will lead to a bridge deck contraction and an abutment displacement towards the bridge deck and away from the backfill. This establishes a pattern of abutment displacement behaviour that may be linked to a recognised pattern of temperature change. The integral bridge structure is therefore subjected to temperature increase or decrease from the temperature at construction completion up to the peak summer or winter months, and a general increase or decrease in deck length, and thereafter, cyclic increase and decrease in deck length as the seasons change through the years.

As the thermal induced displacements commences immediately following the construction completion, the season in which the construction is completed would determine the general pattern of loading the backfill soil would be subjected to as illustrated in Figures 7.1, 7.2 and 7.4. Due to the largely cyclic nature of the temperature variations experienced within the life span of an Integral bridge, the temperature values and the pattern of cyclic abutment

lateral displacements recorded within the bridge structure at any given moment or time duration will likely reoccur.

7.3.1. Summer & Winter Construction

An established pattern of a clear temperature cycle with relatively high summer months' temperatures and low winter months' temperatures is defined by the United Kingdom climate pattern. This implies that within a typical year in the United Kingdom, the general trend of temperature change beyond the peak summer month would be falling temperatures and likewise, that beyond the peak winter month would be rising temperatures.

Where construction is completed in the peak of the summer months, bridge deck contraction and abutment displacement will tend to occur only away from the backfill soil as time progresses towards the winter months and the temperature drops. Beyond the winter months and towards the next summer, the temperature rises and the abutment displacement will tend to occur towards the backfill and subsequently return to the relative neutral position (0mm - see Figure 7.3). The bridge deck expansion will in theory not exceed its length at the neutral position as the next peak of the summer month would have an approximately equal temperature value as the previous peak summer month in which the bridge was constructed.

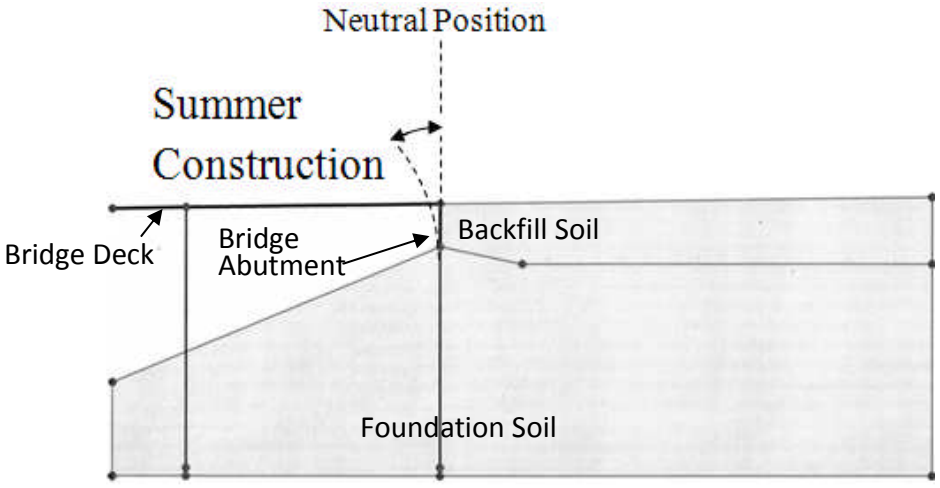

Figure 7.1: Displacement pattern defining a typical integral bridge abutment displacement when construction is completed in the peak summer month.

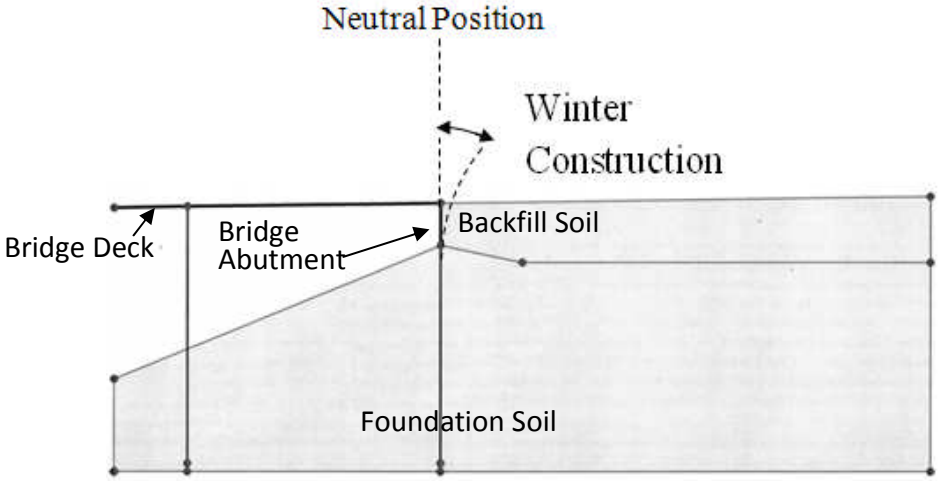

Figure 7.2: Displacement pattern defining a typical integral bridge abutment displacement when construction is completed in the peak winter month.

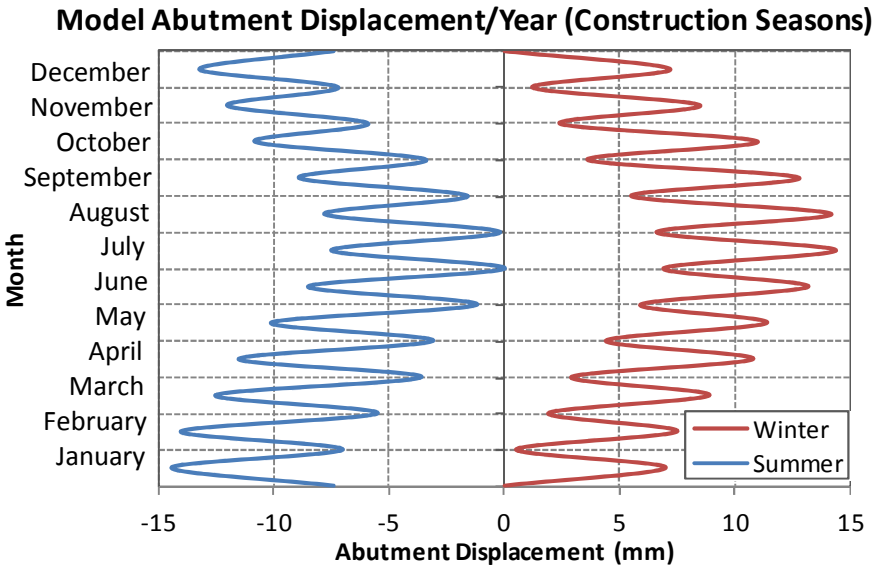

Figure 7.3: Abutment displacement pattern (developed from Table 7.1) defined by construction completion in the peak summer and winter months showing minimum and maximum displacement cycle within a month. Construction completion displacement (neutral position) is 0mm.

Construction completed in the peak winter months will tend to have bridge deck expansion and abutment displacement towards the backfill soil as time progresses and temperature rises leading to the summer. The bridge deck contracts and the abutment displacement occur away from the backfill and back to the relative neutral position (0mm - see Figure

7.3) as the temperature cycle returns leading to the next winter months. The bridge deck contraction will in theory not go below its length at the neutral position as the next peak temperature value of the winter month, is approximately equal to the temperature value recorded in the previous peak winter month in which the bridge was constructed.

7.3.2. Spring & Autumn Construction

Through the cycle of rising and falling temperatures that occur in a typical year, periods of mid temperature values between the highest and lowest temperatures are experienced. These mid-value temperatures are generally associated with the periods of spring and autumn. While the spring and autumn months may have similar temperature values, the temperature changes that are experienced within these two seasons are a reverse of each other, leading to abutment displacements in opposite directions. The spring experiences a general trend of rising temperatures hence abutment displacement into the backfill while the autumn experiences falling temperatures and abutment displacement away from the backfill.

When the bridge is constructed in the peak spring months, abutment displacement occurs towards the backfill soil as the temperature rises and the bridge deck expands. As time progresses beyond the summer months, the displacement of the abutment reverses direction away from the backfill soil and back to the relative neutral position (0mm - see Figure 7.5) leading to the winter months. However, unlike in the winter construction, because the lowest temperature the bridge deck may be subjected to is not the temperature that was experienced in the neutral position at the time of construction, the abutment displacement away from the backfill continues beyond the relative neutral position up to the displacement experienced in the peak winter month. The duration beyond the peak winter month and up to the next spring will result in another temperature rise within this cycle, bringing the abutment back to the relative neutral position as the temperature matches the temperature of the previous spring construction period.

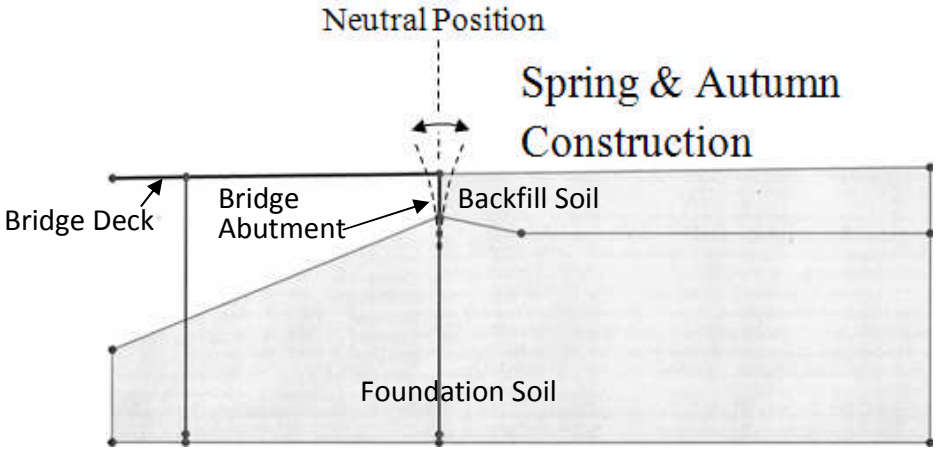

Figure 7.4: Displacement pattern defined by a typical integral bridge abutment when construction is completed in the peak spring or autumn month.

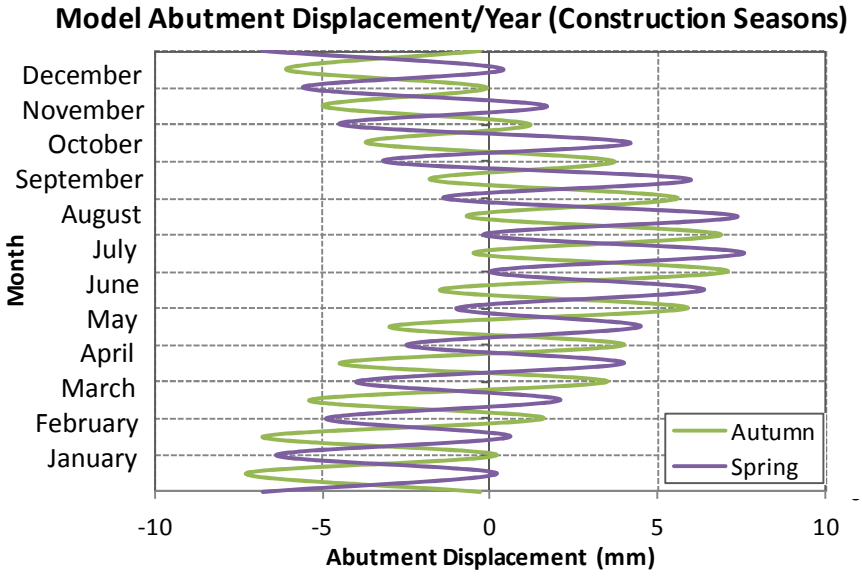

Figure 7.5: Abutment displacement pattern (developed from Table 7.1) defined by construction completion in the peak spring and autumn months showing minimum and maximum displacement cycle within a month. Construction completion displacement (neutral position) is 0mm.

When the bridge construction is completed in the peak of the autumn months, abutment displacement will tend to occur away from the backfill soil as the temperature drops leading to the winter months. As time progresses beyond the winter months and towards the summer, the abutment displacement direction will be reversed towards the backfill and

back to the relative neutral position (0mm - see Figure 7.5), as the bridge deck begins to expand. The abutment displacement will exceed the relative neutral position as it proceeds towards the backfill soil because the bridge will be subjected to higher temperatures than was experienced at the neutral construction position in the previous autumn season. As the temperature begins to drop beyond the peak of the summer month, subsequently matching that of the previous autumn, the abutment displacement direction reverses again away from the backfill soil and returns to the relative neutral position.

7.3.3. Modified Abutment Displacement

A graphical display of the model abutment displacement pattern in autumn and spring as defined by the monthly temperature data obtained from the UK met office is shown in Figure 7.5. This presents spring and autumn displacements not accurately aligned with a spring displacement range of -6.8mm to +7.6mm and an autumn displacement range of -7.3mm to +7.6mm (see April and October displacement range in Table 7.1).

This variation is as a result of the mid temperature of the monthly temperatures values identified for use in Table 7.1 (see Appendix 2 and 3). While analysis involving the winter and summer construction seasons evaluate the effect of the series of abutment displacement pattern limited to either side of the abutment neutral position, analysis involving the autumn and spring construction seasons evaluate the effect of the series of abutment displacement pattern that cross the abutment neutral position depending on the construction completion season. An appropriate comparison of the effect of the autumn and spring construction season would therefore require that the variation in the relative abutment neutral position be eliminated.

A review of the temperature range as published by the UK met office however shows that the mid temperature of the annual temperature range does occur immediately after the peak autumn month (October) temperature value and immediately before the peak spring month (April) temperature value. The temperature table was therefore modified to show the mid value temperature common to both seasons of autumn and spring in order to eliminate the effect of the relative positioning of the series of displacement (Table 7.2). The graphical

result of this modification, used as the model abutment displacement, can be seen in Figure 7.6. This figure show the cyclic relative displacement of the abutment with respect to the neutral position similar in magnitude and direction for construction completed in the autumn and spring seasons. The difference between these seasons now remains the pattern of the initial series of displacement, either towards the backfill soil (passive side) or away from the backfill soil (active side). Figure 7.7 show abutment displacement pattern modelling construction completion in specific seasons.

Modified Mid Autumn/Spring Construction Temperature (Monthly Cycle) (Integral Bridge Deck/Abutment Link Maximum Temperature and Displacement)					
Months	Mid Temp.	Calculated Model Abutment Disp. (mm)	Relative Mid Disp. (mm)	Relative Min. Disp. (mm)	Relative Max. Disp. (mm)
January	2.3	7.0 (±3.5)	-3.6	-7.1	-0.1
February	3.3	**7.0 (±3.5)**	-3.1	-6.6	0.4
March	6.5	**7.0 (±3.5)**	-1.6	-5.1	1.9
April	**10.1**	**7.9 (±4.0)**	0	-4.0	4.0
May	11.8	**7.0 (±3.5)**	0.8	-2.7	4.3
June	15.4	**7.3 (±3.7)**	2.4	-1.3	6.1
July	17.9	**7.5 (±3.8)**	3.6	-0.2	7.4
August	17.4	**7.6 (±3.8)**	3.3	-0.5	7.1
September	14.7	**7.3 (±3.7)**	2.1	-1.6	5.8
October	**10.1**	**7.4 (±3.7)**	0	-3.7	3.7
November	6.5	**6.1 (±3.1)**	-1.6	-4.7	1.5
December	3.9	**6.0 (±3.0)**	-2.8	-5.8	0.2

Table 7.2: Mid temperature values and month of occurrence (modified from Table 7.1) showing calculated model abutment displacement where the displacement at construction completion in autumn and spring (neutral position) is 0mm

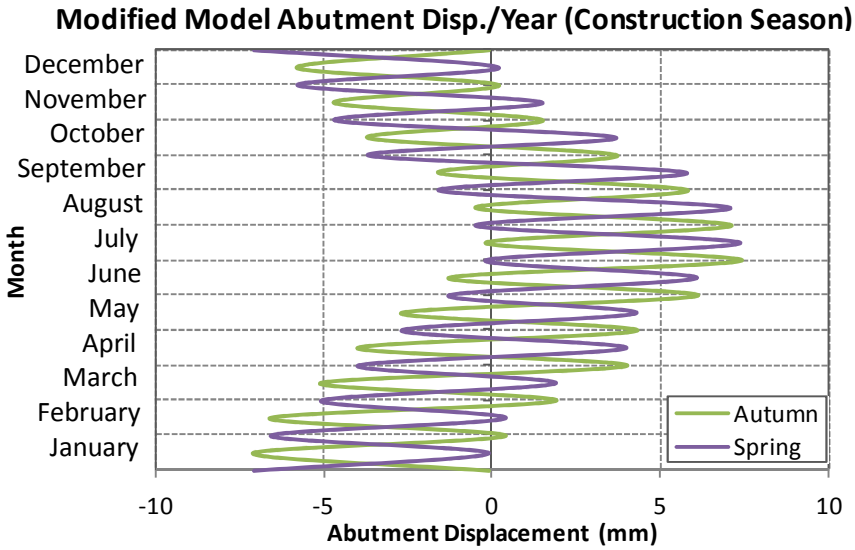

Figure 7.6: Abutment displacement pattern (developed from Table 7.1) defined by construction completion in the peak spring and autumn months showing minimum and maximum displacement cycle within a month. Construction completion displacement (neutral position) is 0mm.

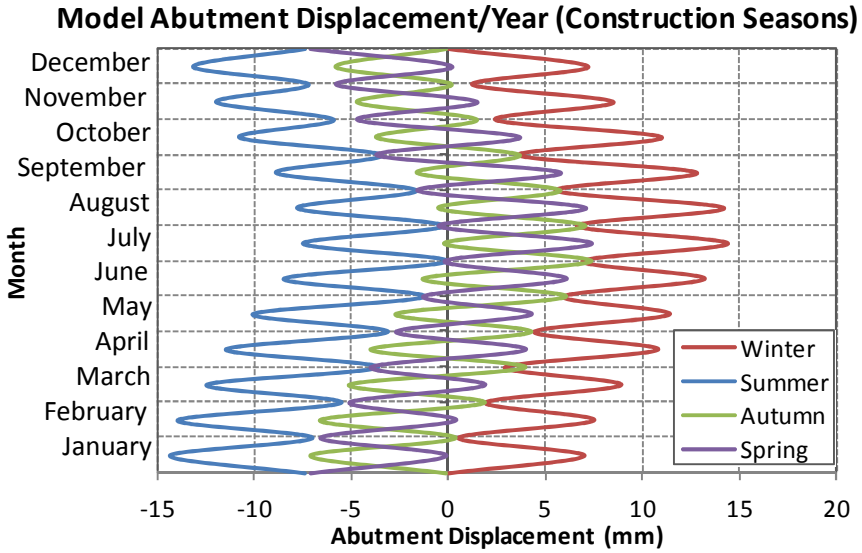

Figure 7.7: Model abutment displacement pattern of all construction seasons with respect to abutment neutral position. Displacements illustrated show a minimum and maximum displacement cycle within a month where construction completion displacement (abutment neutral position) is 0mm.

7.4. Construction season and Soil behavior

Abutment displacement effect within the backfill soil as a result of an increase in the bridge deck length may be described as passive side displacement and as a result of a decrease in deck length, active side displacement. There exist four clearly defined combinations of these displacement patterns defined by the construction completion time of integral bridges constructed within the four distinct seasons in the United Kingdom. These different patterns of abutment displacements present unique and characteristic soil behaviour and consequential earth pressures. This is largely attributed to the fact that the behaviour of a soil mass, irrespective of the strains and stresses it may be currently subjected to, is dependent on its history.

The relationship between the horizontal and vertical effective stress within a soil mass is defined within the limits of the coefficient of earth pressure, K. However, during thermal loading, the relationship between the horizontal and vertical effective stress in the backfill soil at any given time may be defined within the limits of the coefficient of active earth pressure, K_a; and within the limits of the coefficient of passive earth pressure, K_p. The relationships that may apply depend on the relative displacement position of the abutment to the backfill soil.

$$K_a = tan^2(45° - \frac{1}{2}ø') \quad \text{…….. (7.1)}$$

$$K_p = tan^2(45° + \frac{1}{2}ø') \quad \text{…….. (7.2)}$$

These coefficients have different values as calculated using Equations 7.1 and 7.2 and as illustrated in Figure 7.6. Under an equal magnitude of displacement from the abutment neutral position in the active side displacement and passive side displacement, a retained soil mass, such as the backfill soil behind the integral bridge abutment, will generate

different earth pressure values. On return to the abutment relative neutral position, the earth pressures recorded within the backfill soil would be influenced by several factors including the elastoplastic properties of the material thus resulting in slightly different earth pressure values between the active side and the passive side abutment displacements. Where the cyclic lateral loading is sustained on either side, different soil behaviour patterns may therefore be expected as a result of the different stress paths that will be defined. The relationship within the limits of the coefficient of earth pressures, the soil loading pattern controlled by the season in which construction is completed, and the elastic properties of the backfill material, are factors that influence the extent of the variation in the soil behaviour.

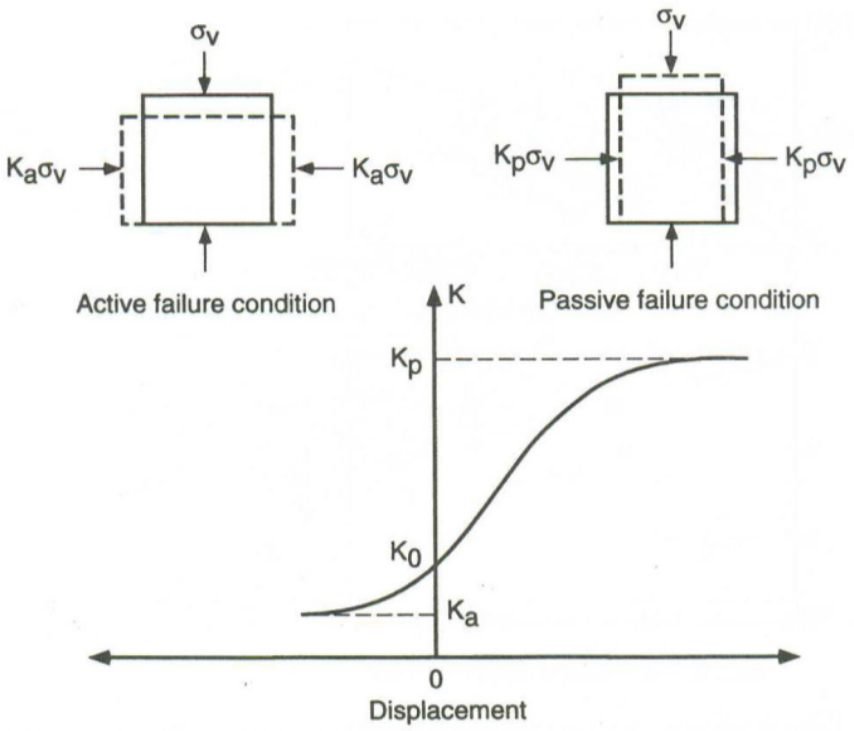

Figure 7.8: Relationship between displacement and the coefficient of active and passive earth pressure (Mitchell and Soga, 2005).

Stresses generated from strain controlled cyclic loading on granular material progressively become more predictable with significantly less changes in successive cycles as the number of cycles increase. In a study carried out by Carder and Hayes, the typical stress strain

behaviour of granular material under strain controlled cyclic loading (Carder and Hayes, 2000) show progressively stabilizing behaviour between the second and tenth cycle and relatively insignificant changes in cycles beyond that. Integral bridge backfill materials are predominantly subjected to strain control loading type. This finding on the effect of strain controlled cyclic loading is therefore considered to apply within this study as the backfill soil being modelled is granular in nature. This informs the decision to carry out a full cyclic loading simulation on the integral bridge backfill soil model up to the tenth cycle.

7.5. Modeling Construction Seasons

A primary challenge in modelling the impact of the construction completion season within the United Kingdom is the adoption of a temperature model that simulates the realistic effect an actual United Kingdom temperature pattern has on an integral bridge structure. While the adoption of a model environmental temperature pattern appears direct and simple, modelling the actual abutment displacement behaviour presents several challenges including establishing an appropriate environmental temperature model, accommodating the thermal properties of the bridge material components, accommodating the environmental conditions, and establishing the abutment displacement characteristics. For this study, environmental temperature data provided by the UK Met office is assumed to be the model bridge EBT.

The process of cyclic loading within an integral bridge backfill is only achieved when the EBT (estimated bridge temperature) of the bridge structure changes from a referenced temperature value and returns to the same value after a period in a continuous manner. This is because the EBT accounts for the actual bridge deck expansion that occurs. The integral bridge structure is generally subjected to two cyclic temperature loading patterns, the daily temperature cycle and the yearly temperature cycle. Smaller temperature variations with a higher frequency of occurrence are experienced in the daily temperature cycle while larger temperature variations with a lower frequency of occurrence are experienced in the yearly temperature cycle.

The daily temperature cycle could be attributed to the change in daily temperatures that occur as a result of heat from the sun's radiation by day and cooling by night. Within the United Kingdom, the yearly temperature cycle could be attributed to the seasonal temperature extremes of winter and summer. While the daily minimum and maximum temperature cycle proceeds, there is a gradual change in temperature reflecting the changing seasons. Temperature changes across the seasons within a year from a maximum temperature season, summer, to a minimum temperature season, winter, thus defining a yearly maximum and minimum temperature cycle. Consequently, these two temperature cycles occur simultaneously. There are 365 typical daily temperature cycles that make up 1 typical yearly temperature cycle.

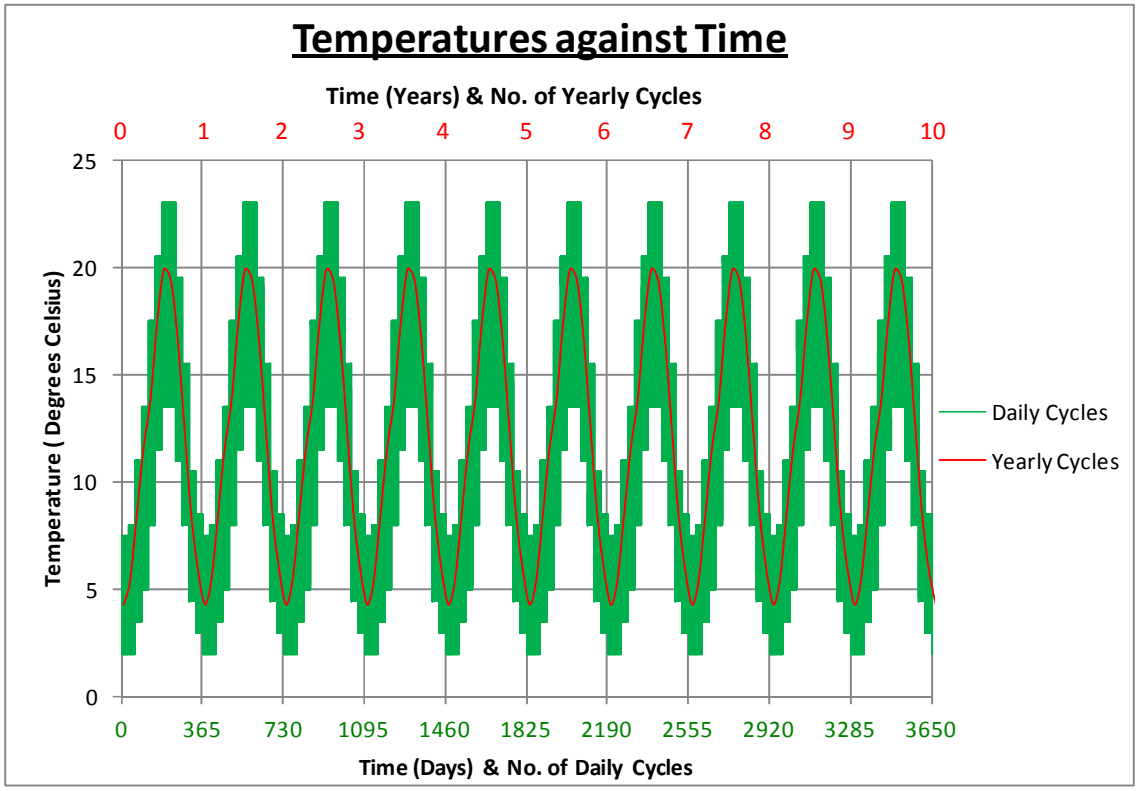

Figure 7.9: Temperature against time - 3650 days (10 years). Showing 365 maximum and minimum daily temperatures cycles (in green) in 1 maximum and minimum yearly temperature cycle (in red).

Temperature data obtained from the UK met office, presented in monthly considerations also consists of the mean daily maximum and minimum temperature recorded at specific

stations, over time (Met.Office, 2012). This data provide an average daily temperature range for each month of the year. The average daily maximum and minimum temperature data across a given month may be used in developing a daily temperature cycle for modelling the impact of daily temperature variation in an annual cycle. As the months change, this would take into account the impact of the changing seasons as well. The monthly maximum and minimum temperature data may also be used in developing a daily temperature cycle. This would involve a daily cycle modelling the monthly limits and changing as the months change to accommodate the seasons in an annual cycle.

7.5.1. Modeling Thermal Effect

Integral bridge structures and the backfill soils are ideally expected to experience 365 daily cycles in one annual cycle. However, the evidence gathered from research does not support this expectation and has shown that the actual cyclic behaviour of a constructed integral bridge differs. Integral bridge abutment displacement and the corresponding environmental temperature measured at consistent regular intervals on sites reveal a less consistent immediate (short duration) temperature-displacement trend (Kerokoski and Laaksonen, 2005, Kerokoski, 2006, Darley et al., 1998, Darley et al., 1996).

The less consistent temperature-displacement trend characteristically does not follow any defined pattern and is not certain to repeat any established pattern. This may be attributed to the fact that the EBT pattern may rise consistently for days and/or fall consistently within the same month even when the general temperature trend of the changing season suggest otherwise. It may also be attributed to the fact that the EBT does not respond instantly to immediate temperature changes. Erratic short-term temperature behaviour is also regularly experienced within the seasons. This less consistent temperature-displacement trend is most appreciated where consistent and regular interval temperature measurement with more than one frequency per day is taken. This trend would also be lost in the event the temperature data is averaged over time.

In theory, a complete cyclic temperature pattern, where the maximum and minimum temperatures are repeated, would not occur in the daily temperature cycles because of the

gradual change in temperature from one day to the next, attributed to the change in seasons. Without the impact of climate change, a complete cyclic temperature pattern will occur in two or more complete yearly cycles. Within the assumptions made in this research, the yearly cycle would entail two calculation phases in simulating the effect of thermal loading on the backfill soil – an abutment displacement in opposite directions, representing the maximum and minimum annual temperature effect. However, a study of the impact of the construction completion season using the yearly cycle (average yearly maximum and minimum temperatures) will present an over simplified account of the activities and developments that may be experienced within the backfill soil. The yearly cycle will also eliminate a prime feature of the integral bridge backfill soil loading - the primary cyclic loading effect that occurs as a result of the daily cyclic loading.

The daily model cycle replicates the average daily temperature pattern experienced within a given month. This model would define a yearly cycle pattern by repeating the daily cycle limits through a month with changes occurring at the beginning of the next month accounting for the limits of the next month and sustained through it. This approach would entail two calculation phases modelling abutment displacement in opposite directions, representing the maximum and minimum temperature effect for every given day. In modelling the effect of thermal induced abutment displacement for 10 years, this translates into a minimum of 7,300 finite element calculation phases.

While the daily temperature model would appear to generate a more detailed abutment displacement output from the large number of calculation required, it has been found that the daily temperature variation does not reflect the actual behaviour of an integral bridge structure subjected to daily temperature changes. Immediate and short term temperature changes have been documented to have little or no effect on the EBT of the bridge deck (Russell and Gerken, 1994). As a result of the constant changes to the temperature values within the day, and the frequency of the cyclic temperature change in the daily cycles, the effect on the integral bridge structure has been found to be largely introducing a thermal gradient through the vertical depth of the structure (Russell and Gerken, 1994).

However, the general temperature trend over a longer period of time (seasonal temperature change) primarily affects the change in the length of the bridge deck (Russell and Gerken, 1994) which controls the actual abutment displacement. This suggests that the daily temperature changes have little impact on the displacements that actually influence the behaviour of the abutment displacement. This behaviour is directly influenced by the seasonal changes in temperature that persist long enough to introduce sustainable thermal change through the depth of the structure and an appreciable displacement. Consequently, the EBT changes may appropriately be attributed to the seasonal temperature change rather than the daily change in temperature.

The temperature range within the daily cycle presents some challenges as well. The temperature data from the UK met office presents an average daily maximum and minimum temperature for each month, which may be adopted in simulating a daily temperature cycle. This would imply that in modelling, a consistent daily temperature maximum and minimum value, representative of the month, is used throughout each month. However, the recorded temperature variation over the months show temperatures that routinely exceed the average daily maximum and minimum temperatures of the referenced month, the previous month and the next month by substantial margins, and therefore cannot be ignored.

This limited daily temperature range was also observed by Springman et al. (Springman et al., 1996). Springman et al. (1996) established that for at least 96% of the days in a typical year within the United Kingdom, the temperature variation is less than 4.5^{o}C. The limited daily temperature range highlights a significant shortcoming in the use of daily temperature maximum and minimum averages values in defining a model temperature pattern, across the months of a typical year in the United Kingdom.

A consideration was given to adopting a higher temperature range that would accommodate the limits routinely attained each month for the daily temperature model. However, the challenge this option presents is that the daily frequency of this higher limits would amount to an extreme scenario most unlikely to occur as the frequency of attaining these limits

within the month is significantly less than the frequency that would be modelled in this scenario.

7.5.2. Thermal Model

While taking into consideration the resources required in achieving the daily temperature model simulation, it will also be appreciated that given the available data, this model would either lack the typical temperature range that may be experienced within a given month if based on the daily temperature averages or would over emphasise the frequency of occurrence of the monthly temperature limits if based on monthly temperature averages. Besides, it is evident from research and field measurement carried out on instrumented integral bridge structures that the behaviour of the backfill soil is to a large extent not dependent on the environmental daily temperature variation depicted in the daily cycle (Russell and Gerken, 1994).

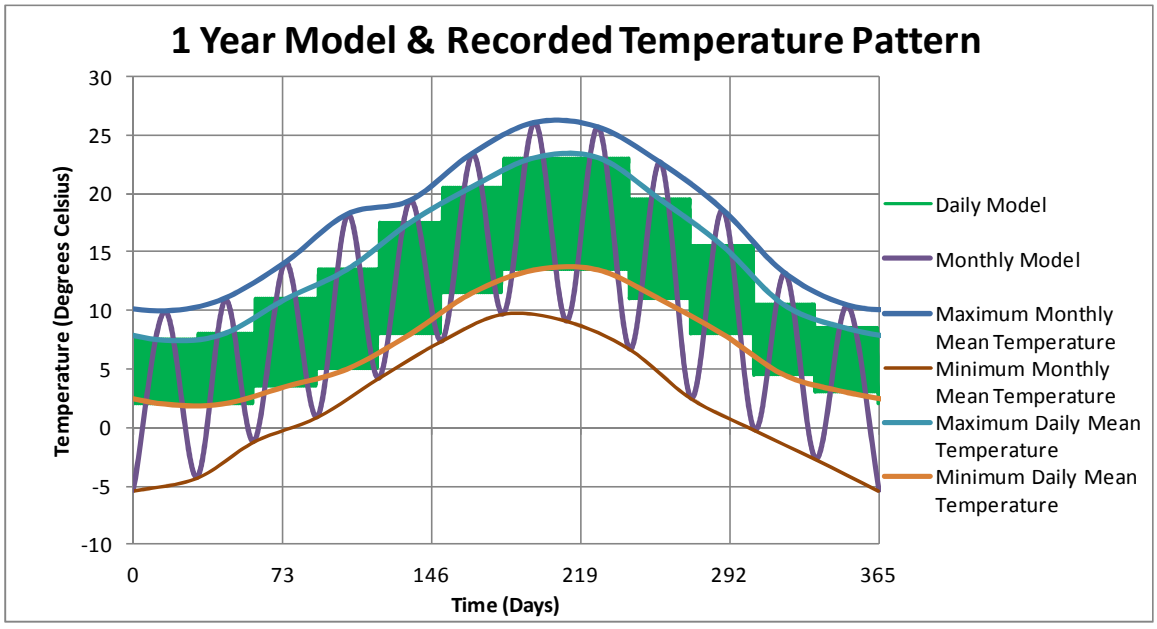

Figure 7.10: Day 1 to 365: Temperature models and limits through a typical year starting January day 1 to December day 365.

Consequently, simulating the thermal induced loading of an integral bridge model using the daily cycle temperature model will generate results that would under estimate the earth

pressures where the temperature is based on the daily temperature averages. Where the temperature model is based on the monthly temperature averages the daily cycle will generate over estimated earth pressure results. In all cases, the daily cycle model would present misleading backfill soil behaviour pattern.

The temperature model data was modified to present a temperature data set that simulates a more realistic backfill soil loading response from a thermal induced abutment displacement. To introduce the required change, features considered less relevant such as daily temperature variation were deemphasised. Features considered more relevant in modelling the actual abutment displacement behaviour such as lower frequency monthly limits, primary cyclic temperature variation within the secondary cyclic variation, and a more appropriate monthly temperature range were emphasised. The governing principle adhered to in this modification was to adopt a temperature model that reflects the characteristics of an abutment season-displacement behaviour in modelling the characteristics of integral bridge obtained through instrumentation and site measurements.

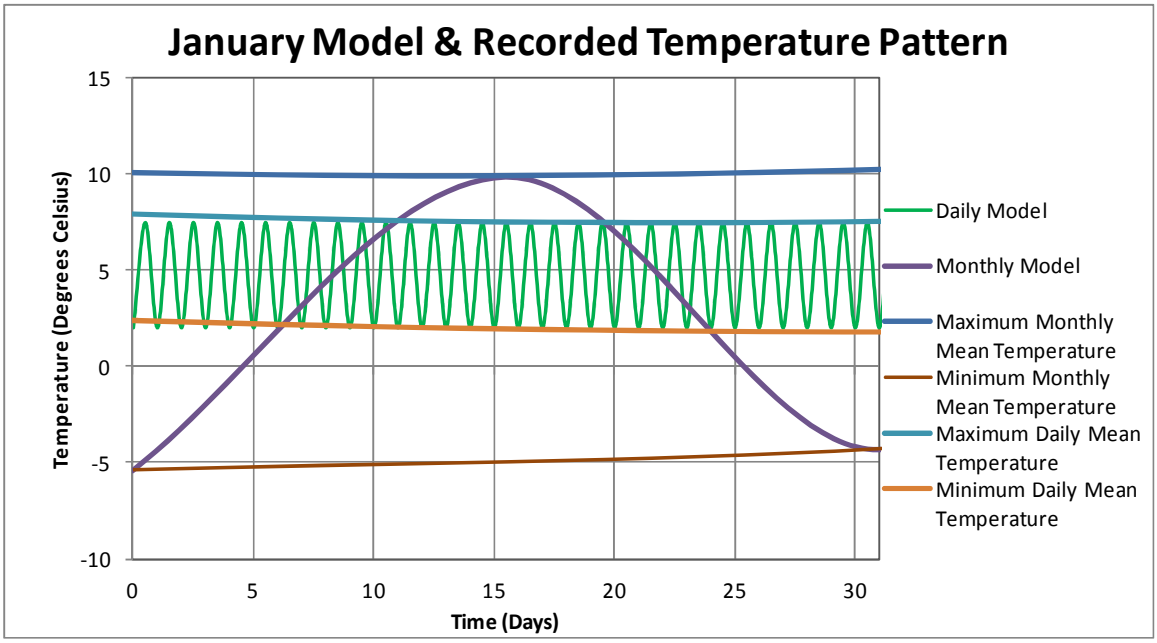

Figure 7.11: Day 1 to 31: Temperature models and limits through a typical month highlighting January day 1 to day 31 as shown in Figure 7.10.

Monthly temperature average data is adopted to accommodate the temperature limits attained within the months. To model the impact of a general temperature trend over a longer period, the monthly limits are assumed to be attained through the duration of a month and within a single cycle. It is therefore assumed that the EBT of the bridge within a month attains both maximum and minimum limit proceeding gradually from one limit at the beginning of the month to the other limit by mid month and returning as the month proceeds towards the end. This assumption was implemented in a monthly model temperature cycle (see Figure 7.12).

While the monthly model temperature cycle does not incorporate the actual daily cycle experienced, the impact of the primary cycle, albeit with lower frequency, is accounted for through the 12 primary cycles in a single secondary cycle accounting for the monthly temperature limits within the months of a year. This model would entail two calculation phases a month in simulating abutment displacement in opposite direction through a model 10 year duration. It accommodates a more realistic temperature range within the months, models backfill soil behaviour dependent on seasonal temperature change and can generate more realistic and reliable results using the available data and resources.

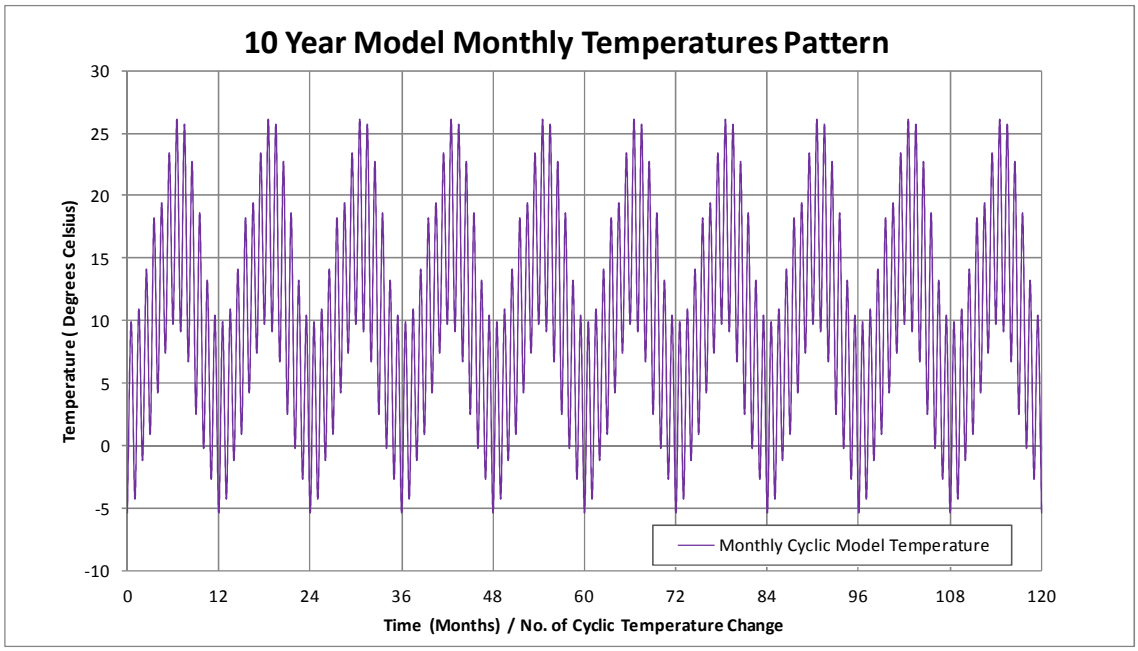

Figure 7.12: Monthly temperature model adopted for use in the model bridge abutment displacement simulation showing temperature variation in time.

7.6. Model Abutment Displacement/Backfill Loading Overview

A combination of sequential lateral displacements within and across the passive and active side in alternate directions was carried out to model the typical displacement pattern of the abutment. Abutment displacement modelling construction completion in specific seasons is shown in Figure 7.7 where passive side abutment displacement is positive and active side abutment displacement is negative. Accordingly, the model, simulating an integral bridge construction completed in the peak summer month, being the period with the maximum temperature of the year, had the bridge deck length at its maximum length in the neutral position. Bridge construction completed in the peak winter month, being the period with the minimum temperature, had the bridge deck simulated at its minimum length in the neutral position. Bridge construction completed in the spring and the autumn months, had the bridge deck simulated at its mid length in the neutral position.

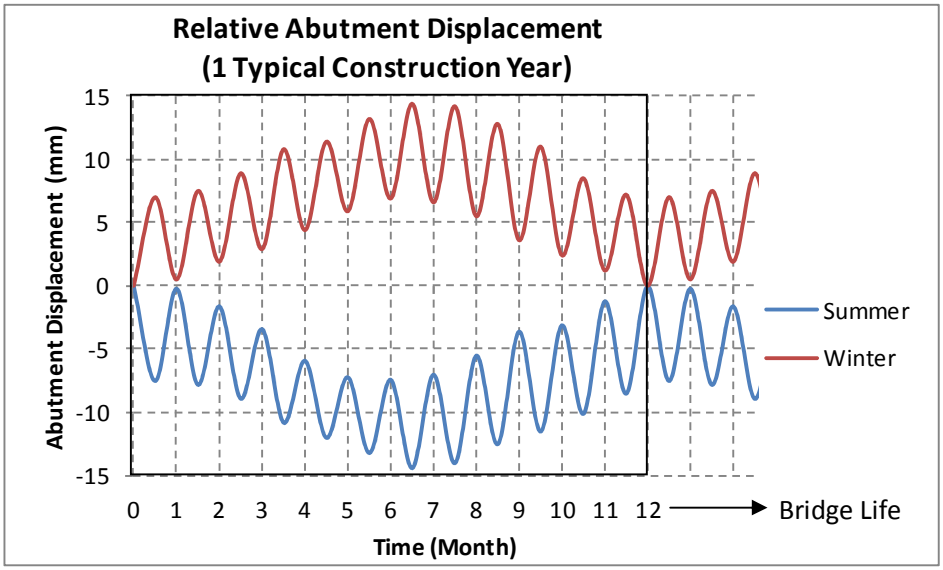

Figure 7.13: A typical year relative abutment displacement highlighting the exclusive displacements relationships of construction completed in the summer against construction completed in the winter as time progresses.

An evaluation of the displacement patterns of an integral bridge abutment with respect to the season in which construction is completed has clearly defined two displacement conditions that may influence the performance of the integral bridge backfill. In one displacement condition, change in performance of the backfill soil may be largely attributed

to the general trend of displacement the backfill soil is subjected to - either passive or active type displacement only. The effect of the passive or active 'type displacement only' may be evaluated by comparing the earth pressure developed as a result of construction completed in the peak summer months to construction completed in the peak winter month where there would be no chance of any significant displacement into the opposite side of the abutment neutral position (see summer and winter displacement curves in Figure 7.13 where construction completion displacement is 0mm).

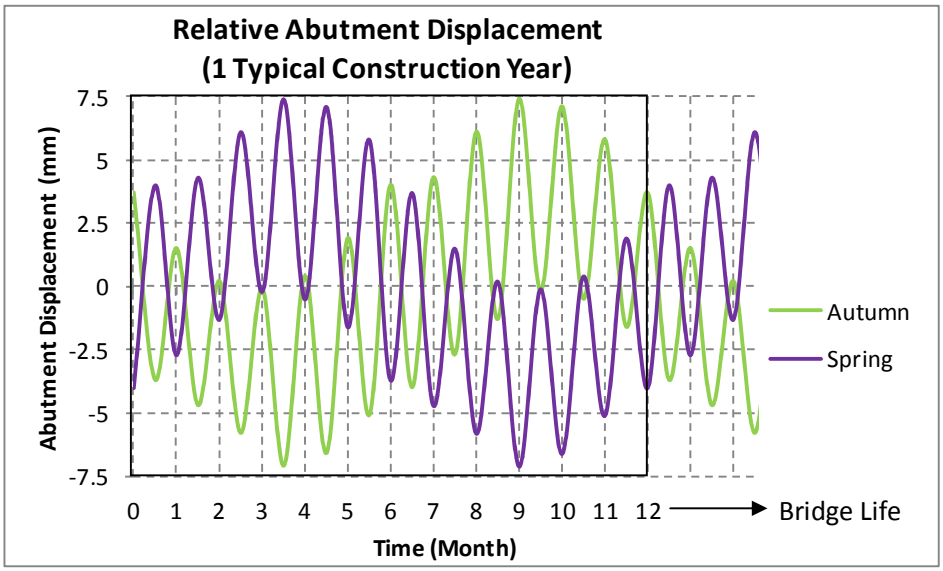

Figure 7.14: Autumn and spring: A typical year relative abutment displacement highlighting the reverse displacements relationships of construction completed in the autumn against construction completed in the spring as time progresses.

In the second displacement condition, abutment displacements occur on both sides crossing the abutment neutral position within complete cycles. Under this displacement condition, change in performance of the backfill soil may be largely attributed to the different stress paths defined by the initial series of abutment displacement - either initially passive or initially active. This effect may be evaluated by a direct comparison of the earth pressure developed as a result of construction completed in the peak autumn month to construction completed in the peak spring month. In each of these case, the initial set of displacements gradually proceed to the maximum displacement in the opposite directions on either side of the abutment neutral position before returning to the maximum displacement on the other

side across the abutment neutral position (see autumn and spring displacement curves in Figure 7.14 where construction completion displacement is 0mm).

The backfill and foundation soil parameters are shown in Table 6.1. Two models, the initial model and the fully drained models were simulated as described in Section 5.5.3.1 to evaluate the impact of the assumptions within the foundation soil on the earth pressure. Changes to the backfill soil stiffness within the parallel models were also simulated. The typical United Kingdom yearly temperature modelled assumed no influence of climate change.

7.7. Results & Discussion

Results obtained from simulating thermal induced displacement on a model integral bridge abutment constructed in the peak season of summer, winter, autumn and spring within the United Kingdom is presented in this section. The yearly average maximum and minimum earth pressures are calculated by finding the average of the maximum and minimum earth pressures of the months within a typical year. The axis indicating the time (months) in the graphs Figures 7.15 – 7.20 commences at month 12 and terminates at month 108 in a 120 months modelling duration. This is to eliminate the effect of a partial year average that may be caused by the different construction completion seasons within a year in order to secure a full 12 month average for every construction completion season.

When subjected to similar temperature variations, the summer and winter displacement patterns present cases of extremes displacement from the abutment neutral position while the autumn and spring presents cases with concurrent minimum displacements on either sides of the abutment neutral position.

7.7.1. Results

Simulation results presenting the impact of the season of construction on the magnitude of earth pressure are presented in Section 7.7.1.1. Simulation results presenting the impact of

the assumptions of fully drained and undrained fine grained soils in the foundation materials on the results generated by modelling the seasons of construction are presented in Section 7.7.1.2. The results presented indicate the stiffness parameter values evaluated at 50MPa, 92.1MPa (model soil with no stiffness change), 150MPa and 250MPa. Initial and fully drained model parameters are as identified in Table 6.1.

As a result of the volume of data generated in this parametric study, and to better appreciate the impact of construction seasons, the results of the summer construction are compared with winter construction and spring construction compared with autumn construction using similar backfill stiffness values and modelled under the same assumptions (initial or fully drained models).

7.7.1.1. Impact of Construction Seasons

Figures 7.15 - 7.18 present the results of evaluating the impact of the season of construction on the magnitude of earth pressure with a backfill stiffness value of 50MPa. Results generated using backfill stiffness values of 92.1MPa, 150MPa and 250MPa are presented in Appendix 6.

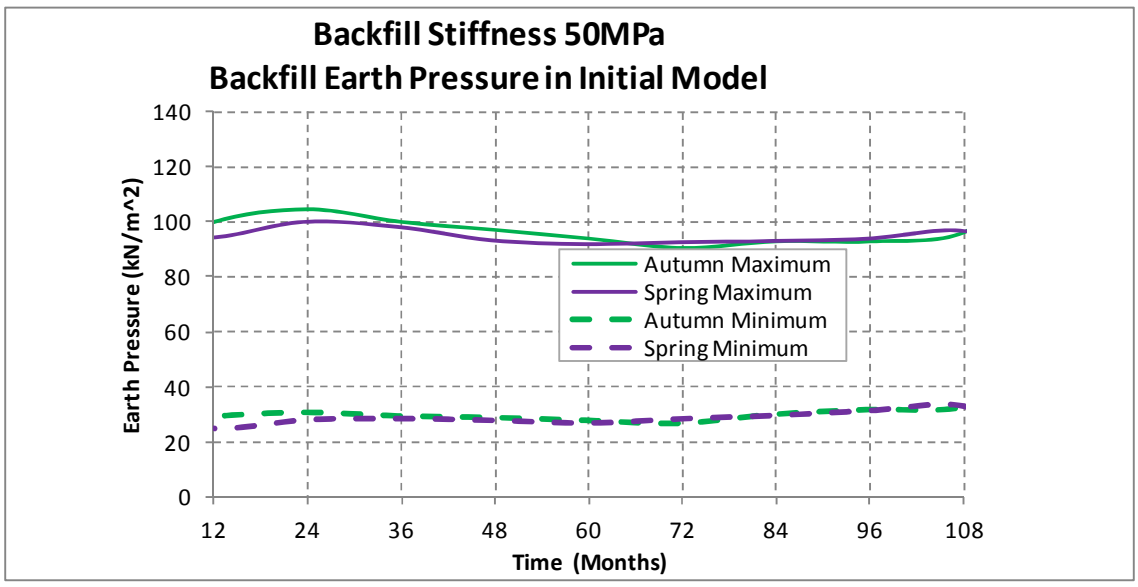

Figure 7.15: Initial model autumn construction against spring construction earth pressures at 50MPa backfill stiffness.

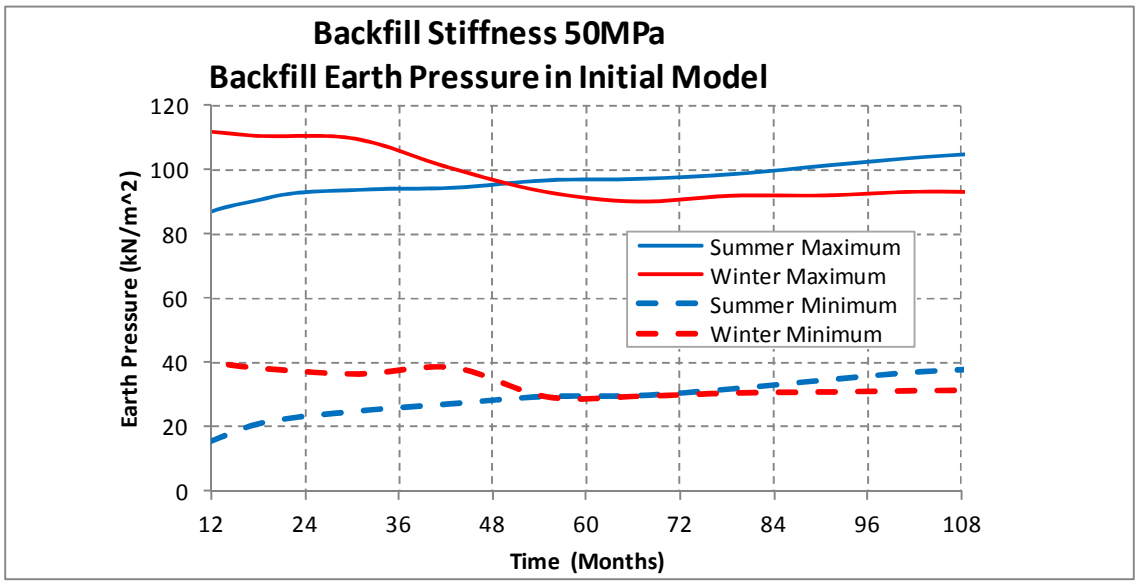

Figure 7.16: Initial model summer construction against winter construction earth pressures at 50MPa backfill stiffness.

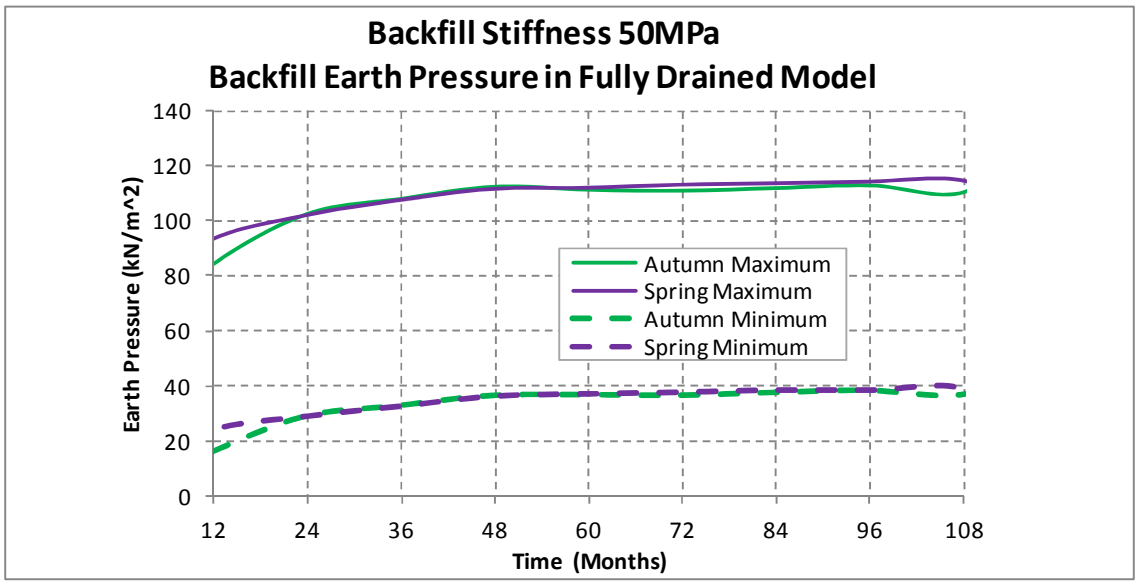

Figure 7.17: Fully drained model autumn construction against spring construction earth pressures at 50MPa backfill stiffness.

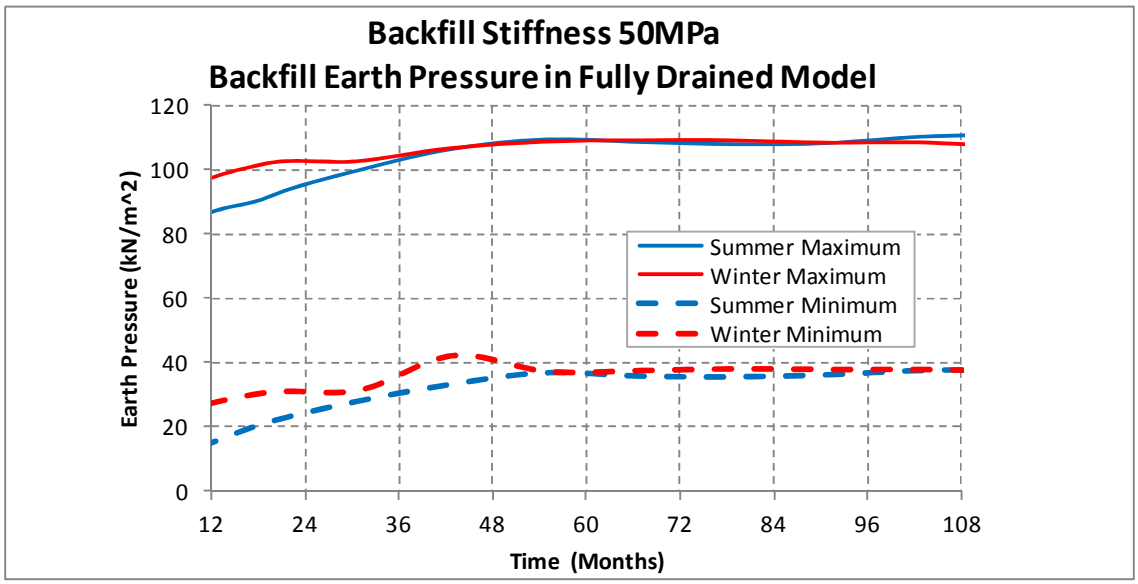

Figure 7.18: Fully drained model summer construction against winter construction earth pressures at 50MPa backfill stiffness

7.7.1.2. Impact of Foundation Soil State

Figures 7.19 and 7.20 present the impact of assuming fully drained or undrained conditions under loading within the fine grained soils in the foundation materials in modelling the seasons of construction using a backfill soil stiffness value of 50MPa. Results generated using backfill soil stiffness values of 92.1MPa, 150MPa and 250MPa are presented in Appendix 7. Within the graphs presented in this section, Full Dr represents fully drained model, Initial represents initial model. Autumn, spring, summer and winter are represented by Aut, Spr, Sum, and Win respectively.

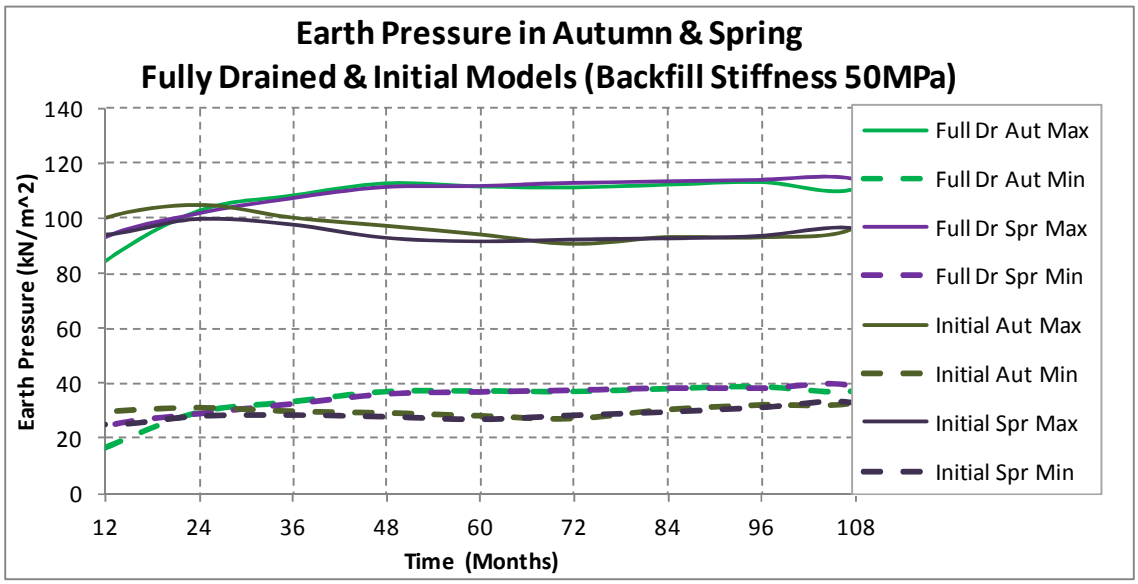

Figure 7.19: Autumn & spring construction fully drained against initial model at 50MPa backfill stiffness - earth pressure values.

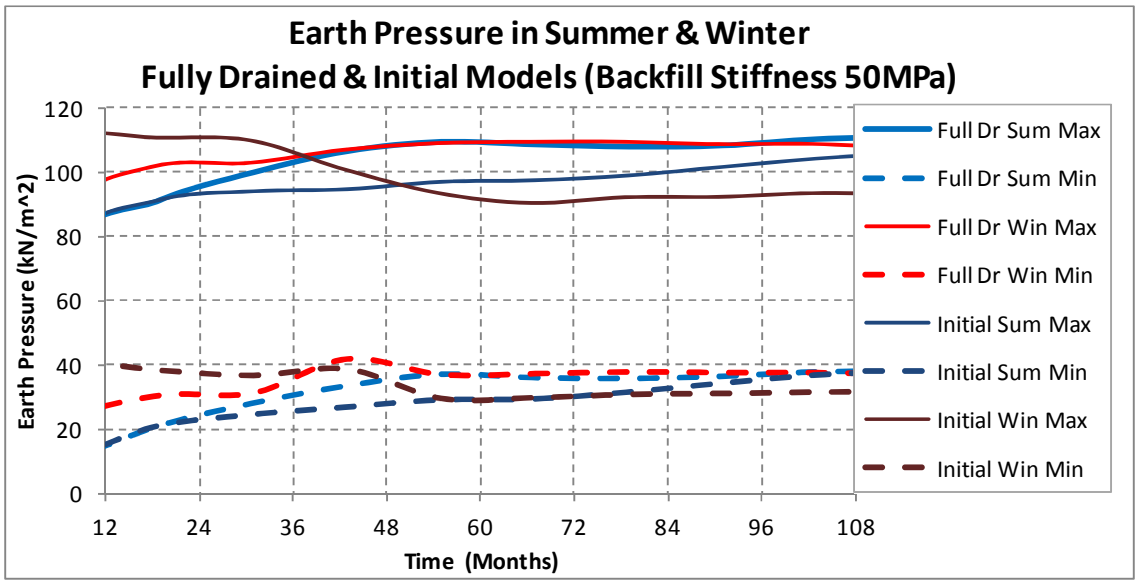

Figure 7.20: Summer and winter construction fully drained against initial model at 50MPa backfill stiffness - earth pressure values.

7.7.2. Discussion

A total of 32 simulations reflecting four stiffness values across four seasons in the initial and fully drained models were carried out. Patterns of behaviour emerged through the comparison of earth pressures developed from construction completed in different seasons and across varying backfill stiffness parameter values.

Lower Earth Pressures Generated in Initial Model Simulations																
Figure & Backfill Stiffness Value		Beginning of 2nd Cycle					Beginning of 10th Cycle					Cumulative				
		A	Sp		Su	W	A	Sp		Su	W	A	Sp		Su	W
7.15	50	-	√				√	-				-	√			
7.16	MPa				√	-				-	√				√	-
7.19	92.1	√	-				-	√				-	√			
7.20	MPa				√	-				-	√				√	-
7.23	150	√	-				-	√				√	-			
7.24	MPa				√	-				√	-				√	-
7.27	250	√	-				√	-				√	-			
7.28	MPa				√	-				√	-				√	-

Table 7.3: Summary of simulation results from the initial model generating lower earth pressures.

The results presented in Figures 7.15 – 7.18 and Appendix 6 show that relatively lower cumulative and peak earth pressures are often developed where construction is completed in the summer against the winter and where construction is completed in the autumn against the spring. However, the results do not suggest any consistent or appreciable difference in the earth pressures developed within the backfill soil as a result of construction completed between the summer and autumn seasons and between the winter and spring seasons. This may be appreciated in the results comparing all seasons in Appendix 9.

Lower Earth Pressures Generated in Fully Drained Model Simulations																
Figure & Backfill Stiffness Value		Beginning of 2nd Cycle					Beginning of 10th Cycle					Cumulative				
		A	Sp		Su	W	A	Sp		Su	W	A	Sp		Su	W
7.17	50	√	-				√	-				√	-			
7.18	MPa				√	-				√	-				√	-
7.21	92.1	√	-				√	-				√	-			
7.22	MPa				√	-				√	-				√	-
7.25	150	√	-				√	-				√	-			
7.26	MPa				√	-				√	-				√	-
7.29	250	√	-				√	-				√	-			
7.30	MPa				√	-				√	-				√	-

Table 7.4: Summary of simulation results from the fully drained model generating lower earth pressures.

A summary of the simulation results generating lower earth pressures from modelling the season of construction and backfill soil stiffness values in the initial and fully drained models are presented in Tables 7.3 and 7.4 respectively. Two seasons are compared along the rows in adjacent columns. A tick represents the season with lower earth pressure. At the beginning of the second cycle, the result summary indicate that autumn and summer constructions predominantly develop relatively lower earth pressures when compared with winter and spring constructions due to the cyclic displacement of the model abutment. More consistency was however observed in the fully drained model result summary (Table 7.4). At the beginning of the tenth cycle, the result summary also indicate (largely due to the fully drained model) that autumn and summer construction predominantly developed relatively lower earth pressures compared with winter and spring. Through the 10 year duration modelled, the results show that cumulatively lower earth pressures were developed in the autumn and summer construction when compared with winter and spring.

These results define a pattern that suggest relatively lower earth pressures may be developed in constructions completed with the initial cumulative abutment displacement proceeding away from the backfill soil, such as may be experienced in the summer to autumn construction seasons, against constructions completed with the initial cumulative abutment displacements proceeding towards the backfill soil, such as may be experienced in the winter to spring construction seasons.

The results also show a high degree of consistency in the fully drained model with lower earth pressures in all cases simulated, developed in the autumn and summer construction against the spring and winter construction respectively. This highlights a variation in the behaviour of the backfill soil when compared with the initial model in which in 7 out of 24 cases, lower earth pressure where found to develop in the spring and winter construction against the autumn and summer construction respectively (see Table 7.3).

Results presented in Figures 7.19 – 7.20 and Appendix 7a -7b (simulations modelling 50MPa backfill soil stiffness) show a more significant effect of the fully drained model and the initial model on the earth pressures developed behind the abutment. Results presented in Appendix 7c – 7f (simulations modelling backfill soil stiffness of 92.1MPa and greater) show little effect arising from the initial or fully drained model. These results suggest that the effect of an assumption of fully drained or fully undrained fine grain soils behaviour within the foundation material may be more significant at lower stiffness values.

England et al. (2000) carried out studies evaluating the impact of construction in the winter, spring and summer seasons. While the studies by England et al. (2000) did not take into consideration the effect of the assumptions of the behaviour of fine grain soils within the foundation material, or consider the performance of construction in the autumn season, the results published showed that summer construction generated cumulatively lower maximum wall reaction ratio or Kelvin stress ratio (England et al., 2000) than winter construction.

7.8. Conclusion

Results of the study carried out to determine the impact of change in the season in which an integral bridge construction is completed, with the assumptions of fully drained or undrained fine grain soils within the foundation material, on the magnitude of earth pressure behind the abutment of an integral bridge model, was presented in this chapter. The impact of the change in the stiffness values on the performance in these circumstances was also evaluated. The average earth pressures generated from the models simulating construction within the different seasons modelling a typical United Kingdom temperature pattern, through a model time duration of 10 years, were compared.

It was found that modelling the season in which an integral bridge construction is completed affects the magnitude of earth pressure experienced within the backfill soil behind the abutment in a characteristic manner. The results suggest that integral bridges constructed in the autumn and summer seasons predominantly developed lower earth pressures than integral bridges constructed in the spring and winter seasons from the thermal induced abutment displacement. These results suggest a relationship between the earth pressure developed behind the abutment, and the initial cumulative series of abutment displacement direction. Lower earth pressures were found to develop in an initially active side abutment displacement relative to the backfill soil.

The results also show an appreciable effect on the earth pressure as a result of the assumptions of fully drained or undrained fine grain soils within the foundation material. In all simulations carried out, lower earth pressures were consistently found to develop in autumn and summer constructions against spring and winter constructions. The consistency of this event was appreciably lower where the fine grain soils within the foundation material was assumed undrained under loading. This suggests an appreciable effect on the behaviour of the backfill soil because of the assumptions. The effect of this assumption was found to be more significant at lower stiffness values.

These results indicate that the state of the integral bridge foundation soil under thermal induced loading may have an appreciable effect on the behaviour of the backfill soil performance. The stiffness of the backfill soil may influence this effect. The findings also

indicate that there are relative gains to be made where the season of construction is taken into consideration. This indicate that greater efficiency may be obtained in the performance of the integral bridge where these findings are taken into consideration within a detailed model of a proposed integral bridge, before the final design details are established and recommended for construction.

Chapter 8 : CONCLUSION

8.1. Summary

Integral bridges are generally considered to have lower construction and maintenance costs than conventional bridges for short and medium span bridges. However, the integral bridge presents challenges caused by the increased level of soil-structure interaction activity in construction and use. This arises from the limited understanding of the soil-structure interaction behaviour in response to the thermal induced lateral displacement of the abutment.

The soil-structure interaction problems primarily occur within the soil. Although the application of this concept presents challenges to engineers and academics alike, generally acceptable design or construction guidelines have not been developed. This thesis reports the findings of a parametric study carried out using the finite element method to better understand the impact of thermal load on the earth pressures behind the integral bridge abutment. The parametric study was carried out with a view to establish design guidelines based on its findings, towards a more efficient integral bridge design, construction and use.

Detailed explanation of the concept of the integral bridge was presented in this thesis. A comprehensive literature review was carried out. The literature review highlighted the increasing use of the integral bridge concept. The advantages of constructing an integral bridge and the challenges encountered through its use were discussed. Previous and ongoing research efforts to solve integral bridge problems as well as proposed solutions were presented. Literature review was carried out to gain an insight into soil behaviour applicable to the characteristic loading of the soil arising from the soil-structure interaction of the integral bridge. The literature review was also carried out to appreciate the principles and application of the finite element numerical modelling method and how they could be applied to an integral bridge.

A comprehensive integral bridge model was developed through the application of the principles of the finite element method using Plaxis 2D version 9.0. This model was developed with data obtained from an instrumented integral bridge site. The process of developing this model overcame challenges typically encountered in developing a realistic finite element integral bridge model. These challenges were solved generating results that realistically depicted the soil-structure interaction activities. This is evident in the results obtained from the model that closely matched the results obtained from the instrumented bridge site.

Parametric studies were carried out to determine the impact that changes in specific backfill soil parameters, with the assumption of a fully undrained behaviour and a fully drained behaviour within the fine grained soils in the foundation materials, have on the earth pressure developed behind the abutment of an integral bridge. The backfill soil parameters identified for evaluation included the stiffness, cohesion, friction angle, dilatancy and unit weight. The impact of change in the Poisson's ratio was also evaluated. Loading simulations defining the pattern of abutment displacement recorded on an instrumented bridge site were carried out. Secondary loading simulations defining an established cyclic loading pattern due to temperature changes were also carried out. These loading simulations were carried out varying the values of the soil parameters within the model backfill soil and varying the state of the fine grained foundation soil materials (fully undrained and fully drained) under loading. The results showed a similar pattern of behaviour in both cases (measured and cyclic abutment displacements).

Parametric studies to determine the impact of change in the season in which an integral bridge is constructed, with the assumption of a fully undrained behaviour and a fully drained behaviour, within the fine grained soils in the foundation materials, on the magnitude of earth pressure behind the abutment of the integral bridge was also carried out. The impact of the change in the stiffness values on the performance in these circumstances was evaluated. The average earth pressures generated from the models simulating construction within the different seasons using a typical United Kingdom temperature pattern were compared.

Knowledge obtained from finding solutions to the challenges of developing a realistic model of the instrumented integral bridge identified for this study, led to a greater understanding of the processes involved in developing a model integral bridge. Data generated from the parametric studies carried out on the integral bridge model developed were analysed for a greater insight into the functioning of a typical integral bridge in practical conditions. The findings of these studies were presented.

8.2. Contribution & Relevance.

Due to the cost and time implications required for the implementation and feedback of research findings in constructing and monitoring an integral bridge, the more practical solutions to the problems of developing and using integral bridges may be predominantly sought through numerical modelling approach such as used in this study. In general, this study highlights challenges of using the finite element method in modelling an integral bridge to enhance knowledge on modelling, and provides recommendations aimed at improving the integral bridge performance.

The problem of the integral bridge is complex. The concept involves relatively small displacements (when compared to the length of the bridge span) that accounts for significant changes in earth pressures. There are currently varying restrictions on bridge length from different authorities arising from these displacements. These length limits, considered safe in the opinion of the various administering authorities are determined on the basis of the perceived sensitivity of the soil-structure interaction activity to the thermal induced displacements. The length restrictions also limit the use of the bridge. However, because these small displacements determine the effect of relatively large lengths, improvements in the management of these small displacements may translate into a significant increase in the span of the bridge. The development of more efficient integral bridges will therefore benefit from the development of cumulative knowledge such as is provided in this thesis. The contributions and relevance of this study is evaluated in terms of the objectives set out.

1. Carry out a comprehensive literature review on integral bridges and integral bridge soil-structure interaction problems as it relates to the backfill and foundation soil.

	Objectives	**Objectives Accomplished**
a.	Review the concept of the integral bridge.	Concept of the integral bridge is reviewed across Chapters 1 and 2.
b.	Establish the benefit of using integral bridges.	Integral bridge advantages are established and presented in Chapters 1 and 2. Further details in Section 2.4.
c.	Identify the issues surrounding the integral bridge.	Issues surrounding the integral bridge are identified and presented in Chapter 2.
d.	Establish current practice in integral bridge design and construction.	Design and construction of the bridge structure are standardised. However, managing the soil-structure interaction is largely left to the discretion of the design engineer. Some highway authorities have recommendations but no standardised design guidelines.
e.	Establish research undertaken and the knowledge gaps.	Research areas explored are identified and presented in Section 2.8. However, the impact of the foundation soil on the backfill soil-structure interaction is not documented. Impact of excess pore pressures on the behaviour of the backfill soil, developed in the fine grained soil within the foundation material as a result of the thermal induced loading, is unknown.

Contribution & Relevance:

- This presented a greater insight into the challenges that remain as a result of the knowledge gap in the integral bridge problem.

2. Develop a comprehensive finite element model of an integral bridge using an appropriate constitutive soil model capable of generating realistic results within the backfill and foundation soil, closely modelling established backfill soil behaviour from an existing bridge.

	Objectives	**Objectives Accomplished**
a.	Review relevant soil mechanics concepts applicable in developing an integral bridge model.	Relevant soil mechanics concepts are reviewed and presented in Chapter 3.
b.	Review relevant finite element numerical modelling concepts applicable in developing the model.	Relevant finite element numerical modelling concepts are reviewed and presented in Chapter 4.
c.	Identify an appropriate constitutive soil model.	An elastoplastic soil model as constituted in Plaxis software is considered appropriate. Details are presented in Section 4.4.2.1.
d.	Identify an instrumented integral bridge with sufficient data to model the concept of the integral bridge.	An instrumented integral bridge presenting data on bridge temperature, abutment displacement, bridge dimensions, earth pressure recordings, as well as backfill and foundation soil geometry, composition and parameters are identified. Details are presented in Chapter 5.
e.	Build a finite element model of an integral bridge soil-structure interaction problem.	A comprehensive model of an instrumented integral bridge was developed in Plaxis. Details of the soil-structure interaction modelling are presented in Chapter 5.
f.	Compare the finite element model output with measured site data to validate the model's output and establish realism.	The finite element model output is compared to measured site data with closely matching results. Details are presented in Chapter 5.

Contribution & Relevance:

- It is appreciated from this study that developing a highly accurate model of an integral bridge problem involves modelling the soil-structure interaction activity

through detailed modelling of several components within the model. This requires an in-depth understanding of the relevance of the units to each other.

- Modelling an integral bridge remains a complex undertaking even with advanced finite element numerical method software. Where taking into consideration the foundation soil, the compound effect of modelling the soil-structure interaction were found to be highly sensitive, and may provide misleading results where general assumptions that tend to ignore finer details are used. With the aid of improvements in computing technology, fine details hitherto considered less significant should be incorporated in the models to improve the result's accuracy leading to more efficient structures.
- This research demonstrates that there is a measurable effect as a result of the assumptions on the state of the fine grained foundation soil materials during thermal induced loading (fully undrained or fully drained). This results in an appreciable change in the behaviour of the backfill soil. Consequently, the state of the foundation soil should be taken into consideration in the analysis during integral bridge design for greater efficiency in performance through the service life of the bridge.
- It is also appreciated that the relationship between an actual abutment displacement and the design abutment displacement exist in a ratio that may be assumed constant with a specific value for each abutment with reasonable accuracy. This may be used for long-term projection or predicting actual abutment displacements.

3. Investigate the effect of changes in the backfill soil parameters on the earth pressure developed behind the abutment, and the effect of the assumption of a fully undrained behaviour and a fully drained behaviour within the fine grained soils in the foundation materials on these changes.

	Objectives	**Objectives Accomplished**
a.	Identify relevant backfill soil parameters.	Relevant backfill soil parameters were identified in Chapter 5.

b.	Determine the backfill soil parameter range for variation.	Backfill soil parameter ranges were identified in Section 6.3.
c.	Establish simulation plan.	The simulation plan was established and presented in Section 6.4.
d.	Carryout parametric studies simulations, investigating the effect of changes in the backfill soil parameters on the earth pressure developed behind the abutment.	Parametric studies involving the integral bridge loading simulations were carried out. The results are presented in Chapter 6.
e.	Analyse results and draw conclusions.	Results of the parametric studies were analysed. The conclusions drawn from this study are presented in Sections 6.6 & 6.7.

Contribution & Relevance:

- The research demonstrates that changes in the value of any of the backfill soil parameters evaluated, affect to some extent the magnitude of earth pressure experienced within the backfill soil.
- The results indicate that the magnitude of earth pressure developed behind the abutment of an integral bridge as a result of thermal induced loading is primarily controlled by the stiffness of the backfill soil. Changes in other backfill soil parameters have a negligible impact on the earth pressure. This finding agrees with other published studies.
- The foundation soils have an appreciable effect on the earth pressure values. There is an appreciable difference in the earth pressure developed behind the abutment where the results generated from the assumption of a fully undrained behaviour in the fine grained soils within the foundation materials was compared with that of fully drained behaviour.

4. Investigate the effect of changes in the seasons of construction, with the assumption of a fully undrained behaviour and a fully drained behaviour in the fine grained soils within the foundation materials on the earth pressure developed behind the

abutment. Investigate the effect of change in the backfill soil parameters on the season changes and foundation soil assumptions.

	Objectives	**Objectives Accomplished**
a.	Establish a typical United Kingdom annual temperature pattern	A typical United Kingdom annual temperature pattern is established and presented in Section 7.2.
b.	Establish characteristics of abutment displacements in construction seasons	Characteristics of abutment displacements in construction seasons are established and presented in Chapter 7.
c.	Carryout parametric studies simulations investigating the effect of changes in the seasons of construction, with the assumption of a fully undrained behaviour and a fully drained behaviour in the fine grained soils within the foundation materials.	Parametric study simulations investigating the effect of changes in the seasons of construction with the assumption of a fully undrained behaviour and a fully drained behaviour in the fine grained soils was carried out. Details of these studies are presented in Chapter 7.
d.	Carryout parametric studies simulations investigating the effect of changes in backfill soil parameters on 4c above - changes in the seasons of construction, with the assumption of a fully undrained behaviour and a fully drained behaviour in the fine grained soils within the foundation materials.	Changes in the backfill soil stiffness parameter were found to predominantly control the magnitude of earth pressure developed behind the abutment. Effects of changes in other backfill soil parameters were found to be negligible. Details of these findings are presented in Chapter 6. Consequently, parametric study simulations investigating the effect of changes in the backfill soil stiffness parameter, and changes in the seasons of construction with the assumption of a fully undrained behaviour and a fully drained behaviour in the fine grained soils was carried out. Details of these studies are presented in Chapter 7.
e.	Analyse results and draw conclusions	Results of these parametric studies were analysed. The conclusions are presented in Sections 7.7 & 7.8.

Contribution & Relevance:

- It was found that modelling the season in which an integral bridge construction is completed, affects the magnitude of earth pressure experienced within the backfill soil behind the abutment. The results show that modelling integral bridges constructed in the autumn and summer seasons predominantly developed lower earth pressures behind the abutment than modelling integral bridges constructed in the spring and winter seasons.
- The results also show that modelling the behaviour of fine grained soils within the foundation materials as either fully undrained or fully drained have an appreciable effect on the behaviour of the backfill material and the earth pressure developed behind the abutment.
- The effect of the assumption of a fully undrained behaviour and a fully drained behaviour in the fine grained soils was found to be more significant during the seasons of construction at lower stiffness values. This indicates that the lower the stiffness of the backfill the greater impact there is on the earth pressures regardless of the pore pressure development in the foundation soils.

5. Design recommendations for integral bridge designs.

Recommendations:

- Fine details generally considered insignificant, have an appreciable effect on the behaviour of the integral bridge model as a result of the complex soil-structure interaction. This research demonstrated that the continuum properties of the finite element method on the load distribution within the backfill soil had an appreciable effect on the earth pressure results generated. It is now possible to consider these details and not use general assumptions. These assumptions can be misleading and may not lead to gains in efficiency in integral bridge design and construction.
- Optimum efficiency in the service of the bridge may not be achieved with separate analysis for the backfill soil and the structures. The inter relationship between the structure and the foundation soil has a significant effect on the earth pressure developed in the backfill soil. Consequently, simultaneous analysis of the effects of

the structure, backfill soil and foundation soil on each other should be carried out for better clarity on the soil-structure interaction performance and improved efficiency.

- An assumption of a fully undrained behaviour and a fully drained behaviour in the fine grained soils within the foundation materials has an appreciable effect on the earth pressure developed behind the backfill soil. The state of the backfill soil with respect to these assumptions should be taken into account in the analysis involving the foundation soil to enhance the efficiency of the design.
- The stiffness property of the backfill soil is predominantly responsible for the magnitude of earth pressure developed behind the abutment. Consequently, this property should be prominent in considerations towards enhancing the efficiency of the integral bridge design as it may be manipulated in construction.
- Analyses involving the season of construction have shown that cumulatively, relatively lower earth pressure may be achieved by construction in certain seasons against others. This study shows that modelling construction in autumn and summer seasons develop relatively lower earth pressures than modelling construction in spring and winter. This analysis should be taken into consideration for enhanced efficiency in integral bridge design.

8.3. Future Research Suggestions

This research originated from the problems caused by the soil-structure interaction activity of the integral bridge, and addressed only a fraction of it. There was a limitation on available resources to facilitate a more elaborate approach to this study. However, while this research appears conclusive in its findings within its limitations, several other possibilities are observed with unanswered questions and may be further explored in future research efforts.

Primarily, there is limited information available on integral bridge performance. This limits the ability to conduct research on integral bridges. There is also limited available information on integral bridge construction materials. A better appreciation of the practical

soil-structure interaction behaviour currently requires long-term instrumentation of bridges for more reliable field data. The development of accurate models for research is based on information obtained from the field data. New knowledge is obtained from the models, and the application of the new knowledge is implemented on newly constructed bridges with the performance monitored through bridge instrumentation. It is therefore suggested that more bridges are instrumented for data collection. This instrumentation affords better research values where the backfill and foundation soil parameters are concurrently documented. Results obtained may also be analysed with a view to establishing a possible correlation of performance between the backfill and foundation soil.

The findings of this research establish new considerations in the design and construction of integral bridges. While the integral bridge model developed using Plaxis software generated realistic earth pressure results from abutment displacements, this study was dependent on one integral bridge model developed from an instrumented bridge. As a result of the resources and data limitations, these findings were not explored in other models. This implies that the findings may be case specific. Consequently, further research on these findings may be carried out with the following variations.

- Using other numerical model integral bridge with different material and geometric parameters for the bridge structure, foundation soils and backfill soil.
- Through a dynamic analysis of the thermal effect on the bridge structure over an extended time period.
- Developing a comprehensive laboratory model for the analysis.
- Using new numerical modelling concepts that involves coupling numerical methods such as the finite element method (FEM) and the discrete element method (DEM) to more accurately model the detailed behaviour of the granular backfill soil, currently evaluated under the general assumption of a continuum in the finite element approach used in this study (Villard et al., 2009b, Yan et al., 2010).

REFERENCES

ABAQUS 2000. *ABAQUS/Standard User's Manual, Volume II, Version 6.1,* Pawtucket, Hibbitt, Karlsson & Sorensen, Inc.

ABENDROTH, R. E. & GREIMANN, L. F. 2005. Field testing of integral abutments." Final Rep. No. HR-399, Iowa State Univ., Iowa Dept. of Transportation, Ames, Ia.

ABUSHARAR, S. W., ZHENG, J.-J. & CHEN, B.-G. 2009. Finite Element Modeling of the Construction Behavior of Multi-Column Supported Road Embankment. *Computer and Geotechnics,* 36**,** 676-685.

ALAMPALLI, S. & YANNOTTI, A. P. 1998. In-Service Performance of Integral Bridges and Jointless Decks. *Transportation Research Record: Journal of the Transportation Research Board,* Vol. 1624.

ANANDARAJAH, A. 2010. *Computational Methods in Elasticity and Plasticity: Solids and Porous Media,* New York, Springer.

ARDUINO, P. & MACARI, E. J. 1998. Numerical modeling of spread footings at bridge-embankment interfaces. *Liquefaction, Differential Settlement, and Foundation Engineering***,** 61-67.

AROCKIASAMY, M., BUTRIENG, N. & SIVAJUMAR, M. 2004. State-of-the-Art of Integral Abutment Bridges: Design and Practice. *JOURNAL OF BRIDGE ENGINEERING,* 9**,** 497-506.

AROCKIASAMY, M. & SIVAJUMAR, M. 2005. Time-Dependent Behavior of Continuous Composite Integral Abutment Bridges. *Practical Periodical on Structural Design and Construction,* 10**,** 161-170.

ARSOY, S. 2004. Mobilization of Passive Earth Pressure Behind Abutments of Jointless Bridges. *Transportation Research Record: Journal of the Transportation Research Board,* 1868**,** 199-204.

ARSOY, S. 2008. Proposed Mathematical Model for Daily and Seasonal Thermal Bridge Displacements. *Transportation Research Record: Journal of the Transportation Research Board,* 2050**,** 3-12.

ARSOY, S., BARKER, R. M. & DUNCAN, J. M. 1999. The Behavior of Integral Abutment Bridges. Charlottesville: Virginia Transportation Research Council.

ARSOY, S., DUNCAN, J. M. & BAKER, R. M. 2002. Performance of Piles Supporting Integral Bridges. *Transportation Research Record: Journal of the Transportation Research Board,* 1808**,** 162-167.

ARSOY, S., DUNCAN, J. M. & BARKER, R. M. 2004. Behavior of a Semiintegral Bridge Abutment under Static and Temperature-Induced Cyclic Loading. *Journal of Bridge Engineering,* 9**,** 193-199.

ATKINSON, J. 2007. *The Mechanics of Soil and Foundations,* London, Taylor & Francis.

ATKINSON, J. H. & BRANSBY, P. L. 1978. *The Mechanics of Soil; An Introduction to Critical State Soil Mechanics,* Berkshire, McGraw-Hill.

ATKINSON, J. H., EVANS, J. S. & RICHARDSON, D. 1986. Effects of Stress Path and Stress History on the Stiffness of Reconstituted London Clay. *Engineering Geology Special Publications,* 2**,** 139-144.

ATKINSON, J. H. & SALLFORS, G. 1991. Experimental determination of soil properties. *In Proc. 10th ECSMFE.* Florence.

BA42/96 2003. The Highways Agency, The Design of Integral Bridges; BA 42/96, Amendment No. 1. *Design Manual for Roads and Bridges (DMRB).* UK: Department for Transport.

BAKKER, K. J., BEZUIJEN, A., BROERE, W. & KWAST, E. A. (eds.) 2006. *Geotechnical Aspect of Underground Construction in Soft Ground,* London: Taylor & Francis/Balkema.

BARKER, K. J. & CARDER, D. R. 2000. Performance of the two integral bridges forming the A62 Manchester road overbridge. *TRL Rep. 436.* Crowthorne, Berkshire: Transport Research Laboratory.

BARKER, K. J. & CARDER, D. R. 2001. Performance of an integral bridge over the M1-A1 link road at bramham crossroads. *TRL Rep. 521.* Crowthorne, Berkshire: Transport Research Laboratory.

BARR, P., STANTON, J. & EBERHARD, M. 2005. Effects of Temperature Variations on Precast, Prestressed Concrete Bridge Girders. *Journal of Bridge Engineering,* 10**,** 186-194.

BD30/87 1987. The Highways Agency, Backfilled Retaining Walls and Bridge Abutments; Vol. 2, Sec. 1. (Part 5 - BD30/87). *Design Manual for Roads and Bridges (DMRB).* UK: Department For Transport.

BD37/01 2001. The Highways Agency, Loads for Highway Bridges; Vol.1; Sec.3, (BD37/01). *Design Manual for Roads and Bridges (DMRB).* UK: Department For Transport.

BD57/01 2001. The Highways Agency, Design for Durability (BD57/01). *Design Manual for Roads and Bridges (DMRB).* UK: Department For Transport.

BELL, F. G. 2000. *Engineering Properties of Soil and Rock,* London, Blackwell Science Ltd.

BLOODWORTH, A. G., XU, M., BANKS, J. R. & CLAYTON, C. R. I. 2012. Predicting the earth pressure on integral bridge abutments. *Journal of Bridge Engineering,* 17**,** 371-381.

BOLTON, M. D. 1986. STRENGTH AND DILATANCY OF SANDS. *Geotechnique,* 36**,** 65-78.

BOLTON, M. D. & STEEDMAN, R. S. CENTRIFUGAL TESTING OF MICROCONCRETE RETAINING WALLS SUBJECTED TO BASE SHAKING. Soil Dynamics & Earthquake Engineering, Proceedings of the Conference., 1982 Southampton, Engl. A. A. Balkema, 311-329.

BOULON, M. & NOVA, R. 1990. Modelling of soil-structure interface behaviour a comparison between elastoplastic and rate type laws. *Computers and Geotechnics,* 9**,** 21-46.

BOWLES, J. E. 1984. *Physical and Geotechnical Properties of Soil,* New York, McGraw-Hill

BOWLES, J. E. 1997. *Foundation Analysis and Design,* New YorK, McGraw-Hill.

BRIAUD, J. L., JAMES, R. W. & HOFFMANN, S. B. 1997. NCHRP Synthesis of Highway Practice 234; Settlement of Bridge Approaches- The Bump at the End of the Bridge. *TRB, National Research Council.* Washington, D. C.

BRINKGRENE, R. B. J., BROERE, W. & WATERMAN, D. (eds.) 2008. *General Information, PLAXIS 2D-Version 9.0 Manual,* Netherlands: PLAXIS bv.

BRITTO, A. M. & GUNN, M. J. 1987. *Critical state soil mechanics viafinite elements,* Chichester, Ellis Horwood.

BURKE, M. P. 1996. An introduction to the design and construction ofintegral bridges. *Workshop on Integral abutment bridges.* Pittsburgh, PA.

BURKE, M. P. 2009. *Integral and Semi-integral Bridges,* West Sussex, Wiley-Blackwell.

BURLAND, J. B. 1987. Nash Lecture: The Teaching of Soil Mechanics - a Personal View. *9th ECSMFE.* Dublin.

CARD, G. B. & CARDER, D. R. 1993. Literature Review of the Geotechnical Aspects of the Design of Integral Bridge Abutments. *TRL Report; 52.* Crowthorne: Transport Research Laboratory.

CARDER, D. R. & CARD, G. B. 1997. Innovative Structural Backfills to Integral Bridge Abutments. *TRL Report; 290.* Crowthorne: Transport Research Laboratory.

CARDER, D. R., DARLEY, P. & BUSH, D. I. 2002. Specification for Suitability Testing of Stress Absorbing Materials behind Integral Bridge Abutments. *TRL Report; 553.* Crowthorne: Transportation Research Labouratory.

CARDER, D. R. & HAYES, J. P. 2000. Performance under Cyclic Loading of the Foundations of Integral Bridges. *TRL Report; 433.* Crowthorne: Transport Research Laboratory.

CHANG, M. F. 1997. Lateral earth pressures behind rotating walls. *Canadian Geotechnical Journal,* 34**,** 498-509.

CHARLES, W. W., SPRINGMAN, S. M. & NORRISH, A. R. M. 1998. Centriruge Modeling of Spread-Base Integral Bridge Abutments. *Journal of Geotechnical and Geoenvironmental Engineering***,** 376-388.

CHEN, F., DRUMM, E. C. & GUIOCHON, G. 2011. Coupled discrete element and finite volume solution of two classical soil mechanics problems. *Computers and Geotechnics,* 38**,** 638-647.

CHEN, W.-F. & DUAN, L. (eds.) 2000. *Bridge Engineering Handbook,* London: CRC Press LLC.

CHOU, W.-I. & BOBET, A. 2002. Predictions of Ground Deformations in Shallow Tunnels in Clay. *Tunneling and Underground Space Technology,* 17**,** 3-19.

CIVJAN, S. A., BONCZAR, C., BRENA, S. F., DEJONG, J. & CROVO, D. 2007. Integral Abutment Bridge Behavior: Parametric Analysis of a Massachusetts Bridge. *JOURNAL OF BRIDGE ENGINEERING,* 12**,** 64-71.

CLAYTON, C. R. I., XU, M. & BLOODWORTH, A. 2006. A Laboratory Study of the Development of Earth Pressure Behind Integral Bridge Abutments. *Geotechnique,* 58**,** 561-571.

COLE, R. T. & ROLLINS, K. M. 2006. Passive Earth Pressure Mobilization during Cyclic Loading. *Journal of Geotechnical and Geoenvironmental Engineering,* 132**,** 1154-1164.

COLLINS, I. F. 2005. Elastic/plastic models for soils and sands. *International Journal of Mechanical Sciences,* 47**,** 493-508.

CRAIG, R. F. 2004. *Craig's Soil Mechanics,* London, Spon Press.

CUI, K. & ZHOU, Q. 2009. A new processing method for modelling the vertical stress distribution at the soil surface. *International Conference on Information Engineering and Computer Science. ICIECS*

CUNDALL, P. A. & STRACK, O. D. L. 1979. A discrete numerical model for granular assemblies. *Geotechnique,* 29**,** 47-65.

DARLEY, P., CARDER, D. R. & ALDERMAN, G. H. 1996. Seasonal Thermal Effects on the Shallow Abutment of an Integral Bridge in Glasgow. *TRL Report; 178.* Crowthorne: Transport Research Laboratory.

DARLEY, P., CARDER, D. R. & BARKER, K. J. 1998. Seasonal Thermal Effects over Three Years on the Shallow Abutment of an Integral Bridge in Glasgow. *TRL Report; 344.* Crowthorne: Transport Research Laboratory.

DAS, B. M. 2008. *Advanced soil mechanics,* London ; New York, Taylor & Francis.

DAVIDS, W. G., SANDFORD, T., ASHLEY, S., DELANO, J. & LYONS, C. 2010. Field-Measured Response of an Integral Abutment Bridge with Short Steel H-Piles. *JOURNAL OF BRIDGE ENGINEERING,* 15**,** 32-43.

DAVIS, E. H. & POULOS, H. G. 1968. The use of elastic theory for settlement prediction under three dimensional conditions. *Geotechnique,* 18**,** 67-91.

DE JOSSELIN DE JONG, G. 1976. ROWE'S STRESS-DILATANCY RELATION BASED ON FRICTION. *Geotechnique,* 26**,** 527-534.

DEMIR, A., ORNEK, M., LAMAN, M., YILDIZ, A. & MISIR, G. 2009. Model studies of circular foundations on soft soils. *Geotechnics of Soft Soils***,** 219-226.

DESAI, C. S. & ABEL, J. F. 1972. *Introduction to the Finite Element Method,* New York, Van Nostrand Reinhold Company.

DESAI, C. S. & CHRISTIAN, J. T. (eds.) 1977. *Numerical Methods in Geotechnical Engineering,* New York: McGraw-Hill.

DICLELI, M. 2000a. A Rational Design Approach for Prestressed-Concrete-Girder Integral Bridge. *Engineering Structures,* 22**,** 230-245.

DICLELI, M. 2000b. Simplified model for computer-aided analysis of integral bridges. *Journal of Bridge Engineering,* 5**,** 240-248.

DICLELI, M. 2005. Integral Abutment-Backfill Behaviour on Sand Soil-Pushover Analysis Approach. *JOURNAL OF BRIDGE ENGINEERING,* 10**,** 354-364.

DICLELI, M. & ALBHAISI, S. M. 2004a. Effect of cyclic thermal loading on the performance of steel H-piles in integral bridges with stub-abutments. *Journal of Constructional Steel Research,* 60**,** 161-182.

DICLELI, M. & ALBHAISI, S. M. 2004b. Estimation of Length Limits for Integral Bridges Built on Clay. *JOURNAL OF BRIDGE ENGINEERING,* 9**,** 572-581.

DICLELI, M. & ALBHAISI, S. M. 2004c. Performance of Abutment-Backfill System under Thermal Variation in Integral Bridges Built on Clay. *Engineering Structures,* 26**,** 949-962.

DICLELI, M. & ALBHAISI, S. M. 2005. Analytical formulation of maximum length limits of integral bridges on cohesive soils. *Canadian Journal of Civil Engineering,* 32**,** 726-38.

DICLELI, M. & ERHAN, S. 2008. Effect of Soil and Substructure Properties on Live-Load Distribution in Integral Abutment Bridges. *Journal of Bridge Engineering,* Vol. 13.

DICLELI, M. & ERHAN, S. 2010. Effect of Soil-Bridge Interaction on the Magnitude of Internal Forces in Integral Abutment Bridge Components due to Live Load Effects. *Engineering Structures,* 32**,** 129-145.

DRUCKER, D. C. & PRAGER, W. 1952. Soil mechanics and plastic analysis or limit design. *Quarterly of Applied mathematics,* 10.

DUNCAN, J. & MOKWA, R. 2001. Passive Earth Pressures: Theories and Tests. *JOURNAL OF GEOTECHNICAL AND GEOENVIRONMENTAL ENGINEERING,* 127**,** 248-257.

DUNCAN, J. M. & CHANG, C. Y. 1970. Nonlinear Analysis of Stress and Strain in Soil. *ASCE Journal of the Soil Mechanics and Foundations Div.,* 96**,** 1629-1653.

DUTTA, S. C. & ROY, R. 2002. A critical review on idealization and modeling for interaction among soil-foundation-structure system. *Computers & Structures,* 80**,** 1579-94.

ENGLAND, G. L. & DUNSTAN, T. Shakedown Solutions for Soil Containing Structures as Influenced by Cyclic Temperatures - Integral Bridge and Biological Filter. 3rd International Conference on Structural Engineering, 1994 Singapore.

ENGLAND, G. L., TSANG, N. C. M. & BUSH, D. I. 2000. *Integral Bridges; A fundamantal approach to the time-temperature loading problem,* London, Thomas Telford.

ERKEN, A. & ULKER, B. M. C. 2007. Effect of Cyclic Loading on Monotonic Shear Strength of Fine-Grained Soils. *Engineering Geology,* 89**,** 243-257.

FANG, Q., TSUCHIYA, T. & YAMAMOTO, T. 2002. Finite difference, finite element and finite volume methods applied to two-point boundary value problems. *Journal of Computational and Applied Mathematics,* 139**,** 9-19.

FARAJI, S., TING, J. M., CROVO, D. S. & ERNST, H. 2001. Nonlinear Analysis of Integral Bridges: Finite-Element model. *Journal of Geotechnical and Geoenvironmental Engineering,* Vol. 127.

FENNEMA, J. L., LAMAN, J. A. & LINZELL, D. G. 2005. Predicted and Measured Response of an Integral Abutment Bridge. *Journal of Bridge Engineering,* 10**,** 666-677.

FMI. 2012. *Weather Observations in Finland* [Online]. Finnish Meteorological Institute, Ministry of Transport and Communications. Available: http://en.ilmatieteenlaitos.fi/observations-in-finland 2012].

FORD, A. 1999. *Modeling the Environment: An Introduction to System Dynamics Models of Environmental Systems,* Washington D.C., Island Press.

GANGARAO, H., THIPPESWAMY, H., DICKSON, B. & FRANCO, J. 1996. Survey and design of integral abutment bridges. *Workshop on Integral abutment bridges,.* Pittsburgh, PA.

GIRTON, D. D., HAWKINSON, T. R. & GREIMANN, L. F. 1991a. Validation of Design Recommendations for Integral-Abutment Piles. *Journal of Structural Engineering,* 117**,** 2117-2134.

GIRTON, D. D., HAWKINSON, T. R. & GREIMANN, L. F. 1991b. Validation of design recommendations for integral-abutment piles. *Journal of structural engineering New York, N.Y.,* 117**,** 2117-2134.

GLANVILLE, W. H., CLARE, K. E., CRONEY, D., DAVIS, E. H. & LEWIS, W. A. 1952. *Road Research Laboratory; Soil Mechanics for Road Engineers,* London, H.M.S.O.

GOEL, R. K. 1997. Earthquake characteristics of bridges with integral abutments. *Journal of structural engineering New York, N.Y.,* 123**,** 1435-1443.

GONG, X. L. & ZHAO, J. 2009. Numerical Simulating of Layered Buried Embankment Based On PLAXIS. *Icicta: 2009 Second International Conference on Intelligent Computation Technology and Automation, Vol Ii, Proceedings***,** 128-131.

GREENBERGER, M., CRENSON, M. & CRISSEY, B. 1976. *Models in the policy process,* New York, Russell Sage Foundation.

GREIMANN, L. F., WOLDE-TINSAAE, A. M. & YANG, P. S. 1983. Transportation Research Record 903: Skewed bridges with integral abutments. Washington D.C.: National Research Council.

HAMMOURI, N. A., MALKAWI, A. I. H. & YAMIN, M. M. A. 2008. Stability analysis of slopes using the finite element method and limiting equilibrium approach. *Bulletin of Engineering Geology and the Environment,* 67**,** 471-478.

HAZIRBABA, K. & RATHJE, E. M. 2009. Pore pressure generation of silty sands due to induced cyclic shear strains. *JOURNAL OF GEOTECHNICAL AND GEOENVIRONMENTAL ENGINEERING,* 135**,** 1892-1905.

HAZIRBABA, K., ZHANG, Y. & LEROY HULSEY, J. 2011. Evaluation of temperature and freeze-thaw effects on excess pore pressure generation of fine-grained soils. *Soil Dynamics and Earthquake Engineering,* 31**,** 372-384.

HILL, R. 1958. *The mathematical theory of plasticity* New York, Oxford University Press.

HOEK, E. 1990. Estimating Mohr-Coulomb friction and cohesion values from the Hoek-Brown failure criterion. *International journal of rock mechanics and mining sciences & geomechanics abstracts,* 27**,** 227-229.

HOEK, E. & BROWN, E. T. 1980. EMPIRICAL STRENGTH CRITERION FOR ROCK MASSES. *Journal of the Geotechnical Engineering Division,* 106**,** 1013-1035.

HOPPE, E. J. & GOMEZ, J. P. 1996. Field study of an integral backwall bridge. *Virginia Transportation Research Council.*

HORVATH, J. S. 2000. Integral-Abutment Bridges: Problems and Innovative Solutions Using EPS Geofoam and Other Geosynthetics. *Manhattan College Research Report No. CE/GE-00-2.* New York, USA: Manhattan College.

HORVATH, J. S. 2005. Integral - Abutment Bridges: Geotechnical Problems and Solutions Using Geosynthetics and Ground Improvement. *The 2005 FHwA Conference on Integral Abutment and Jointless Bridges.* Baltimore, USA.

HOWARD, I. L. & WARREN, K. A. 2009. Finite-Element Modeling of Instrumented Flexible Pavements under Stationary Transient Loading. *Journal of Transportation Engineering-Asce,* 135**,** 53-61.

HUANG, J., SHIELD, C. K. & FRENCH, C. 2005. Time-Dependent Behavior of a Concrete Integral Abutment Bridge. *Transportation Research Record: Journal of the Transportation Research Board,* CD 11-S**,** 299-309.

HUANG, J., SHIELD, C. K. & FRENCH, C. 2008. Parametric Study of Concrete Integral Abutment Bridge. *JOURNAL OF BRIDGE ENGINEERING,* 13**,** 511-526.

ILES, D. C. Integral Bridges in United Kingdom. International Workshop on the Bridges with Integral Abutmants, 2006 Lulea, Sweden. Lulea University of Technology, 13-24.

JARDINE, R. J., POTTS, D. M., FOURIE, A. B. & BURLAND, J. B. 1986. Studies of the influence of non-linear stress-strain characteristics in soil-structure interaction. *Geotechnique,* 36**,** 377-396.

JOHNSON, I. D. (ed.) 1994. *Performance of Deck Expansion Joints,* London: E & FN Spon.

KALALA, J. T. & MOYS, M. H. 2004. Discrete element method modelling of liner wear in dry ball milling. School of Process and Materials Engineering, University of the Witwatersrand, Johannesburg.

KAMEL, M. R., BENAK, J. V., TADROS, M. K. & JAMSHIDI, M. 1996. Prestressed concrete piles in jointless bridges. *PCI Journal,* 41**,** 56-67.

KANG, J., PARKER, F., KANG, Y. J. & YOO, C. H. 2008. Effects of Frictional Forces Acting on Sidewalls of Buried Box Culverts. *International Journal for Numerical and Analytical Methods in Geomechanics,* 32**,** 289-306.

KATSIKADELIS, J. T. & NERANTZAKI, M. S. 1999. The boundary element method for nonlinear problems. *Engineering Analysis with Boundary Elements,* 23**,** 365-373.

KELLN, C., SHARMA, J., HUGHES, D. & GRAHAM, J. 2008. An improved elastic-viscoplastic soil model. *Canadian Geotechnical Journal,* 45**,** 1356-1376.

KEROKOSKI, O. 2006. *Soil-Structure Interaction of Long Jointless Bridges with Integral Abutments.* Doctor of Technology, Tampere University of Technology.

KEROKOSKI, O. & LAAKSONEN, A. Soil-Structure Interaction of Jointless Bridges. FHWA CONFERENCE; Integral Abutment and Jointless Bridges 2005 Baltimore, Maryland

KHAN, M. A. Modeling and seismic analysis of integral abutments. Proceedings of the 2004 Structures Congress - Building on the Past: Securing the Future, May 22, 2004 - May 26, 2004, 2004 Nashville, TN, United states. American Society of Civil Engineers, 1275-1283.

KHODAIR, Y. A. & HASSIOTIS, S. 2005. Analysis of Soil-Pile Interaction in Integral Abutment. *Computer and Geotechnics,* 32**,** 201-209.

KIM, W. & LAMAN, J. A. 2010. Integral Abutment Bridge Response Under Thermal Loading. *Engineering Structures,* 32**,** 1495-1508.

KIM, W. & LAMAN, J. A. 2012. Seven-Year Field Monitoring of Four Integral Abutment Bridges. *Journal of Performance of Constructed Facilities,* 26**,** 54-64.

KLEIN TANK, A. M. G., WIJNGAARD, J. B., KONNEN, G. P., BOHM, R., DEMAREE, G., GOCHEVA, A., MILETA, M., PASHIARDIS, S., HEJKRLIK, L., KERN-HANSEN, C., HEINO, R., BESSEMOULIN, P., MULLER-WESTERMEIER, G., TZANAKOU, M., SZALAI, S., PALSDOTTIR, T., FITZGERALD, D., RUBIN, S., CAPALDO, M., MAUGERI, M., LEITASS, A., BUKANTIS, A., ABERFELD, R., VAN ENGELEN, A. F. V., FORLAND, E., MIETUS, M., COELHO, F., MARES, C., RAZUVAEV, V., NIEPLOVA, E., CEGNAR, T., LOPEZ, J. A., DAHLSTROM, B., MOBERG, A., KIRCHHOFER, W., CEYLAN, A., PACHALIUK, O. & ALEXANDER, L. V. 2002. Daily dataset of 20th-century surface air temperature and precipitation series for the European Climate Assessment. *International Journal of Climatology,* 22**,** 1441-53.

KNICKERBOCKER, D., BASU, P. K. & WASSERMAN, E. P. Behavior of two-span integral bridges unsymmetrical about the pier line. Proc., 2005 FHWA Conf., Integral Abutment and Jointless Bridges (IAJB 2005), 2005 Washington, D.C., 244–253.

KNICKERBOCKER, D. J., BASU, P. K., HOLLORAN, M. A. & WASSERMAN, E. P. 2003. Recent experience with high-performance concrete jointless bridges in Tennessee. *Design of Structures 2003***,** 104-114.

KONDNER, R. 1963. Hyperbolic stress-strain response: cohesive soils. *Proceedings of the Journal of Soil Mechanics and Foundation Division (ASCE),* 98**,** 115-143.

KUMAR, J. & RAO, K. S. S. 1997. Passive pressure coefficients, critical failure surface and its kinematic admissibility. *Geotechnique,* 47**,** 185-192.

KUMAR, P. 1998. Shear failure envelope of Hoek-Brown criterion for rockmass. *Tunnelling and Underground Space Technology,* 13**,** 453-458.

KUNIN, J. & ALAMPALLI, S. 2000. Integral Abutment Bridges: Current Practice in United States and Canada. *Journal of Performance of Constructed Facilities,* 14**,** 104-111.

LABUZ, J. F. & ZANG, A. 2012. Mohr-Coulomb Failure Criterion. *Rock Mechanics and Rock Engineering,* 45**,** 975-9.

LAMBE, T. W. 1964. Methods of estimating settlement. *Proc. Am. Socy. Civil Engrs,* Vol. 90 (SM5)**,** 42-67.

LAWVER, A., FRENCH, C. & SHIELD, C. K. 2000. Field Performance of Intergal Bridge. *Transportation Research Record: Journal of the Transportation Research Board,* 1740**,** 108-117.

LEHANE, B. M., KEOGH, D. L. & O'BRIEN, E. J. 1999. Simplified Elastic Model for Restraining Effects of Backfill Soil on Integral Bridges. *Computer and Structures,* 73**,** 303-313.

LEONG, E. C., CAHYADI, J. & RAHARDJO, H. Stiffness of a compacted residual soil. 4th International Conference on Unsaturated Soils, April 2, 2006 - April 5, 2006, 2006 Carefree, AZ, United states. American Society of Civil Engineers, 1168-1180.

LEVEQUE, R. J. 2002. *Finite Volume Methods for Hyperbolic Problems,* New York, Cambridge University Press.

LOVISA, J., SHUKLA, S. K. & SIVAKUGAN, N. 2010. Behaviour of prestressed geotextile-reinforced sand bed supporting a loaded circular footing. *Geotextiles and Geomembranes,* 28**,** 23-32.

MAGNIER, S. A. & DONZE, F. V. 1998. Numerical simulation of impacts using a discrete element method. *Mechanics of Cohesive-Frictional Materials,* 3**,** 257-276.

MARFURT, K. J. 1984. Accuracy of finite-difference and finite-element modelling of the scalar and elastic wave equation. *Geophysics,* 49**,** 533-549.

MARURI, R. F. & PETRO, S. H. 2005. Integral Abutment and Jointless Bridges (IAJB) 2004 Survey Summary. *FHWA Conference on Integral Abutment and Jointless Bridges.* Washington, D. C.: Federal Highway Administration.

MATTIUSSI, C. 1997. An Analysis of Finite Volume, Finite Element, and Finite Difference Methods Using Some Concepts from Algebraic Topology. *Journal of Computational Physics,* 133**,** 289-309.

MCNALLY, G. H. 1998. *Soil and Rock Construction Materials,* London, Taylor & Francis.

MET.OFFICE. 2012. *Weather Extremes* [Online]. Available: http://www.metoffice.gov.uk/climate/uk/extremes/ [Accessed 22 JULY 2012].

MINDESS, S., YOUNG, J. F. & DARWIN, D. 2002. *Concrete,* London, Prentice Hall,.

MITCHELL, J. K. & SOGA, K. 2005. *Fundamentals of Soil Behavior,* Hoboken, John Wiley & Sons, Inc.

MODONI, G., KOSEKI, J. & DAN, L. Q. A. 2010. Cyclic stress-strain response of compacted gravel. *Geotechnique,* 61**,** 473-85.

MOHAMMADI, S. 2003. *Discontinuum Mechanics; Using Finite and Discrete Element,* USA, WIT Press.

MOHR, O. 1900. The relation of the elastic limit to the rupture of a material

Welche Umstande Bedingen die Elastizitatsgrenze und den Bruch eines Materiales? *Zeitschrift des Vereines Deutscher Ingenieure*.

MONTGOMERY, D. C. & RUNGER, G. C. 2007. *Applied Statistics and Probability for Engineers*, John Wiley & Sons, Inc.

MONTGOMERY, D. C., RUNGER, G. C. & HUBELE, N. F. 2007. *Engineering Statistics*, John Wiley & Sons, Inc.

MONTORO, M. A. & FRANCISCA, F. M. 2010. Soil Permeability Controlled by Particle-fluid Interaction. *Geotechnical and Geological Engineering,* 28**,** 851-64.

MOORTY, S. & ROEDER, C. 1992. Temperature-Dependent Bridge Movements. *Journal of Structural Engineering,* 118**,** 1090-1105.

MUNJIZA, A. 2004. *The combined finite-discrete element method,* West Sussex, Wiley.

MURTHY, V. N. S. 2003. *Geotechnical Engineering: Principles and Practices of Soil Mechanics and Foundation Engineering,* New York, Marcel Dekker, Inc.

NADAI, A. 1950. *Theory of flow and fracture of solids,* New York, NY, United States, McGraw-Hill Book Co.

NAGTEGAAL, J. C., PARKS, D. M. & RICE, J. R. 1974. On numerically accurate finite element solutions in the fully plastic range. *Computer Methods in Applied Mechanics and Engineering,* 4**,** 153-77.

NAYLOR, D. J. 1974. Stresses in Nearly Incompressible Materials by Finite Elements with Application to the Calculation of Excess Pore Water Pressure. *International Journal for Numerical Methods in Engineering,* 8**,** 443-460.

NEVILLE, A. M. 1995. *Properties of concrete,* Harlow, Longman Scientific & Technical.

NEVILLE, A. M. & BROOKS, J. J. 1987. *Concrete Technology,* Harlow, Longman Scientific & Technical.

NG, C. W. W., SPRINGMAN, S. M. & NORRISH, A. R. M. 1998. Centrifuge modeling of spread-base integral bridge abutments. *JOURNAL OF GEOTECHNICAL AND GEOENVIRONMENTAL ENGINEERING,* 124**,** 376-388.

NICHOLSON, B. A. (ed.) 1994. *Effect of Temperature, Shrinkage and Creep on Integral Bridges,* London: E & FN Spon.

NILSSON, M. 2008. *Evaluation of In-situ Measurements of Composite Bridge with Integral Abutments.* Luleå University of Technology.

OOI, P. S. K., LIN, X. & HAMADA, H. S. 2010a. Field Behaviour of an Integral Abutment Bridge Supported on Drilled Shafts. *JOURNAL OF BRIDGE ENGINEERING,* 15**,** 4-18.

OOI, P. S. K., LIN, X. B. & HAMADA, H. S. 2010b. Numerical Study of an Integral Abutment Bridge Supported on Drilled Shafts. *JOURNAL OF BRIDGE ENGINEERING,* 15**,** 19-31.

PANDE, G. N. & ZIENKIEWICZ, O. C. 1982. *Soil Mechanics - Transient and Cyclic Loads,* Chichester, John Wiley & Sons.

PARASCHOS, A. & AMDE, A. M. 2011. *A survey on the status of use, problems, and costs associated with Integral Abutment Bridges* [Online]. Randall Reilly. Available: http://www.betterroads.com/integral-abutment-bridges/ [Accessed 30th Nov. 2012].

PARSONS, A. W. 1992. *Compaction of soils and granular materials : a review of research performed at the Transport Research Laboratory,* London, HMSO.

PAUL, M., LAMAN, J. A. & LINZELL, D. G. Thermally induced superstructure stresses in prestressed girder integral abutment bridges. Transportation Research Board - 6th International Bridge Engineering Conference: Reliability, Security, and Sustainability in Bridge Engineering, July 17, 2005 - July 20, 2005, 2005 Boston, MA, United states. Transportation Research Board, 287-297.

PEIRO, J. & SHERWIN, S. 2005. Handbook of Materials Modeling. Volume 1. *In:* YIP, S. (ed.). Springer.

PETURSSON, H., COLLIN, P., MILAN, V. & JORGEN, A. 2011. Monitoring of a swedish integral abutment bridge. *Structural Engineering International: Journal of the International Association for Bridge and Structural Engineering (IABSE),* 21**,** 175-180.

PLAXIS. 2010a. *Plaxis 2D Material Models Manual Version 9.0* [Online]. Available: http://www.plaxis.com.

PLAXIS. 2010b. *Plaxis 2D Reference Manual Version 9.0* [Online]. Available: http://www.plaxis.com.

POTTS, D. M. & ZDRAVKOVIC, L. 1999. *Finite Element Analysis in Geotechnical Engineering: Theory,* London, Thomas Telford

POWRIE, W. 2004. *Soil Mechanics; Concepts and Application,* London, Spon Press.

PUGASAP, K., KIM, W. & LAMAN, J. A. 2009. Long-Term Response Prediction of Integral Abutment Bridges. *JOURNAL OF BRIDGE ENGINEERING,* 14**,** 129-139.

RAO, S. S. 2005. *The Finite Element Method in Engineering*, Butterworth-Heinemann.

REDDY, J. N. 1993. *An Introduction to the Finite Element Method,* New York, McGraw-Hill.
REDDY, J. N. 2004. *An introduction to nonlinear finite element analysis,* Oxford, Oxford University Press.
REYNOLDS, C. E., STEEDMAN, J. C. & THRELFALL, A. J. 2008. *Reynold's Reinforced Concrete Designer Handbook,* New York, Taylor & Francis.
RICHARDS, B. G. & PETH, S. 2009. Modelling soil physical behaviour with particular reference to soil science. *Soil and Tillage Research,* 102**,** 216-224.
RICHARDS, K., BITHELL, M., DOVE, M. & HODGE, R. 2004. Discrete-element modelling: methods and applications in the environmental sciences. *Phil. Trans. R. Soc. Lond. A,* 362**,** 1797-1816.
ROSCOE, K. H. & BURLAND, J. B. 1968. On the generalised stress-strain behaviour of 'wet' clay. In Engineering Plasticity. *In:* HEYMAN, J. & LECKIE, F. A. (eds.) *Engineering Plasticity.* Cambridge: Cambridge University Press.
ROWE, P. W. 1954. A stress-strain theory for cohesionless soil with applications to earth pressure at rest and moving walls. *Geotechnique,* 4**,** 70-88.
ROWE, P. W. 1962. The stress-dilatancy relation for static equilibrium of an assembly of particles in contact. *Proceedings of the Royal Society of London, Series A (Mathematical and Physical Sciences),* 269**,** 500-527.
RUSSELL, H. G. & GERKEN, L. J. 1994. Jointless Bridges - the Knowns and the Unknowns. *Concrete International,* 16**,** 44-48.
RYALL, M. J., PARKE, G. A. R. & HARDING, J. E. (eds.) 2000. *The Manual of Bridge Engineering,* London: Thomas Telford.
SCHANZ, T. & VERMEER, P. A. 1998. Special Issue on Pre-Failure Deformation Behavior of Geomaterials. *Geotechnique,* 48**,** 383-387.
SCHWEIGER, H. F. 1994. ON THE USE OF DRUCKER-PRAGER FAILURE CRITERIA FOR EARTH PRESSURE PROBLEMS. *Computers and Geotechnics,* 16**,** 223-246.
SHAMSABADI, A., ROLLINS, K. M. & KAPUSKAR, M. 2007. Nonlinear soil-abutment-bridge structure interaction for seismic performance-based design. *JOURNAL OF GEOTECHNICAL AND GEOENVIRONMENTAL ENGINEERING,* 133**,** 707-720.
SHERIF, M. A., ISHIBASHI, I. & LEE, C. D. 1982. Earth pressures against rigid retaining walls. *Journal of the Geotechnical Engineering Division,* 108**,** 679-695.
SIMPSON, M. J. & CLEMENT, T. P. 2003. Comparison of finite difference and finite element solutions to the variably saturated flow equation. *Journal of Hydrology,* 270**,** 49-64.
SIVAKUGAN, N. D. B. M. 2010. *Geotechnical engineering : a practical problem solving approach,* Ft. Lauderdale, FL, J. Ross Pub.
SLOAN, S. W. & RANDOLPH, M. F. 1982. NUMERICAL PREDICTION OF COLLAPSE LOADS USING FINITE ELEMENT METHODS. *International Journal for Numerical and Analytical Methods in Geomechanics,* 6**,** 47-76.
SMADI, M. 2012. *Geotechnical Directory* [Online]. Available: http://www.geotechnicaldirectory.com/page/Software/Numerical_analysis_(soil)_.html [Accessed 31/01/2012.
SMITH, M. R., COLLIS, L. & FOOKES, P. G. (eds.) 2001. *Aggregates : sand, gravel and crushed rock aggregates for construction purposes,* London: The Geological Society.
SOLTANI, A. A. & KUKRETI, A. R. 1996. Performance evaluation ofintegral abutment bridges,. *Workshop on Integral abutment bridges.* Pittsburgh, PA.
SOUBRA, A. H. 2000. Static and seismic passive earth pressure coefficients on rigid retaining structures. *Canadian Geotechnical Journal,* 37**,** 463-478.
SPRINGMAN, S. M. & NORRISH, A. R. M. (eds.) 1994. *Soil-Structure Interaction: Centrifuge Modeling of Integral Bridge Abutments,* London: E & FN Spon.

SPRINGMAN, S. M., NORRISH, A. R. M. & NG, C. W. W. 1996. Cyclic Loading of Sand Behind Integral Bridge Abutments. *TRL Report; 146.* Crowthorne: Transport Research Laboratory.

SPYRAKOS, C. & LOANNIDIS, G. 2003. Seismic Behavior of a Post-Tensioned Integral Bridge Including Soil-Structure Interaction (SSI). *Soil Dynamics and Earthquake engineering,* 23**,** 53-63.

STEELE, D. P. & SNOWDON, R. A. 1996. In situ states of compaction of structural backfill. *TRL report; 206.* Crowthorne.

TACHIBANA, S., IIZUKA, A., KAWAI, K., KOBAYASHI, I., PIPATPONGSA, T. & OHTA, H. 2007. Numerical investigation on the failure criterion of normally consolidated clays. *International Journal for Numerical and Analytical Methods in Geomechanics,* 31**,** 809-833.

TAKE, W. A. & BOLTON, M. D. 2011. Seasonal ratcheting and softening in clay slopes, leading to first-time failure. *Geotechnique,* 61**,** 757-69.

TAN, Y. 2008. Finite element analysis of highway construction in peat bog. *Canadian Geotechnical Journal,* 45**,** 147-160.

TERZAGHI, K. 1936a. A fundamental fallacy in earth pressure calculations. *Boston Society of Civil Engineers Journal.*

TERZAGHI, K. The Shearing Resistance of Saturated Soils. Proceedings of the First International Conference on Soil Mechanics, 1936b. 54-56.

TERZAGHI, K. & PECK, R. B. 1967. *Soil Mechanics in Engineering Practice,* New York, John Wiley & Sons Inc.

THOMSON, J. T. A. & LUTENEGGER, A. J. Passive Earth Pressure Tests on Integral Bridge Abutment. Proceedings of the 4th International Conference on Case Histories in Geotechnical Engineering, 1998. 733-739.

TILLY, G. P. (ed.) 1994. *Historical Review of the Development of Continuity and Joints in Bridges,* London: E & FN Spon.

TSANG, N. C. M., ENGLAND, G. L. & DUNSTAN, T. 2002. Soil/Structure Interaction of Integral Bridge with Full Height Abutments. *15th ASCE Engineering Mechanics Conference June 2-5, 2002, Columbia University.* New York.

UNITED STATES. FEDERAL HIGHWAY, A., NATIONAL COOPERATIVE HIGHWAY RESEARCH, P., NEWCOMB, D. E., AMERICAN ASSOCIATION OF STATE, H., TRANSPORTATION, O., BIRGISSON, B. & NATIONAL RESEARCH COUNCIL . TRANSPORTATION RESEARCH, B. 1999. *Measuring in situ mechanical properties of pavement subgrade soils,* Washington, D.C., National Academy Press.

VERSTEEG, H. K. & MALALASEKERA, W. 2007. *An introduction to computational fluid dynamics : the finite volume method*, Harlow : Pearson Prentice Hall.

VILADKAR, M. N., GODBOLE, P. N. & NOORZAEI, J. 1994. Modelling of interface for soil-structure interaction studies. *Computers and Structures,* 52**,** 765-779.

VILLARD, P., CHEVALIER, B., HELLO, B. L. & COMBE, G. 2009a. Coupling between finite and discrete element methods for the modelling of earth structures reinforced by geosynthetics. *Computers and Geotechnics,* 36**,** 709-717.

VILLARD, P., CHEVALIER, B., LE HELLO, B. & COMBE, G. 2009b. Coupling between finite and discrete element methods for the modelling of earth structures reinforced by geosynthetic. *Computers and Geotechnics,* 36**,** 709-17.

VON MISES, R. 1913. Mechanik der festen Körper im plastisch- deformablen Zustand. *Nachrichten von der Gesellschaft der Wissenschaften zu Göttingen, Mathematisch-Physikalische Klasse,* 1913**,** 582-592.

WANG, B., CHEN, G. & JIN, D. 2010. Pore water pressure increment model for saturated Nanjing fine sand subject to cyclic loading. *Earthquake Engineering and Engineering Vibration,* 9**,** 569-76.

WANG, C.-J. & SHIH, M.-H. 2007. Performance Study of a Bridge Involving Sliding Decks and Pounded Abutment During a Violent Earthquake. *Engineering Structures,* 29**,** 802-812.
WASSERMANN, E. P. & WALKER, J. H. 1996. Integral Abutments for continuous steel bridges,. *Workshop on Integral abutment bridges,.* Pittsburgh, PA.
WEBB, J. D. C. & MEADEN, G. T. 2000. Daily Temperature Extremes for Britain. *Weather Vol. 55.*
WHITE, H. 2007. Integral Abutment Bridges: Comparison of Current Practice between European Countries and the United States of America. *Special Report 152.* New York: Transportation Research and Development Bureau.
WHITE, H., PTURSSON, H. & COLLIN, P. 2010. Integral abutment bridges: The European way. *Practice Periodical on Structural Design and Construction,* 15**,** 201-208.
WICKS, J. 2011. Understanding our Analysis: Flood Modeling. 19 September ed.: Institute of Civil Engineers.
WOOD, D. M. 1990. *Soil Behaviour and Critical State Soil Mechanics,* New York, Cambridge University Press.
WOOD, D. M. 2004. *Geotechnical Modeling,* London, E & FN Spoon.
WOOD, D. M. & NASH, D. 2000. Earth Pressure on an Integral Bridge Abutment; A Numerical Case Study. *SOILS AND FOUNDATION; THE JAPANESE GEOTECHNICAL SOCIETY,* 40**,** 23-38.
WOODWARD, P. K. 1997. Earth pressure coefficients based on the Lade-Duncan failure criterion. *Engineering Structures,* 19**,** 733-737.
XU, M. & BLOODWORTH, A. G. The earth pressure behind full-height integral abutments. Structures and Extreme Events. IABSE Symposium, 14-17 Sept. 2005, 2006 Zurich, Switzerland. ETH Honggerberg, 316-17.
XU, M., BLOODWORTH, A. G. & CLAYTON, C. R. I. 2007. Behavior of a Stiff Clay Behind Embedded Integral Abutments. *Journal of Geotechnical and Geoenvironmental Engineering,* 133**,** 721-730.
YAN, B., REGUEIRO, R. A. & STURE, S. 2010. Three-dimensional ellipsoidal discrete element modeling of granular materials and its coupling with finite element facets. *Engineering Computations (Swansea, Wales),* 27**,** 519-550.
YANG, P. S., WOLDE-TINSAE, A. M. & GREIMANN, L. F. 1985. Effects of Predrilling and Layered Soils on Piles. *Journal of Geotechnical Engineering,* 111**,** 18-31.
YASUHARA, K. Drainage Effect Importance in Cyclic Behaviour of Clay. 10th European Conference on Soil Mechanics and Foundation Engineering, 1991 Florence. 1285-1287.
ZHANG, J.-M., SHAMOTO, Y. & TOKIMATSU, K. 1998. Evaluation ofearth pressure under any lateral deformation. *Soils and Foundation (Japanese Geotechnical Society),* 38**,** 15-33.
ZHANG, L. 2006. *Engineering Properties of Rocks*, Elsevier.
ZHAO, Q., VASHEGHANI-FARAHANI, R. & BURDETTE, E. G. Seismic Analysis of Integral Abutment Bridge Including Soil-Structure Interaction. Structures Congress 2011, 2011

Las Vegas, Nevada. American Society of Civil Engineers.
ZHU, D. Y. & QIAN, Q. 2000. Determination of passive earth pressure coefficients by the method of triangular slices. *Canadian Geotechnical Journal,* 37**,** 485-491.
ZIENKIEWICZ, O. C., KELLY, D. W. & BETTESS, P. 1977. The Coupling of the Finite Element Method and Boundary Solution Procedures. *International Journal for Numerical Methods in Engineering,* 11**,** 377-375.
ZORDAN, T., BRISEGHELLA, B. & LAN, C. 2011. Parametric and pushover analyses on integral abutment bridge. *Engineering Structures,* 33**,** 502-515.

APPENDIX 1

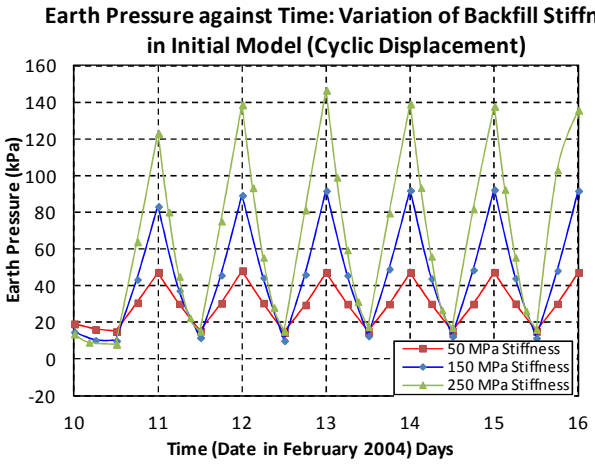

Appendix 1a: Change in backfill stiffness (cyclic displacement in initial Model).

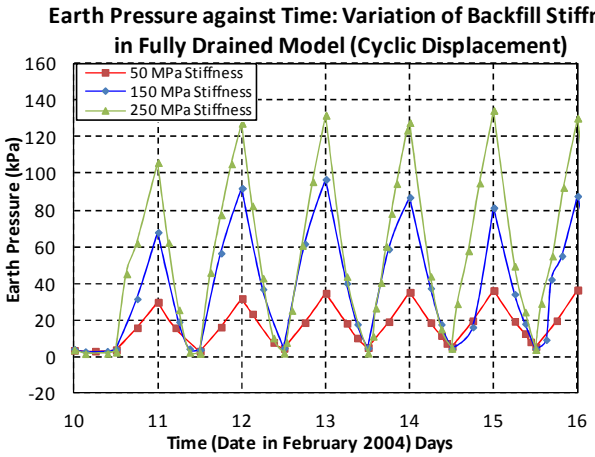

Appendix 1b: Change in backfill stiffness (cyclic displacement in fully Drained Model).

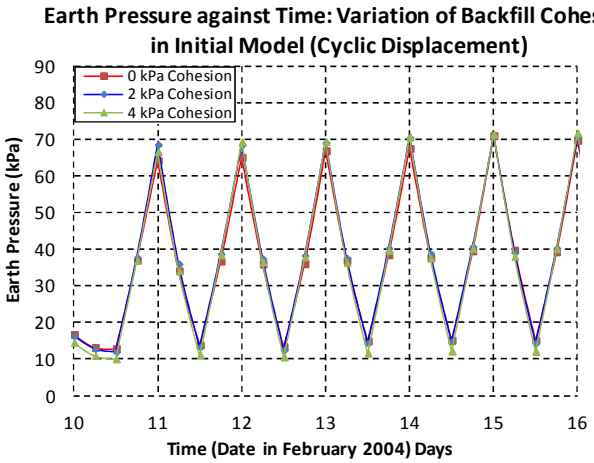

Appendix 1c: Change in backfill cohesion (cyclic displacement in initial Model).

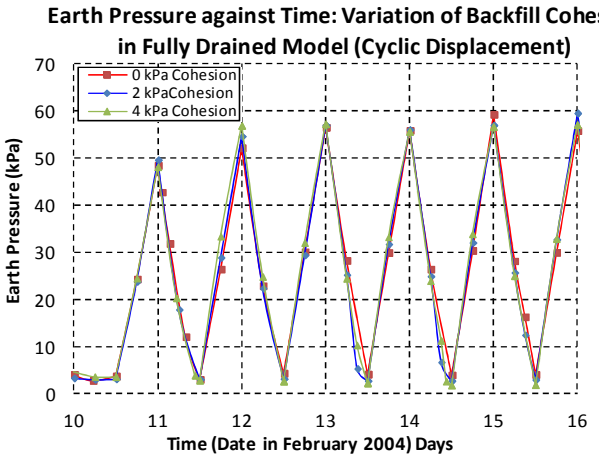

Appendix 1d: Change in backfill cohesion (cyclic displacement in fully Drained Model).

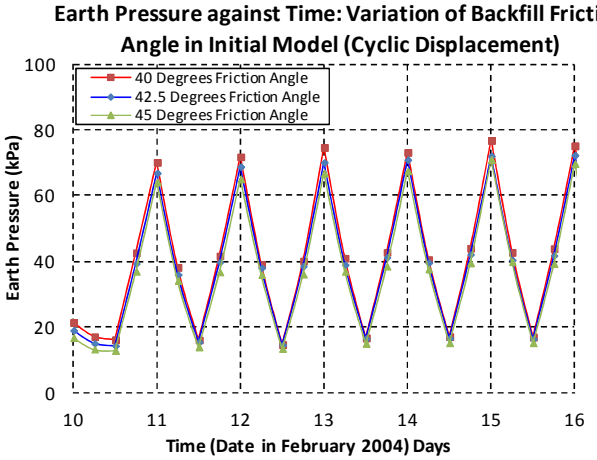

Appendix 1e: Change in backfill friction angle (cyclic displacement in initial Model).

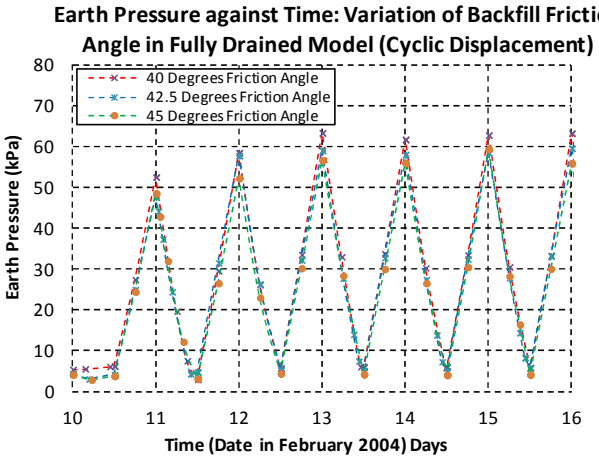

Appendix 1f: Change in backfill friction angle (cyclic displacement in fully Drained Model).

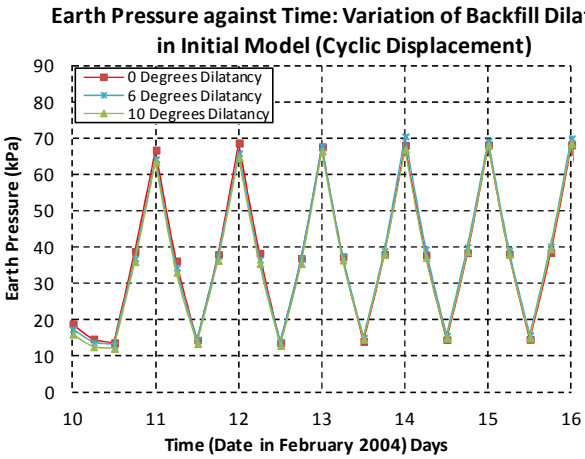

Appendix 1g: Change in backfill dilatancy (cyclic displacement in initial Model).

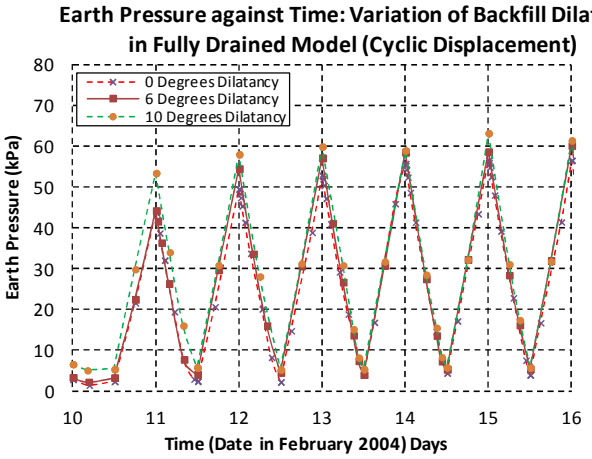

Appendix 1h: Change in backfill dilatancy (cyclic displacement in fully Drained Model).

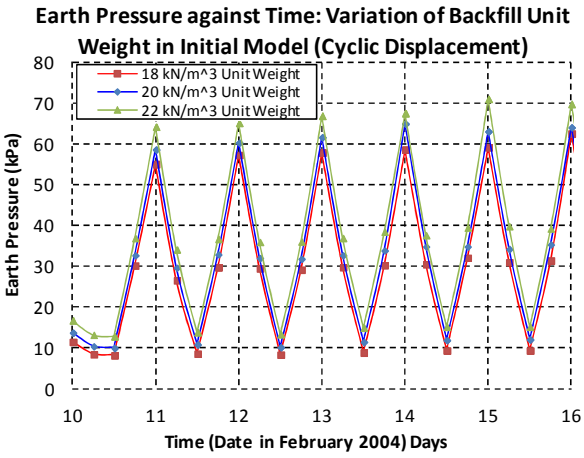

Appendix 1i: Change in backfill unit weight (cyclic displacement in initial Model).

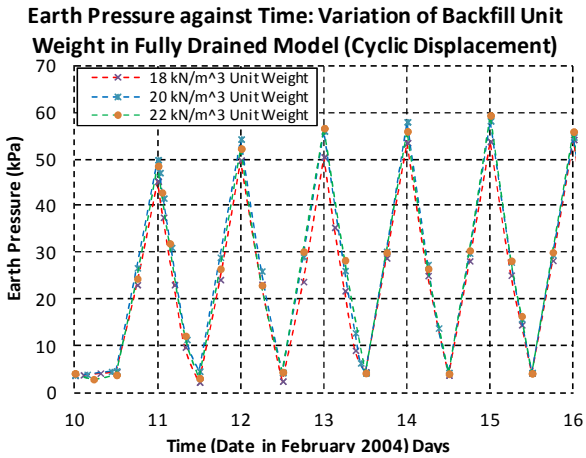

Appendix 1j: Change in backfill unit weight (cyclic displacement in fully Drained Model).

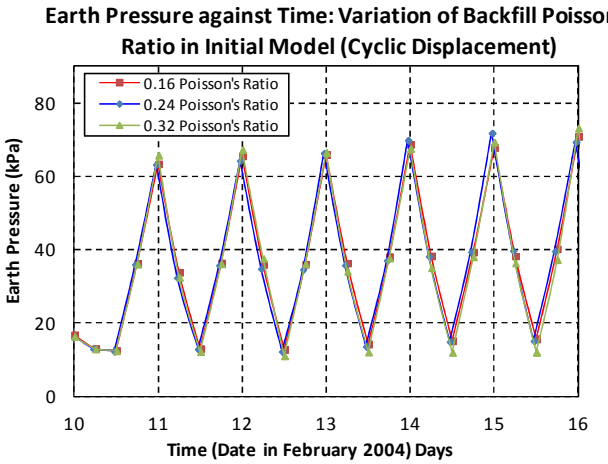

Appendix 1k: Change in backfill Poisson's Ratio (cyclic displacement in Initial Model).

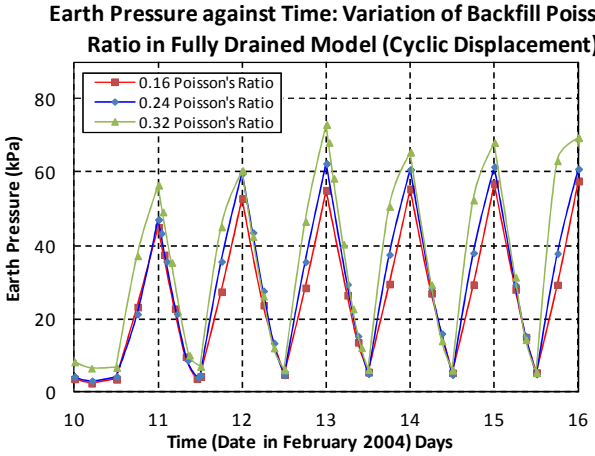

Appendix 1l: Change in backfill Poisson's Ratio (cyclic displacement in fully Drained Model).

APPENDIX 2

Autumn Construction Abutment Displacement Model (Monthly Cycle) (Integral Bridge Deck/Abutment Link Temperature and Displacement)					
Months	Mid Temp.	Calc. Model Abutment Disp. (mm)	Relative Mid Disp. (mm)	Relative Min. Disp. (mm)	Relative Max. Disp. (mm)
January	2.3	**7.0 (±3.5)**	-3.8	-7.3	-0.3
February	3.3	**7.0 (±3.5)**	-3.3	-6.8	0.2
March	6.5	**7.0 (±3.5)**	-1.9	-5.4	1.6
April	9.6	**7.9 (±4.0)**	-0.5	-4.5	3.5
May	11.8	**7.0 (±3.5)**	0.5	-3	4.0
June	15.4	**7.3 (±3.7)**	2.2	-1.5	5.9
July	17.9	**7.5 (±3.8)**	3.3	-0.5	7.1
August	17.4	**7.6 (±3.8)**	3.1	-0.7	6.9
September	14.7	**7.3 (±3.7)**	1.9	-1.8	5.6
October	10.6	**7.4 (±3.7)**	0	-3.7	3.7
November	6.5	**6.1 (±3.1)**	-1.9	-5.0	1.2
December	3.9	**6.0 (±3.0)**	-3.1	-6.1	-0.1

APPENDIX 3

Spring Construction Abutment Displacement Model (Monthly Cycle) (Integral Bridge Deck/Abutment Link Temperature and Displacement)					
Months	Mid Temp.	Calc. Model Abutment Disp. (mm)	Relative Mid Disp. (mm)	Relative Min. Disp. (mm)	Relative Max. Disp. (mm)
January	2.3	**7.0 (±3.5)**	-3.3	-6.8	0.2
February	3.3	**7.0 (±3.5)**	-2.9	-6.4	0.6
March	6.5	**7.0 (±3.5)**	-1.4	-4.9	2.1
April	9.6	**7.9 (±4.0)**	0	-4.0	4.0
May	11.8	**7.0 (±3.5)**	1.0	-2.5	4.5
June	15.4	**7.3 (±3.7)**	2.7	-1.0	6.4
July	17.9	**7.5 (±3.8)**	3.8	0.0	7.6
August	17.4	**7.6 (±3.8)**	3.6	-0.2	7.4
September	14.7	**7.3 (±3.7)**	2.3	-1.4	6.0
October	10.6	**7.4 (±3.7)**	0.5	-3.2	4.2
November	6.5	**6.1 (±3.1)**	-1.4	-4.5	1.7
December	3.9	**6.0 (±3.0)**	-2.6	-5.6	0.4

APPENDIX 4

Summer Construction Abutment Displacement Model (Monthly Cycle) (Integral Bridge Deck/Abutment Link Temperature and Displacement - Warmest Period)				
Months	Max. Temp.	Calc. Model Abutment Disp. (mm)	Relative Max. Disp. (mm)	Relative Min. Disp. (mm)
January	9.9	**7.0**	-7.4	-14.4
February	10.9	**7.0**	-7.0	-14.0
March	14.1	**7.0**	-5.5	-12.5
April	18.2	**7.9**	-3.6	-11.5
May	19.4	**7.0**	-3.1	-10.1
June	23.4	**7.3**	-1.2	-8.5
July	26.1	**7.5**	0	-7.5
August	25.7	**7.6**	-0.2	-7.8
September	22.7	**7.3**	-1.6	-8.9
October	18.6	**7.4**	-3.4	-10.8
November	13.2	**6.1**	-5.9	-12.0
December	10.4	**6.0**	-7.2	-13.2

APPENDIX 5

Winter Construction Abutment Displacement Model (Monthly Cycle) (Integral Bridge Deck/Abutment Link Temperature and Displacement - Coldest Period)				
Months	Min. Temp.	Calc. Model Abutment Disp. (mm)	Relative Min. Disp. (mm)	Relative Max. Disp. (mm)
January	-5.4	**7.0**	0	7.0
February	-4.3	**7.0**	0.5	7.5
March	-1.2	**7.0**	1.9	8.9
April	0.9	**7.9**	2.9	10.8
May	4.2	**7.0**	4.4	11.4
June	7.4	**7.3**	5.9	13.2
July	9.7	**7.5**	6.9	14.4
August	9.1	**7.6**	6.6	14.2
September	6.7	**7.3**	5.5	12.8
October	2.5	**7.4**	3.6	11.0
November	-0.2	**6.1**	2.4	8.5
December	-2.7	**6.0**	1.2	7.2

APPENDIX 6

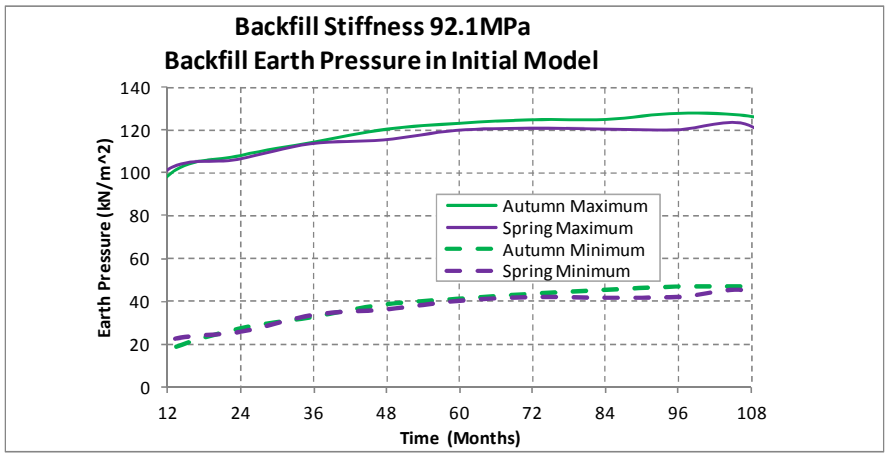

Appendix 6a: Initial model autumn against spring earth pressures at 92.1MPa backfill stiffness.

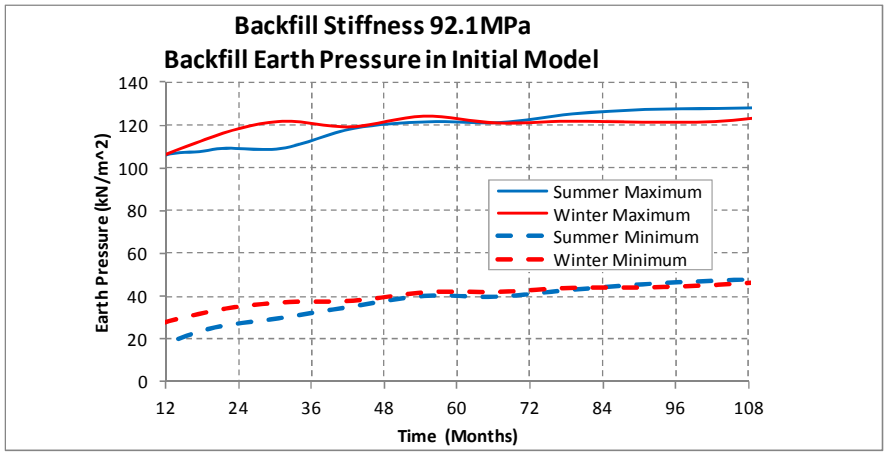

Appendix 6b: Initial model summer against winter earth pressures at 92.1MPa backfill stiffness.

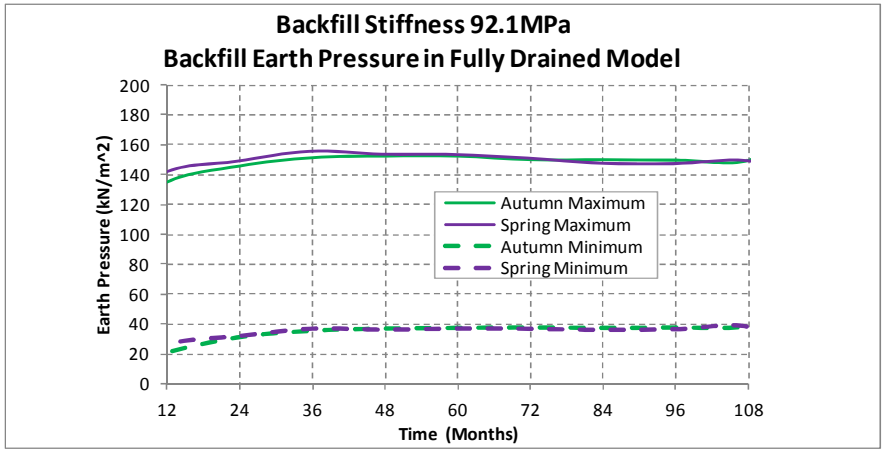

Appendix 6c: Fully drained model autumn against spring earth pressures at 92.1MPa backfill stiffness.

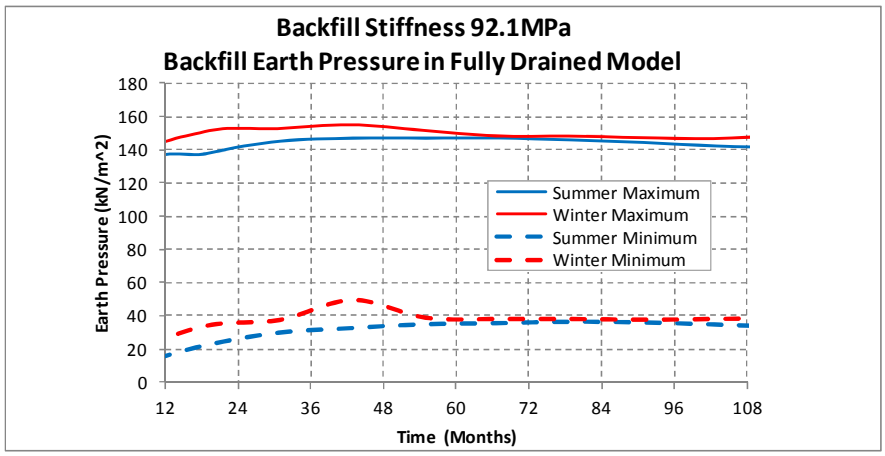

Appendix 6d: Fully drained model summer against winter earth pressures at 92.1MPa backfill stiffness

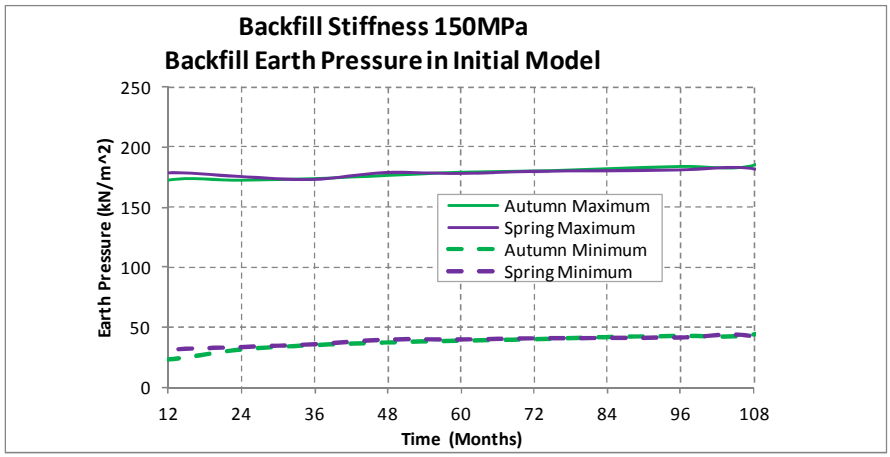

Appendix 6e: Initial model autumn against spring earth pressures at 150MPa backfill stiffness.

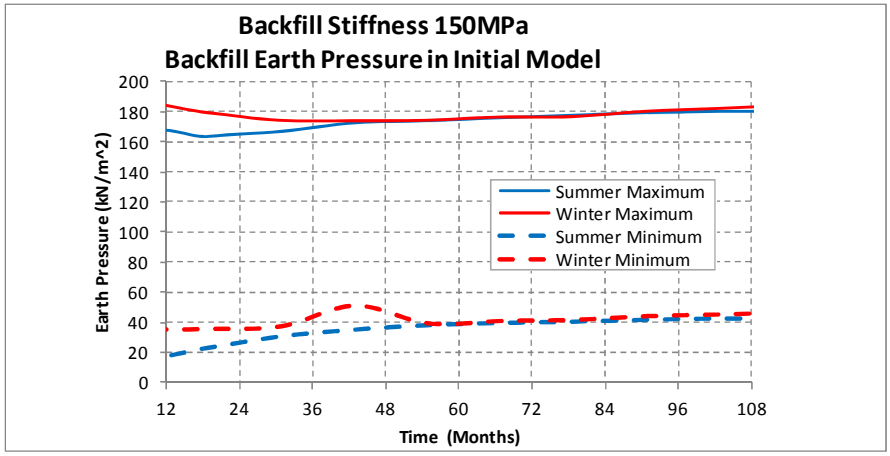

Appendix 6f: Initial model summer against winter earth pressures at 150MPa backfill stiffness.

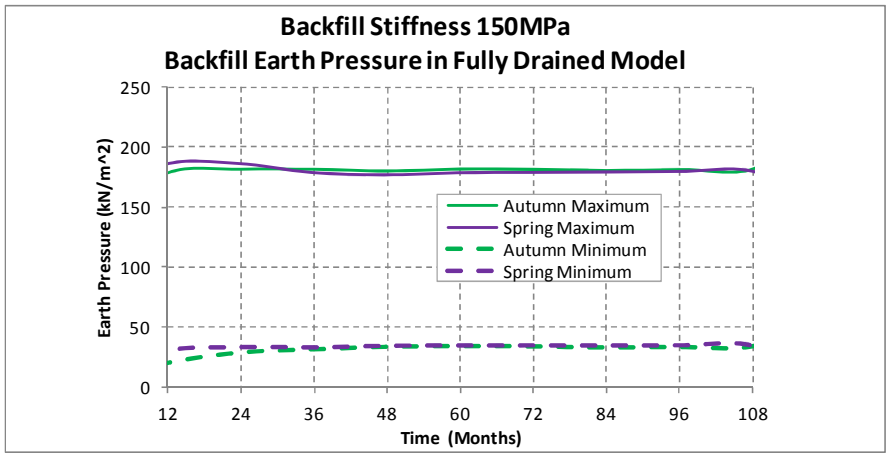

Appendix 6g: Fully drained model autumn against spring earth pressures at 150MPa backfill stiffness.

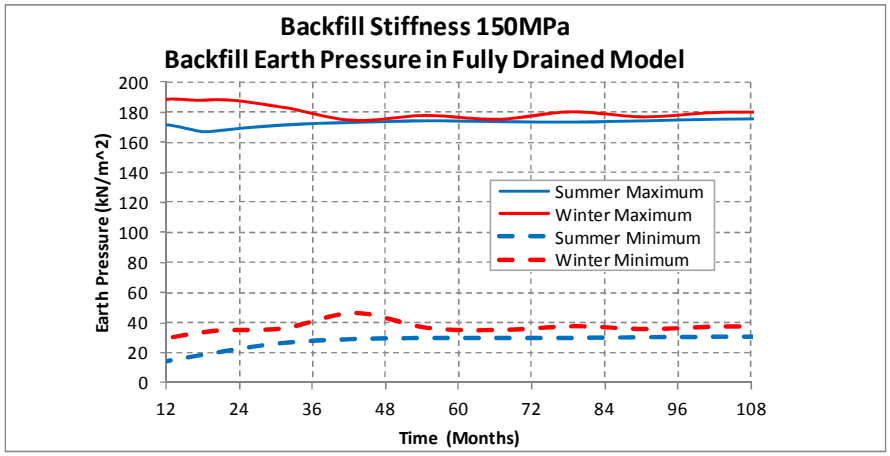

Appendix 6h: Fully drained model summer against winter earth pressures at 150MPa backfill stiffness

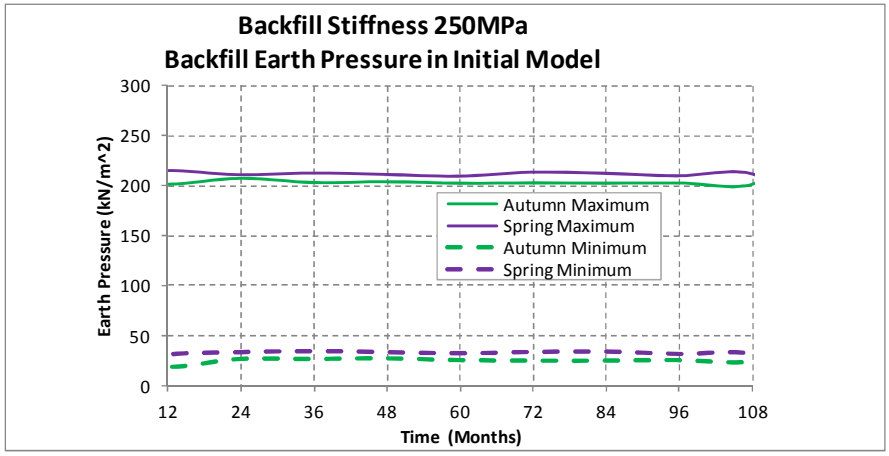

Appendix 6i: Initial model autumn against spring earth pressures at 250MPa backfill stiffness.

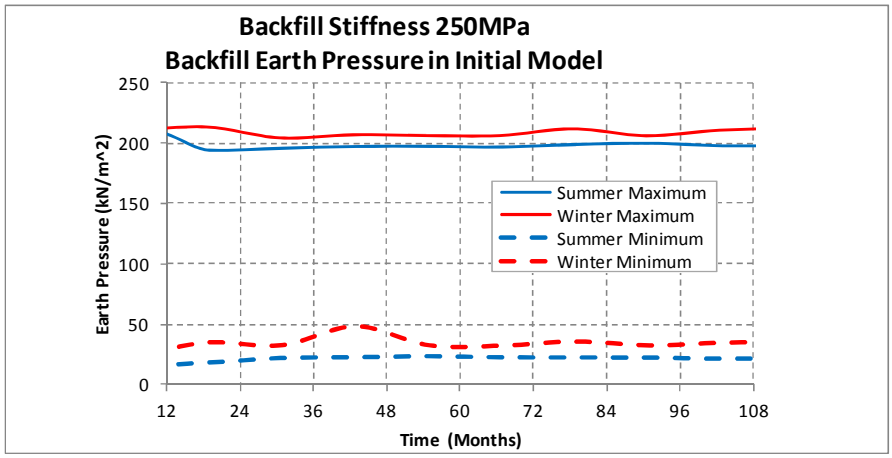

Appendix 6j: Initial model summer against winter earth pressures at 250MPa backfill stiffness.

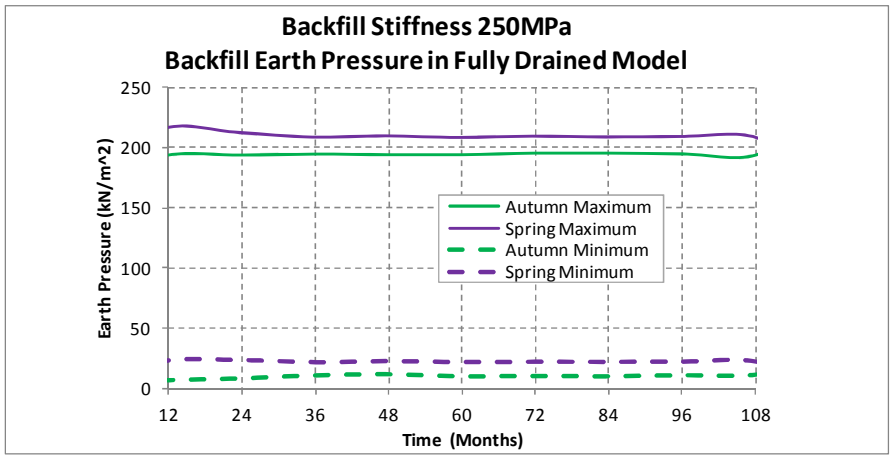

Appendix 6k: Fully drained model autumn against spring earth pressures at 250MPa backfill stiffness.

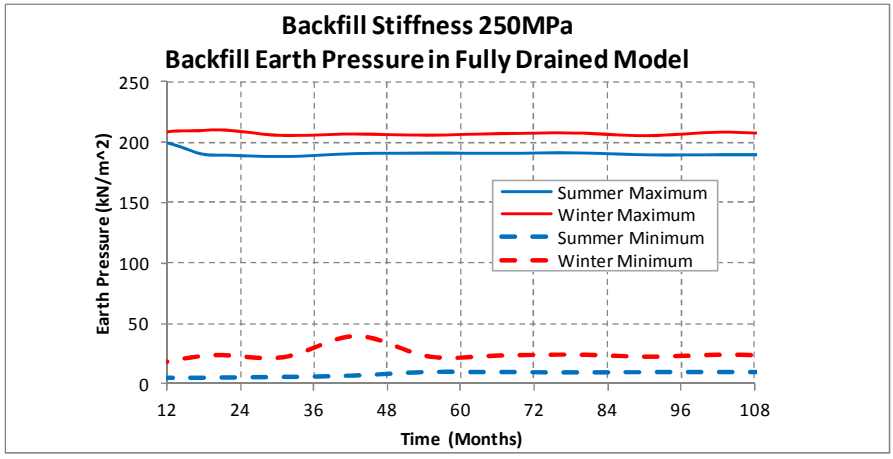

Appendix 6l: Fully drained model summer against winter earth pressures at 250MPa backfill stiffness

APPENDIX 7

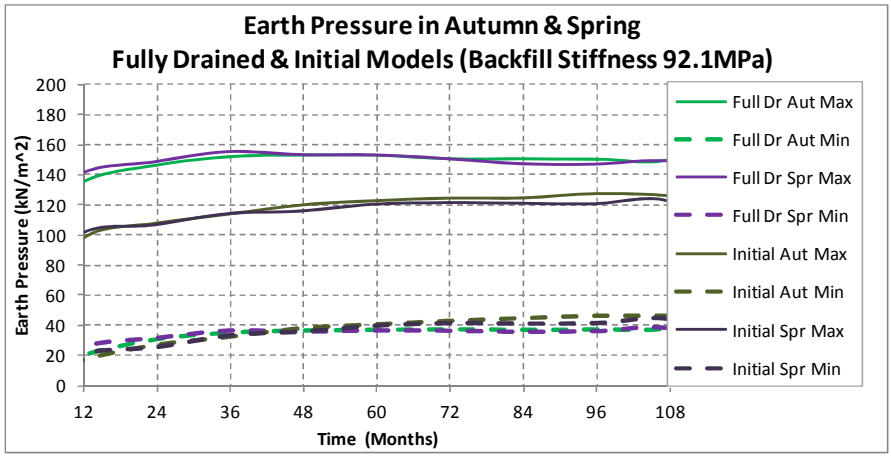

Appendix 7a: Autumn and spring fully drained against initial model at 92.1MPa backfill stiffness - earth pressure values.

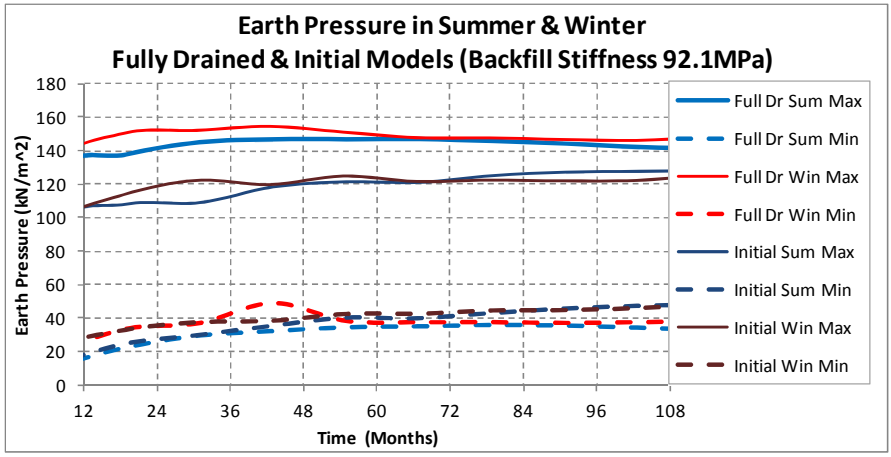

Appendix 7b: Summer and winter fully drained against initial model at 92.1MPa backfill stiffness - earth pressure values.

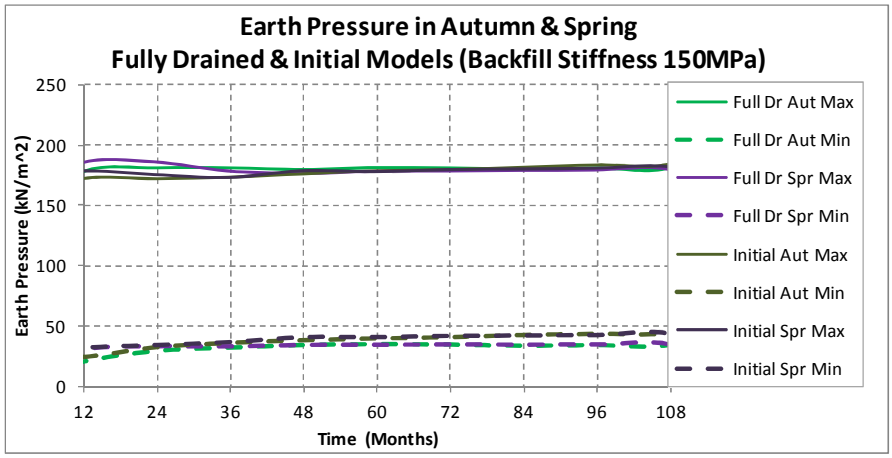

Appendix 7c: Autumn and spring fully drained against initial model at 150MPa backfill stiffness - earth pressure values.

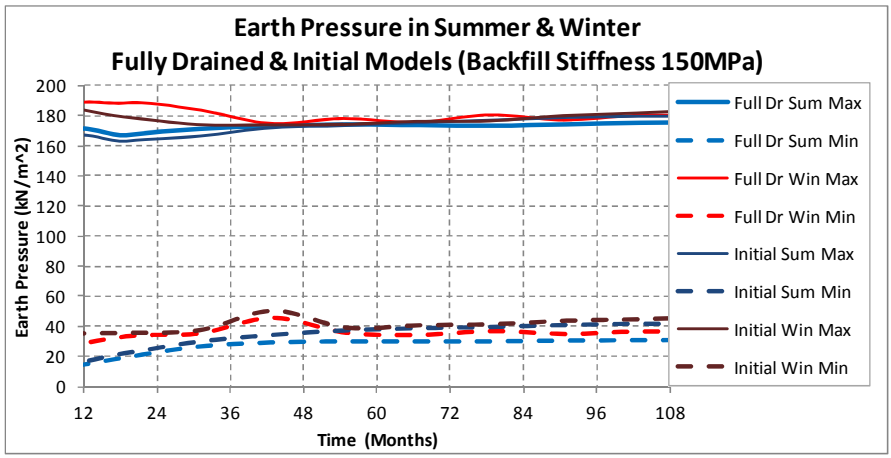

Appendix 7d: Summer and winter fully drained against initial model at 150MPa backfill stiffness - earth pressure values.

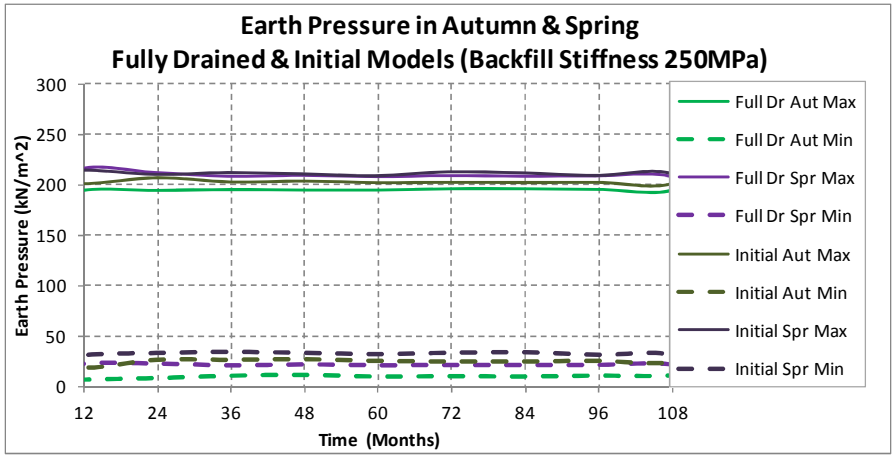

Appendix 7e: Autumn and spring fully drained against initial model at 250MPa backfill stiffness - earth pressure values.

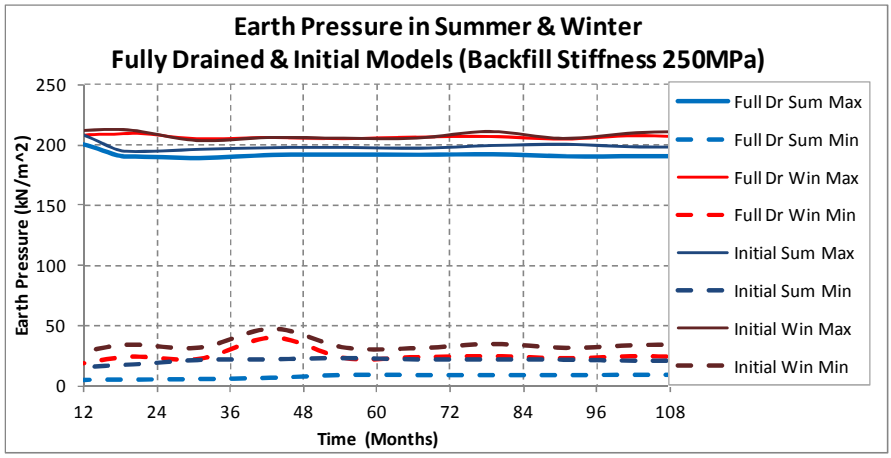

Appendix 7f: Summer and winter fully drained against initial model at 250MPa backfill stiffness - earth pressure values.

APPENDIX 8

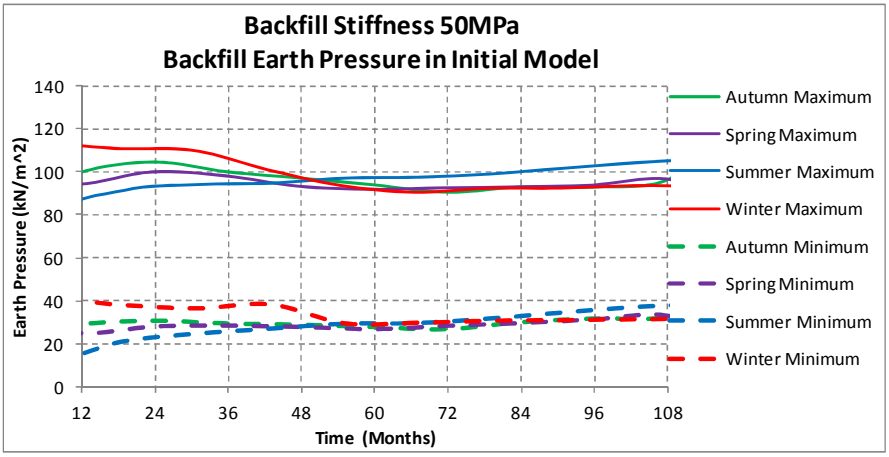

Appendix 8a: 50MPa backfill stiffness (Initial Model).

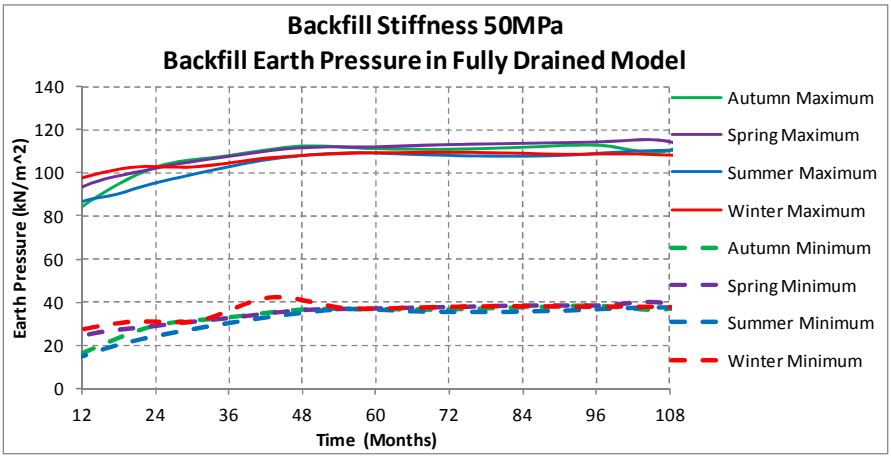

Appendix 8b: 50MPa backfill stiffness (Fully Drained Model).

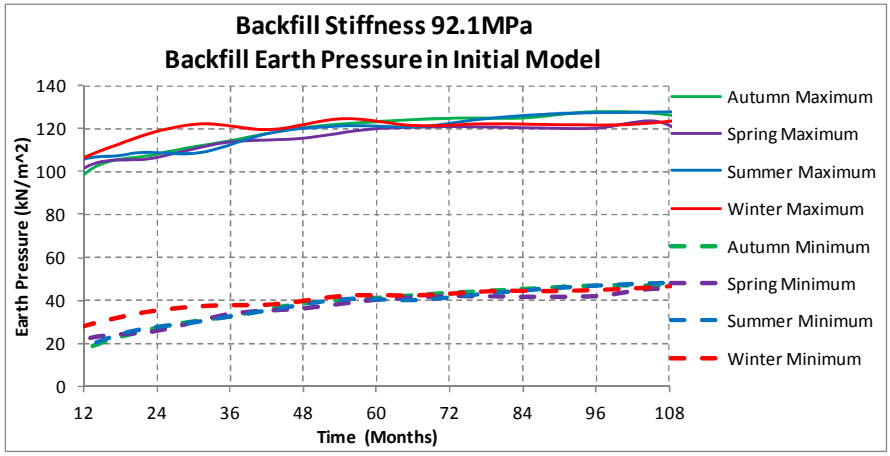

Appendix 8c: 92.1MPa backfill stiffness (Initial Model).

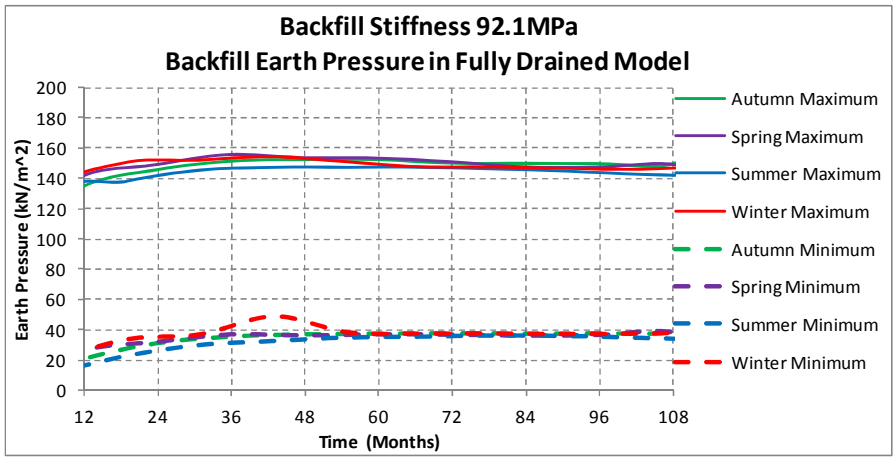

Appendix 8d: 92.1MPa backfill stiffness (Fully Drained Model).

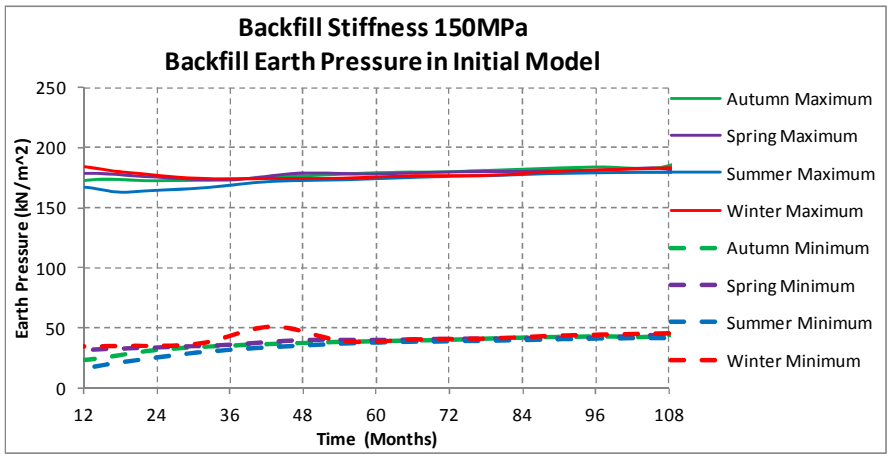

Appendix 8e: 150MPa backfill stiffness (Initial Model).

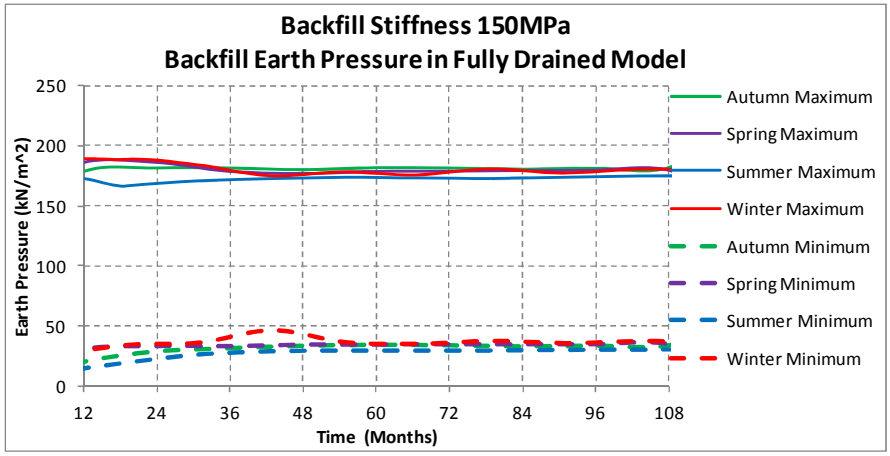

Appendix 8f: 150MPa backfill stiffness (Fully Drained Model).

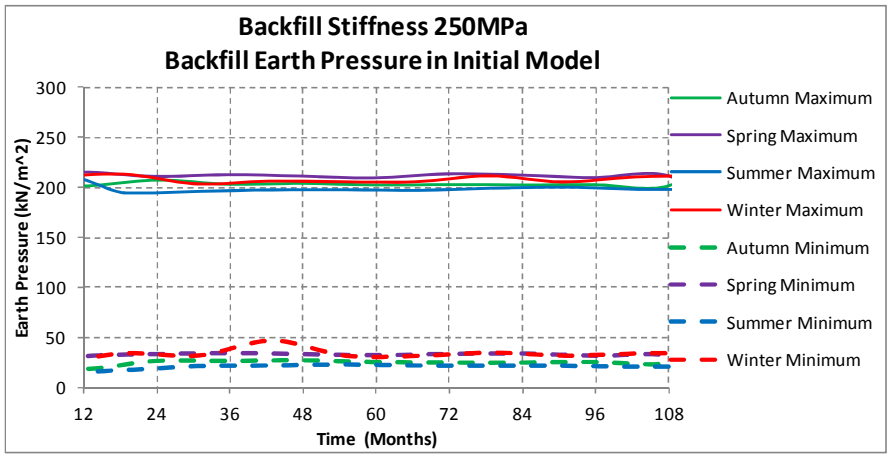

Appendix 8g: 250MPa backfill stiffness (Initial Model).

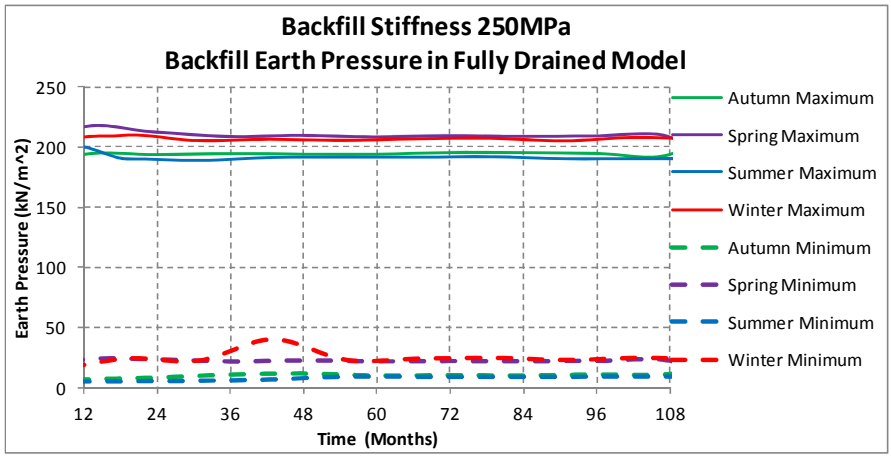

Appendix 8h: 250MPa backfill stiffness (Fully Drained Model).

APPENDIX 9

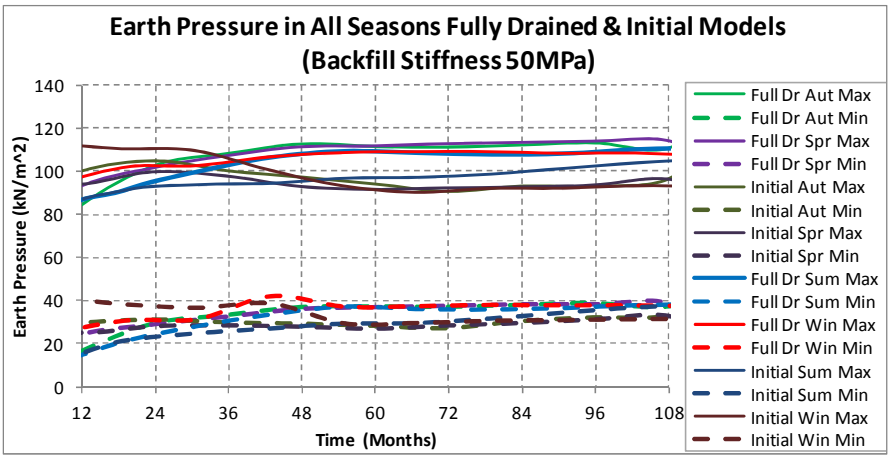

Appendix 9a: Earth pressures in construction seasons (50MPa backfill stiffness).

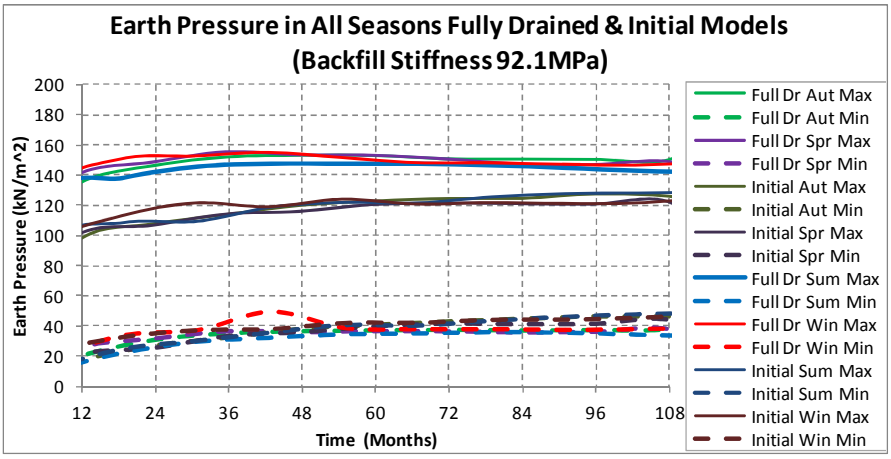

Appendix 9b: Earth pressures in construction seasons (92.1MPa backfill stiffness).

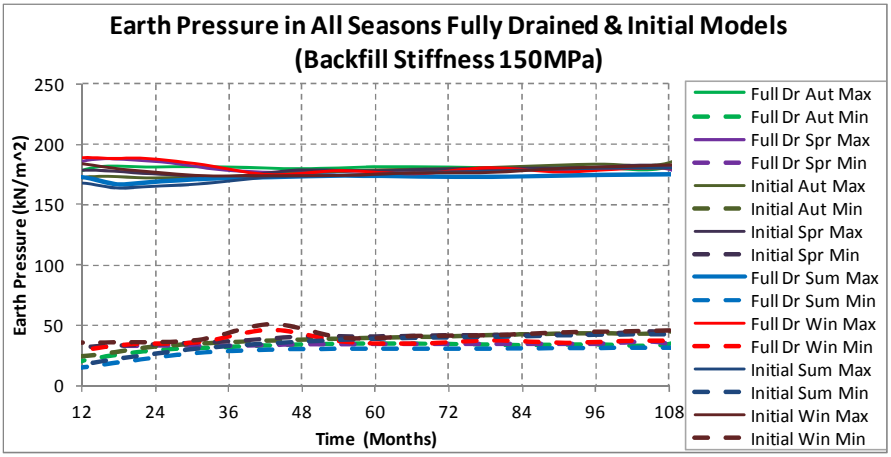

Appendix 9c: Earth pressures in construction seasons (150MPa backfill stiffness).

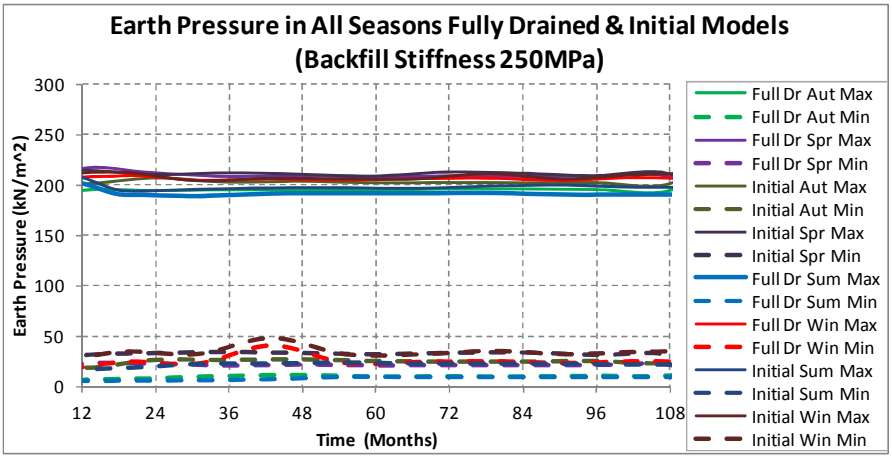

Appendix 9d: Earth pressures in construction seasons (250MPa backfill stiffness).